

Ministry of Higher Education and Scientific Research
Hassiba Benbouali University of Chlef
Faculty of Civil Engineering and Architecture
Department of Civil Engineering



THESIS

Submitted for the

DOCTORAL DEGREE

Field: Civil Engineering

Specialty: Earthquake Engineering and Geo-environment

By

BENDRISS Faïçal

Theme:

Reliability Study of Bearing Capacity of Foundations under Dynamic Loadings

Defended on 05/23/2024, before the jury consisting of:

Belkacem LAMRI	Professor	University of Chlef	President
Zine El Abidine RAHMOUNI	Professor	University of M'sila	Examiner
Abdelaziz MEDDAH	Professor	University of M'sila	Examiner
Mohamed MEKKI	Professor	University of USTO	Examiner
Mohamed GHRICI	Professor	University of Chlef	Examiner
Zamila HARICHANE	Professor	University of Chlef	Reporter

Ministère de l'Enseignement Supérieur et de la Recherche Scientifique

Université Hassiba Benbouali de Chlef

Faculté Génie civil et d'architecture

Département Génie civil



THÈSE

Présentée pour l'obtention du diplôme de

DOCTORAT

Filière : Génie civil

Spécialité : Génie parasismique et Géo-environnement

Par

BENDRISS Faïçal

Thème :

Etude fiabiliste de la capacité portante des fondations sous chargements dynamiques

Soutenue le 23/05/2024, devant le jury composé de :

Belkacem LAMRI	Professeur	Université de Chlef	Président
Zine El Abidine RAHMOUNI	Professeur	Université de M'sila	Examineur
Abdelaziz MEDDAH	Professeur	Université de M'sila	Examineur
Mohamed MEKKI	Professeur	Université d'USTO	Examineur
Mohamed GHRICI	Professeur	Université de Chlef	Examineur
Zamila HARICHANE	Professeur	Université de Chlef	Rapporteur

Dedications

I dedicate this arduous work to my beloved parents to express my deep gratitude for the attention, constant support, trust, and encouragement they have continuously shown towards me throughout these long years, and for being by my side throughout my entire life to witness me become who I am.



Gratitudes

At the end of this work, I would like to first thank ALLAH, the Merciful and Compassionate, for blessing me with good health to undertake this endeavor.

I would like to express my deepest gratitude and sincere thanks to my supervisor Dr. Zamila HARICHANE, Professor at Hassiba Benbouali University of Chlef, for providing the scientific guidance for this work, for her patience, trust, and especially for her valuable advice, encouragement, as well as all the suggestions and remarks she provided throughout this endeavor.

It is my great pleasure to extend my heartfelt gratitude to Dr. Belkacem LAMRI, Professor at Hassiba Benbouali University of Chlef, for the honor of chairing the jury.

I would like to thank Dr. Zine El Abidine RAHMOUNI and Dr. Abdelaziz MEDDAH, Professors at the University of M'sila, Dr. Mohamed MEKKI, Professor at the University of Oran (USTO), and Dr. Mohamed GHRICI, Professor at Hassiba Benbouali University of Chlef, for agreeing to evaluate my thesis.

My warmest thanks also go to the entire academic team of the Faculty of Civil Engineering and Architecture, especially those who facilitated our advancement in the doctoral program in Earthquake Engineering and Geo-environment.

Finally, I would like to thank my parents, as well as my siblings, for their support throughout these years, without which I would not be where I am today.

ملخص

الهدف الرئيسي لهذه الأطروحة هو دراسة تأثير عدم الإرتيابات على قدرة تحمل الأساسات السطحية تحت تحميل الزلازل باستخدام النهج الاحتمالي. في المرحلة الأولى من هذه الرسالة، تم استخدام طريقة توسيع Karhunen-Loève (KL) في سياق نظرية الحقل العشوائي لاستكشاف تأثير عشوائية معطيات التربة والزلازل على قدرة تحمل الزلازل. تم تطبيق معادلات قدرة التحمل الزلزالية التي وضعها كونتي (2018) في التحليل لنوعين من التربة التي تدعم القواعد السطحية: تربة متماسكة بحتة وتربة متماسكة احتكاكية. أشارت النتائج إلى أنه، في سياق النتائج الإحصائية والاحتمالية، من الضروري إعطاء الأولوية لمعامل التباين لالتقاط التباين بدقة وإجراء استدلالات موثوقة. في المرحلة الثانية من الأطروحة، تم تقديم صياغة لتحديد معامل قدرة تحمل الزلازل لقاعدة شريطية سطحية تتأثر بانتشار الأمواج السطحية الإلتوائية وتقع على تربة غير متجانسة ذات خواص متباينة. تم استخدام طريقة التوازن الحدودي بالاشتراك مع النهج الشبه ديناميكي. بالإضافة إلى ذلك، تم إجراء تحليل موثوقية استنادًا إلى المحاكاة المونتي كارلو لدمج الإرتيابات في التربة والزلازل ودراسة تأثيراتها. وُجد أن عامل القدرة التحملية المقترح للزلازل يمكن أن يكون قابلاً للتطبيق من أجل قياس انتشار الموجات الإلتوائية، والتباين في الخواص، وعدم تجانس خصائص التربة.

كلمات مفتاحية: الإرتيابات؛ قدرة التحمل؛ الأساسات السطحية؛ زلازل؛ الموجة؛ حقل عشوائي؛ موثوقية؛ مونتي كارلو؛ احتمالية.

Abstract

The main objective of this thesis is to investigate the impact of uncertainties on the bearing capacity of shallow foundations under seismic loading by employing probabilistic approaches. At the first stage, the Karhunen-Loève (KL) expansion method within the context of random field theory was utilized to explore the influence of soil and earthquake parameter randomness on the seismic bearing capacity. The seismic bearing capacity equations established by Conti (2018) were applied in the analysis for two soil types supporting shallow strip footings: purely cohesive soil and cohesive-frictional soil. The results indicated that, in the context of statistical and probabilistic results, prioritizing the coefficient of variation is essential for accurately capturing the variability and making reliable inferences. At the second stage, a formulation for determining the seismic bearing capacity factor of a shallow strip footing influenced by torsional surface wave propagation and resting on anisotropic non-homogeneous soil was presented. The limit equilibrium method in conjunction with the pseudo-dynamic approach are used. In addition to that, a reliability analysis based on Monte Carlo simulation was conducted in order to incorporate the soil-earthquake uncertainties and investigating their effects. It was found that the proposed seismic bearing capacity factor can be applicable in order to quantify the torsional wave propagation, the anisotropy and the non-homogeneity of the soil properties.

Keywords: Uncertainties; bearing capacity; shallow foundations; torsional wave; Random field; Reliability; Monte Carlo; probability.

Résumé

Le principal objectif de cette thèse est d'étudier l'impact des incertitudes sur la capacité portante des fondations superficielles sous chargement sismique en utilisant des approches probabilistes. Dans la première étape, la méthode d'expansion Karhunen-Loève (KL) dans le contexte de la théorie des champs aléatoires a été utilisée pour explorer l'influence du caractère aléatoire des paramètres du sol et du séisme sur la capacité portante sismique. Les équations de la capacité portante sismique établies par Conti (2018) ont été appliquées dans l'analyse pour deux types de sol soutenant des semelles superficielles : sol purement cohérent et sol cohésif-frictionnel. Les résultats ont indiqué que, dans le contexte des résultats statistiques et probabilistes, il est essentiel de prioriser le coefficient de variation pour capturer avec précision la variabilité et faire des inférences fiables. Dans la deuxième étape, une formulation pour déterminer le facteur de capacité portante sismique d'une semelle superficielle influencée par la propagation des ondes de surface torsionnelles et reposant sur un sol hétérogène anisotrope a été présentée. La méthode d'équilibre limite en conjonction avec une approche pseudo-dynamique est utilisée. De plus, une analyse fiabiliste basée sur les simulations de Monte Carlo a été réalisée afin d'incorporer les incertitudes du système sol-séisme et d'étudier leurs effets. Il a été constaté que le facteur de capacité portante sismique proposé peut être applicable afin de quantifier la propagation des ondes de torsion, l'anisotropie et le non-homogénéité des propriétés du sol.

Mots-clés : Incertitudes ; capacité portante ; fondations superficielles ; onde de torsion ; champ aléatoire ; Fiabiliste ; Monte Carlo ; probabilité.

TABLE OF CONTENTS

Dedications.....	I
Gratitudes.....	II
ملخص	III
Abstract	IV
Résumé	V
Table of Contents.....	VI
List of Figures.....	XI
List of Tables.....	XXI
List of Symbols.....	XXIII

General Introduction

1. Problematic and objectives.....	2
3. Thesis organization.....	3

Chapter 1: Bibliographic Research

1.1. Introduction	6
1.2. Overview of geotechnical seismic engineering on the history of earthquakes.....	6
1.2.1 El-Asnam Earthquake (1980).....	6
1.2.2 Mexico City Earthquake (1985).....	7
1.2.3. Loma Prieta Earthquake (1989).....	8
1.2.4. Kobe Earthquake (1995).....	8
1.2.5. Boumerdès Earthquake (2003).....	8
1.2.6. Haiti Earthquake (2010).....	9
1.2.7. Christchurch Earthquake (2010-2011).....	10
1.2.8. Nepal Earthquake (2015).....	11
1.3. Failure mechanism of shallow foundations under static load.....	12
1.4. Failure mechanism of shallow foundations under seismic load.....	15
1.5. Approaches for determination of bearing capacity	16
1.5.1. Limit equilibrium method	16

1.5.2. Limit analysis method.....	17
1.5.2.1. Lower-bound theorem.....	17
1.5.2.2. Upper-bound theorem	18
1.5.3. Slip line method	18
1.5.4. Characteristic method.....	19
1.6. Traditional Bearing Capacity Assessment: An In-depth Overview	19
1.6.1. Terzaghi’s theory	19
1.6.2. Meyerhof’s theory	20
1.6.3. Hansen’s theory	21
1.6.4. Vesic’s theory	23
1.6.5. Standard European code (Eurocode 7).....	24
1.6.6. Standard Algerian code DTR-BC 2.331.....	25
1.7. Assessment of Bearing Capacity under Seismic Conditions.....	25
1.7.1. Sarma’s theory.....	26
1.7.2. Richard’s theory.....	28
1.7.3. Budhu’s theory.....	31
1.7.4. Choudhury’s theory.....	33
1.8. Conclusion.....	34

Chapter 2: Synthesis of Previous Works

2.1. Introduction.....	37
2.2. Previous studies on the bearing capacity under earthquake loading	37
2.3. Uncertainty in Soil Properties: Implications for Geotechnical Engineering	48
2.4. Inherent (Spatial) variability of soil properties	49
2.5. Random field theory	50
2.6. Geostatistics	52
2.7. Discretization of random field theory	53
2.7.1. Karhunen-Loéve (K-L) Expansion approach.....	53
2.7.2. Covariance Matrix Decomposition approach.....	54
2.7.3. Local Average Subdivision approach.....	55

2.8. Ranges of variability in some geotechnical soil properties	55
2.8.1. Coefficient of variations (COVs).....	55
2.8.2. Correlation coefficients.....	56
2.8.3. Scale of fluctuations.....	57
2.9. Previous works on reliability analysis.....	58
2.9.1. Essential principles of reliability.....	58
2.9.2. Reliability analysis methods.....	60
2.9.2.1. First order reliability method.....	60
2.9.2.2. Monte Carlo Simulation method.....	61
2.9.2.3. Importance Sampling method.....	62
2.9.2.4. Additional methods.....	63
2.9.3. Quantification of geotechnical uncertainties	63
2.10. Conclusion.....	66

Chapter 3: Reliability-based analysis of seismic bearing capacity

3.1. Introduction.....	68
3.2. Numerical procedure.....	68
3.3. Validation examples.....	69
3.3.1. Random field realizations.....	69
3.3.2. Validation of the statistical moments associated with the static bearing capacity..	71
3.3.3. Validation of the failure probability associated with the static bearing capacity...	73
3.4. Results and discussions.....	77
3.4.1. Impact of Autocorrelation functions (ACFs) on the seismic bearing capacity.....	77
3.4.2. Impact of the COVs of the seismic coefficients and the strength parameters on seismic bearing capacity.....	79
3.4.3. Impact of scale of fluctuations (SOFs) on the seismic bearing capacity.....	82
3.5. Conclusion.....	85

Chapter 4: Seismic Bearing Capacity of Shallow Foundations in Anisotropic Non-Homogeneous media

4.1. Introduction.....	88
4.2. Torsional wave motions	88
4.3. Anisotropy and non-homogeneity of soils.....	93
4.4. Analysis method	95
4.4.1. Model definition and assumptions	95
4.4.2. Pseudo dynamic analysis.....	98
4.4.2.1. Seismic inertia forces.....	98
4.4.2.2. Determination of the active pressure (P_A) and passive resistance (P_P).....	99
4.4.2.3. Pseudo dynamic bearing capacity factor	101
4.5. Conclusion.....	103

Chapter 5: Deterministic and reliability analyses of seismic Bearing Capacity due to torsional waves

5.1. Introduction.....	105
5.2. Optimization of the dynamic bearing capacity factor.....	105
5.3. Validation of the model.....	106
5.4. Parametric study.....	111
5.4.1. Impact of the internal soil friction angle ϕ	112
5.4.2. Impact of the interface wall friction angle δ	112
5.4.3. Impact of the embedment depth ratio D_f/B	113
5.4.4. Impact of the dimensionless cohesion $2c_v / \gamma_0 B$	114
5.4.5. Impact of the wavelength and the seismic acceleration of the torsional wave.....	115
5.4.6. Impact of soil anisotropy.....	116
5.4.7. Impact of soil non-homogeneity.....	119
5.5. Reliability analysis.....	121
5.5.1. Validation.....	122

5.5.2. Determination of the required number of realizations.....	123
5.5.3. Effects of the COV_{φ} and COV_{k_h} on the statistical moments of $N_{\gamma E}$ and on the failure probability.....	123
5.5.4. Effects of soil anisotropy on the statistical moments of $N_{\gamma E}$ and on the failure probability.....	126
5.5.5. Effect of soil non-homogeneity on the statistical moments of $N_{\gamma E}$ and on the failure probability.....	132
5.5.6. Effect of wavelength on the failure probability.....	136
5.5.7. Effect of FOS on P_f	137
5.6. Conclusion.....	138

General Conclusions and Recommendations for Future Work

1. General conclusions.....	141
2. Recommendations for future work.....	142
Bibliographic references.....	144
Appendix.....	156

LIST OF FIGURES

N°	Title of Figure	Page
Fig. 1.1	Extent of Building Damage Caused by the El Asnam Earthquake Ait-Meziane et al. (2018).	7
Fig. 1.2	Settlement of building and foundation failure during Mexico earthquake 1985, Britannica Editors of Encyclopaedia (2023).	7
Fig. 1.3	Buildings collapse during Loma Prieta earthquake 1989, Sturzenegger (2015).	9
Fig. 1.4	Building settlement during Kobe Earthquake 1995, Britannica Editors of Encyclopaedia (2008).	10
Fig. 1.5	Damage in the affected areas in Boumerdes-Algiers region Ait-Meziane et al. (2018).	10
Fig. 1.6	Damaged buildings in Port-au-Prince, Haiti after earthquake magnitude 7, Center for Disaster Philanthropy (2022).	11
Fig. 1.7	Building collapse and soil liquefaction during Christchurch Earthquake 2010-2011, Wikipedia (2024).	11
Fig. 1.8	Building collapse, land sliding, settlement, soil liquefaction during Nepal earthquake 2015, Taylor (2016)	12
Fig. 1.9	General failure mechanism - strip footing model during the centrifugal test (Bond and Harris, 2008).	13
Fig. 1.10	General failure mechanism with: (a) soil failure at surface; (b) load-settlement curve.	13
Fig. 1.11	Local shear failure with: (a) soil failure at surface; (b) load-settlement curve.	14

Fig. 1.12	Punching shear failure with: (a) soil failure at surface; (b) load-settlement curve.	14
Fig. 1.13	Prandtl failure mechanism modified by Richard et al. (1993).	16
Fig. 1.14	Mec2 failure mechanism assumed by Paolucci and Pecker (1997).	16
Fig. 1.15	Failure mechanism used in Sarma and Iossifelis (1990) analysis.	27
Fig. 1.16	Interslice thrusts given by Sarma and Iossifelis (1990).	27
Fig. 1.17	Seismic bearing capacity factors obtained by Sarma and Iossifelis (1990).	28
Fig. 1.18	Seismic Coulomb failure mechanism.	31
Fig. 1.19	Normalized seismic bearing capacity factors for various friction angles.	32
Fig. 1.20	Seismic bearing capacity factors of Choudhury and Subba Rao (2005).	34
Fig. 2.1	Normalized seismic bearing capacity factors to static factors obtained by Richard et al. (1993).	38
Fig. 2.2	Effect of horizontal seismic acceleration coefficient and slope inclination angle on the bearing capacity factors Yamamoto (2010).	41
Fig. 2.3	Effect of the horizontal and vertical acceleration coefficient as well as amplification factor on the seismic bearing capacity Zhou et al. (2015).	42
Fig. 2.4	Effect of the horizontal seismic acceleration coefficient and load inclination on the bearing capacity Conti (2018) with: (a) cohesive-frictional soil; (b) purely cohesive soil.	43

Fig. 2.5	Effect of the horizontal and vertical acceleration coefficient on the bearing capacity factors Chen et. al (2007).	44
Fig. 2.6	Effect of seismic acceleration coefficient on the equivalent seismic bearing capacity factor Debnath and Ghosh (2018).	45
Fig. 2.7	Effect of seismic acceleration on the equivalent bearing capacity factor Nadgouda and Choudhury (2019).	45
Fig. 2.8	Effect of earthquake force on the bearing capacity factors Kumar and Mohan Rao (2002).	46
Fig. 2.9	Effect of the horizontal acceleration coefficient on the bearing capacity factors for both smooth and rough base foundations Cascone and Casablanca (2016).	47
Fig. 2.10	Effect of Love wave frequency and seismic acceleration coefficient on the equivalent seismic bearing capacity factor Izadi et al. (2022).	48
Fig. 2.11	Statistical representation of soil variability (Phoon and Kulhawy, 1999a).	50
Fig. 2.12	Variation of semivariogram with separation distance.	53
Fig. 2.13	Transformation of random variables into standard normal random variables.	61
Fig. 2.14	Influence of COV _{cu} and correlation length on the mean bearing capacity (Griffiths et al., 2002).	64
Fig. 2.15	Influence of rock parameters uncertainties on the PDF of bearing capacity (Al-Bittar & Soubra, 2016).	65
Fig. 3.1	The mesh employed for discretizing the random fields.	69
Fig. 3.2	Simulation of Gaussian random field with $\delta h=20\text{m}$ and $\delta y=2\text{m}$ for: (a) soil cohesion with $\mu c = 30 \text{ kPa}$ and $\sigma c = 9 \text{ kPa}$, (b) soil	70

friction angle with $\mu\phi = 30$ kPa and $\sigma\phi = 9$.

- Fig. 3.3** Comparison between the normalized bearing capacity obtained in the present study and that reported by Griffiths et al. (2002) for a case of $\mu_{cu} = 100$ kPa, $\delta_x = \delta_y = 2$ m and $k_h = 0$. 71
- Fig. 3.4** Comparison between the coefficient of variation (COV) of the bearing capacity factor (N_c) obtained in the present study and that reported by Luo and Bathurst (2017) for a case of $\mu_{cu} = 20$ kPa, $\gamma = 20$ kN/m³ and $k_h = 0$. 72
- Fig. 3.5** Validation of the statistical characteristics of the static bearing capacity obtained in the present study compared to those reported by Cho and Park (2010) for a case of $r(c,\phi) = -0.5$, $COV_c = 30\%$, $COV_\phi = 20\%$, $\delta_v = 1$ m and $k_h = 0$. 74
- Fig. 3.6** Validation of the statistical characteristics of the static bearing capacity obtained in the present study compared to those reported by Cho and Park (2010) for a case of $r(c,\phi) = -0.5$, $COV_c = 30\%$, $COV_\phi = 20\%$, $\delta_h = 10$ m and $k_h = 0$. 75
- Fig. 3.7** Validation of the failure probability associated with the bearing capacity obtained in the present study compared to that reported by Massih et al. (2008) and Krishnan and Chakraborty (2021) for: $r(c, \phi) = -0.5$, $\mu_\phi = 30^\circ$, $\mu_c = 20$ kPa, $COV_\phi = 10\%$, $COV_c = 20\%$ and $k_h = 0$. 76
- Fig. 3.8** Impact of different types of autocorrelation functions (ACFs), with $\delta_h = 20$ m and $\delta_v = 2$ m, on the seismic bearing capacity of a shallow strip footing resting on: (a) cohesive frictional soil, (b) purely cohesive soil. 78
- Fig. 3.9** The Probability Density Function (PDF) of the seismic bearing capacity of strip footing resting on cohesive frictional soil for $\delta_h = 20$ m and $\delta_v = 2$ m for various COVs of: (a) seismic 81

coefficient, (b) cohesion, (c) frictional angle.

Fig. 3.10	The Probability Density Function PDF of seismic bearing capacity of strip footing resting on purely cohesive soil for $\delta h = 20\text{m}$ and $\delta v = 2\text{m}$ for various COVs of: (a) seismic coefficient, (b) undrained shear strength.	82
Fig. 3.11	Probability density function and failure probability of the seismic bearing capacity of a strip footing on cohesive frictional soil for various values of: (a) and (b) horizontal SOF and $\delta v = 2\text{m}$, (c) and (d) vertical SOF and $\delta h = 20\text{m}$.	84
Fig. 3.12	Probability density function and failure probability of the undrained seismic bearing capacity of a strip footing on a purely cohesive soil for various values of: (a) and (b) horizontal SOF and $\delta v = 2\text{m}$, (c) and (d) vertical SOF and $\delta h = 20\text{m}$.	85
Fig. 4.1	A non-homogeneous anisotropic layer over a heterogeneous half-space.	91
Fig. 4.2	Roots of the dispersion equation.	92
Fig. 4.3	Anisotropy of soil cohesion.	94
Fig. 4.4	Non-homogeneity of soil cohesion.	94
Fig. 4.5	Seismic Coulomb failure mechanism.	96
Fig. 4.6	Body forces: (a) active wedge, (b) passive wedge.	97
Fig. 5.1	Algorithm for optimizing the dynamic bearing capacity factor.	106
Fig. 5.2	Validation of the present static bearing capacity factor with published results: (a) $\varphi = 30^\circ$ and $\delta = \varphi / 2$, (b) $\delta = \varphi / 2$ and $2c_v/\gamma_0 B = 0.25$.	108
Fig. 5.3	Validation of the present N_γ static bearing capacity factor with published results for isotropic homogeneous condition of soil unit weight for: $D_f/B = 0$, $\beta_r^{-1} = 1$ and $v_p = 0$.	109

Fig. 5.4	Validation of the present N_c bearing capacity factor with published results for different anisotropic degree values of soil cohesion.	110
Fig. 5.5	Validation of the present N_c bearing capacity factor with published results for different non-homogeneity degree values of soil cohesion.	111
Fig. 5.6	Validation of the present N_γ static bearing capacity factor with published results for different anisotropic degree values of soil friction angle for: $2c_v/\gamma_0B = 0.0$, $D_f/B = 0$, $\delta = \phi$, $\beta_r^{-1} = 1$ and $\nu_p = 0$.	111
Fig. 5.7	Variation of the pseudo dynamic bearing capacity factor versus the acceleration coefficient for different values of the soil friction angle for $D_f/B = 0.5$, $2c_v/\gamma_0B = 0.25$, $\delta = \phi/2$, $\beta_r^{-1} = 0.7$, $\beta_\phi = 1.5$, $\beta_c^{-1} = 0.5$, $\nu_p = 0.1$ and $\nu_c = 15$.	112
Fig. 5.8	Variation of the pseudo dynamic bearing capacity factor versus the acceleration coefficient for different values of the wall friction angle for $\varphi = 30^\circ$, $D_f/B = 0.5$, $2c_v/\gamma_0B = 0.25$, $\beta_r^{-1} = 0.7$, $\beta_\phi = 1.5$, $\beta_c^{-1} = 0.5$, $\nu_p = 0.1$ and $\nu_c = 15$.	113
Fig. 5.9	Variation of the pseudo dynamic bearing capacity factor versus the acceleration coefficient for different values of the embedment ratio for: $\varphi = 30^\circ$, $2c_v/\gamma_0B = 0.25$, $\delta = \varphi/2$, $\beta_r^{-1} = 0.7$, $\beta_\phi = 1.5$, $\beta_c^{-1} = 0.5$, $\nu_p = 0.1$ and $\nu_c = 15$.	114
Fig. 5.10	Variation of the pseudo dynamic bearing capacity factor versus the acceleration coefficient for different dimensionless values of the cohesion ratio for: $\varphi = 30^\circ$, $D_f/B = 0.5$, $\delta = \varphi/2$, $\beta_r^{-1} = 0.7$, $\beta_\phi = 1.5$, $\beta_c^{-1} = 0.5$, $\nu_p = 0.1$ and $\nu_c = 15$.	114
Fig. 5.11	Variation of the pseudo dynamic bearing capacity factor versus the torsional wave frequency for different values of the seismic	115

acceleration coefficient for: $\varphi = 30^\circ$, $D_f/B = 0.5$, $2c_v/\gamma_0B=0.25$, $\delta = \varphi/2$, $\beta_r^{-1} = 0.7$, $\beta_\phi = 1.5$, $\beta_c^{-1} = 0.5$, $v_p = 0.1$ and $v_c = 15$.

- Fig. 5.12** Variation of the pseudo dynamic bearing capacity factor versus the acceleration coefficient for different values of anisotropy degree of rigidity for: $\varphi = 30^\circ$, $D_f/B = 0.5$, $2c_v/\gamma_0B=0.25$, $\delta = \varphi/2$, $\beta_\phi = 1.5$, $\beta_c^{-1} = 0.5$, $v_p = 0.1$ and $v_c = 15$. 117
- Fig. 5.13** Variation of the pseudo dynamic bearing capacity factor versus the acceleration coefficient for different values of anisotropy degree of internal friction angle for: $\varphi = 30^\circ$, $D_f/B = 0.5$, $2c_v/\gamma_0B=0.25$, $\delta = \varphi/2$, $\beta_r^{-1} = 0.7$, $\beta_c^{-1} = 0.5$, $v_p = 0.1$ and $v_c = 15$. 118
- Fig. 5.14** Variation of the pseudo dynamic bearing capacity factor versus the acceleration coefficient for different values of the inverse anisotropy degree of cohesion for: $\varphi = 30^\circ$, $D_f/B = 0.5$, $2c_v/\gamma_0B = 0.25$, $\delta = \varphi/2$, $\beta_r^{-1} = 0.7$, $\beta_\phi = 1.5$, $v_p = 0.1$ and $v_c = 15$. 118
- Fig. 5.15** Variation of the pseudo dynamic bearing capacity factor versus the acceleration coefficient for different values of non-homogeneity parameter for: $\varphi = 30^\circ$, $D_f/B=0.5$, $2c_v/\gamma_0B = 0.25$, $\delta = \varphi/2$, $\beta_\phi = 1.5$, $\beta_c^{-1} = 0.5$ and $v_c = 15$. 120
- Fig. 5.16** Variation of the pseudo dynamic bearing capacity factor versus the acceleration coefficient for different values of non-homogeneity coefficient of cohesion for: $\varphi = 30^\circ$, $D_f/B=0.5$, $2c_v/\gamma_0B = 0.25$, $\delta = \varphi/2$, $\beta_\phi = 1.5$, $\beta_c^{-1} = 0.5$, $\beta_r^{-1} = 0.7$, $v_p = 0.1$. 121
- Fig. 5.17** Comparison of probability of failure with published results for $\varphi = 30^\circ$, $c = 20$ kPa, $COV_\varphi = 10\%$, $COV_c = 20\%$, and $k_h = 0$. 122
- Fig. 5.18** Convergence of the failure probability with respect to the number of simulations for $\varphi=30^\circ$, $k_h = 0.2$, $COV_\varphi = 10\%$, $COV_{k_h} = 15\%$, $\beta_r^{-1} = 0.7$, $\beta_\phi = 1.5$, $\beta_c^{-1} = 0.5$, $v_p = 0.1$ and $v_c =$ 123

15.

- Fig. 5.19** Variation of statistical moments of pseudo dynamic bearing capacity factor versus the torsional wave frequency for different *COV*: (a) and (b) $\varphi = 30^\circ$, $\beta_r^{-1} = 0.7$, $\beta_\phi = 1.5$, $\beta_c^{-1} = 0.5$, $\nu_p = 0.1$, $\nu_c = 15$. (c) and (d) $\varphi = 30^\circ$, $k_h = 0.2$, $\beta_r^{-1} = 0.7$, $\beta_\phi = 1.5$, $\beta_c^{-1} = 0.5$, $\nu_p = 0.1$, $\nu_c = 15$. 124
- Fig. 5.20** Variation of the failure probability of $N_{\gamma E}$ factor for $\mu_\varphi = 30^\circ$ and $\mu_{kh} = 0.2$ with respect to the torsional wave frequency. 126
- Fig. 5.21** Variation of the statistical moments of the pseudo dynamic bearing capacity factor versus the torsional wave frequency for different values of anisotropy degree of rigidity for: $\mu_\varphi = 30^\circ$, $\mu_{kh} = 0.2$, $COV_\varphi = 10\%$, $COV_{kh} = 5\%$, $\beta_\phi = 1.5$, $\beta_c^{-1} = 0.5$, $\nu_\gamma = 0.1$ and $\nu_c = 15$. 127
- Fig. 5.22** Variation of the failure probability of the pseudo dynamic bearing capacity factor versus the torsional wave frequency for different values of non-homogeneity degree for: $\mu_\varphi = 30^\circ$, $\mu_{kh} = 0.2$, $COV_\varphi = 10\%$, $COV_{kh} = 5\%$, $\beta_\phi = 1.5$, $\beta_c^{-1} = 0.5$, $\nu_\gamma = 0.1$ and $\nu_c = 15$. 128
- Fig. 5.23** Variation of the statistical moments of the pseudo dynamic bearing capacity factor versus the torsional wave frequency for different values of anisotropy degree of friction angle for: $\mu_\varphi = 30^\circ$, $\mu_{kh} = 0.2$, $COV_\varphi = 10\%$, $COV_{kh} = 5\%$, $\beta_r^{-1} = 0.7$, $\beta_c^{-1} = 0.5$, $\nu_p = 0.1$ and $\nu_c = 15$. 129
- Fig. 5.24** Variation of the failure probability of the pseudo dynamic bearing capacity factor versus the torsional wave frequency for different values of anisotropy degree of friction angle for: $\mu_\varphi = 30^\circ$, $\mu_{kh} = 0.2$, $COV_\varphi = 10\%$, $COV_{kh} = 5\%$, $\beta_r^{-1} = 0.7$, $\beta_c^{-1} = 0.5$, $\nu_p = 0.1$ and $\nu_c = 15$. 130

- Fig. 5.25** Variation of the statistical moments of the pseudo dynamic bearing capacity factor versus the torsional wave frequency for different values of anisotropy degree of cohesion for: $\mu_\phi = 30^\circ$, $\mu_{kh} = 0.2$, $COV_\phi = 10\%$, $COV_{kh} = 5\%$, $\beta_r^{-1} = 0.7$, $\beta_\phi = 1.5$, $\nu_p = 0.1$ and $\nu_c = 15$. 131
- Fig. 5.26** Variation of the failure probability of the pseudo dynamic bearing capacity factor versus the torsional wave frequency for different values of anisotropy degree of cohesion for: $\mu_\phi = 30^\circ$, $\mu_{kh} = 0.2$, $COV_\phi = 10\%$, $COV_{kh} = 5\%$, $\beta_r^{-1} = 0.7$, $\beta_\phi = 1.5$, $\nu_p = 0.1$ and $\nu_c = 15$. 132
- Fig. 5.27** Variation of the statistical moments of the pseudo dynamic bearing capacity factor versus the torsional wave frequency for different values of non-homogeneity parameter for: $\mu_\phi = 30^\circ$, $\mu_{kh} = 0.2$, $COV_\phi = 10\%$, $COV_{kh} = 5\%$, $\beta_\phi = 1.5$, $\beta_c^{-1} = 0.5$, $\beta_r^{-1} = 0.7$ and $\nu_c = 15$. 133
- Fig. 5.28** Variation of the failure probability of the pseudo dynamic bearing capacity factor versus the torsional wave frequency for different values of non-homogeneity coefficient for: $\mu_\phi = 30^\circ$, $\mu_{kh} = 0.2$, $COV_\phi = 10\%$, $COV_{kh} = 5\%$, $\beta_\phi = 1.5$, $\beta_c^{-1} = 0.5$, $\beta_r^{-1} = 0.7$ and $\nu_c = 15$. 134
- Fig. 5.29** Variation of the statistical moments of the pseudo dynamic bearing capacity factor versus the torsional wave frequency for different values of non-homogeneity coefficient of cohesion for: $\mu_\phi = 30^\circ$, $\mu_{kh} = 0.2$, $COV_\phi = 10\%$, $COV_{kh} = 5\%$, $\beta_r^{-1} = 0.7$, $\beta_\phi = 1.5$, $\beta_c^{-1} = 2$ and $\nu_p = 0.1$. 135
- Fig. 5.30** Variation of the failure probability of the pseudo dynamic bearing capacity factor versus the torsional wave frequency for different values of non-homogeneity coefficient of cohesion for: $\mu_\phi = 30^\circ$, $\mu_{kh} = 0.2$, $COV_\phi = 10\%$, $COV_{kh} = 5\%$, $\beta_r^{-1} = 0.7$, 136

$$\beta_\phi = 1.5, \beta_c^{-1} = 2 \text{ and } \nu_p = 0.1.$$

- Fig. 5.31** Variation of the failure probability of $N_{\gamma E}$ factor for different torsional wave frequencies for $\mu_\phi = 30^\circ$, $\mu_{kh} = 0.2$, $COV_\phi = 10\%$, $COV_{kh} = 5\%$, $\beta_\phi = 1.5$, $\beta_c^{-1} = 0.5$, $\beta_r^{-1} = 0.7$, $\nu_p = 0.1$ and $\nu_c = 15$. 137
- Fig. 5.32** Variation of the failure probability of $N_{\gamma E}$ factor with respect to the FOS for different values of the COV_ϕ for $\mu_\phi = 30^\circ$, $K_{TH} = 0.25$, $\beta_\phi = 3$, $\beta_c^{-1} = 0.4$, $\beta_r^{-1} = 0.5$, $\nu_p = 0.5$ and $\nu_c = 30$. 138

LIST OF TABLES

N°	Title of Table	Page
Table 1.1	Seismic bearing capacity factors and ratios to static values (Richard et al. 1993).	30
Table 2.1	Effect of the seismic acceleration coefficient on the bearing capacity factor $N_{\gamma E}$ Soubra (1997).	38
Table 2.2	Effect of the seismic acceleration coefficient on the bearing capacity factor N_{cE} of Soubra (1997).	39
Table 2.3	Effect of the seismic acceleration coefficient on the bearing capacity factor N_{qE} of Soubra (1997).	40
Table 2.4	Various forms of autocorrelation functions (ACFs).	51
Table 2.5	Coefficient of variation of soil parameter.	56
Table 2.6	Correlation coefficients of (c, ϕ).	56
Table 2.7	Scale of fluctuation for different soil properties.	57
Table 3.1	Comparison between the exact and estimated values of soil properties obtained using the KL method and LAS method.	70
Table 3.2	Statistical parameters for the cohesive frictional soil.	77
Table 3.3	Statistical parameters for the purely cohesive soil.	77
Table 3.4	Impact of the type of the autocorrelation functions (ACFs) on the statistical moments of the seismic bearing capacity of a shallow strip footing for $\delta_h = 20m$ and $\delta_v = 2m$.	79
Table 3.5	Impact of the coefficients of variation (COVs) of the seismic coefficient (k_h), cohesion (c), and friction angle (ϕ) on the statistical characteristics of the seismic bearing capacity of a shallow strip footing resting on cohesive frictional soil for $\delta_h = 20m$ and $\delta_v = 2m$.	80
Table 3.6	Impact of the coefficients of variation (COVs) of the seismic coefficient (k_h) and undrained shear strength (c_u) on the statistical characteristics of the seismic bearing capacity of a shallow strip footing resting on purely cohesive soil for $\delta_h = 20m$ and $\delta_v = 2m$.	80

Table 3.7	Impact of the horizontal SOF on the statistical moments of the seismic bearing capacity of a shallow strip footing for $\delta_v=6m$.	83
Table 3.8	Impact of the vertical SOF on the statistical moments of the seismic bearing capacity of a shallow strip footing for $\delta_h=60m$.	84
Table 5.1	Summary of the parameters used in the reliability analysis.	122
Table A.1	Seismic bearing capacity formulas for cohesive-frictional and purely cohesive soils (Conti 2018)	157
Table A.2	Static bearing capacity factor $N_{\gamma s}$.	158
Table A.3	Equivalent pseudo dynamic bearing capacity factor $N_{\gamma E}$ for different anisotropy degree of rigidity and non-homogeneity parameter when $k_h=0.2$	159
Table A.4	Equivalent pseudo dynamic bearing capacity factor $N_{\gamma E}$ for different anisotropy degree of internal friction angle for $k_h=0.2$.	160
Table A.5	Equivalent pseudo dynamic bearing capacity factor $N_{\gamma E}$ for different anisotropy degree and non-homogeneity coefficient of cohesion for $k_h = 0.2$.	161

LIST OF SYMBOLS

λ	Wavelength
$K_T H$	Torsional wave frequency
$N_{\gamma E}$	Equivalent seismic bearing capacity factor
β_ϕ	Friction angle anisotropy
β_c^{-1}	Inverse of the cohesion anisotropy
β_r^{-1}	Inverse of the rigidity anisotropy
μ	Mean
μ_c	Cohesion mean value
μ_{qu}	Seismic bearing capacity mean value
μ_ϕ	Mean friction angle
ACF	Auto correlation function
B	breadth of footing
BN	Binary noise
c	Cohesion
CE	Cosine exponential
COV	Coefficient of variation
COV_c	Coefficient of variation of the cohesion
COV_{cu}	Coefficient of variation of the undrained shear strength
COV_{kh}	Coefficient of variation of the horizontal seismic acceleration coefficient
COV_{Nc}	Coefficient variation of bearing capacity factor
COV_ϕ	Coefficient of variation of the friction angle
COV_{qu}	Coefficient of variation of the seismic bearing capacity
c_u	Undrained shear strength
D_f	Depth of footing
FOS	Factor of safety
$J_1(kr)$	Bessel's function
k_h	Horizontal seismic acceleration coefficient
KL	Karhunen-Loève expansion method
LAS	Local average subdivision method
N_c	Bearing capacity factor
N_{sim}	Number of simulations

P_A	Active pressure
PDF	Probability density function
P_f	Probability of failure
P_L	Ultimate bearing capacity
P_p	Passive resistance
$RFEM$	Random finite element method
SNE	Single exponential
SOF	Scale of fluctuation
SOM	Second-order Markov
SQE	Squared exponential
t	Time
$V(z)$	Amplitude
v_s	Shear wave velocity
v_{sI}	Shear wave velocity bed Rock
v_T	Torsional wave velocity
β	Inclination angle in passive wedge
δ_h	Horizontal scale of fluctuation
δ_v	Vertical scale of fluctuation
v_c	Non-homogeneity of cohesion
v_P	Non-homogeneity parameter
σ	Standard deviation
σ_c	Standard deviation value of cohesion
σ_{qu}	Standard deviation value of seismic bearing capacity
σ_ϕ	Standard deviation value of friction angle
τ_x	Absolute horizontal distance between two points within the soil unit
τ_y	Absolute vertical distance between two points within the soil unit
α	Inclination angle in active wedge
γ	Unit weigh
δ	Wall friction angle
ω	Pulsation

GENERAL INTRODUCTION

1. Problematic and objectives

The shallow foundation is the part of a structure that ensures the safe transfer of the structure's loads to the ground. Typically hidden underground, shallow foundation systems may be subjected to dynamic loading. This dynamic loading can manifest in different forms, including (a) monotonic loading with varying velocities, (b) earthquake loading, (c) cyclic loading, and (d) transient loading. Consequently, it leads to a decrease in the bearing capacity of shallow foundations and amplifies the risk of settlement. Earthquake loading poses a terrible and frequently occurring dynamic force capable of causing significant damage to shallow foundations. For this reason, the effect of the seismic loading on the bearing capacity of shallow foundations is the topic of this thesis.

Because earthquake engineering focuses on the impact of earthquakes on humans and their surroundings, particularly those situated on or close to the Earth's surface, surface waves hold significant importance. They attenuate more slowly with distance compared to body waves, further emphasizing their relevance in seismic analysis and design. In earthquake engineering, two primary types of surface waves hold significant importance. The Rayleigh wave is evident in a homogeneous elastic half-space while the Love wave necessitates a surface layer with lower S-wave velocity compared to the underlying half-space. Although other surface wave types exist, their relevance in earthquake engineering is comparatively minor. The study of those both surface waves is more focused in homogeneous condition than in heterogeneous one in the literature studies.

Recently, the impact of Rayleigh wave and Love wave on the bearing capacity of shallow foundations have been investigated by [Saha and Ghosh \(2017\)](#) and [Izadi et al. \(2022\)](#), respectively.

Because of the Earth's inhomogeneous nature, there is a significant need for intensive study of wave propagation in inhomogeneous media. Torsional waves, which are a type of surface waves, exclusively propagate in non-homogeneous media ([Meissner, 1921](#); [Rayleigh, 1945](#)). In light of this point, this surface wave should be taken into consideration during the estimation of the bearing capacity of shallow foundations in inhomogeneous (heterogeneous) media. For this purpose, the impact of the surface torsional wave is investigated in chapters 4 and 5.

On the other hand, the seismic bearing capacity analysis is usually conducted for homogeneous soils under the assumption of a set of deterministic soil and earthquake properties. Nevertheless, it is well known that the soil properties such as shear strength parameters involve

a significant level of uncertainty, despite being in a single soil layer (Johari et al., 2017). Hence, a reliability analysis is an adequate way to consider the uncertainties incorporated in the properties and to provide a rational framework for adopting the appropriate bearing capacity that provides power tools to succor geotechnical designers in checking how reliable their designs are?

In light of what has been argued, the present work primarily focuses on investigating the impact of randomly varying soil and earthquake parameters on the seismic bearing capacity of shallow foundations. This is accomplished by applying random field theory to existing bearing capacity formulas. After that, a seismic bearing capacity model of a strip footing, which considers the influence of soil non-homogeneity and torsional surface wave propagation is proposed. Furthermore, a reliability-based analysis is carried out to incorporate uncertainties in soil and earthquake parameters and to examine their impact.

2. Thesis organization

Following the motivations and objectives of the thesis, the organization of the dissertation is presented below:

The first chapter consists in a bibliographic research focused on the methods employed in estimating the bearing capacity of shallow foundations under both static and seismic loading conditions. Additionally, various mathematical models proposed by different researchers for determining the bearing capacity in static and dynamic scenarios are presented.

The second chapter started first with a synthesis of previous works on the seismic bearing capacity of shallow foundations. After that, it presented (1) the different sources of soil properties uncertainty in geotechnical field, (2) the spatial variability of soil properties, (3) the methods of characterization of spatial variability and (4) the reliability analysis methods. At the end, a synthesis previous works on the quantification of geotechnical uncertainties in the seismic bearing capacity field is included.

In the third chapter, the Karhunen-Loève (KL) expansion method within the context of random field theory was utilized to explore the influence of soil and earthquake parameter randomness on the seismic bearing capacity. The seismic bearing capacity equations established by Conti (2018) were applied in the analysis for two soil types supporting shallow strip footings: purely cohesive soil and cohesive-frictional soil.

The fourth chapter exhibits a formulation of the seismic bearing capacity factor for strip footings, utilizing a combination of the limit equilibrium method and the pseudo-dynamic approach. This formulation incorporates soil heterogeneity parameters and the propagation of the torsional wave in determining the seismic factor.

Finally, the chapter five presents the validation and comparison of the seismic bearing capacity factor obtained with existing literature studies. Also, a parametric study reveals the effect of the heterogeneity, seismic torsional wave parameters and the other parameters governing this seismic factor. Later on, a reliability analysis based on the Monte Carlo simulations is also carried out with the aim to incorporate the uncertainties around the main soil and earthquake parameters that govern the seismic bearing capacity of shallow foundations (soil internal friction angle and seismic acceleration coefficient) and to study their effects.

The dissertation ends with overarching conclusions, along with recommendations and prospects for future research endeavors.

BIBLIOGRAPHIC RESEARCH

1.1. Introduction

During the earthquake loading, the shallow foundations may experience a reduction in bearing capacity and increment in the susceptibility to settlement. This reduction of bearing capacity of foundations increases the potential of building failure and consequently may leading to human casualties. The evaluation of seismic bearing capacity of foundations is a crucial step in the design phase.

1.2. Overview of geotechnical seismic engineering on the history of earthquakes

Earthquakes have emerged as one of the most devastating natural disasters throughout history, leading to significant loss of life and infrastructure damage, particularly in densely populated regions prone to seismic activity. In the past few years, numerous cities worldwide have suffered from the destructive consequences of earthquakes, leading to widespread damage and a range of associated challenges.

From a geotechnical engineering perspective, foundations represent a critical focal point in ensuring the safety of superstructures and mitigating potential losses of life and infrastructure during seismic events. Numerous instances worldwide underscore the profound impact of powerful earthquakes on cities, revealing their varied effects on diverse types of civil engineering structures.

1.2.1. El-Asnam Earthquake (1980)

The 1980 El Asnam Earthquake, one of the most destructive seismic events recorded in northern Africa and the Western Mediterranean Basin, struck the northern region of Algeria with a moment magnitude of 7.1. It devastated the city of El Asnam, which had an estimated population of 125,000, as well as nearby towns and villages. The earthquake resulted in a significant loss of life, with casualties reportedly ranging from 5,000 to 20,000, largely due to the collapse of buildings (Fig. 1.1). In many areas, particularly along the Chlef riverbanks, large amounts of sandy soil were ejected onto the ground surface. The earthquake also caused substantial damage to civil and hydraulic structures, including earth dams, embankments, bridges, slopes, and buildings.



Fig 1.1 Extent of Building Damage Caused by the El Asnam Earthquake [Ait-Meziane et al. \(2018\)](#).

1.2.2. Mexico City Earthquake (1985)

The magnitude 8.1 earthquake that struck Mexico City resulted in substantial damage to buildings and infrastructure. Numerous structures suffered foundation failures, culminating in collapses and loss of life. The city's soil conditions, characterized by the presence of soft clay and lake sediments, amplified the seismic waves, amplifying ground shaking and inflicting damage on foundational structures ([Fig. 1.2](#)).



Fig. 1.2 Settlement of building and foundation failure during Mexico earthquake 1985, [Britannica Editors of Encyclopaedia \(2023\)](#).

1.2.3. Loma Prieta Earthquake (1989)

The Loma Prieta earthquake, with a magnitude of 6.9, struck the San Francisco Bay Area in California. It caused significant damage to various types of foundation structures. Many buildings experienced foundation settlement, where the soil beneath the foundation shifted, leading to cracks in walls and floors. Some buildings suffered from differential settlement, causing uneven settling and structural damage. In extreme cases, the foundations failed completely, resulting in building collapse (Fig. 1.3).

1.2.4. Kobe Earthquake (1995)

The Kobe earthquake, also known as the Great Hanshin earthquake, struck the city of Kobe in Japan with a magnitude of 6.9. The earthquake resulted in extensive damage to buildings and infrastructures. Numerous buildings encountered both foundation settling and differential settlement, leading to structural instability and collapse. The soft and loose soil conditions in the region exacerbated the effects of the earthquake on foundation structures (Fig. 1.4).

1.2.5. Boumerdès Earthquake (2003)

The 2003 Boumerdès Earthquake, also known as the Zemmouri Earthquake, struck northern Algeria on May 21, 2003, with a magnitude of 6.8 on the Richter scale. The epicenter was near the town of Zemmouri, approximately 60 kilometers east of the capital, Algiers. This seismic event was a result of tectonic activity along the convergent boundary between the African and Eurasian Plates.

The earthquake's impact on buildings was catastrophic, causing widespread destruction across the region. Thousands of residential buildings collapsed or were severely damaged, leaving many people homeless and highlighting deficiencies in construction practices and building materials. Modern structures, despite being designed to withstand earthquakes, also suffered significant damage, including cracked walls, compromised foundations, and the failure of non-structural elements such as facades and interior partitions (Fig. 1.5).



Fig. 1.3 Buildings collapse during Loma Prieta earthquake 1989, [Sturzenegger \(2015\)](#).

1.2.6. Haiti Earthquake (2010)

The magnitude 7.0 earthquake that struck Haiti caused catastrophic damage and loss of life. Many buildings, particularly in the capital city of Port-au-Prince, suffered either complete or partial collapse. The lack of proper construction practices and poor-quality materials contributed to the vulnerability of the structures ([Fig. 1.6](#)). The shallow foundations of many buildings were unable to withstand the seismic forces, leading to widespread foundation failure.



Fig 1.4. Building settlement during Kobe Earthquake 1995, [Britannica Editors of Encyclopaedia \(2008\)](#).



Fig. 1.5 Damage in the affected areas in Boumerdes-Algiers region [Ait-Meziane et al. \(2018\)](#).

1.2.7. Christchurch Earthquake (2010-2011)

A series of earthquakes struck the city of Christchurch in New Zealand, with the most devastating one occurring in February 2011, with a magnitude of 6.3. The earthquakes inflicted substantial damage on buildings and infrastructure, resulting in foundation cracking, settlement, and lateral spreading in numerous structures. The extensive liquefaction of the soil led to widespread foundation failure and structural damage, resulting in the collapse of numerous buildings ([Fig. 1.7](#)).



Fig. 1.6 Damaged buildings in Port-au-Prince, Haiti after earthquake magnitude 7, [Center for Disaster Philanthropy \(2022\)](#).



Fig. 1.7 Building collapse and soil liquefaction during Christchurch Earthquake 2010-2011, [Wikipedia \(2024\)](#).

1.2.8. Nepal Earthquake (2015)

The earthquake with a magnitude of 7.8 that occurred in Nepal caused widespread devastation, particularly in the capital city of Kathmandu and surrounding areas. Many buildings, including historic structures, suffered from foundation failure and collapse. The combination of inadequate construction practices, heavy loadings, and the region's geology contributed to the vulnerability of the foundations. Soil liquefaction and landslides further exacerbated the damage ([Fig. 1.8](#)).



Fig. 1.8 Building collapse, land sliding, settlement, soil liquefaction during Nepal earthquake 2015, [Taylor \(2016\)](#).

1.3. Failure mechanism of shallow foundations under static load

The results of tests on rigid foundations show that there are three potential failure mechanisms involving a limited volume of soil. The first is a general mechanism characterized by the formation of a wedge beneath the foundation base, which displaces the soil laterally along slip lines that emerge at the surface ([Fig. 1.9](#)). The foundation settlement generally leads to an uplift of the soil, which is more pronounced when the structure is less deformable. This is the case for relatively strong soils ([Fig. 1.10](#)). The second is a mechanism of localized shearing, extending only in the immediate vicinity of the foundation. There is also uplift of the soil, but it occurs after significant settlement, particularly in very compressible soils like loose sands ([Fig. 1.11](#)). The third mechanism is a failure by punching, where the foundation penetrates vertically into the ground without disturbing the soil not directly beneath the foundation ([Fig. 1.12](#)).

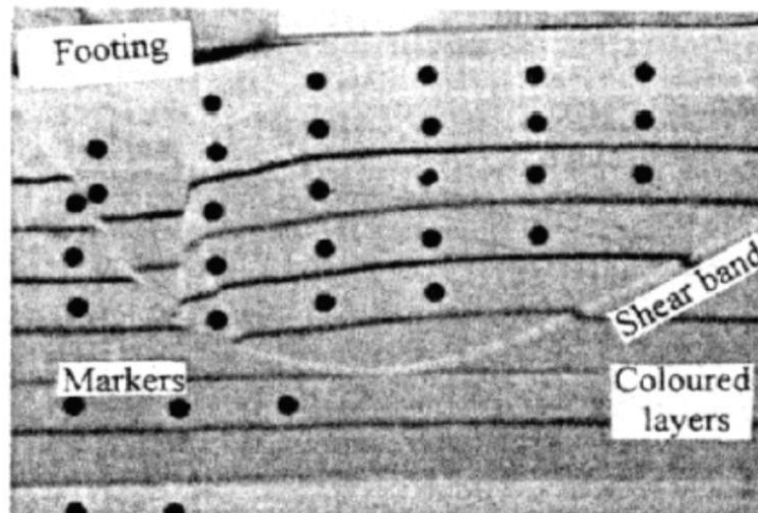


Fig. 1.9 General failure mechanism - strip footing model during the centrifugal test (Bond and Harris, 2008).

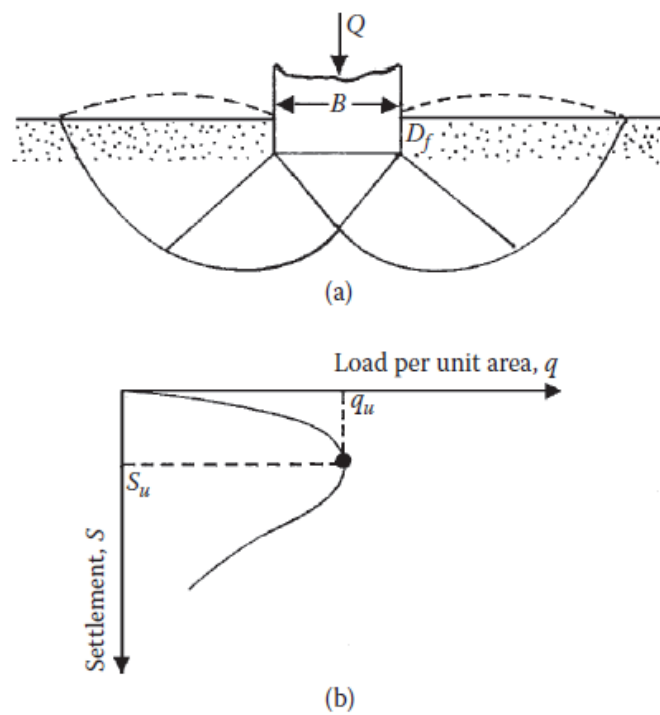


Fig. 1.10 General failure mechanism with: (a) soil failure at surface; (b) load-settlement curve.

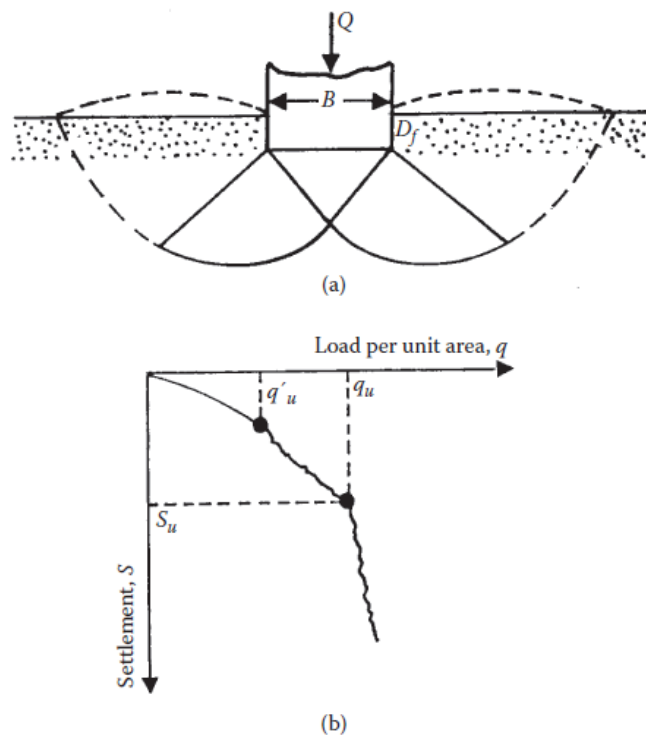


Fig. 1.11 Local shear failure with: (a) soil failure at surface; (b) load-settlement curve.

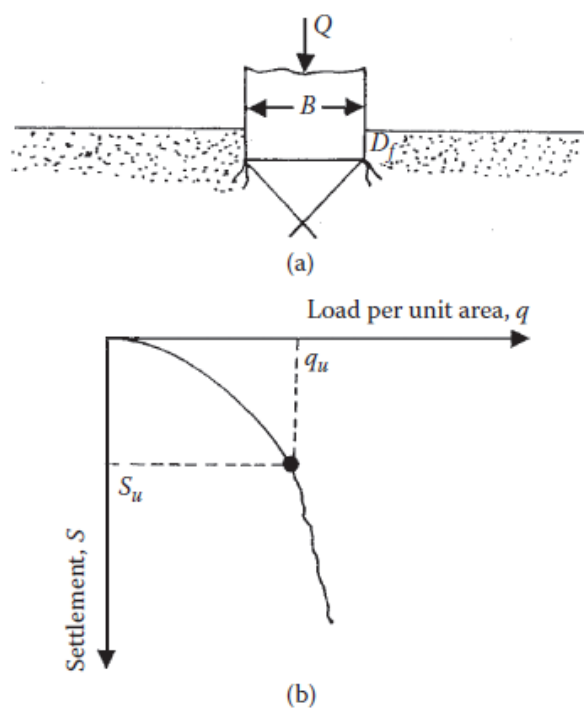


Fig. 1.12 Punching shear failure with: (a) soil failure at surface; (b) load-settlement curve.

1.4. Failure mechanism of shallow foundations under seismic load

Various analytical approaches in the existing literature have addressed the seismic bearing capacity problem. These methods include solutions based on limit equilibrium analysis (Richard et al. 1993 and Budhu and Al-Karni 1993), upper-bound kinematic analyses (Soubra 1999 and Paolucci and Pecker 1997), and lower-bound analyses using the method of stress characteristics (Kumar and Mohan Rao 2002). In all these approaches, earthquake loads and accelerations are considered as pseudo-static, with adjustments made for modifying soil inertia due to horizontal accelerations represented by $k_h.g$ and vertical accelerations represented by $k_v.g$, where 'g' denotes the acceleration due to Earth's gravity.

Both Richard et al. (1993) and Budhu and Al-Karni (1993) approached the problem by assuming the formation of an asymmetrical Prandtl failure surface, as illustrated in Fig. 1.13. For analytical purposes, this was simplified to a two-part Coulomb sliding wedge mechanism in Richard et al. (1993), while Budhu and Al-Karni (1993) analyzed the same mechanism without this simplification. In both cases, the superstructure forces included the vertical load resulting from the structure's weight and the horizontal load due to the structure's inertia during the earthquake. The foundation failure occurred through rotation about one corner, specifically the right-hand corner in Fig. 1.13. It is noteworthy that as the magnitude of horizontal acceleration increases, the size of the failure mechanism diminishes, consequently reducing the bearing capacity.

Considering that the majority of structures have their center of mass positioned well above the soil–foundation interface, and given that this interface is where horizontal inertial loads are applied, it becomes apparent that substantial moments are induced on the foundation due to these inertial forces. These moments result in the foundation rotating about a point that may not necessarily be at a corner, and the extent of rotation depends on the magnitude of the applied moment. Consequently, this rotation can lead to uplift along a portion of the foundation. An upper-bound kinematic analysis, which accounts for these moment effects, is presented in Paolucci and Pecker (1997). In this analysis, the failure mechanism, referred to as Mec 2, has been adjusted to incorporate uplift by introducing the parameter λ , as depicted in Fig. 1.14.

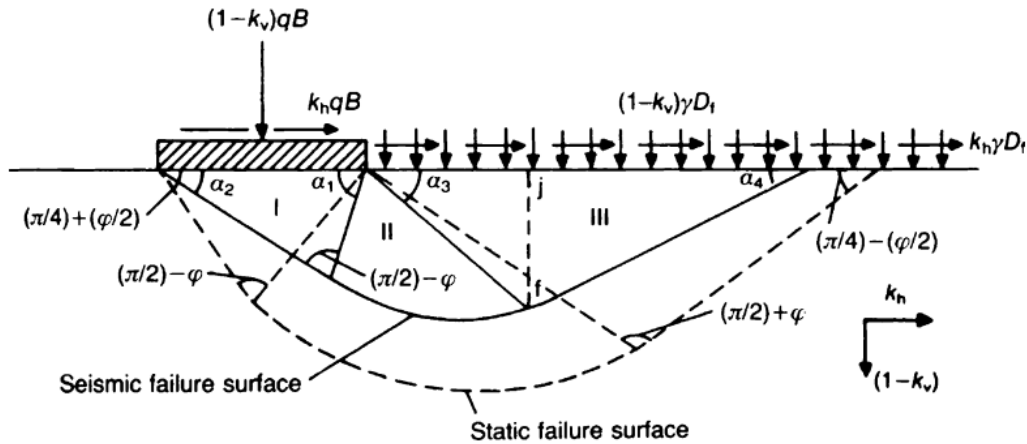


Fig. 1.13 Prandtl failure mechanism modified by Budhu and Al-Karni (1993).

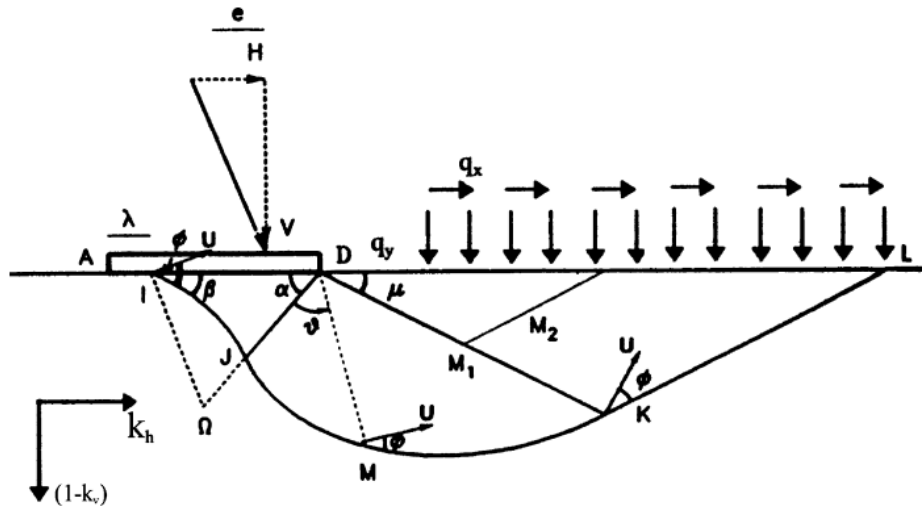


Fig. 1.14 Mec2 failure mechanism assumed by Paolucci and Pecker (1997).

1.5. Approaches for Determining Bearing Capacity

1.5.1. Limit equilibrium method

The limit equilibrium method is a commonly used engineering approach to analyze and design structures or geotechnical systems, especially in the context of soil mechanics and slope stability analysis. This method is employed to determine whether a given structure or slope will remain stable or if it is at risk of failure under specific conditions. The approach is based on the concept of equilibrium, which means that the forces and moments acting on a structure or soil mass must balance for it to remain stable.

The solutions of Terzaghi (1943) and Taylor (1948), which are widely used in building codes and soil mechanics courses, are obtained through the limit equilibrium method.

In Terzaghi's 1943 work, the concept of "superposition" concerning the bearing capacity of a cohesive and frictional medium with a given unit weight and a surface surcharge was introduced. In his well-known formula (Eq. 1.1), Terzaghi described the bearing capacity as the sum of three independent terms.

$$q_u = cN_c + qN_q + \frac{1}{2}\gamma BN_\gamma \quad (1.1)$$

In which c , q and γ denote respectively the cohesion, the surcharge load and soil unit weight, while N_c , N_q and N_γ are the bearing capacity factors.

1.5.2. Limit analysis method

The limit analysis method is an engineering approach used to assess the safety and stability of structures, particularly in geotechnical and structural engineering. This method focuses on determining the critical load or the maximum load-carrying capacity that a structure can withstand before failure occurs. The limit analysis method is widely used in the design of various engineering structures, such as foundations, retaining walls, and bridges.

The method is built upon the idealized stress-strain relationship of soil, which is termed normality or the flow rule, forming the basis for the limit theorems central to limit analysis. Under this theoretical framework, the approach is rigorous and, in certain scenarios, provides simpler techniques in comparison to the limit equilibrium method. For stability issues such as determining the critical heights of unsupported vertical cuts or assessing the bearing capacity of nonhomogeneous soils, the plastic limit theorems introduced by [Drucker et al. \(1952\)](#) can be conveniently applied to establish both upper and lower bounds for the collapse load.

The necessary conditions for establishing either an upper-bound or a lower-bound solution are fundamentally as follows:

1.5.2.1. Lower-bound theorem

The loads obtained solely from the distribution of stress, which adheres to (a) equilibrium equations, (b) stress boundary conditions, and (c) doesn't violate the yield criterion anywhere, do not exceed the actual collapse load. Such a stress distribution that fulfills these criteria is termed a statically admissible stress field for the specific problem. Therefore, the lower-bound theorem can be summarized as follows: If a statically admissible stress distribution is attainable, plastic flow will not occur at a load lower than this. Notably, the lower-bound

technique primarily takes into account equilibrium and yield and does not factor in soil kinematics.

1.5.2.2. Upper-bound theorem

The loads, determined by setting the external rate of work equal to the internal rate of dissipation within an assumed deformation mode (or velocity field) that adheres to (a) velocity boundary conditions and (b) strain and velocity compatibility conditions, do not fall below the actual collapse load. The energy dissipation during plastic flow related to this field can be calculated using the idealized stress/strain rate relation, often referred to as the flow rule. A velocity field that satisfies the aforementioned conditions is termed a kinematically admissible velocity field. Therefore, the upper-bound theorem asserts that if a kinematically admissible velocity field can be identified, uncontrolled plastic flow either threatens or has occurred in the past. The upper-bound technique primarily considers velocity or failure modes and energy dissipation, without requiring stress distribution to be in equilibrium, and it is defined solely within the deforming regions of the mode.

Through the appropriate selection of stress and velocity fields, these two theorems allow for the collapse load to be closely approximated as needed for the specific problem at hand.

1.5.3. Slip line method

Impending plastic deformation of the soil occurs when a sufficiently large portion of the soil beneath a footing reaches its yield or limiting condition, allowing unrestricted plastic flow beneath the footing. During this impending plastic flow, both equilibrium and yield conditions are met in the region near the footing. The widely-used Coulomb criterion is applied to soils to define this yield condition. By combining the Coulomb criterion with the equations of equilibrium, a set of differential equations for plastic equilibrium in this region is established. When coupled with stress boundary conditions, these differential equations can be used to examine the stress distribution in the soil beneath a footing or behind a retaining wall at the point when plastic flow is about to take place. To address specific engineering problems, it is practical to transform this set of equations into curvilinear coordinates, where the directions of these coordinates align with the directions of potential failure or slip planes. These directions are referred to as slip lines, and the entire pattern is known as the slip-line field.

[Kötter \(1903\)](#) was the pioneer in formulating the slip-line equations, particularly for cases of plane deformations. [Prandtl \(1920\)](#) made a significant contribution by being the first to derive an analytical closed-form solution for these equations, focusing on a footing placed on

a weightless soil. In his analysis, he introduced a singular point and a set of straight slip-lines radiating from it. These findings were subsequently utilized by [Reissner \(1924\)](#) and [Novotortsev \(1938\)](#) to address specific issues related to the bearing capacity of footings on weightless soil. Their work was particularly valuable when straight slip-lines from at least one family were involved, allowing for solutions in closed form.

Nonetheless, the introduction of soil weight significantly complicates the mathematical solution, prompting the development of numerous approximate methods. [Sokolovskii \(1965\)](#) employed a numerical technique that relies on finite difference approximations of the slip-line equations. This approach was particularly useful for solving challenging problems related to the bearing capacity of footings, slopes, and the pressure exerted by fill against retaining walls, where closed-form solutions were elusive. In contrast, [De Jong \(1957\)](#) took a different route and devised a graphical method for arriving at solutions. Other forms of approximate solutions encompass the use of perturbation methods ([Spencer, 1962](#)) and series expansion methods ([Dembicki et al., 1964](#)).

1.5.4. Characteristic method

The method of characteristics is specifically designed to determine stress states that satisfy equilibrium and the failure criterion only within the failure zone near the footing. [Smith's \(2005\)](#) research and [Martin's \(2005\)](#) work suggest that when soil behavior adheres to the associated flow rule, this method can precisely address the bearing capacity problem. It accomplishes this when the calculations of the three terms in the bearing capacity formula align with a single collapse mechanism. Importantly, the method of characteristics has the benefit of eliminating the need for arbitrary assumptions about the shape of the slip surface and accurately identifies the depth of the failure zone.

1.6. Traditional Bearing Capacity Assessment: An In-depth Overview

Over the past seven decades, numerous theories have emerged to estimate the ultimate bearing capacity of shallow foundations. This section provides a summary of key contributions and significant advancements in this field.

1.6.1. Terzaghi's theory

[Terzaghi \(1943\)](#) introduced a well-formulated theory for calculating the ultimate bearing capacity of a shallow foundation. This foundation is characterized by being rough, rigid, continuous (strip), and supported by a homogeneous soil layer extending to significant depths.

Terzaghi (1943) specifically defined a shallow foundation as one in which the width (B) is either equal to or less than its depth (D_f). It's bearing capacity formula for a soil cohesion, friction and weight defined as:

$$q_u = cN_c + qN_q + \frac{1}{2}\gamma BN_\gamma \quad (1.2)$$

where, N_c , N_q and N_γ are the bearing capacity factors given as:

$$N_q = \frac{\exp 2 \left(\frac{3\pi}{4} - \frac{\varphi}{2} \right) \tan \varphi}{2 \cos^2 \left(45 + \frac{\varphi}{2} \right)} \quad (1.3a)$$

$$N_c = \cot \varphi (N_q - 1) \quad (1.3b)$$

$$N_\gamma = \frac{1}{2} K_{p\gamma} \tan^2 \varphi - \frac{\tan \varphi}{2} \quad (1.3c)$$

1.6.2. Meyerhof's theory

Meyerhof (1963) introduced a bearing capacity theory applicable to foundations characterized by rough surfaces and varying depths, accommodating considerations such as foundation shape, load inclination, eccentricity, and the resistance of soil above the foundation base. This led to the modification of Terzaghi's general bearing capacity formula by Meyerhof to encompass these additional factors.

$$q_u = cN_c s_c d_c i_c + qN_q s_q d_q i_q + \frac{1}{2}\gamma BN_\gamma s_\gamma d_\gamma i_\gamma \quad (1.4)$$

where, s_i , d_i and i_i are the shape, depth and load inclination factors respectively given in Eqs. (1.10) to (1.17).

Meyerhof (1963) developed his bearing capacity formula by incorporating expressions from Prandl (1920) for the N_c factor, Reissner (1924) for the N_q factor, and his own formula (Meyerhof, 1961) for the N_γ factor.

$$N_q = \exp(\pi \tan \varphi) \tan^2 \left(\frac{\pi}{4} + \frac{\varphi}{2} \right) \quad (1.5a)$$

$$N_c = \cot \varphi (N_q - 1) \quad (1.5b)$$

$$N_\gamma = (N_q - 1) \tan(1.4\varphi) \quad (1.5c)$$

Shape factor proposed by Meyerhof (1963):

$$s_q = s_\gamma = 1 \quad \text{if } \varphi = 0^\circ \quad (1.6a)$$

$$s_c = 1 + 0.2 \tan^2 \left(\frac{\pi}{4} + \frac{\varphi}{2} \right) \frac{B}{L} \quad (1.6b)$$

$$s_\gamma = s_q = 1 + 0.1 \tan^2 \left(\frac{\pi}{4} + \frac{\varphi}{2} \right) \frac{B}{L} \quad \text{if } \varphi > 0^\circ \quad (1.6c)$$

Depth factor proposed by Meyerhof (1963):

$$d_q = d_\gamma = 1 \quad \text{if } \varphi = 0^\circ \quad (1.7a)$$

$$d_c = 1 + 0.2 \tan^2 \left(\frac{\pi}{4} + \frac{\varphi}{2} \right) \frac{D}{B} \quad (1.7b)$$

$$d_\gamma = d_q = 1 + 0.1 \tan^2 \left(\frac{\pi}{4} + \frac{\varphi}{2} \right) \frac{D}{B} \quad \text{if } \varphi > 0^\circ \quad (1.7c)$$

Load inclination factor proposed by Meyerhof (1963):

$$i_q = i_c = \left(1 - \frac{\delta}{90} \right)^2 \quad (1.8a)$$

$$i_\gamma = \left(1 - \frac{\delta}{\varphi} \right)^2 \quad (1.8b)$$

1.6.3. Hansen's theory

Hansen (1970) introduced an approximated relationship for the N_γ factor in the following form:

$$N_\gamma = 1.5(N_q + 1) \tan \varphi \quad (1.9)$$

Hansen provided expressions accounting for the influence of the foundation shape, soil resistance above the foundation, and applied load inclination, detailed from Eqs. (1.10) to (1.13).

Shape factor given by Hansen (1970):

$$s_q = 1 + \frac{B}{L} \sin\varphi \quad (1.10a)$$

$$s_c = 1 + \left(\frac{N_q B}{N_c L}\right) \varphi \neq 0 \quad (1.10b)$$

$$s_c = 1 + \left(0.2 \frac{B}{L}\right) \varphi = 0$$

$$s_\gamma = 1 - 0.4 \frac{B}{L} \quad (1.10c)$$

Depth factor given by Hansen (1970):

- For $D \leq B$:

$$d_q = 1 + 2 \tan\varphi (1 - \sin\varphi)^2 \frac{D}{B} \quad (1.11a)$$

$$d_c = d_q - \frac{1 - d_q}{N_q \tan\varphi} \quad (1.11b)$$

$$d_c = 1 + 0.4 \frac{D}{B} (\varphi = 0)$$

$$d_\gamma = 1 \quad (1.11c)$$

- For $D > B$:

$$d_q = 1 + 2 \tan\varphi (1 - \sin\varphi)^2 \tan^{-1} \frac{D}{B} \quad (1.12a)$$

$$d_c = 1 + 0.4 \tan^{-1} \left(\frac{D}{B}\right) \quad (1.12b)$$

$$d_\gamma = 1 \quad (1.12c)$$

Load inclination factor given by Hansen (1970):

$$i_q = \left(1 - \frac{0.5H}{V + Ac \cot\varphi}\right)^5 \quad (1.13a)$$

$$i_c = i_q - \left(\frac{1 - i_q}{N_q - 1}\right) \quad (1.13b)$$

$$i_\gamma = \left(1 - \frac{0.7H}{V + Ac \cot\varphi}\right)^5 \quad (1.13c)$$

Which, H and V represent the horizontal and the vertical components of the inclined load applied on the footing.

[Hansen \(1970\)](#) proposed the incorporation of two factors in the bearing capacity equation to consider both base and ground inclination effects. Their expressions are given as follow:

Base inclination factor given by [Hansen \(1970\)](#):

$$b_q = \exp(-2\alpha \tan\varphi) \quad (1.14a)$$

$$b_c^a = \frac{2\alpha}{\pi + 2} \quad (1.14b)$$

$$b_\gamma = \exp(-2.7\alpha \tan\varphi) \quad (1.14c)$$

where, α represents the angle of inclination of the foundation base.

Ground inclination factor given by [Hansen \(1970\)](#):

$$g_q = (1 - 0.5 \tan\beta)^5 \quad (1.15a)$$

$$g_c^a = \frac{2\beta}{\pi + 2} \quad (1.15b)$$

$$g_\gamma = g_q \quad (1.15c)$$

where, β represents the angle of inclination of the ground adjacent to the foundation.

1.6.4. Vesic's theory

[Vesic \(1973\)](#) recommended representing the N_γ factor values provided by [Caquot and Kérisel \(1953\)](#) with an error of less than 10% within the range of 15 to 45 degrees of soil friction angle (with less than 5% error specifically between 20 and 40 degrees). This representation is achieved through the following expression:

$$N_\gamma = 2(N_q + 1)\tan\varphi \quad (1.16)$$

where, [Vesic \(1973\)](#) used the bearing capacity factors N_c and N_q of [Prandl \(1920\)](#) and [Reissner \(1924\)](#) respectively.

Vesic (1973) gave the following expressions for shape factors:

$$s_q = 1 + \frac{B}{L} \tan\varphi \quad (1.17a)$$

$$s_c = 1 + \frac{N_q B}{N_c L} \quad (1.17b)$$

$$s_\gamma = 1 - 0.4 \frac{B}{L} \quad (1.17c)$$

The inclination factors, developed by Vesic in 1975 to account the applied load inclination on the foundation, are presented as follows:

$$i_q = \left(1 - \frac{H}{V + Ac \cot\varphi}\right)^m \quad (1.18a)$$

$$i_c = \frac{i_q N_q - 1}{N_q - 1} \quad (1.18b)$$

$$i_\gamma = \left(1 - \frac{H}{V + Ac \cot\varphi}\right)^{m+1} \quad (1.18c)$$

1.6.5. Standard European code (Eurocode 7)

Eurocode 7 (EN 1997) for geotechnical design, particularly in the context of bearing capacity calculations, generally follows the Vesic method with some modifications. One notable adjustment is the use of Chen's equation for calculating the bearing capacity factor N_γ , which assumes a rough base condition.

$$N_\gamma = 2(N_q - 1)\tan\varphi \quad (1.19)$$

The Eurocode 7 bearing capacity calculation method does not include a depth factor to increase the bearing capacity based on foundation depth and does not allow for foundations on top of slopes. Depth factors are considered unreliable and relatively small for shallow foundations, leading to their omission. Consequently, the EN 1997-1 method tends to produce slightly conservative values compared to other methods.

Eurocode (2004) gave the following expressions for shape factors:

$$s_q = 1 + \frac{B}{L} \tan\varphi \quad (1.20a)$$

$$s_c = \frac{S_q N_q - 1}{N_q - 1} \quad (1.20b)$$

$$s_\gamma = 1 - 0.3 \frac{B}{L} \quad (1.20c)$$

1.6.6. Standard Algerian code DTR-BC 2.331

The Algerian Geotechnical Code (DTR) relies on the Meyerhof method for calculating the bearing capacity of shallow foundations. The Meyerhof method is known for providing conservative bearing capacity factor values, ensuring a safer design by incorporating higher margins of safety.

The DTR code incorporates shape factors similar to those proposed by Costet and Sanglerat (1983) to account for the effects of foundation shape.

$$s_q = 1 \quad (1.21a)$$

$$s_c = 1 + 0.2 \frac{B}{L} \quad (1.21b)$$

$$s_\gamma = 1 - 0.2 \frac{B}{L} \quad (1.21c)$$

For inclined loads applied to footings, the DTR code utilizes Meyerhof's coefficients.

1.7. Assessment of Bearing Capacity under Seismic Conditions

In the presence of dynamic loads, foundations experience inertia forces. When subjected to a low vertical force, foundations designed with a safety factor $FS > 3$ against static loads can effectively withstand seismic loading (Chatzigogos, 2007). However, a substantial reduction in bearing capacity due to inertia forces becomes noteworthy under high vertical forces. Foundations with a static safety factor $FS < 2$ are particularly vulnerable, even under moderate seismic conditions (Chatzigogos, 2007). Consequently, evaluating bearing capacity under dynamic conditions, considering inertia forces, becomes imperative.

In this subsection, various studies from the literature addressing the bearing capacity of shallow foundations under earthquake loading will be presented.

1.7.1. Sarma's theory

Sarma and Iossifelis (1990) assessed formulas for seismic bearing capacity factors using limit equilibrium with inclined slices. They assumed a failure mechanism consisting of an active wedge, a passive wedge, and an internal shear zone positioned between the two wedges, as depicted in Fig. 1.15. The form of the failure surface that defines the shear zone is assumed to be a log-spiral. Sarma and Iossifelis (1990) indicated that the angles defining these wedges are initially unknown and are determined through an iterative process to yield the minimum bearing capacity factors.

The seismic bearing capacity expressions are provided under the assumption that the center of the log-spiral is at point O, as illustrated in Fig. 1.15, and that all interslice slip surfaces intersect at the same point:

$$N_q = L \times \frac{M}{A} \quad (1.22a)$$

$$N_c = \frac{D}{A} \quad (1.22b)$$

$$N_\gamma = \frac{R}{A} \quad (1.22c)$$

where L , M , A , D and R are listed in the Eqs. (A.1) to (A.4) in the Appendix.

When the center of the log-spiral is situated at a different point, while the interslice slip surfaces pass through point O, the ultimate seismic bearing capacity is numerically determined by the following expression:

$$E_{i+1} \cos(2\varphi - \beta_i - \delta_{i+1}) \sec\varphi = a_i - p_i k_c + E_i \cos(2\varphi - \beta_i - \delta_i) \sec\varphi \quad (1.23)$$

The parameters a_i , p_i , R_i , and S_i are detailed in the Eqs. (A.13) to (A.16) in the Appendix, while b_i represents the slice width, d_i is the length of the inclined interslice slip surface, β_i is the inclination of the slip surface to the horizontal, and δ_i is the inclination of the slip surface to the vertical, as depicted in Fig. 1.16.

Sarma and Iossifelis (1990) visually represented seismic bearing capacity factors in relation to the horizontal acceleration coefficient for various internal friction angles of soil. This graphical representation can be observed in Fig. 1.17.

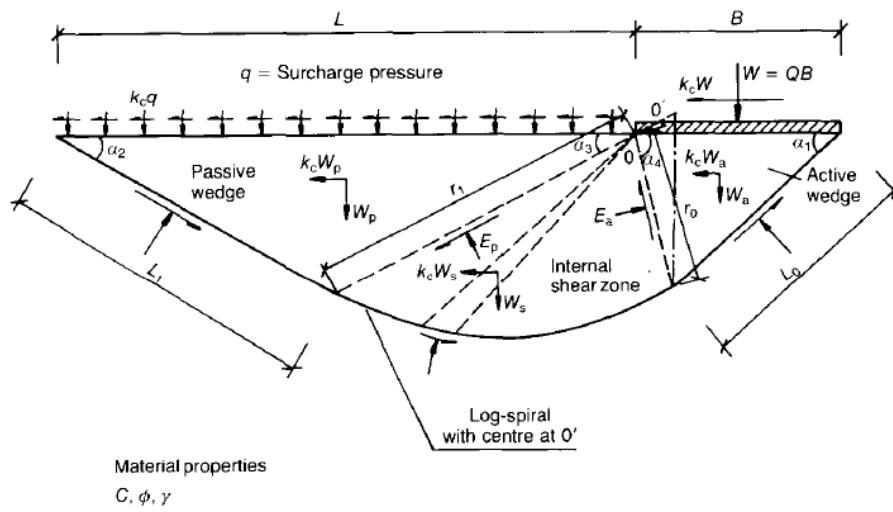


Fig. 1.15 Failure mechanism used in Sarma and Iossifelis (1990) analysis.

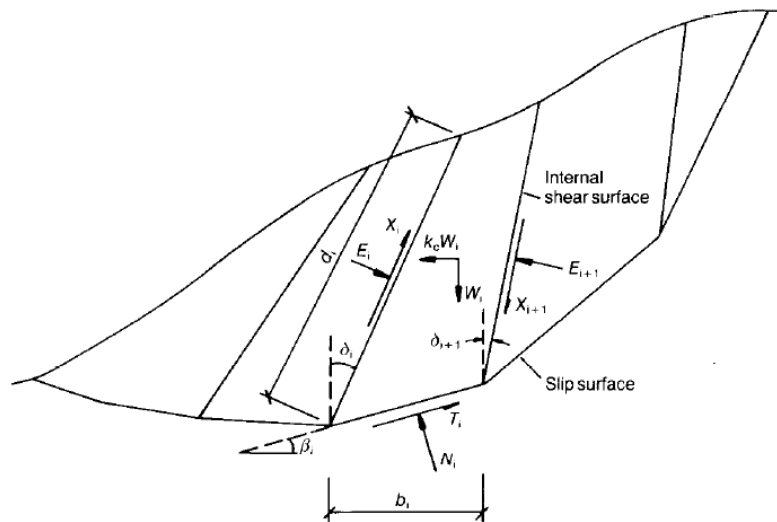


Fig. 1.16 Interslice thrusts given by Sarma and Iossifelis (1990).

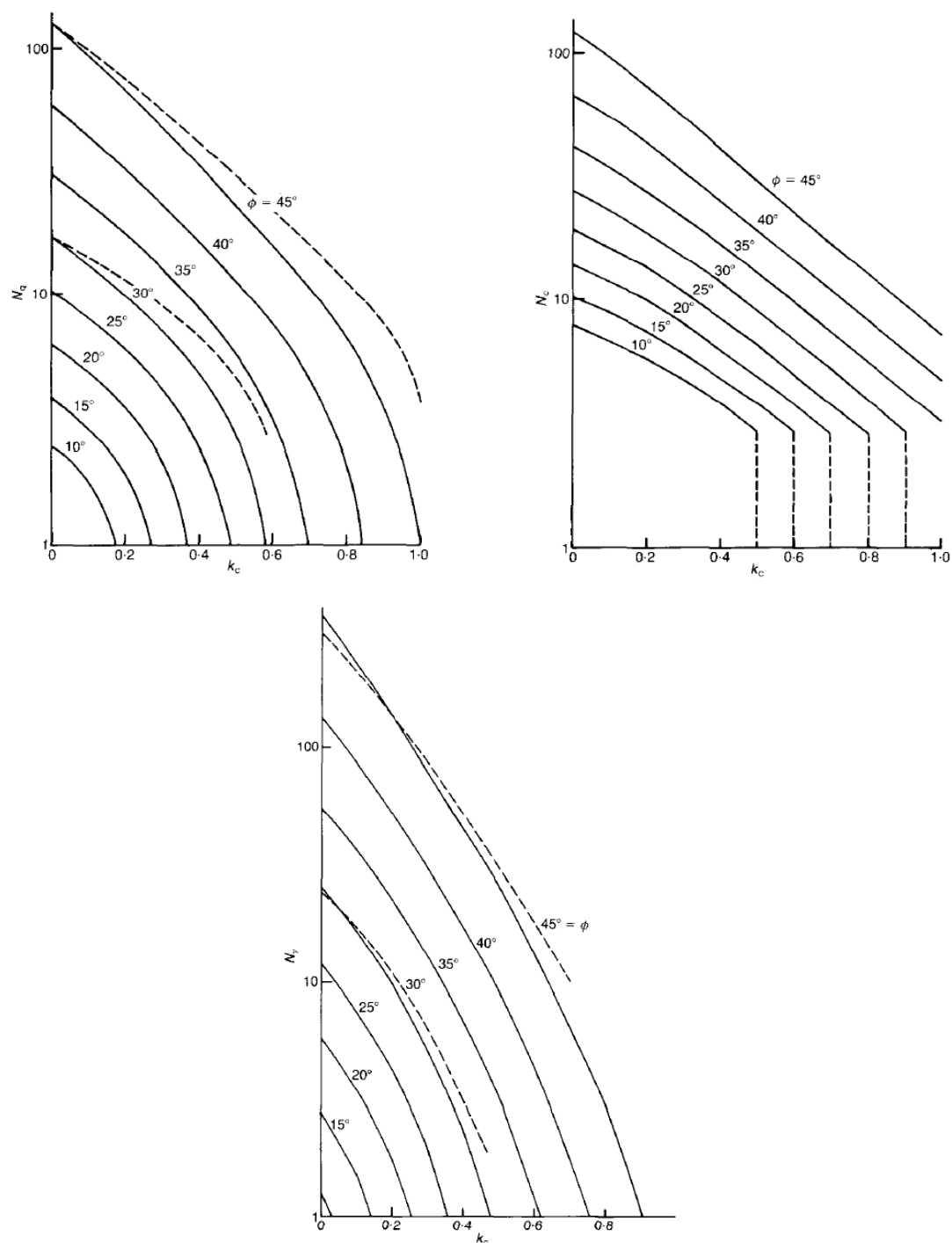


Fig. 1.17 Seismic bearing capacity factors obtained by [Sarma and Iossifelis \(1990\)](#).

1.7.2. Richard's theory

[Richard et al. \(1993\)](#) employed the limit analysis method to establish precise formulations for the seismic bearing capacity factors explicitly linked to their static components.

A Coulomb-type failure mechanism under dynamic situation caused by earthquake loading including inertial forces in the soil and on the footing shows the equilibrium forces in

the active and passive wedges (Fig. 1.18). The figure illustrates the presence of inertial forces $k_h.W_i$ and $k_v.W_i$ in the soil layer resulting from the earthquake accelerations $k_h.g$ and $k_v.g$ respectively. α_{AE} and α_{PE} represent Coulomb's failure wedges for active and passive conditions, determined by the following expressions:

$$\alpha_{AE} = \alpha + \tan^{-1} \left\{ \frac{\sqrt{(1 + \tan^2 \alpha)[1 + \tan(\delta + \theta) \cot \alpha]} - \tan \alpha}{1 + \tan(\delta + \theta)(\tan \alpha + \cot \alpha)} \right\} \quad (1.24a)$$

$$\alpha_{PE} = -\alpha + \tan^{-1} \left\{ \frac{\sqrt{(1 + \tan^2 \alpha)[1 + \tan(\delta - \theta) \cot \alpha]} + \tan \alpha}{1 + \tan(\delta + \theta)(\tan \alpha + \cot \alpha)} \right\} \quad (1.24b)$$

where,

$$\alpha = \phi - \theta \quad (1.25)$$

and

$$\theta = \tan^{-1} \frac{k_h}{1 - k_v} \quad (1.26)$$

Richard et al. (1993) recommended in the computation of the seismic bearing capacity factors it is advisable to designate the angle of wall friction δ to be equal to half of the friction angle ϕ ($\delta = \phi/2$).

The density γ and friction angle ϕ are suggested to be constant. The equilibrium of pseudo static forces gives the earth pressure coefficient in the seismic case K_{AE} (active pressure) and K_{PE} (passive pressure) as follow:

$$K_{AE} = \frac{\cos^2(\phi - \theta)}{\cos \theta \cos(\delta + \theta) \left[1 + \sqrt{\frac{\sin(\phi + \delta) \sin(\phi - \theta)}{\cos(\delta + \theta)}} \right]^2} \quad (1.27a)$$

$$K_{PE} = \frac{\cos^2(\phi - \theta)}{\cos \theta \cos(\delta + \theta) \left[1 - \sqrt{\frac{\sin(\phi + \delta) \sin(\phi - \theta)}{\cos(\delta + \theta)}} \right]^2} \quad (1.27b)$$

Richard et al. (1993) substituted these seismic earth pressure to directly obtain the seismic bearing capacity factors N_{qE} , $N_{\gamma E}$ and N_{cE} :

$$N_{qE} = \frac{K_{PE}}{K_{AE}} \quad (1.28a)$$

$$N_{\gamma E} = \tan \alpha_{AE} \left(\frac{K_{PE}}{K_{AE}} - 1 \right) \quad (1.28b)$$

$$N_{cE} = (N_{qE} - 1) \cot \phi \quad (1.28c)$$

Their values are shown in Table 1.1 for different acceleration intensity when $\phi = 30^\circ$. Tables containing seismic bearing capacity factors for a comprehensive range of friction angles can be assembled for seismic design, intended for use alongside their dynamic counterparts

$$P_{LE} = cN_{cE} + qN_{qE} + 0.5\gamma BN_{\gamma E} \quad (1.29)$$

where, P_{LE} is the ultimate seismic bearing capacity.

Table 1.1 Seismic bearing capacity factors and ratios to static values (Richard et al. 1993).

Acceleration Intensity $\tan \theta$	Seismic bearing capacity factors			Seismic-Static bearing capacity factors ratio		
	N_{qE}	$N_{\gamma E}$	N_{cE}	N_{qE} / N_{qS}	$N_{\gamma E} / N_{\gamma S}$	N_{cE} / N_{cS}
0.000	16.51	23.76	26.86	1.00	1.00	1.00
0.087	12.86	15.34	20.55	0.78	0.65	0.77
0.176	09.84	9.45	15.31	0.60	0.40	0.57
0.268	7.30	5.36	10.91	0.44	0.23	0.41
0.364	5.12	2.61	7.14	0.31	0.11	0.27
0.466	3.21	0.88	3.83	0.19	0.04	0.14
0.577	1.00	0.00	0.00	0.06	0.00	0.00

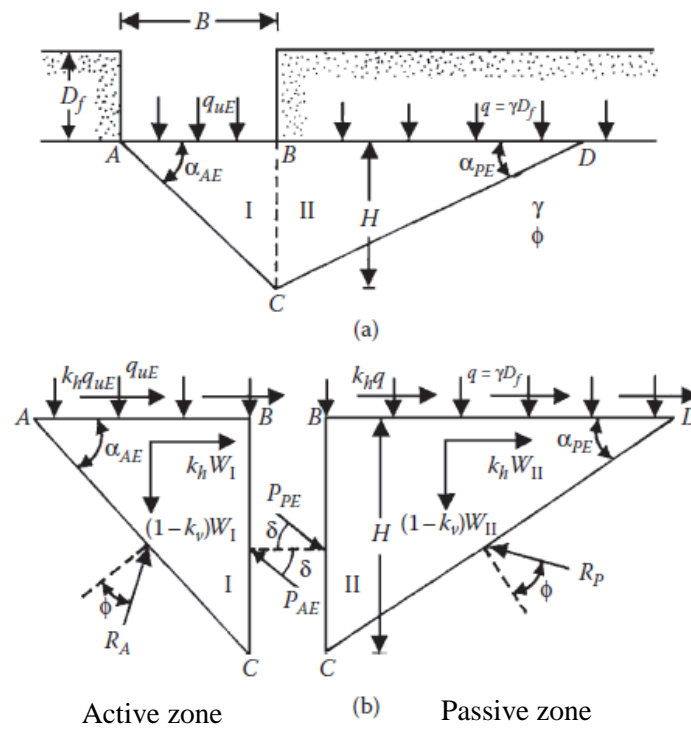


Fig. 1.18 Seismic Coulomb failure mechanism (Richard et al. 1993).

1.7.3. Budhu's theory

Budhu and Al-Karni (1993) presented in their technical note a method for assessing seismic bearing capacity factors based on their static counterparts. Their relationships can be given as follows:

$$N_{qE} = (1 - k_v) N_{qS} \exp(\beta_q) \quad (1.30a)$$

$$N_{\gamma E} = \left(1 - \frac{2}{3} k_v\right) N_{\gamma S} \exp(-\beta_\gamma) \quad (1.30b)$$

$$N_{cE} = N_{cS} \exp(\beta_c) \quad (1.30c)$$

where β_q , β_γ and β_c represent the seismic factors related to the static bearing capacity factors N_{qS} , $N_{\gamma S}$ and N_{cS} proposed by Vesic (1973) respectively. Which can be expressed as:

$$\beta_q = \frac{5.3 k_h^{1.2}}{1 - k_v} \quad (1.31a)$$

$$\beta_\gamma = \frac{9k_h^{1.1}}{1 - k_v} \tag{1.31b}$$

$$\beta_c = 4.3 k_h^{1+D} \tag{1.31c}$$

In which, $D (= c/\gamma h)$ is the stability factor

$$h = \frac{0.5B}{\cos\left(\frac{\pi}{4} + \frac{\phi}{2}\right)} \exp\left(\frac{\pi}{2} \tan\phi\right) + D_f \tag{1.32}$$

Fig. 1.19 shows the normalized seismic bearing capacity factors N_{qE} , $N_{\gamma E}$ and N_{cE} to the static factors N_{qS} , $N_{\gamma S}$ and N_{cS} .

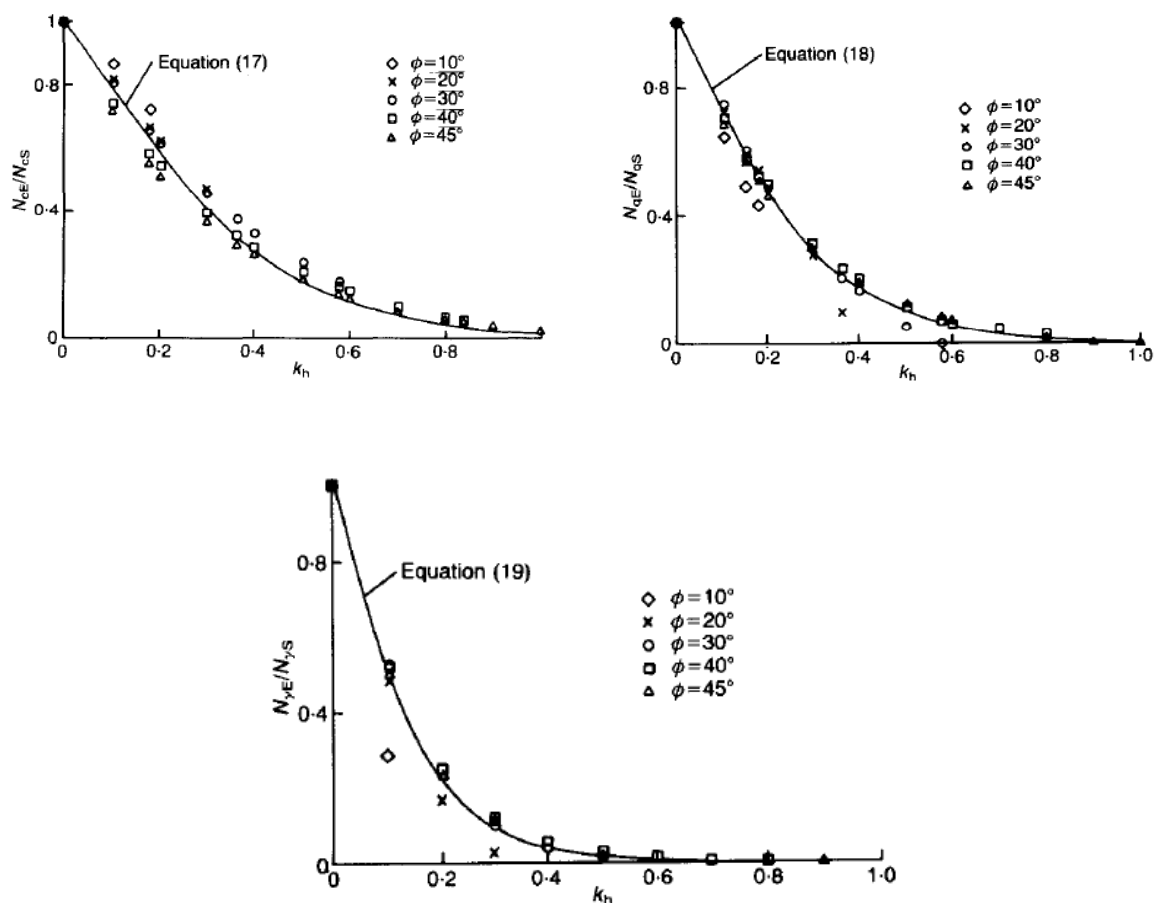


Fig. 1.19 Normalized seismic bearing capacity factors for various friction angles (Budhu and Al-Karni 1993).

1.7.4. Choudhury's theory

Choudhury and Subba Rao (2005) introduced seismic bearing capacity factors within the framework of pseudo-static analysis, employing the limit equilibrium method and incorporating a composite failure surface. Their expressions are given as follows:

$$N_{cd} = \frac{1}{k_h} \left[\frac{\frac{K_{pcd1}}{\cos \varphi} \sin(\alpha_1 - \varphi) - \frac{mK_{pcd2}}{\cos \varphi_2} \sin(\alpha_2 - \varphi_2)}{\frac{1}{\tan \alpha_1} + \frac{1}{\tan \alpha_2}} + \frac{\sin \alpha_1 \tan \varphi_2 \cos \alpha_2}{\sin(\alpha_1 + \alpha_2) \tan \varphi} - \frac{\sin \alpha_2 \cos \alpha_1}{\sin(\alpha_1 + \alpha_2)} \right] \quad (1.33a)$$

$$N_{qd} = \frac{1}{k_h} \left[\frac{\frac{K_{pcd1}}{\cos \varphi} \sin(\alpha_1 - \varphi) - \frac{mK_{pcd2}}{\cos \varphi_2} \sin(\alpha_2 - \varphi_2)}{\frac{1}{\tan \alpha_1} + \frac{1}{\tan \alpha_2}} \right] \quad (1.33b)$$

$$N_{\gamma d} = \frac{1}{k_h} \left[\frac{\frac{K_{pcd1}}{\cos \varphi} \sin(\alpha_1 - \varphi) - \frac{mK_{pcd2}}{\cos \varphi_2} \sin(\alpha_2 - \varphi_2)}{\left(\frac{1}{\tan \alpha_1} + \frac{1}{\tan \alpha_2}\right)^2} \right] - \frac{1}{\left(\frac{1}{\tan \alpha_1} + \frac{1}{\tan \alpha_2}\right)} \quad (1.33c)$$

where K_{pcd} , K_{pqd} and K_{pyd} are given as:

$$K_{pcd} = \frac{P_{pcd} \cos \delta}{2cH} \quad (1.34c)$$

$$K_{pqd} = \frac{P_{pqd} \cos \delta}{qH} \quad (1.34c)$$

$$K_{pyd} = \frac{2P_{pyd} \cos \delta}{\gamma H^2} \quad (1.34c)$$

The seismic passive pressures P_{pcd} , P_{pqd} and P_{pyd} values can be found in Choudhury and Subba Rao (2002) analysis. Fig. 1.20 illustrates the variation of seismic bearing capacity factors in relation to the horizontal acceleration coefficient k_h .

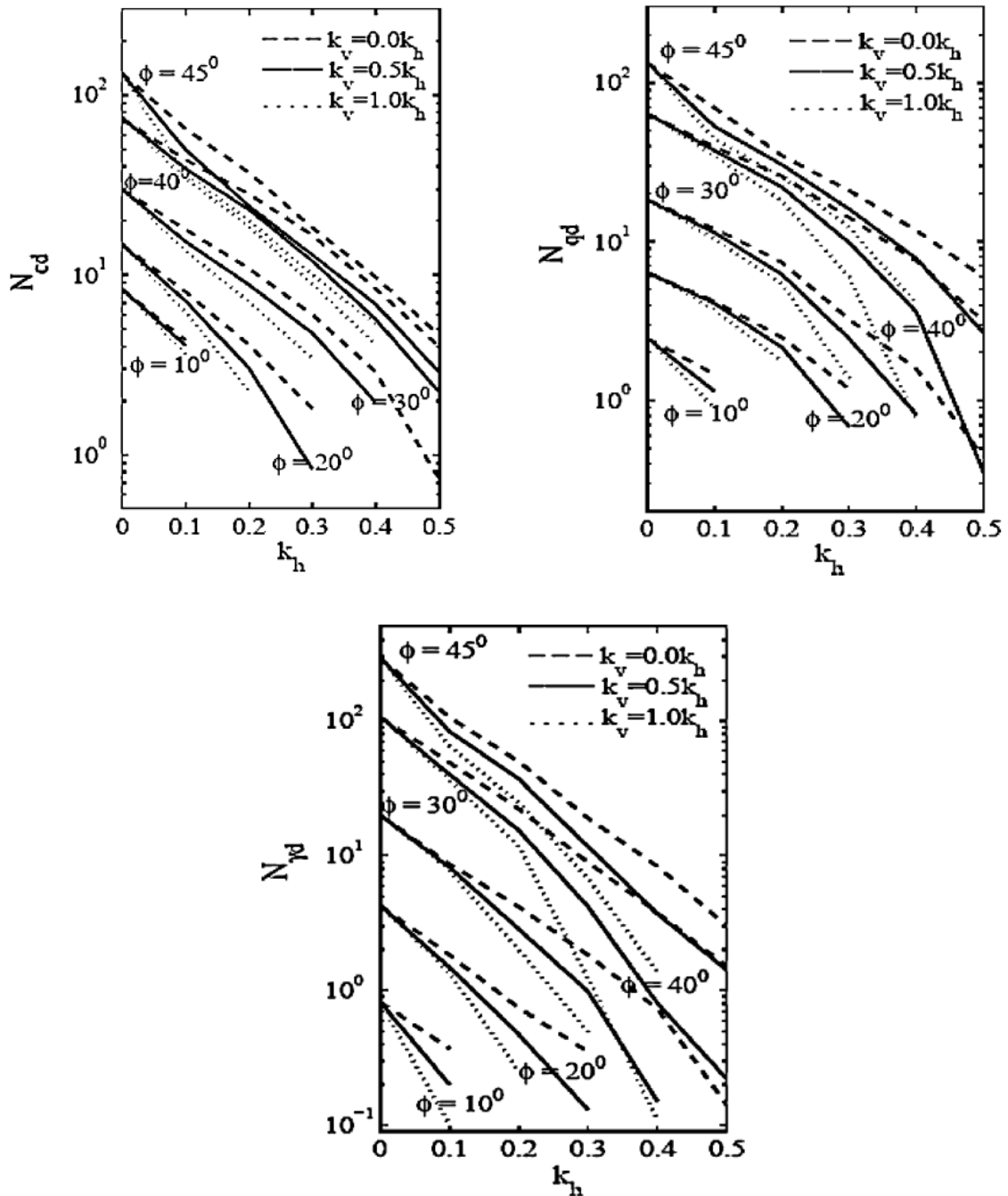


Fig. 1.20 Seismic bearing capacity factors (Choudhury and Subba Rao 2005).

1.8. Conclusion

This chapter initially provided existing examples of the foundations failure caused by numerous earthquakes that occurred in different regions of the world. The various damages to infrastructure of cities in general, and foundations in particular have been discussed. After that,

the different failure mechanisms of shallow foundations in static and seismic cases were presented.

Traditional methods such as limit equilibrium, limit analysis, slip line method and characteristic method can be employed to address these mechanisms for evaluating the foundation bearing capacity. As a result of this, several theories exist in the literature for both static and seismic cases, enabling geotechnical engineering to estimate the allowable bearing capacity in structural design.

SYNTHESIS OF PREVIOUS WORKS

2.1. Introduction

In geotechnical structure analysis and design, input data inherently carry uncertainty, resembling random variables or stochastic processes. Despite engineers' recognition of this uncertainty, traditional deterministic models oversimplify by treating uncertain parameters as deterministic and addressing uncertainties with a global safety factor a somewhat arbitrary "factor of ignorance" derived from past experience. In contrast, a reliability-based approach proves more rational, as it explicitly considers the inherent uncertainty associated with each input variable.

2.2. Previous studies on the bearing capacity under earthquake loading

The seismic bearing capacity assessment of shallow foundations is an important topic for geotechnical engineers in a seismic region. Earthquake loadings diminish the bearing capacity and increase the settlement of shallow foundations. Numerous studies have been conducted on the seismic bearing capacity topic focusing on the determination of the seismic bearing capacity factors following four main approaches: (1) the limit analysis, (2) the limit equilibrium method, (3) the characteristic method and (4) the numerical methods. Additionally, a seismic force within soil is typically characterized using pseudo-static methods, pseudo-dynamic methods and fully dynamic analyses.

[Richard et al. \(1993\)](#) utilized the limit analysis method, incorporating the Coulomb failure mechanism and accounting for inertial forces in both the soil and the footing, to assess the seismic bearing capacity of foundations. Their findings indicated that the bearing capacity of foundations decreases significantly with increasing the seismic acceleration coefficient. ([Fig. 2.1](#)).

[Soubra \(1997\)](#) He calculated the seismic bearing capacity factors of a shallow strip footing using the upper bound of the limit analysis method in conjunction with the pseudo-static approach. He considered two different failure mechanisms, M1 and M2, where the first mechanism consists of a logarithmic sandwich composed of a triangular active wedge, a logarithmic spiral radial shear zone, and a triangular passive wedge. Meanwhile the second mechanism consists of an arc sandwich composed of a triangular active wedge, a circular radial shear zone and a triangular passive wedge. He found that the seismic bearing capacity factors diminish with the increment of the seismic acceleration coefficient for the both mechanisms ([Tables 2.1 to 2.3](#)).

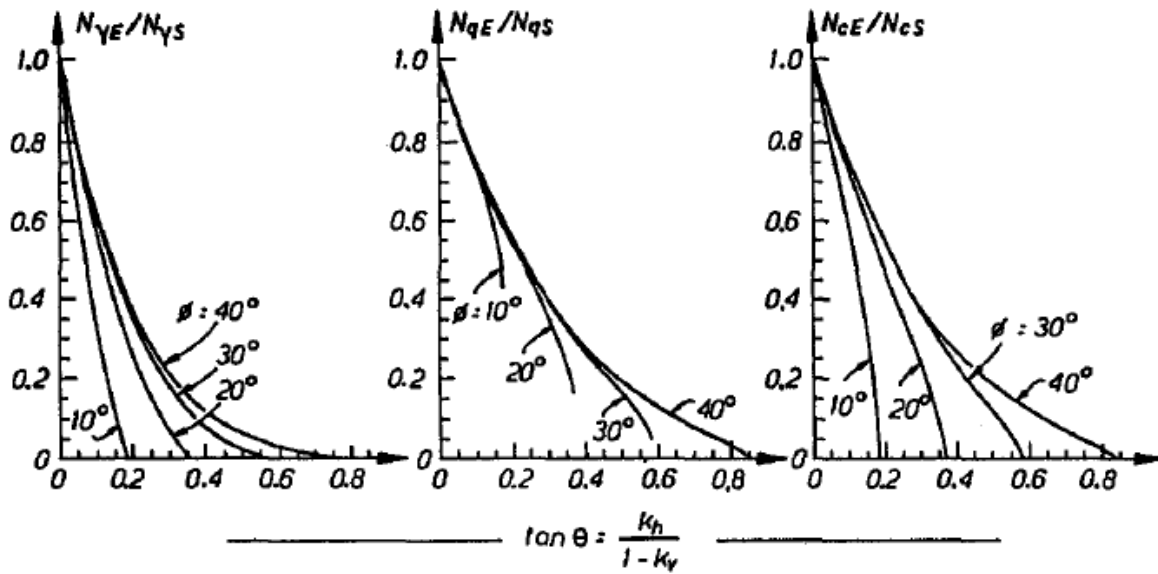


Fig. 2.1 Normalized seismic bearing capacity factors to static factors obtained by Richard et al. (1993).

Table 2.1 Effect of the seismic acceleration coefficient on the bearing capacity factor $N_{\gamma E}$ (Soubra, 1997).

	k_h	Friction angle ϕ (°)					
		15	20	25	30	35	40
M_1	0	2.3	5.2	11.4	25.0	57.1	140.5
	0.1	1.1	3.0	6.9	15.6	36.1	88.4
	0.2	-	1.3	3.6	8.9	21.4	53.0
	0.3	-	-	1.5	4.5	11.7	30.1
	0.4	-	-	-	1.8	5.8	16.0
	0.5	-	-	-	-	2.3	7.8
	0.6	-	-	-	-	-	3.3
M_2	0	2.1	4.8	11.1	31.5	152.2	5444.4
	0.1	-	2.7	6.6	18.9	85.2	2288.7
	0.2	-	1.2	3.4	10.3	44.4	912.1
	0.3	-	-	1.4	4.9	21.3	345.1
	0.4	-	-	-	1.9	9.1	123.2
	0.5	-	-	-	-	3.3	40.6
	0.6	-	-	-	-	0.8	11.7
0.7	-	-	-	-	-	2.5	

Table 2.2 Effect of the seismic acceleration coefficient on the bearing capacity factor N_{cE} of (Soubra, 1997).

	k_h	Friction angle ϕ (°)					
		15	20	25	30	35	40
M_1	0	11.0	14.8	20.7	30.1	46.1	75.3
	0.1	9.5	12.7	17.5	25.0	37.6	60.1
	0.2	7.9	10.5	14.3	20.3	30.0	46.9
	0.3	6.4	8.5	11.5	16.1	23.5	36.1
	0.4	5.1	6.7	9.1	12.6	18.1	27.4
	0.5	4.0	5.2	7.0	9.7	13.8	20.7
	0.6	3.0	4.0	5.4	7.4	10.5	15.5
	0.7	-	-	4.0	5.6	7.9	11.6
	0.8	-	-	-	4.2	5.9	8.7
	0.9	-	-	-	3.1	4.4	6.5
	1	-	-	-	-	3.3	4.9
M_2	0	11.9	18.0	31.3	31.5	280.6	-
	0.1	10.2	15.1	25.3	18.9	193.8	-
	0.2	8.5	12.3	19.9	10.3	130.7	-
	0.3	6.8	9.7	15.3	4.9	86.4	-
	0.4	5.3	7.5	11.4	1.9	56.3	-
	0.5	4.1	5.6	8.4	-	36.1	-
	0.6	-	4.1	6.0	-	22.9	-
	0.7	-	-	4.2	-	14.2	-
	0.8	-	-	-	-	8.6	-

Table 2.3 Effect of the seismic acceleration coefficient on the bearing capacity factor N_{qE} of (Soubra, 1997).

	k_h	Friction angle ϕ (°)					
		15	20	25	30	35	40
M_1	0	3.9	6.4	10.7	18.4	33.3	64.2
	0.1	3.1	5.0	8.3	14.3	25.6	48.7
	0.2	2.1	3.6	6.2	10.7	19.0	35.9
	0.3	-	2.2	4.2	7.5	13.6	25.7
	0.4	-	-	2.5	5.0	9.4	17.9
	0.5	-	-	-	-	6.0	12.0
	0.6	-	-	-	-	3.5	7.8
M_2	0	4.2	7.6	15.6	41.4	197.5	-
	0.1	3.2	5.7	11.5	29.1	125.0	-
	0.2	2.1	4.0	8.0	19.5	76.2	-
	0.3	-	2.4	5.1	12.4	44.6	-
	0.4	-	-	-	7.3	24.9	-
	0.5	-	-	-	3.6	13.0	-
	0.6	-	-	-	-	5.8	-

Yamamoto (2010) developed seismic bearing capacity factors formula of spread and embedded foundations near to a slope using the upper bound of limit analysis method and the pseudo static approach. He observed that the seismic bearing capacity factors decrease considerably with increasing the horizontal seismic coefficient and the slope inclination angle (Fig. 2.2).

Zhou et al (2015) utilized the limit analysis theory with the pseudo dynamic approach to analyze the bearing capacity of shallow foundations rested on rock masses subjected to seismic loads. They indicated that the horizontal and vertical seismic acceleration coefficients and the amplification factor significantly affect the ultimate bearing capacity of shallow foundations (Fig. 2.3).

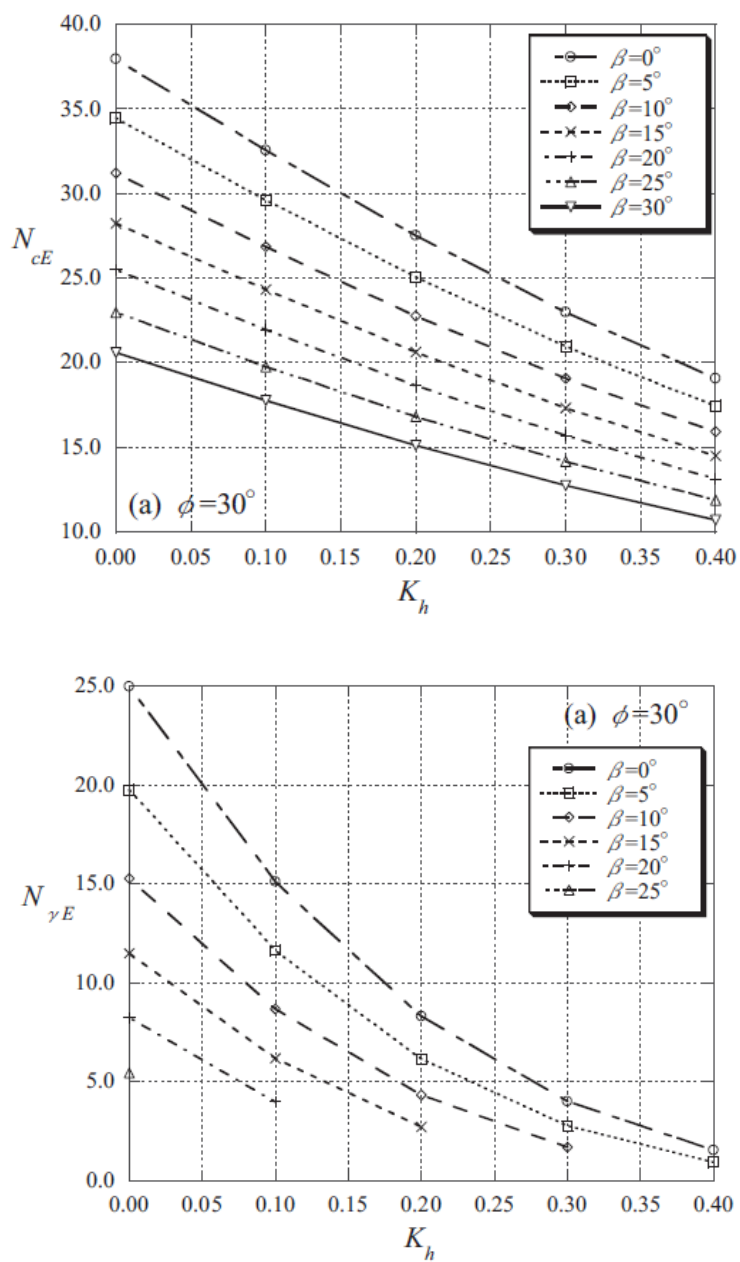


Fig. 2.2 Effect of horizontal seismic acceleration coefficient and slope inclination angle on the bearing capacity factors (Yamamoto, 2010).

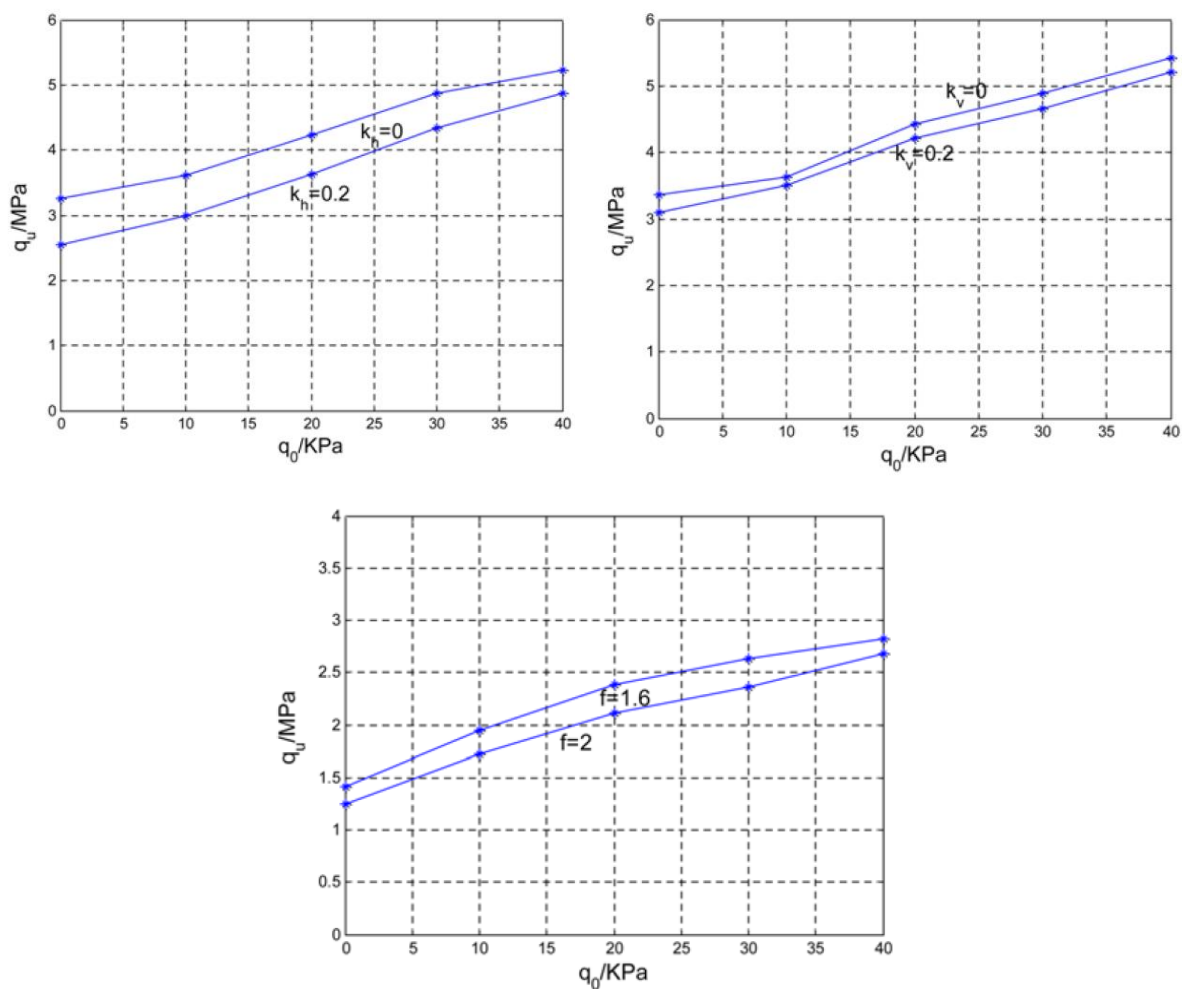


Fig. 2.3 Effect of the horizontal and vertical acceleration coefficient as well as the amplification factor on the seismic bearing capacity (Zhou et al., 2015).

Conti (2018) used the upper bound of the limit analysis method and the pseudo static approach to derive comprehensive seismic bearing capacity formulas of strip footings resting on cohesive-frictional and purely cohesive soils. His findings indicated that the bearing capacity decreases as the seismic acceleration coefficient and the load inclination increase for the both soils (Fig. 2.4).

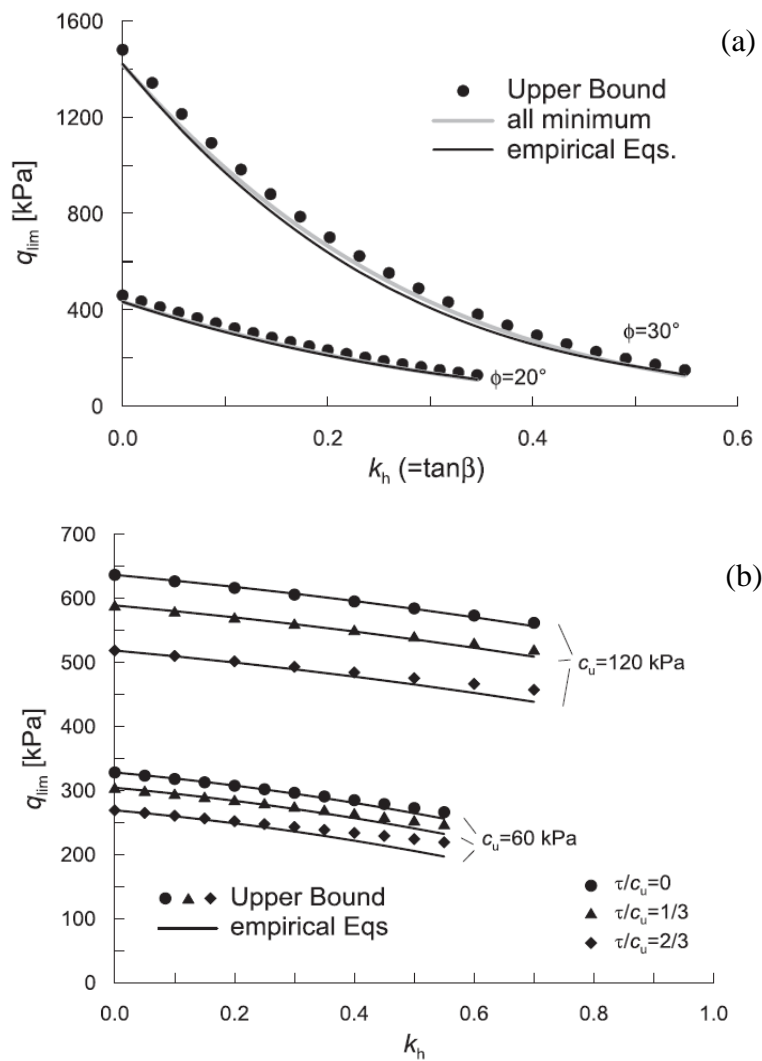


Fig. 2.4 Effect of the horizontal seismic acceleration coefficient and load inclination on the bearing capacity (Conti (2018)) with: (a) cohesive-frictional soil; (b) purely cohesive soil.

Chen et al. (2007) studied the influence of earthquake forces on the bearing capacity factors of shallow strip foundations on a sloping ground by employing the limit equilibrium method and the pseudo static approach, taking into consideration the effect of the intermediate principal stress. Their findings show that the bearing capacity factors are affected by the horizontal and vertical seismic acceleration coefficient (Fig. 2.5).

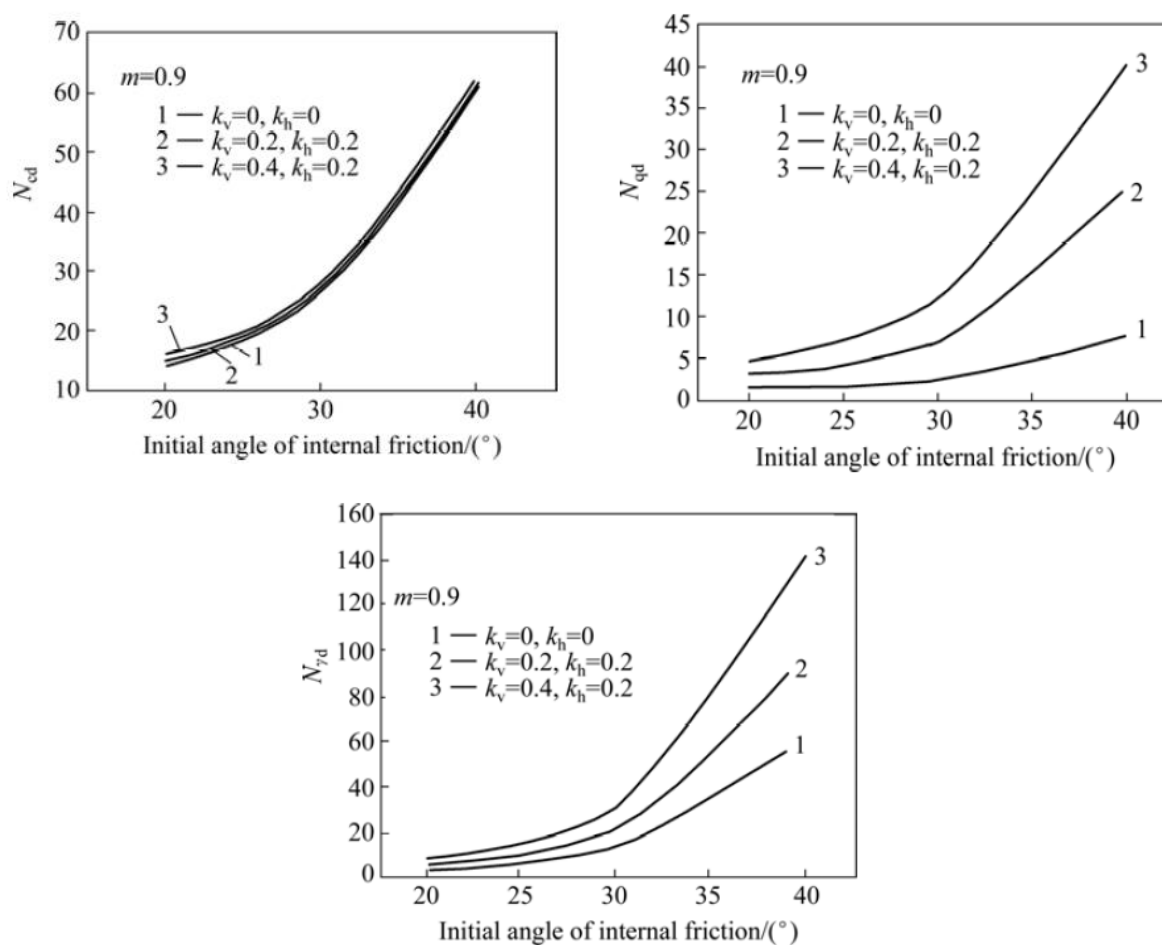


Fig. 2.5 Effect of the horizontal and vertical acceleration coefficients on the bearing capacity factors (Chen et al., 2007).

Debnath and Ghosh (2018) evaluated the seismic bearing capacity of a shallow strip foundation resting on two layered soil using the limit equilibrium method in a pseudo static situation. Their results reveal that the seismic bearing capacity decreases with increasing both of the horizontal and vertical seismic acceleration coefficients (Fig. 2.6).

Nadgouda and Choudhury (2019) derived an equivalent seismic bearing capacity factor for a strip footing resting on a dry cohesionless sand using the limit equilibrium method with the modified pseudo dynamic approach. They found that the bearing capacity factor decreases with increasing the acceleration coefficients (Fig. 2.7).

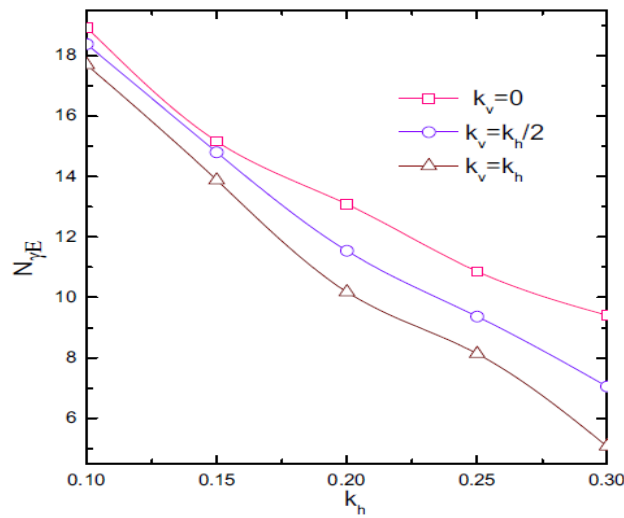


Fig. 2.6 Effect of seismic acceleration coefficient on the equivalent seismic bearing capacity factor (Debnath and Ghosh, 2018).

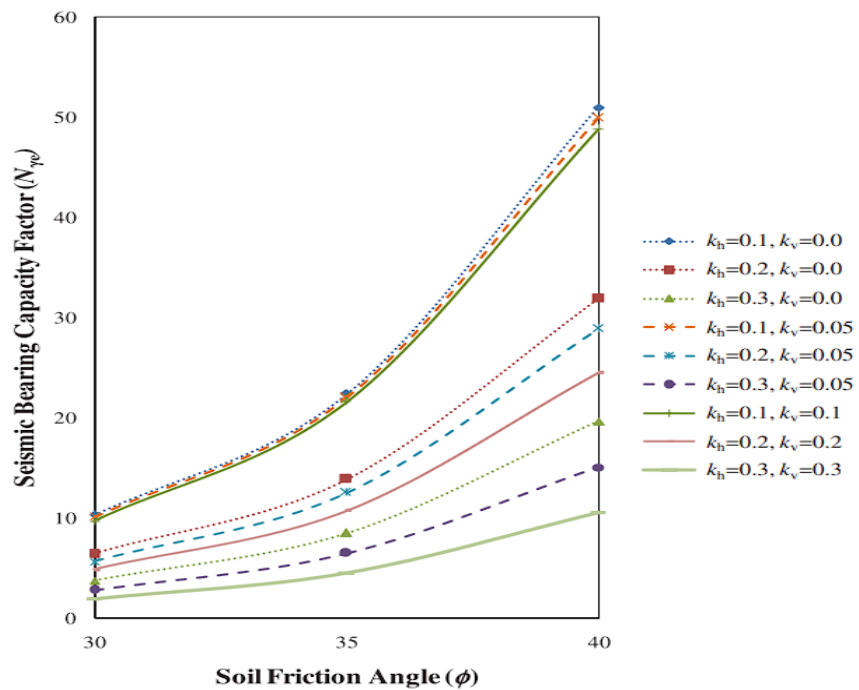


Fig. 2.7 Effect of seismic acceleration on the equivalent bearing capacity factor (Nadgouda and Choudhury, 2019).

Kumar and Mohan Rao (2002) examined the effect of the horizontal earthquake forces on the bearing capacity of shallow foundations by employing the stress characteristics method. They revealed that the bearing capacity factors decrease as the earthquake forces increase (Fig. 2.8).

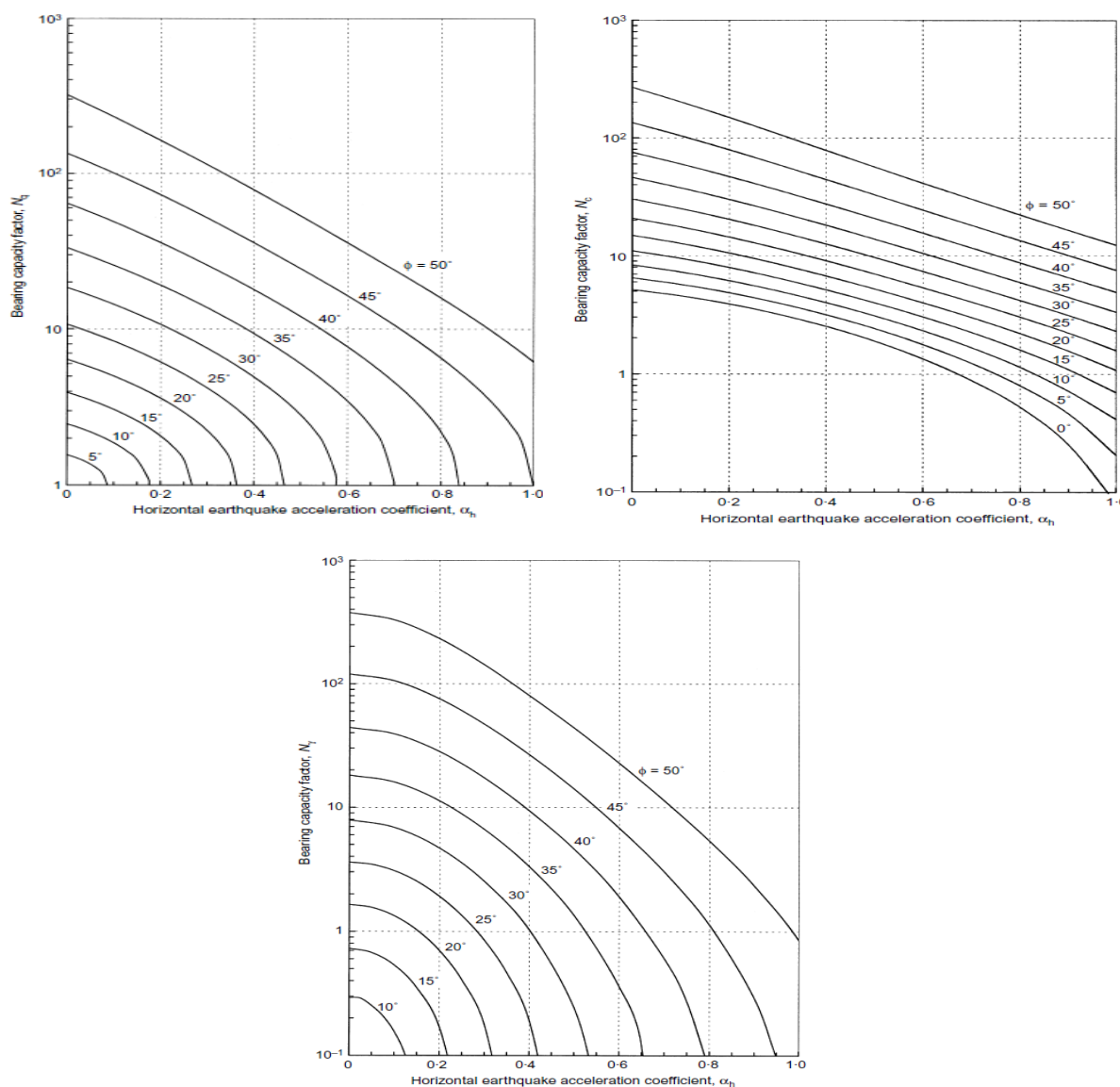


Fig. 2.8 Effect of earthquake forces on the bearing capacity factors (Kumar and Mohan Rao, 2002).

Cascone and Casablanca (2016) assessed the static and seismic bearing capacity factors of a strip footing using the characteristics method with the pseudo static approach. Their results were presented for the both smooth and rough foundations bases. Their results, presented for both smooth and rough foundation bases, indicate that the bearing capacity factors decrease under seismic conditions as the seismic acceleration factors increase. (Fig. 2.9).

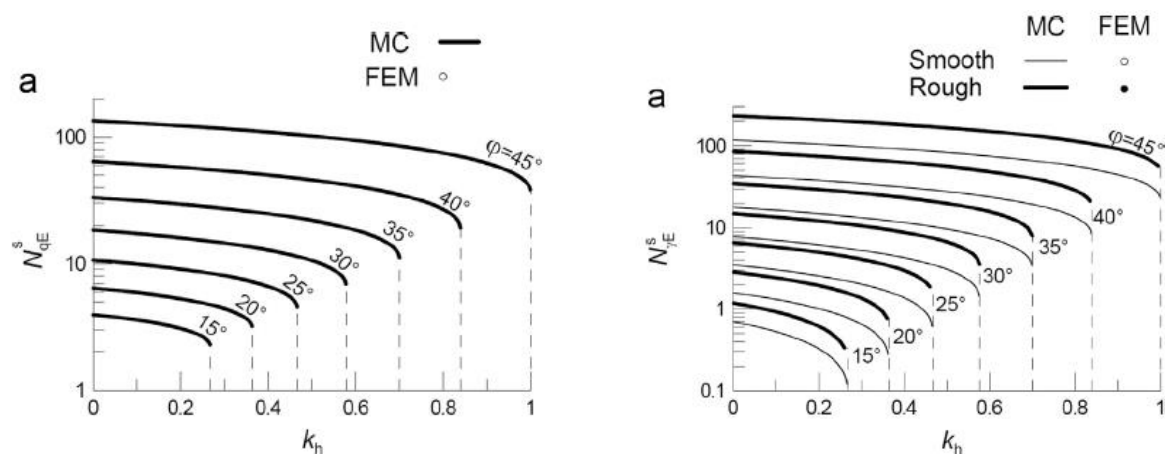


Fig. 2.9 Effect of the horizontal acceleration coefficient on the bearing capacity factors for both smooth and rough base foundations (Cascone and Casablanca, 2016).

Pane et al. (2016) studied the effect of structural and soil inertia due to seismic loads on the bearing capacity of shallow strip footings using a numerical method called finite difference combined with the pseudo-static approach. By estimating reduction factors for both inertia forces, they determined the reduction in the bearing capacity caused by earthquake forces. The results revealed that in certain scenarios, the soil inertia played a significant role in influencing the seismic bearing capacity of the system.

Based on the literature studies, the pseudo static approach is the more applicable by the investigators than the pseudo dynamic approach because of its simplicity and ability to take into account the seismic forces. The pseudo static approach considers the dynamic seismic waves induced by earthquakes as time independent, which means that the magnitude and phase of the acceleration are uniform throughout a soil layer. Despite its proven effectiveness, the pseudo static approach is limited due to its inability to capture the effect of the excitation time duration, excitation frequency and phase differences. These limitations have been surmounted by the pseudo dynamic approach proposed first by Steedman and Zeng (1990) and developed later by Choudhury and Nimbalkar (2005).

Ghosh and Saha (2013) developed a pseudo-dynamic approach that considers the effects of both shear and compression wave velocities to predict the seismic passive resistance on the back of a battered-faced retaining wall. However, it is well known that the surface waves such as Rayleigh waves and Love waves are of utmost importance in earthquake engineering and

the understanding of the causes of damage caused by earthquakes (Katdare and Choudhury, 2012). They have capabilities to cause devastating damage during an earthquake. Thus, their propagation throughout soil profiles may lead to considerable effects on the geotechnical constructions. Over recent years, the consideration of Rayleigh waves in the pseudo dynamic approach has attracted considerable attention. As a result, numerous studies were carried out either to analyze the pseudo-dynamic earth pressure considering Rayleigh waves (Choudhury and Katdare, 2012 and 2013; Ghosh and Saha, 2013 and 2014) or to analyze the problem of pseudo dynamic bearing capacity with considering Rayleigh waves along with primary waves and shear waves (Saha and Ghosh, 2017).

Regarding the Love waves, a single study has been encountered in the literature, which was carried out by Izadi et al. (2022) who addressed the impact of Love wave propagation on the pseudo-dynamic bearing capacity of shallow foundations in terms of the equivalent seismic bearing capacity factor (Fig. 2.10).

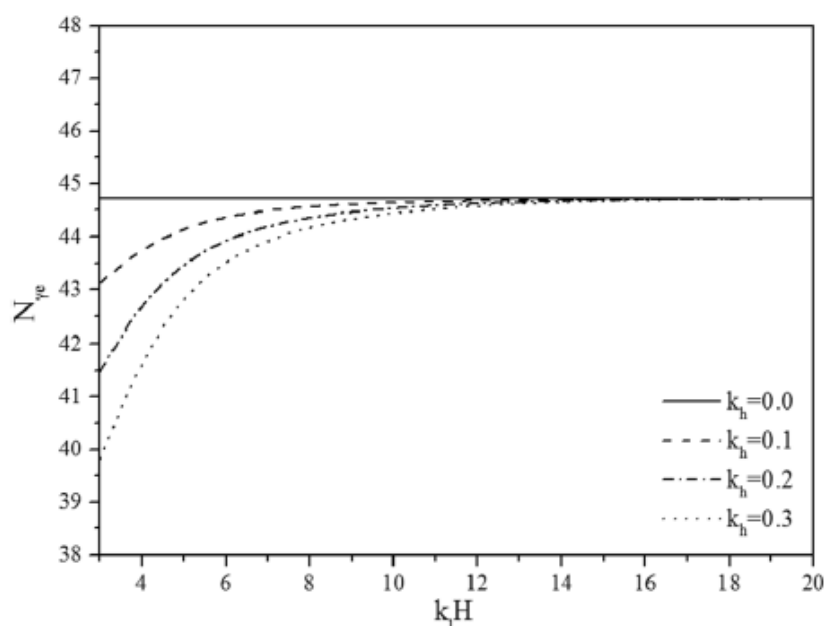


Fig. 2.10 Effect of Love wave frequency and seismic acceleration coefficient on the equivalent seismic bearing capacity factor (Izadi et al., 2022).

2.3. Uncertainty in Soil Properties: Implications for Geotechnical Engineering

The geotechnical engineering practice categorized the uncertainty into three primary sources, which are: (i) natural heterogeneity, (ii) measurement, and (iii) transformation uncertainty, as identified by Phoon and Kulhawy (1999a). Der Kiureghian and Ditlevsen (2009) indicated in

their research paper called “Aleatory or epistemic? Does it matter?” that the uncertainties can be described as epistemic when the modeler realizes an opportunity to reduce them through collecting more data or through refining the transformation models. While, the uncertainties can be described as aleatory when the modeler does not foresee the chance of mitigating them through the collection of additional information.

The measurements and the transformation uncertainties are two types of epistemic uncertainties that can be encountered in the geotechnical engineering domain. The first type arises from the sampling errors induced by a limited amount of available information. Reducing this uncertainty can be possible by incorporating a large number of samples. The second type is employed when the field or laboratory measurements undergo transformation into the design soil properties through the exploitation of empirical or other correlation models.

Natural heterogeneity is regarded as an essential aspect of aleatory or inherent uncertainty. For example, soil properties exhibit spatial variations, while seismic activity varies temporally. The spatial variability, or inherent variability, of soil arises primarily from natural geological processes that influence the in-situ mass. Regarding seismic loading, temporal variability stems from the random nature of acceleration values at different time steps.

2.4. Inherent (Spatial) variability of soil properties

The spatial variability of soils arises primarily from variations in the soil properties between different points in space, attributable to diverse depositional conditions and distinct loading histories (Elkateb et al., 2002). The characterization of the spatial variability of soil properties can be efficiently performed statistically by considering three statistical parameters: (i) mean; (ii) coefficient of variation (or standard deviation) and (iii) autocorrelation distance (or generally the autocorrelation function) (VanMarcke, 1977). Fig. 2.11 exhibits a typical spatial variation of soil properties in a soil profile. This variation is described by the essential parameters such the vertical scale of fluctuation δ_v (or correlation distance r_0), the trend function $t(z)$ and the deviation from the trend $w(z)$, which play an important role in the site characterization.

When conducting probabilistic analysis in geotechnical engineering, it is crucial to employ accurate values of the mean, the standard deviation and the autocorrelation distance of the uncertain soil properties. To achieve this goal, various geotechnical and geophysical tests must

be conducted to quantify these parameters. The difference between those two tests is that the first one covers a small area and requires a large number of tests in order to characterize the variability of a soil property, whereas the second one covers a large area with a smaller number of tests, which represents an efficient option for the geotechnical studies.

Following the collection of various values for a specific soil property, a conventional statistical analysis is employed to determine the mean and standard deviation of this property. While this analysis reveals the variability of the soil property, it does not offer insight into the spatial trend. Therefore, to characterize the spatial variation of a soil property, it is essential to determine the autocorrelation distance. Two mathematical techniques presented in the literature are available for identifying the autocorrelation structure of a soil property: random field theory and geostatistical tools.

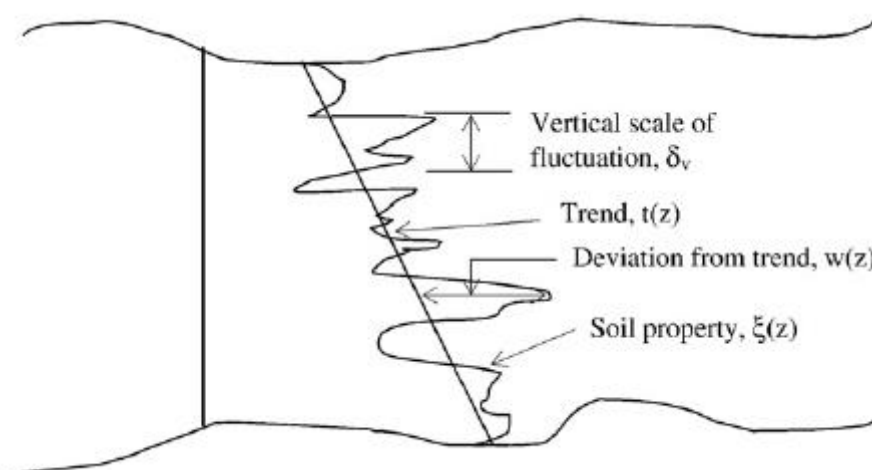


Fig. 2.11 Statistical representation of soil variability (Phoon and Kulhawy, 1999a).

2.5. Random field theory

The random field theory is frequently employed in the literature to characterize the spatial variability of a soil property. VanMarcke (1983) pointed that the random field theory should introduce the observed phenomenon. This theory assumes that the actual value of a soil property at each location to be a realization of a random variable. That values at adjacent locations exhibit greater correlation than those separated by a distance. Thus, an important statistical characteristic, namely the autocorrelation function (ACF), is introduced as well as statistical parameters such as the mean, the standard deviation, or the coefficient of variation. The autocorrelation function (ACF) is a graphical representation of the correlation coefficient

plotted against the distance. This autocorrelation function (ACF) serves the purpose of identifying either the autocorrelation distance or the scale of fluctuation. When denoting the soil property of interest as Z , the correlation coefficient (ρ) between the values of this property at two distinct locations is given by the following equation:

$$\rho(\tau) = \frac{C[Z(X_i), Z(X_{i+\tau})]}{\sigma_z^2} = \frac{1}{\sigma_z^2} E\{[Z(X_i) - \mu_z][Z(X_{i+\tau}) - \mu_z]\} \quad (2.1)$$

where, X is the vector of location. For the case of a one dimensional (1D) random field, the vector is defined by $X = (x)$, for (2D) random field; $X = (x, y)$ and for (3D) random field; $X = (x, y, z)$. $Z(X_i)$ denotes the value of the property Z at a given location X_i . τ is the separation distance between two spatial locations. $E[.]$ is the expectation operator. C represents the covariance, μ_z the mean value of the property Z and σ_z the standard deviation of the same property Z . Five frequently referenced autocorrelation functions (ACFs) are described in the literature as listed in Table 2.4. These ACFs are commonly employed to evaluate the distance over which a property shows strong correlation. In Table 2.4, ρ designates the ACF and τ_x and τ_y signify the absolute horizontal and vertical distances between two points within the soil unit, respectively. δ_h and δ_v designate the horizontal and vertical scale of fluctuation (SOF), respectively.

Table 2.4 Various forms of autocorrelation functions (ACFs).

ACF type	Expression
Single exponential (SNE)	$\rho(\tau_x, \tau_y) = \exp\left[-2\left(\frac{\tau_x}{\delta_h} + \frac{\tau_y}{\delta_v}\right)\right]$
Cosine exponential (CE)	$\rho(\tau_x, \tau_y) = \exp\left[-\left(\frac{\tau_x}{\delta_h} + \frac{\tau_y}{\delta_v}\right)\right] \cos\left(\frac{\tau_x}{\delta_h}\right) \cos\left(\frac{\tau_y}{\delta_v}\right)$
Second-order Markov (SOM)	$\rho(\tau_x, \tau_y) = \exp\left[-4\left(\frac{\tau_x}{\delta_h} + \frac{\tau_y}{\delta_v}\right)\right] \left(1 + \frac{4\tau_x}{\delta_h}\right) \left(1 + \frac{4\tau_y}{\delta_v}\right)$
Squared exponential (SQE)	$\rho(\tau_x, \tau_y) = \exp\left[-\pi\left(\frac{\tau_x^2}{\delta_h^2} + \frac{\tau_y^2}{\delta_v^2}\right)\right]$
Binary noise (BN)	$\rho(\tau_x, \tau_y) = \begin{cases} \left(1 - \frac{\tau_x}{\delta_h}\right) \left(1 - \frac{\tau_y}{\delta_v}\right) & \text{for } \tau_x \leq \delta_h \text{ and } \tau_y \leq \delta_v \\ 0 & \text{otherwise} \end{cases}$

2.6. Geostatistics

In the field of geostatistics, the spatial variability of soil properties is described through the variogram or semivariogram function (Deutsch and Journel, 1997). The variogram is characterized as the variance of the difference $\{Z(X_{i+\tau}) - Z(X_i)\}$

$$2\gamma(\tau) = \text{var}\{Z(X_{i+\tau}) - Z(X_i)\} \quad (2.2)$$

where, $\text{var}[\cdot]$ is the variance operator. By definition, the semivariogram is the half of variogram and can be expressed as:

$$\gamma(\tau) = \frac{1}{2} \text{var}\{Z(X_{i+\tau}) - Z(X_i)\} \quad (2.3)$$

Fig. 2.12 illustrates the variation of the semivariogram function $\gamma(\tau)$ with the separation distance τ . It can be notice that the function $\gamma(\tau)$ increases and tends to be stable at a limiting value called the sill as the separation distance τ increases. This value is at or near to the variance of the stochastic process $C(0) = \sigma^2$. The range where the semivariogram function varies from its initial value $\gamma(0)$ into the sill value is called the range of influence. Occasionally, the variogram may exhibit a discontinuity in its behavior near the origin ($\tau = 0$). This discontinuity, known as the nugget effect, manifests as an apparent intercept at zero separation distance, referred to as the nugget. Small-scale effects or measurement errors can give rise to the nugget effect.

The autocovariance distance, alternatively known as the correlation length, autocorrelation length, or correlation distance, is determined from the variogram function or the autocorrelation function (ACF). It represents the distance at which the spatial variance or autocorrelation has decreased to $1/e$ (37%). Typically falling within the range of 1.4 to 2.0 times the correlation length for exponential, Gaussian, and spherical ACFs (Vanmarcke, 1983). Furthermore, in geostatistics, the ACF is referred to as a correlogram.

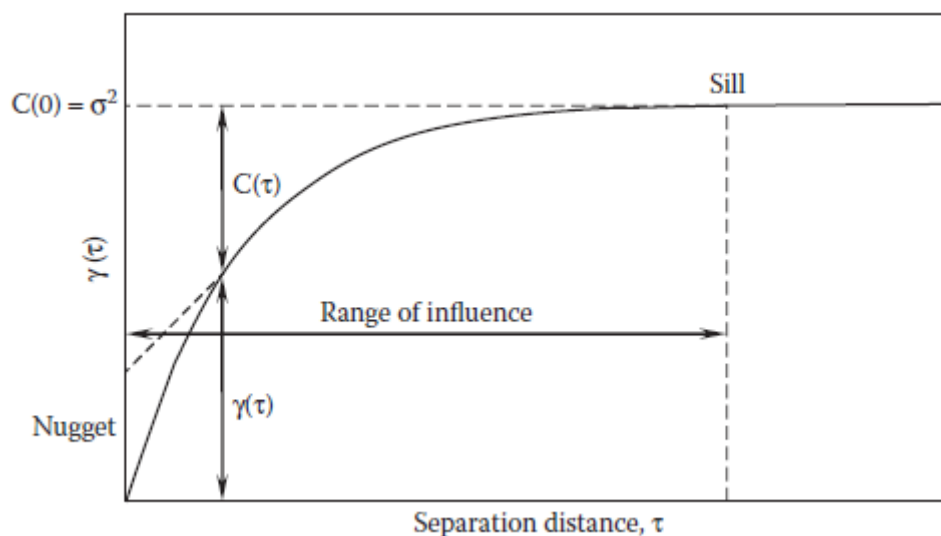


Fig. 2.12 Variation of semivariogram with separation distance.

2.7. Discretization of random field theory

Many geotechnical problems necessitate discrete fields to precisely capture the spatial variability. The commonly used approaches for discretizing the random field theory include the Karhunen–Loève (KL) expansion method, the covariance matrix decomposition method and the local average subdivision method (LAS).

2.7.1. Karhunen-Loève (K-L) Expansion approach

This approach which was introduced in 1991 by Ghanem and Spanos, also known as principal component analysis (PCA), is a mathematical technique used to decompose a random field into a series of uncorrelated modes or eigenfunctions. These modes represent different scales of variability, ordered by their contribution to the overall variance of the field. In this approach, the random field is based on the spectral decomposition of a covariance function:

$$Z(X, \theta) = \mu(X) + \sum_{i=1}^{\infty} \sqrt{\lambda_i} \varphi_i(X) \varepsilon_i(\theta) \quad (2.4)$$

In Eq. (2.4), X represents the coordinate of a point in continuous domain Ω , θ represents the coordinate in the sample space, $\mu(X)$ represents the mean of the random field and $\varepsilon_i(\theta)$ the represent the uncorrelated standard random variables. φ_i and λ_i are the eigenfunctions and eigenvalues of covariance matrix, respectively.

Those eigen parameters (φ_i, λ_i) may be obtained through solving the homogeneous Fredholm integral equation of the second kind:

$$\int_{\Omega} C(X, X')\varphi_i(X')dX' = \lambda_i\varphi_i(X) \quad (2.5)$$

By truncating the ordered series, the approximated random field is defined as follow:

$$Z(X, \theta) = \mu(X) + \sum_{i=1}^M \sqrt{\lambda_i}\varphi_i(X)\varepsilon_i(\theta) \quad (2.6)$$

where M is the truncating level. The optimal choice of this parameter is heavily depending upon the targeted precision and the covariance function inherent in the random field.

2.7.2. Covariance Matrix Decomposition approach

This approach supposes that the parameters at diverse positions in the field are correlated random variables. It is relevant to any configuration of the simulated locations and any covariance model. In a one-dimensional problem, the space is discretized into n points, with the soil property at each point considered as a random variable. A covariance matrix denoted as C is assumed for the correlated random variables. When the covariance matrix is positive, a correlated standard normal random field Z can be generated by utilizing independent standard normal random variables, as expressed in the following expression:

$$Z = LU \quad (2.7)$$

where, L represents the lower triangular matrix which can be obtained through applying the Cholesky decomposition method on $LL^T = C$. U represents the vector of the n -independent standard normal random variables. Z represents the vector of the n -correlated standard normal random variables.

For a single soil property Z' of the normal random field with a mean and standard deviation, the generation of a soil property may be acquired using the generation of the correlated standard normal random variable Z as:

$$Z' = \mu_z I + \sigma_z \cdot Z \quad (2.8)$$

In Eq. (2.8), I represents the unit matrix and μ_z and σ_z represent the mean and standard deviation of Z' .

For non-normal random fields, an appropriate transformation of a normally distribution random field must be implicated. For instance, a log-normally random field can be attained as:

$$Z' = \exp(\mu_{\ln Z} I + \sigma_{\ln Z} \cdot Z) \quad (2.9)$$

where $\mu_{\ln Z}$ and $\sigma_{\ln Z}$ are the mean and standard deviation of $\ln(Z')$, respectively.

2.7.3. Local Average Subdivision approach

Fenton and Vanmarcke (1990) proposed a fast and an accurate approach for generating realizations of a random process called Local Average Subdivision (LAS) method. This approach is constructed on the stochastic subdivision methods (Carpenter, 1980; Fournier et al., 1982) and combines the concept of local averaging. For a better understanding of the basic concept of this approach, Fenton and Vanmarcke (1990) showcased an example that illustrated the LAS procedure for a one-dimensional stationary random field in their research paper.

2.8. Ranges of variability in some geotechnical soil properties

This section presents frequently used values of the coefficient of variations (COVs) for various geotechnical soil properties, as well as correlation coefficients between these properties and their scale of fluctuations.

2.8.1. Coefficient of variations (COVs)

The reported COVs of certain soil parameters from the literature are listed in Table 2.5. In this table, UC denotes the unconfined compression test; UU denotes the unconsolidated-undrained triaxial compression test and CIUC denotes the isotropic consolidated undrained triaxial compression test.

Table 2.5 Coefficients of variation of some soil properties.

Parameter	Type of soil	COV (%)	Authors
Density	All soils	5-10	Lumb (1974)
Unit weight γ (kN/m ³)	Fine grained	3-20	Phoon and Kulhawy (1999)
Dry unit weight γ_d (kN/m ³)	Fine grained	2-13	Phoon and Kulhawy (1999)
D_r (%) (direct method)	Sand	11-36	Phoon and Kulhawy (1999)
D_r (%) (indirect method)	Sand	49-74	Phoon and Kulhawy (1999)
C_u (UC)	Clay	30-50	Lumb (1972)
	Clay	60-85	Lumb (1972)
Undrained shear strength (C_u)	Clay (triaxial)	5-20	Lacasse and Nadim (1996)
Undrained shear strength (C_u)	Clay	10-35	Lacasse and Nadim (1996)
	Clayey silt	10-30	Lacasse and Nadim (1996)
C_u (UC)	Fine grained	6-56	Phoon and Kulhawy (1999)
C_u (UU)	Clay, silt	11-49	Phoon and Kulhawy (1999)
C_u (CIUC)	Clay	18-42	Phoon and Kulhawy (1999)
Undrained cohesion	Clay	20-50	Lumb (1974)
	Sand	2-5	Lacasse and Nadim (1996)
Friction angle ϕ (°)	Clay	40	Kotzias et al. (1993)
	Alluvial	16	Wolff (1996)
	Tailings	5-20	Baecher et al. (1983)
	Sand	5-11	Phoon and Kulhawy (1999)
	Clay, silt	4-50	Phoon and Kulhawy (1999)

2.8.2. Correlation coefficients

A correlation coefficient is a statistical measure that quantifies the degree of association or relationship between two parameters. The cohesion and friction angle are commonly assumed to be correlated geotechnical strength parameters. Table 2.6 shows the reported values of the correlation coefficients between these two parameters.

Table 2.6 Correlation coefficients of (c , ϕ).

Authors	$r_{c, \phi}$
Lumb (1970)	-0.7 to -0.37
Yucemen et al. (1973)	-0.49 to -0.24
Wolff (1985)	-0.47
Cherubini (2000)	-0.61

2.8.3. Scale of fluctuations

In geotechnical engineering, the scale of fluctuation refers to the spatial or temporal range over which variations occur in a specific geotechnical property or parameter. This concept is essential for understanding the heterogeneity or variability of soil characteristics within a given site. Table 2.7 shows the reported values of the scale of fluctuation for different soil properties where CPT denotes the Cone Penetration Test, FVT denotes the Field Vane Test, VST denotes Vane Shear Test and DSS denotes the Direct Simple Shear Test. It can be concluding generally from this table that, the horizontal scale of fluctuation can be varying from 10 to 100m. While the vertical scale of fluctuation varies from 0 to 10m.

Table 2.7 Scale of fluctuation for different soil properties.

Soil	Soil property	Scale of fluctuation δ (m)		Test	Authors
		δ_h	δ_v		
Marine clay (different levels)	Average cone resistance	35-60	-	CPT	Tang (1979)
Marine clay (0- 3m below sea bottom)	Average cone resistance	55	-	CPT	Tang (1979)
Sensitive clay	CPT tip resistance q_c	-	2	CPT	Chiasson et al. (1995)
Glacial sands	CPT tip resistance q_c	20-35	-	CPT	Vrouwenvelder and Calle (2003)
//	CPT tip resistance q_c	-	0.8-1.8	CPT	Popescu et al. (1995)
Clay	CPT tip resistance q_c	-	1	CPT	Vanmarcke (1977)
Offshore soils	CPT tip resistance q_c	14-38	-	CPT	Keaveny et al. (1989)
Silty clay	CPT tip resistance q_c	5-12	1	CPT	Lacasse and de Lamballerie (1995)
Clean sand	CPT tip resistance q_c	-	1.6	CPT	Kulatilake and Ghosh (1988)
Sand, clay	CPT tip resistance q_c	3-80	0.1-2.2	CPT	Phoon and Kulhawy (1996)
Clay	Corrected CPT tip resistance, q_T	23-66	0.2-0.5	CPT	Phoon and Kulhawy (1996)

-	Undrained shear strength c_u	-	2	FVT	Chiasson et al. (1995)
Clay	Undrained shear strength c_u	-	2.5-6	FVT	Asaoka and A-Grivas (1982)
Sensitive clay	Undrained shear strength c_u	23	-	FVT	DeGroot and Baecher (1993)
Sensitive clay	Undrained shear strength c_u	-	1	FVT	Baecher (1982)
Chicago clay	Undrained shear strength c_u	-	0.5	Unconfined compression test	Wu (1974)
Offshore soils	Undrained shear strength c_u	-	0.3-0.6	Triaxial tests and DSS tests	Keaveny et al. (1989)
Clay	Undrained shear strength c_u	-	0.8-6.1	Laboratory test	Phoon and Kulhawy (1996)
Clay	Undrained shear strength c_u	46-60	2-6.2	VST	Phoon and Kulhawy (1996)
Clay, loam	Total unit weight γ	-	2.4-7.9	-	Phoon and Kulhawy (1996)
Clay	Effective unit weight γ	-	1.6	-	Phoon and Kulhawy (1996)

2.9. Previous works on reliability analysis

Reliability calculations offer a way to assess the collective impact of uncertainties and to identify situations where uncertainties are notably high or low. Despite its potential utility, reliability theory is not extensively applied in standard geotechnical practices for two main reasons. Firstly, the theory introduces terms and concepts that are unfamiliar to many geotechnical engineers. Secondly, there is a prevailing perception that integrating reliability theory into practice would demand more data, time, and effort than what is typically available in most situations.

2.9.1. Essential principles of reliability

The initial phase in assessing the reliability of any system, involves identifying the pertinent uncertain input parameters within the geotechnical model. These parameters are referred to as

basic random variables (X_i), and their connection with the system's performance (Z) is established.

$$Z = g(X) = g(X_1, X_2, \dots, X_n) \quad (2.10)$$

In Eq. (2.10), X represents the vector of the random variable X_i and $g(X)$ is the state function or performance function. The failure of the structure is described by the condition $Z < 0$ and the safety (security) of the structure is described by the condition $Z > 0$, thus the limit state function is $Z = 0$ which represents the boundary between safe and failure regions.

The probability of failure corresponds to the probability that the system is unable to execute its intended function, represented by the following integral:

$$P_f = P(Z < 0) = \int_{X \in F} \int \dots \int f_x(x_1, x_2, \dots, x_n) dx_1 dx_2 \dots dx_n \quad (2.11)$$

where $f_x(x_1, x_2, \dots, x_n)$ is the joint probability density function (PDF) for X .

Reliability is characterized as the probabilistic metric assessing the confidence in performance assurance. It is common to represent the reliability through a reliability index (β), which is calculated as the ratio of the mean to the standard deviation of the performance function

$$\beta = \frac{\mu_z}{\sigma_z} \quad (2.12)$$

where μ_z and σ_z are, respectively, the mean and standard deviation of Z .

The probability of failure can be expressed in term of the reliability index (β) as follow:

$$P_f = P(Z < 0) = \Phi\left(\frac{0 - \mu_z}{\sigma_z}\right) = \Phi(-\beta) = 1 - \Phi(\beta) \quad (2.13)$$

where $\Phi(\cdot)$ signifies the cumulative distribution function (CDF) of the standard normal distribution.

2.9.2. Reliability analysis methods

From the perspective of geotechnical engineering, obtaining the integral in Eq. (2.11) is challenging, and the assessment of multiple integrals proves to be exceedingly complex. For this purpose, different reliability analysis methods have been developed to align with the diverse types and complexities of performance functions.

2.9.2.1. First order reliability method

The First-Order Reliability Method (*FORM*) is an analytical probabilistic approach employed for assessing the probable reliability of an engineering problem. FORM solves the failure probability integral given in Eq. (2.11) by approximating the failure function or limit state function(s) $g(X)=0$, using a first-order Taylor series expansion centered at the most probable point (MPP). The FORM analysis contains three fundamental steps: (i) transformation of the random variables, (ii) search for the most probable point (MPP) and (iii) computation of probability of failure (P_f).

The first step concerns a transformation of a vector of random variables $X = [X_1, X_2, \dots, X_n]^T$ (in X -space) into standard normal variables $U = [U_1, U_2, \dots, U_n]^T$ using the Rosenblatt transformation

$$U_i = \Phi^{-1}[F_{X_i}(x_i)], \quad i = 1, 2, \dots, n \quad (2.14)$$

where Φ^{-1} represents the inverse of the cumulative distribution function (CDF) of the standard normal distribution. $F_{X_i}(x_i)$ represents the CDF of the random variable X_i . As a result of that transformation, the limit state function $g(X)=0$ in X -space becomes $g(U)=0$ in U -space. Fig. 2.13 shows a graphic illustration of this space transformation.

The next step is searching for the most probable point (MPP). It is expressed mathematically as follow:

$$\begin{cases} \min \beta = \|U\| \\ \text{s. t. } g(U) = 0 \end{cases} \quad (2.15)$$

where β represents the reliability index, which is the distance between the MPP and the origin in U-space as depicted in Fig. 2.13. An optimization algorithm based on gradients can be employed, where the calculation involves determining the search direction and the corresponding vector with normalized magnitude.

The last step is the computation of the probability of failure. At the Most Probable Point (MPP), the joint Probability Density Function (PDF) of U attains its maximum value on the limit state in U-space. To minimize the loss of accuracy, the Limit State Function (LSF) is linearized at the MPP in U-space. Subsequently, the probability in Eq. (2.11) is analytically calculated using the following equation:

$$F_z(z) = P[Z \leq 0] \cong \Phi(-\beta) \quad (2.16)$$

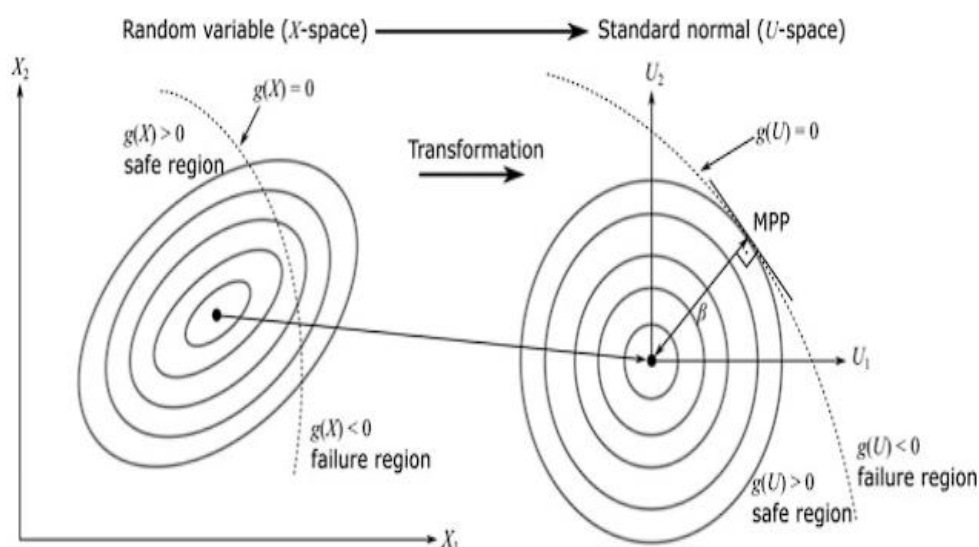


Fig. 2.13 Transformation of random variables into standard normal random variables.

2.9.2.2. Monte Carlo Simulation method

The Carlo simulation is a computational technique used to assess the probability distribution of the output variable based on the probability distributions of a specified set of input random variables. An essential step in the Monte Carlo simulation involves generating suitable values for the random variables, i.e., generating random numbers in alignment with the Probability Density Function (PDF) of the input random variables.

To illustrate the use of the Monté Carlo simulation in assessing failure probability, it's important to initially recognize that the probability of failure can be expressed mathematically as follows:

$$P_f = \int \dots \int I(x) f_x(x) dx \quad (2.17)$$

where $f_x(x)$ is the probability density function and $I(x)$ is the indicator function which is equal to 1 when x is in the failure region while it is equal to 0 when x is in the safe region.

The mean value of the indicator function $I(x)$ describes the failure probability with the following expression:

$$\hat{P}_f \approx \frac{1}{N} \sum_{i=1}^N I(x'_i) \quad (2.18)$$

where \hat{P}_f represents the approximation of the failure probability P_f . x'_i is the i^{th} sample of x and N represents the number of random simulations.

2.9.2.3. Importance Sampling method

The Importance Sampling method is a technique employed to improve the efficiency of Monte Carlo simulations, especially when rare events, such as system failures, are of interest. Concerning Monte Carlo simulations, samples are directly drawn from the probability density function $f_x(x)$ of the random variable X . In contrast, concerning importance sampling, samples are drawn from a distinct sampling function $s(x)$ instead of directly from $f_x(x)$. Thus, Eq. (2.17) is rewritten as follow:

$$P_f = \int \dots \int \{I(x)w(x)\}s(x)dx \quad (2.19)$$

where $w(x)$ denotes a weighting function expressed by the following equation:

$$w(x) = \frac{f_x(x)}{s(x)} \quad (2.20)$$

Therefore, the estimated failure probability linked to an estimator is given as follows (Ang and Tang, 1984):

$$\hat{P}_f \approx \frac{1}{N} \sum_{i=1}^N I(x') w(x') \quad (2.21)$$

2.9.2.4. Additional methods

Numerous reliability analysis methods have been documented in the literature, such as the Second-Order Reliability Method (SORM), Subset Simulation, Response Surface Method (RSM), Advanced First-Order Reliability Method (AFORM) and various Hybrid Methods. Due to space limitations, it is not feasible to comprehensively cover all of these methods in this thesis.

2.9.3. Quantification of geotechnical uncertainties

The seismic bearing capacity analysis is typically performed assuming homogeneous soils and deterministic earthquake properties. However, soil properties, including shear strength parameters, exhibit random variations even within a single soil layer (Johari et al. 2017). Therefore, reliability analysis offers a suitable approach to account for this randomness, providing a rational framework for selecting appropriate bearing capacities. This approach empowers geotechnical designers to assess the reliability of their designs effectively.

Numerous studies have explored the reliability analysis of shallow foundations under static loads considering the stochastic nature of soil properties in terms of statistical moments or failure probability (Griffiths et al., 2002; Al-Bittar and Soubra, 2014; Pula and Chwala, 2015; Al-Bittar and Soubra, 2016; Jha, 2016; Al-Bittar et al., 2018; Brahmi et al., 2018; Pula and Chwala, 2018; Wu et al., 2019; Simoes et al., 2020).

Griffiths et al. (2002) conducted a probabilistic analysis on the bearing capacity of a shallow rough rigid strip footing on weightless cohesive soil. They employed analysis is a combination of the random field theory and the conventional nonlinear finite element algorithm, integrated with Monte Carlo simulations. Their findings indicated that the mean bearing capacity, accounting for spatially varying shear strength, consistently appeared lower than the deterministic bearing capacity. Moreover, they noted a decrease in the bearing capacity with

an increase in both the coefficient of variation of the undrained cohesion (COV_{c_u}) and the spatial correlation length (Fig. 2.14).

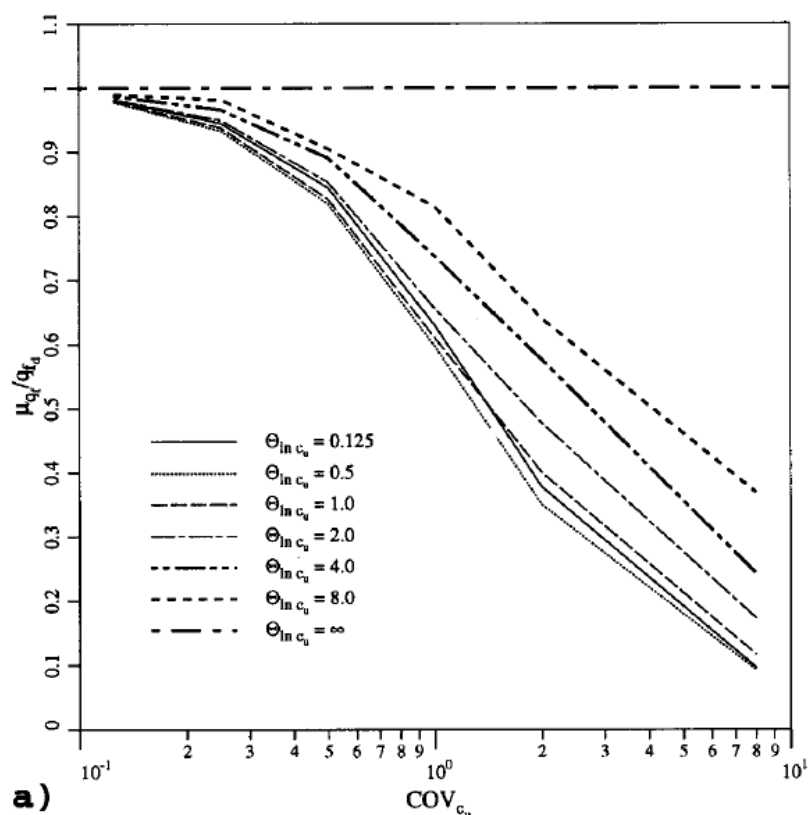


Fig. 2.14 Influence of COV_{c_u} and correlation length on the mean bearing capacity (Griffiths et al., 2002).

Al-Bittar and Soubra, (2016) conducted a probabilistic investigation focused on evaluating the probability density function associated with the bearing capacity of a shallow strip footing. This analysis was carried out considering a rock mass characterized by spatial variability and assuming adherence to the generalized Hoek-Brown failure criterion. Their results revealed that the variability of the bearing capacity increases with the increase of the coefficient of variation of the rock parameters (σ_c and GSI).

Brahmi et al. (2018) integrated a finite element limit analysis with the random field theory to conduct a probabilistic assessment of the undrained bearing capacity of strip footings situated near slopes and subjected to inclined loads. Their results revealed a substantial influence of the coefficients of variation of the undrained cohesion (COV_{c_u}) and the spatial correlation length on the undrained bearing capacity.

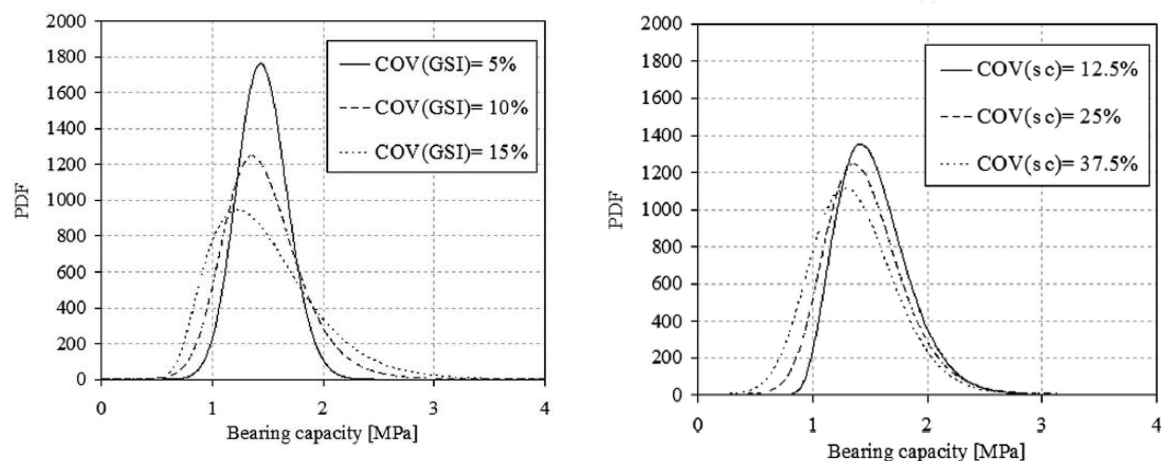


Fig. 2.15 Influence of rock parameters uncertainties on the PDF of bearing capacity (Al-Bittar & Soubra, 2016).

In the dynamic bearing capacity context, only four studies on the reliability analysis of shallow foundations are available. [Massih et al. \(2008\)](#) employed a probabilistic methodology to analyze the behavior of a shallow strip footing subjected to vertical loads, both with and without pseudo-static seismic loads. Their investigation revealed a noteworthy impact on the failure probability of the bearing capacity, specifically driven by variations in the coefficient of friction angle and the horizontal seismic acceleration coefficient. [Johari et al. \(2017\)](#) used the random field theory to evaluate the reliability of the seismic bearing capacity of a strip footing considering the geotechnical and earthquake properties uncertainty. Their results indicated that, the reduction in the correlation length led to an increase in the mean of the seismic bearing capacity and a simultaneous decrease in the standard deviation. [Hamrouni et al. \(2021\)](#) applied the finite difference method to assess the reliability of the pseudo static seismic bearing capacity of a shallow strip footing. They have shown that the option of the negative correlation between the soil shear strength parameters provides a conservative result. [Krishnan et al. \(2021\)](#) incorporated the spatial variability of soil properties into their seismic bearing capacity factor model through the discretization of the random field theory using the KL-expansion method. Their findings revealed that as the vertical correlation distance increased, the seismic bearing capacity factor exhibited a decrease. Furthermore, they noted that the failure probability was not directly influenced by the magnitude of the mean seismic bearing capacity factor.

2.10. Conclusion

This chapter begins with a review of previous studies on the seismic bearing capacity of shallow foundations. After that, it discusses different sources of uncertainties and their characterization. Finally, it introduces the reliability analysis methods for dealing with uncertainty and their application in static and dynamic bearing capacity analyses.

RELIABILITY-BASED ANALYSIS OF
SEISMIC BEARING CAPACITY

3.1. Introduction

The objective of this chapter is to perform a reliability analysis of the seismic bearing capacity for shallow strip footings situated on soils with randomly varying properties and earthquake parameters. This analysis utilizes existing seismic bearing capacity formulas developed by [Conti \(2018\)](#) that considers two types of soil supporting the strip footing: purely cohesive and cohesive-frictional. These formulas extend to more general conditions other literature results, allowing to take into account easily the effects of inertia forces acting both on the superstructure (load inclination and eccentricity) and into the foundation soil. The randomness inherent in soil parameters is accounted for using the Karhunen-Loève (KL) expansion method within the framework of random field theory. The chapter investigates the impact of Autocorrelation Functions (ACFs), Scale of Fluctuations (SOFs), and the coefficients of variation (COVs) of the parameters on the probability density function (PDF), probability of failure (Pf), and statistical moments (mean, standard deviation, and COV) of the seismic bearing capacity.

3.2. Numerical procedure

This work employs a numerical technique that incorporates both probabilistic and reliability assessments to evaluate the impact of spatial variations in soil properties. This method combines simplified seismic bearing capacity formulas with random field theory to account for uncertainties in the soil properties of cohesive or cohesive-frictional soils. It uses the KL expansion method ([Constantine, 2022](#)) to generate realistic variations in the soil properties across one or two dimensions. The seismic bearing capacity analysis proceeds through the following steps:

- 1) **Defining Statistical Inputs:** Establish parameters such as mean value, variance (or coefficient of variation), number of simulations (N_{sim}) and autocorrelation function. For the cohesive frictional soil, determine the cross-correlation coefficient (ρ_{ij}) between the cohesion and the frictional angle. Define horizontal and vertical scales of fluctuation (autocorrelation lengths).
- 2) **Discretizing Random Fields:** Create a mesh around the footing's edge for analysis (refer to [Fig. 3.1](#)).
- 3) **Generating Realizations of Cross-Correlated Random Fields:** Simulate N_{sim} realizations of the cross-correlated random field. Example shear strength parameter realizations (cohesion c and friction angle φ) are depicted in [Fig. 3.2](#).

- 4) Incorporating Realizations into bearing capacity formulas: Utilize the N_{sim} realizations of the random fields for the parameters in a Monte Carlo simulation to compute seismic bearing capacities using the provided formulas in [Table A.1](#) of [Appendix](#).
- 5) Analyzing Statistical Response: Evaluate outputs such as mean, standard deviation, coefficient of variation of bearing capacity, and probability density function.
- 6) Calculating Probability of Failure: Employ bearing capacities from N_{sim} simulations in [Eq. \(2.10\)](#) of the limit state function. Adjust applied load values to transition from the safe domain ($p_f = 0$) to the failure domain $p_f = 1$ at each step.

These steps are implemented in a MATLAB code, permitting the presentation and analysis of results through tables and figures.

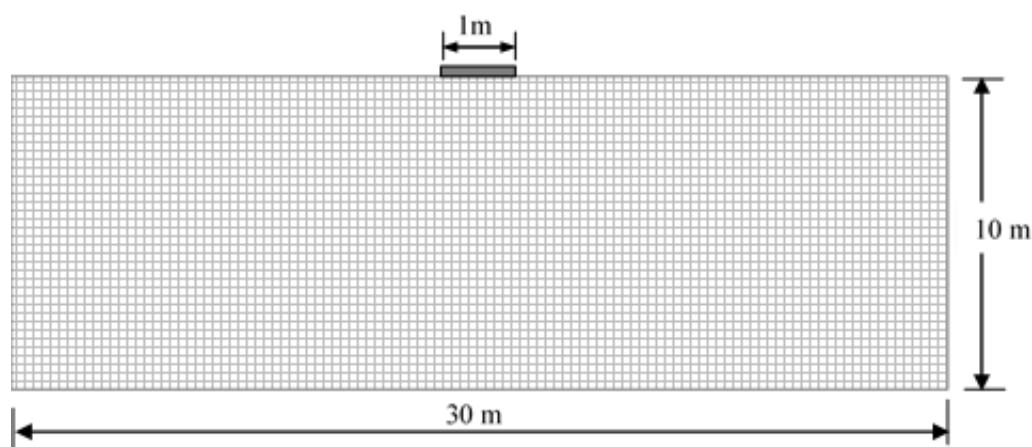


Fig. 3.1 The mesh employed for discretizing the random fields.

3.3. Validation examples

This section conducts validation examples to confirm the accuracy of the obtained results and to compare them with other numerical and rigorous methods.

3.3.1. Random field realizations

To begin, an example of random fields illustrating the cohesion and the friction angle, discretized according to the normal distribution with statistical inputs outlined in [Table 3.1](#), is presented. A mesh measuring 128 x 64 dimensions is utilized. The mean and standard deviation values attained through the Karhunen–Loève (KL) expansion method are compared in [Table 3.1](#) with those derived from the local average subdivision method (LAS) ([Alamanis and Dakouakas, 2019](#)). [Table 3.1](#) demonstrates that the KL method yields mean and standard deviation values for the cohesion (c) and a standard deviation value for the friction angle (ϕ),

which are closest to the exact values when compared to the LAS method. Additionally, a single realization of the random fields for the cohesion and the friction angle is illustrated in Fig. 3.2.

Table 3.1. Comparison between the exact and estimated values of soil properties obtained using the KL method and LAS method.

Parameter	Exact mean (μ)	Attained μ by present KL	Attained μ by LAS	Exact standard deviation (σ)	Attained σ by present KL	Attained σ by LAS
Cohesion c (kPa)	30	30.0453	30.0746	9	8.7336	7.579
Friction angle ϕ (degree)	30	30.0508	30.0096	6	5.8752	5.111

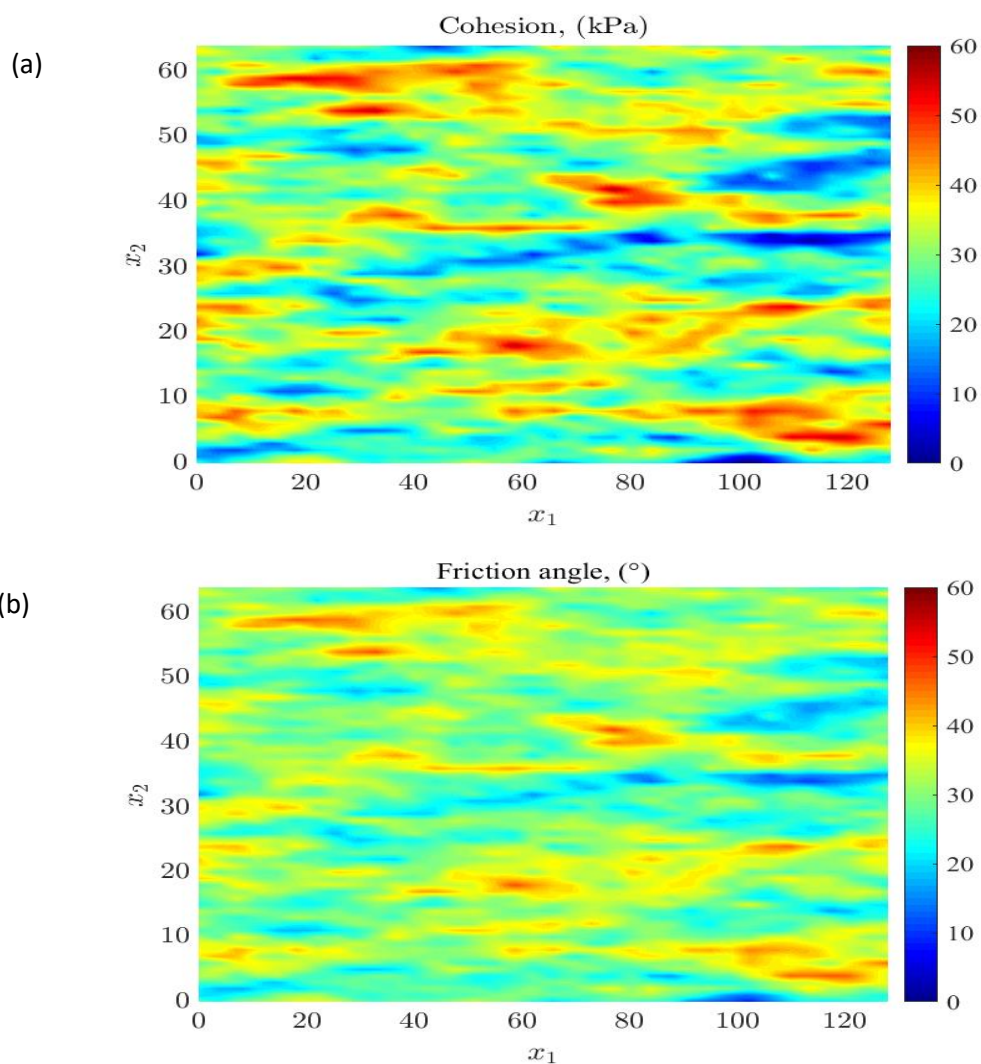


Fig 3.2 Simulation of Gaussian random fields with $\delta_h=20\text{m}$ and $\delta_y=2\text{m}$ for: (a) soil cohesion with $\mu_c = 30 \text{ kPa}$ and $\sigma_c = 9 \text{ kPa}$, (b) soil friction angle with $\mu_\phi = 30 \text{ kPa}$ and $\sigma_\phi = 9$.

3.3.2. Validation of the statistical moments associated with the static bearing capacity

This first example involves verifying the statistical moments of the bearing capacity of a shallow strip footing situated on soils with spatially and randomly varying properties. The comparison is made with previously published results in the static case ($k_h=0$). Since not all statistical moments of the bearing capacity may be available in a single study, various examples of the mean (μ) and standard deviation (σ) or coefficient of variation (COV) values of the strength parameters are considered for comparison.

Fig. 3.3 compares the variation of the mean normalized bearing capacity against the coefficient of variation of the undrained shear strength (cohesion c_u) (COV_{cu}) for a strip footing situated on a purely cohesive soil with a mean value of c_u equal to 100 kPa, to that published by Griffiths et al. (2002). In their study, Griffiths et al. (2002) conducted bearing capacity analyses using a conventional nonlinear finite element algorithm combined with the random field theory, in conjunction with a Monte Carlo method, for a 1m wide strip footing. As depicted in Fig. 3.3, both sets of results exhibit a similar trend, with a maximum relative difference of approximately 28% observed for a COV_{cu} of 50%.

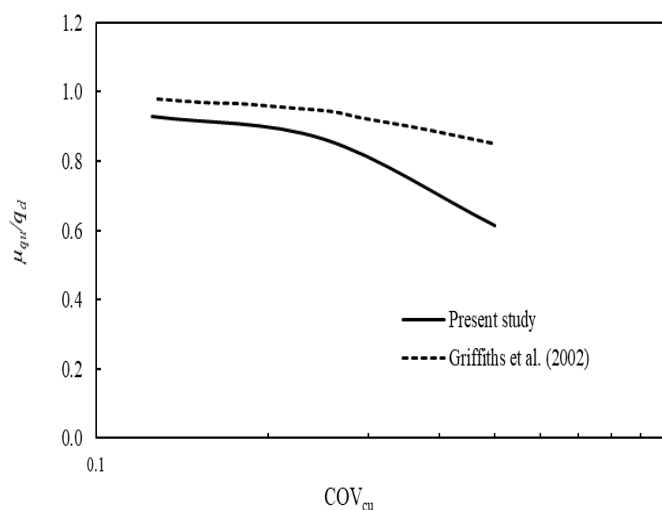


Fig. 3.3 Comparison between the normalized bearing capacity obtained in the present study and that reported by Griffiths et al. (2002) for a case of $\mu_{cu} = 100$ kPa, $\delta_x = \delta_y = 2$ m and $k_h = 0$.

In the second example, the current results obtained using the simplified Conti (2018) formulas are verified against those obtained by Luo and Bathurst (2017) when conducting a reliability bearing capacity analysis of a footing on cohesive soil slopes using the random finite element method (RFEM). Fig. 3.4 illustrates the variation of the coefficient of variation (COV) of the

bearing capacity factor (N_c) for a 1m wide footing resting on purely cohesive soil with unit weight and mean cohesion of 20 kN/m^3 and 20 kPa , respectively. The results presented by [Luo and Bathurst \(2017\)](#) correspond to the scenario of a strip footing on level ground, i.e., without slope. As depicted in the figure, the current results align well with those of [Luo and Bathurst \(2017\)](#) and remain slightly lower, as observed in the previous example.

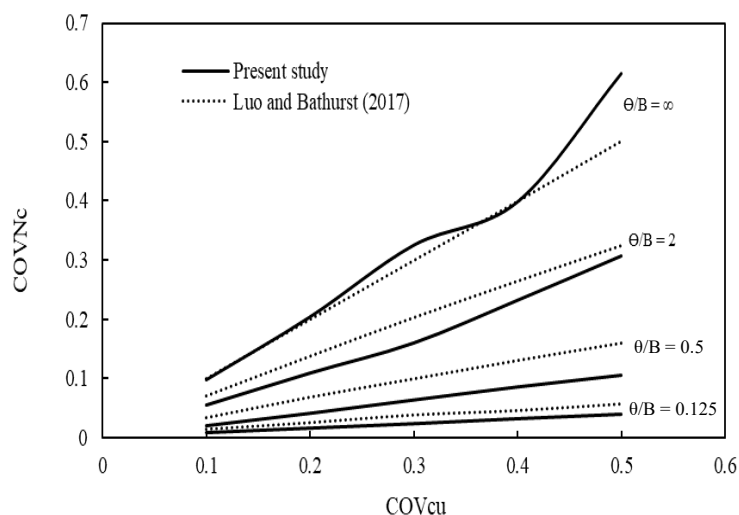


Fig. 3.4 Comparison between the coefficient of variation (COV) of the bearing capacity factor (N_c) obtained in the present study and that reported by [Luo and Bathurst \(2017\)](#) for a case of $\mu_{cu} = 20 \text{ kPa}$, $\gamma = 20 \text{ kN/m}^3$ and $k_h = 0$.

In the third example, we verify the statistical moments of the static bearing capacity obtained in the present study against those provided by [Cho and Park \(2010\)](#). Cho and Park investigated the impact of the spatial variability of the cross-correlated strength parameters (c and ϕ) on the bearing capacity of a strip footing using an approach integrating a commercial finite difference method and random field theory. They generated cross-correlated non-Gaussian random fields based on the Karhunen-Loève method.

It's worth noting that in the deterministic analysis, [Cho and Park \(2010\)](#) estimated the bearing capacity to be 1.01 MPa , which closely matched the value of 1.04 MPa obtained from the [Terzaghi \(1943\)](#) formula. In contrast, in the present study, it is estimated to be 1.03 MPa . This disparity is expected since the [Conti \(2018\)](#) formulas used in our study were based on Terzaghi's equation for vertical bearing capacity.

Figs. 3.5 and 3.6 illustrate the variation of the mean value, standard deviation, and coefficient of variation (COV) of the bearing capacity against the horizontal and vertical standardization of fluctuation (SOF), respectively. It can be observed from these figures that the present results exhibit similar patterns to those of [Cho and Park \(2010\)](#) but are consistently lower. In other words, the present results, based on the simplified [Conti \(2018\)](#) formulas, are always conservative concerning cohesive-frictional soils due to the utilization of the all-minimum procedure as concluded by [Conti \(2018\)](#).

Furthermore, in the case of cohesive-frictional soil, the mean static bearing capacity remains nearly constant as the horizontal standardization of fluctuation (SOF) increases from 5m to 30m, a trend comparable to that identified by [Cho and Park \(2010\)](#) (Fig. 3.5a). [Dobrzański and Kawa \(2021\)](#) also observed this pattern for purely cohesive soil within the same range of SOF.

However, as depicted in Fig. 3.6a, the mean static bearing capacity exhibits minimal fluctuations around a value of 1060 kPa as the vertical SOF increases from 1m to 10m, mirroring the pattern identified by [Cho and Park \(2010\)](#). It's worth noting that this behavior was observed for $COV_c = 30\%$ and $COV_\phi = 20\%$.

In contrast, for purely cohesive soil, [Jha \(2016\)](#) noted that regardless of whether $\delta_h = \delta_v$ or δ_h differs from δ_v , the mean normalized static bearing capacity experiences a slight decrease as the horizontal SOF increases, reaching a minimum, and then slightly increasing. The maximum variation increment is less than 1%. This trend was observed for two values of COV_{cu} (30% and 50%), with the reduction being less pronounced for COV_{cu} of 30%. A similar pattern was also observed in the results obtained by [Pula and Chwala \(2018\)](#).

3.3.3. Validation of the failure probability associated with the static bearing capacity

In this fourth and final validation example, we compare the failure probability of the static bearing capacity obtained in the present study with the results of [Massih et al. \(2008\)](#) and [Krishnan and Chakraborty \(2021\)](#). [Krishnan and Chakraborty \(2021\)](#) explored the seismic bearing capacity of a strip footing over a c- ϕ soil using a finite element lower bound limit analysis formulation in conjunction with a modified pseudo-dynamic approach for considering

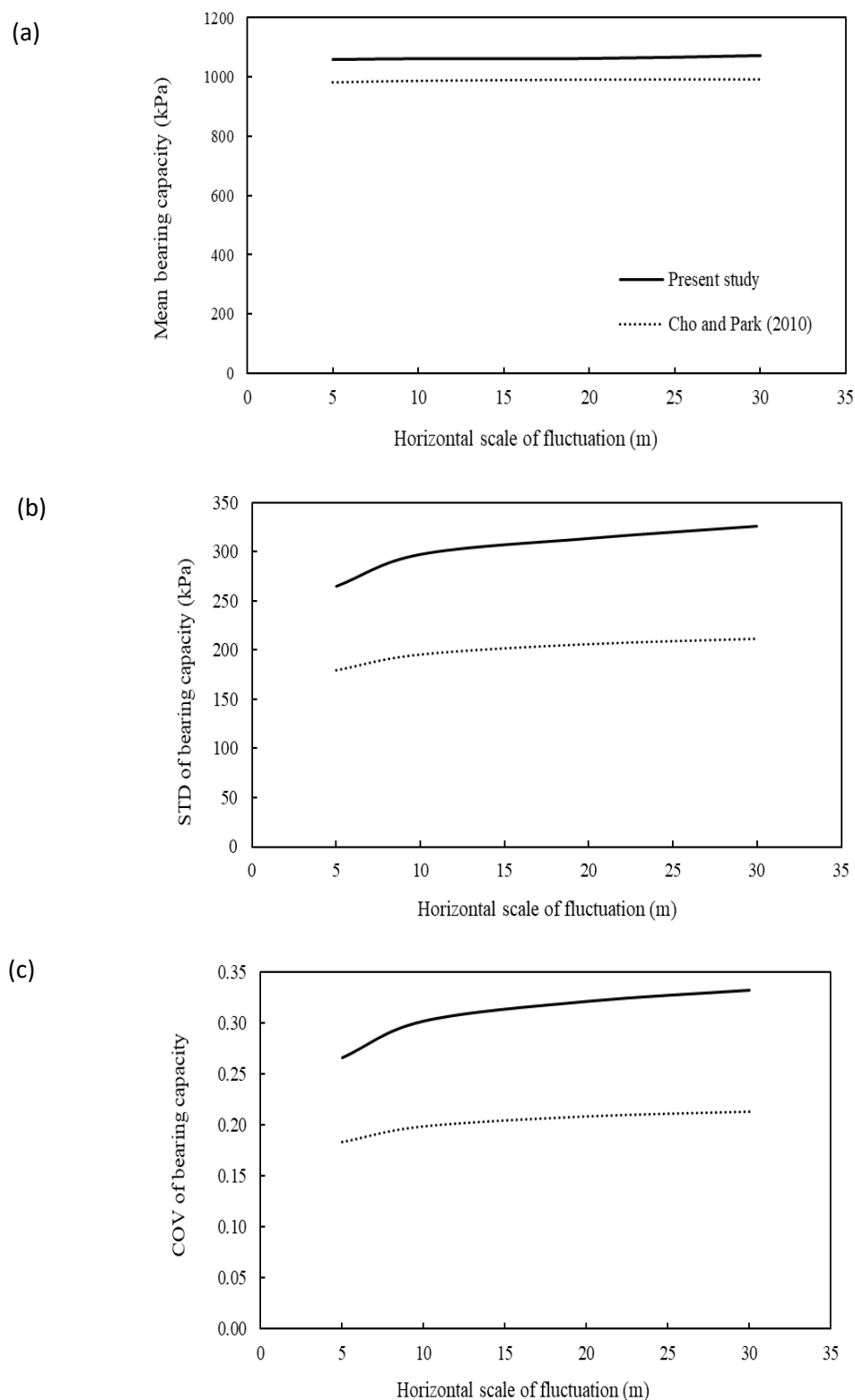


Fig. 3.5 Validation of the statistical characteristics of the static bearing capacity obtained in the present study compared to those reported by [Cho and Park \(2010\)](#) for a case of $r(c, \phi) = -0.5$, $COV_c = 30\%$, $COV_\phi = 20\%$, $\delta_v = 1\text{m}$ and $kh = 0$.

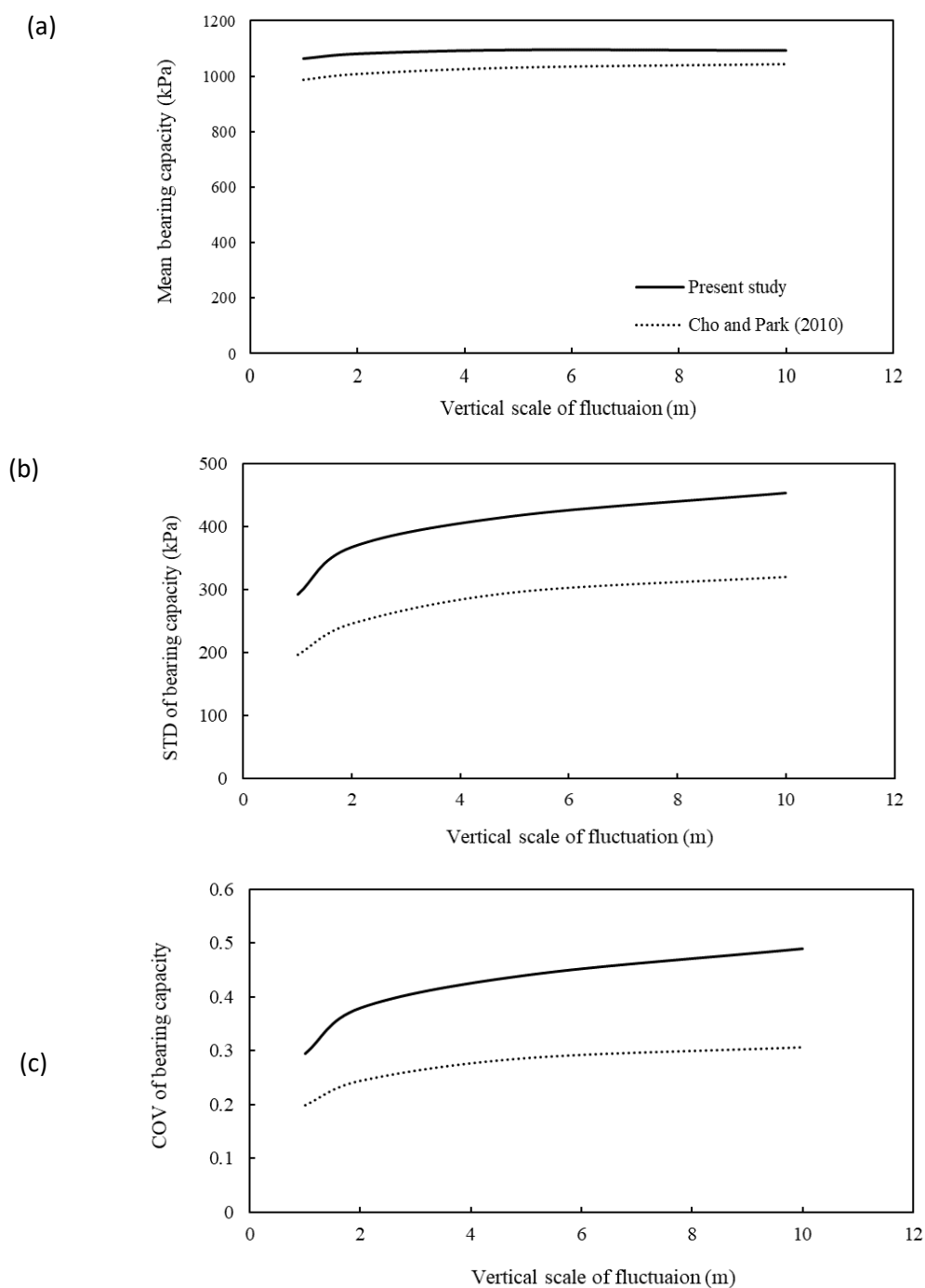


Fig. 3.6 Validation of the statistical characteristics of the static bearing capacity obtained in the present study compared to those reported by [Cho and Park \(2010\)](#) for a case of $r(c, \phi) = -0.5$, $COV_c = 30\%$, $COV_\phi = 20\%$, $\delta_h = 10\text{m}$ and $k_h = 0$.

seismic action. They discretized soil properties (c and ϕ) spatially using the Karhunen-Loève (KL) expansion method and obtained statistical responses via Monte Carlo Simulation.

On the other hand, [Massih et al. \(2008\)](#) investigated the ultimate bearing load of a $c-\phi$ soil in a reliability context using a pseudo-static approach with the help of the upper bound limit analysis. It's noteworthy that in the present study, the random parameters are generated according to the normal distribution, whereas in the other two papers for comparison, they are obtained with the lognormal distribution.

[Fig. 3.7](#) presents a comparison of the failure probability (or cumulative distribution function, CDF) plots of the ultimate bearing capacity for the static case among the three studies. Despite the use of normal distribution for the parameters in the present study versus the lognormal distribution in the other two studies, it is evident from [Fig. 3.7](#) that the present study offers the highest failure probabilities, while of [Massih et al. \(2008\)](#) provides the lowest. In other words, the bearing capacity formulas used in the present analysis, based on the all-minimum procedure, are more conservative than those obtained by the lower bound method ([Krishnan and Chakraborty, 2021](#)) and consequently, those obtained by the upper bound method ([Massih et al. 2008](#)). Unfortunately, there are no results available for comparison in the seismic case.

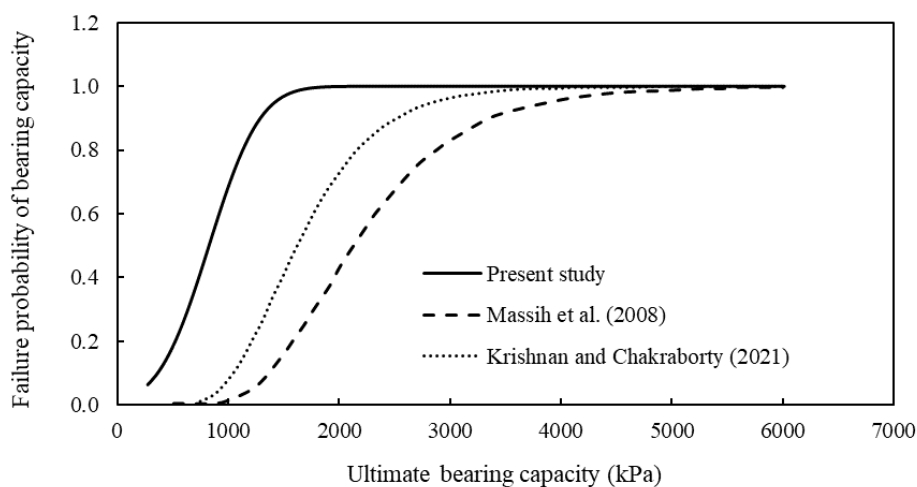


Fig. 3.7 Validation of the failure probability associated with the bearing capacity obtained in the present study compared to that reported by [Massih et al. \(2008\)](#) and [Krishnan and Chakraborty \(2021\)](#) for: $r(c, \phi) = -0.5, \mu_\phi = 30^\circ, \mu_c = 20 \text{ kPa}, \text{COV}_\phi = 10\%, \text{COV}_c = 20\%$ and $k_h = 0$.

3.4. Results and discussions

The objective of this section is to examine the influence of the autocorrelation functions (ACFs), the scale of fluctuations (SOFs) and the coefficient of variation (COV) of the key parameters governing the seismic bearing capacity on the probabilistic outcomes for two distinct soil types.

To achieve this objective, we analyze a shallow strip footing with a width of 1m subjected to seismic loading ($q = 20$ kPa). The strip footing is assumed to rest on two different types of soil: cohesive frictional soil (with $c \neq 0$, $\phi \neq 0$) and purely cohesive soil (with $c = c_u$, $\phi = 0$). Each soil type is characterized by its statistical inputs as provided in [Tables 3.2](#) and [3.3](#).

Table 3.2. Statistical parameters for the cohesive frictional soil.

Parameter	Mean (μ)	Coefficient of variation (COV)	PDF
Cohesion c (kPa)	20	20%	Normal
Friction angle ϕ (degree)	30	10%	Normal
Horizontal seismic coefficient k_h	0.2	25%	Log-Normal

Table 3.3. Statistical parameters for the purely cohesive soil.

Parameter	Mean (μ)	Coefficient of variation (COV)	PDF
Undrained shear strength c_u (kPa)	20	20%	Normal
Horizontal seismic coefficient k_h	0.15	25%	Log-Normal

3.4.1. Impact of Autocorrelation functions (ACFs) on the seismic bearing capacity

In the case of cohesive frictional soil, [Figs. 3.8a](#) and [3.8b](#) depict the Probability Density Function (PDF) and the failure probability, respectively, of the ultimate seismic bearing capacity for five different types of Autocorrelation Functions (ACFs) outlined in [Table 2.4](#) ([Chapter 2](#)). It's evident from these figures that all ACF types yield similar variability (PDF) of the seismic bearing capacity and corresponding probability of failure (P_f) for purely cohesive soil. However, only the SNE ACF yields a PDF and P_f distinct from the other four ACFs for the cohesive frictional soil.

Furthermore, we examine the impact of the ACF type on the statistical moments of the seismic bearing capacity (mean value $\mu(q_u)$, standard deviation $\sigma(q_u)$, coefficient of variation $COV(q_u)$) as presented in [Table 3.4](#). It is notable from [Table 3.4](#) that only the SNE ACF yields statistical

moments of the bearing capacity differing from those provided by the other ACF types and smaller than them, specifically for the cohesive frictional soil. This observation suggests that the commonly used SNE type of ACFs produces conservative results. It is important to note that only the SNE ACF will be utilized in all subsequent applications.

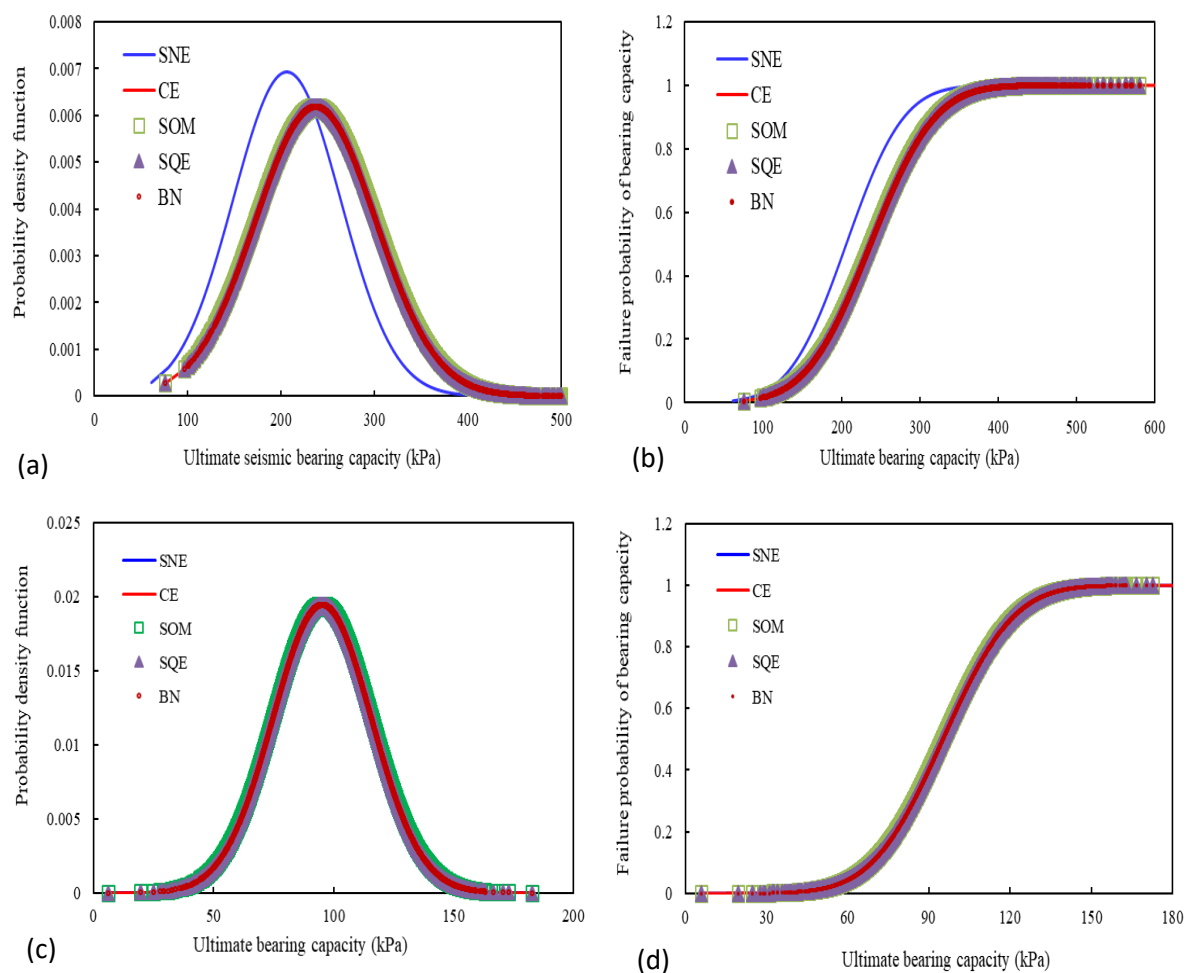


Figure 3.8 Impact of different types of autocorrelation functions (ACFs), with $\delta_h = 20\text{m}$ and $\delta_v = 2\text{m}$, on the probability density function (PDF) and the failure probability (P_f) of the seismic bearing capacity of a shallow strip footing resting on: (a) and (b) cohesive frictional soil, (c) and (d) purely cohesive soil.

Table 3.4. Impact of the type of autocorrelation functions (ACFs) on the statistical moments of the seismic bearing capacity of a shallow strip footing for $\delta_h = 20m$ and $\delta_v = 2m$.

ACF type	Cohesive frictional soil			Purely cohesive soil		
	μ_{qu} (kPa)	σ_{qu} (kPa)	COV_{qu} (%)	μ_{qu} (kPa)	σ_{qu} (kPa)	COV_{qu} (%)
SNE	206.17	57.55	27.91	95.21	20.51	21.54
CE	237.08	64.47	27.19	95.21	20.51	21.54
SOM	237.07	64.47	27.19	95.21	20.51	21.54
SQE	237.07	64.47	27.19	95.21	20.51	21.54
BN	237.07	64.47	27.19	95.21	20.51	21.54

3.4.2. Impact of COVs of seismic coefficients and strength parameters on seismic bearing capacity

In the case of cohesive frictional soil, Figs. 3.9a, 3.9b, and 3.9c illustrate the Probability Density Function (PDF) of the seismic bearing capacity for various values of the coefficient of variation (COV) of the seismic coefficient (COV_{kh}), the cohesion (COV_c) and the friction angle (COV_ϕ), respectively. For each of these figures, the COV of the parameter under consideration is varied while the COVs of the other two parameters remain equal to the values given in Table 3.2. The results indicate that increasing the COV of the cohesion or friction angle enhances the variability of the seismic bearing capacity, while this variability remains unchanged when the COV of the seismic coefficient increases.

Moreover, it is observed that the increase in the variability is more pronounced for the friction angle. The statistical moments of the seismic bearing capacity also exhibit sensitivity to the randomness of the soil parameters, as shown in Tables 3.5 and 3.6. For instance, increasing the COV_c from 10% to 20% (while maintaining COV_ϕ and COV_{kh} at 10% and 25%, respectively) leads to a 22.49% increase in the COV of the seismic bearing capacity (COV_{qu}). Similarly, increasing COV_ϕ from 5% to 10% (with COV_c and COV_{kh} at 20% and 25%, respectively) results in a 32.80% increase in COV_{qu} . On the other hand, increasing COV_{kh} from 20% to 40% leads to only a 0.56% increase in COV_{qu} .

In the case of purely cohesive soil, Figs. 3.10a and 3.10b depict the PDF of the undrained seismic bearing capacity for various values of the COV_{kh} and COV_{cu} (COV of the undrained shear strength), respectively. Each figure follows the same approach as in the previous case of the cohesive frictional soil. The results reveal that increasing the COV_{cu} enhances the variability of the seismic bearing capacity (Fig. 3.10b). Similarly, increasing the COV_{cu} from

15% to 20% (with COV_{k_h} at 25%) results in a 35.22% (Table 3.6) increase in COV_{q_u} . However, the increase in the COV_{k_h} from 20% to 40% does not influence the COV_{q_u} (Table 3.6).

Table 3.5. Impact of the coefficients of variation (COVs) of the seismic coefficient (k_h), cohesion (c), and friction angle (ϕ) on the statistical characteristics of the seismic bearing capacity of a shallow strip footing resting on cohesive frictional soil for $\delta_h = 20m$ and $\delta_v = 2m$

COV_{k_h} (%)	COV_c (%)	COV_ϕ (%)	μ_{q_u} (kPa)	σ_{q_u} (kPa)	COV_{q_u} (%)
20	20	10	678.96	155.03	22.83
40	20	10	677.77	155.65	22.96
60	20	10	675.52	156.72	23.20
25	10	10	584.59	97.77	16.72
25	20	10	563.50	115.40	20.48
25	30	10	509.64	153.44	30.11
25	20	5	571.70	89.92	15.73
25	20	10	563.56	117.72	20.89
25	20	15	549.17	155.85	28.38

Table 3.6. Impact of the coefficients of variation (COVs) of the seismic coefficient (k_h) and undrained shear strength (c_u) on the statistical characteristics of the seismic bearing capacity of a shallow strip footing resting on purely cohesive soil for $\delta_h = 20m$ and $\delta_v = 2m$.

COV_{k_h} (%)	COV_{c_u} (%)	μ_{q_u} (kPa)	σ_{q_u} (kPa)	COV_{q_u} (%)
20	20	98.77	12.87	13.36
40	20	98.77	12.87	13.36
60	20	98.77	12.87	13.36
25	15	100.49	10.12	10.08
25	20	99.09	13.50	13.63
25	25	94.20	16.92	17.97

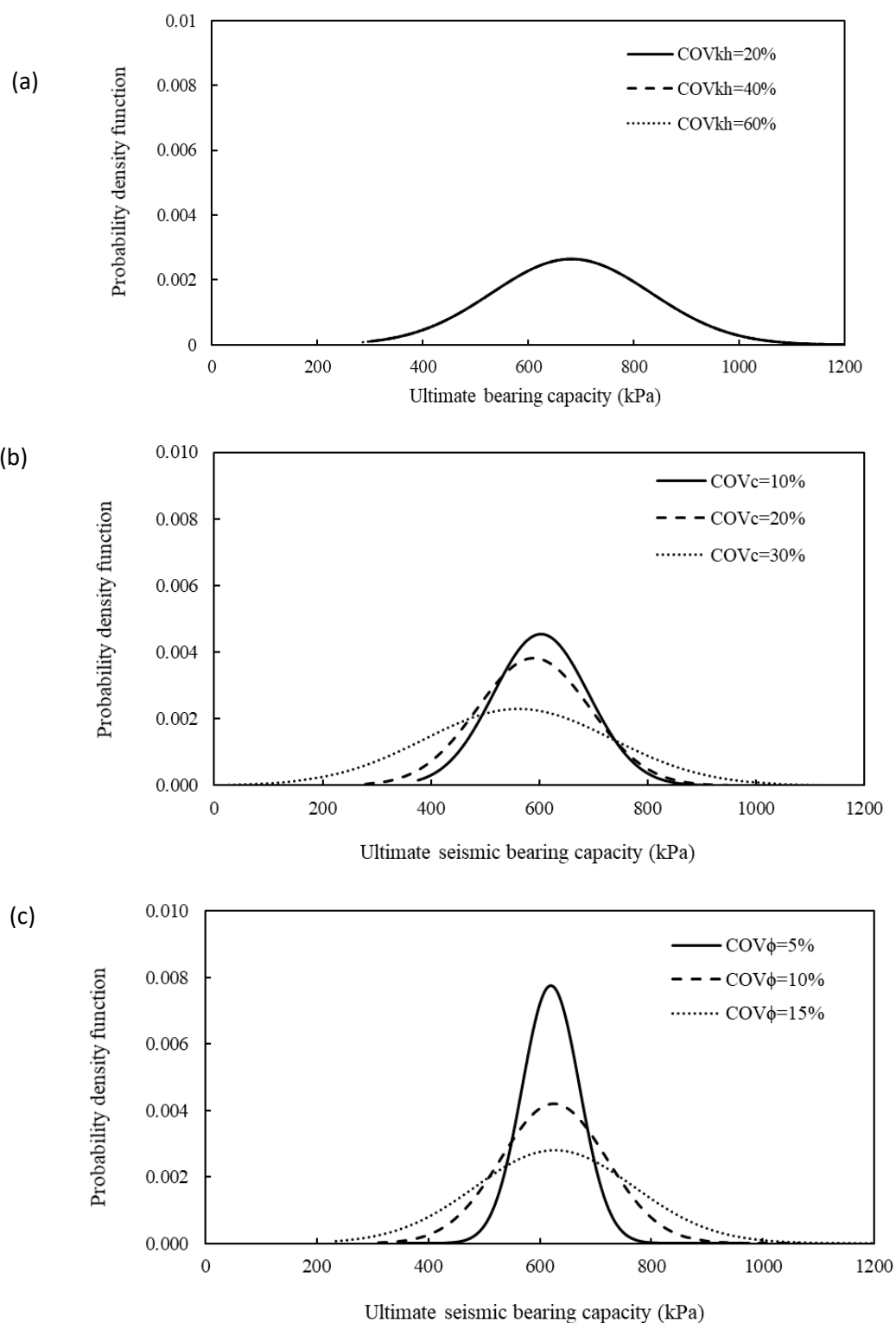


Fig. 3.9 Probability Density Function (PDF) of the seismic bearing capacity of strip footing resting on cohesive frictional soil for $\delta_h = 20m$ and $\delta_v = 2m$ for various $COVs$ of: (a) seismic coefficient, (b) cohesion, (c) frictional angle.

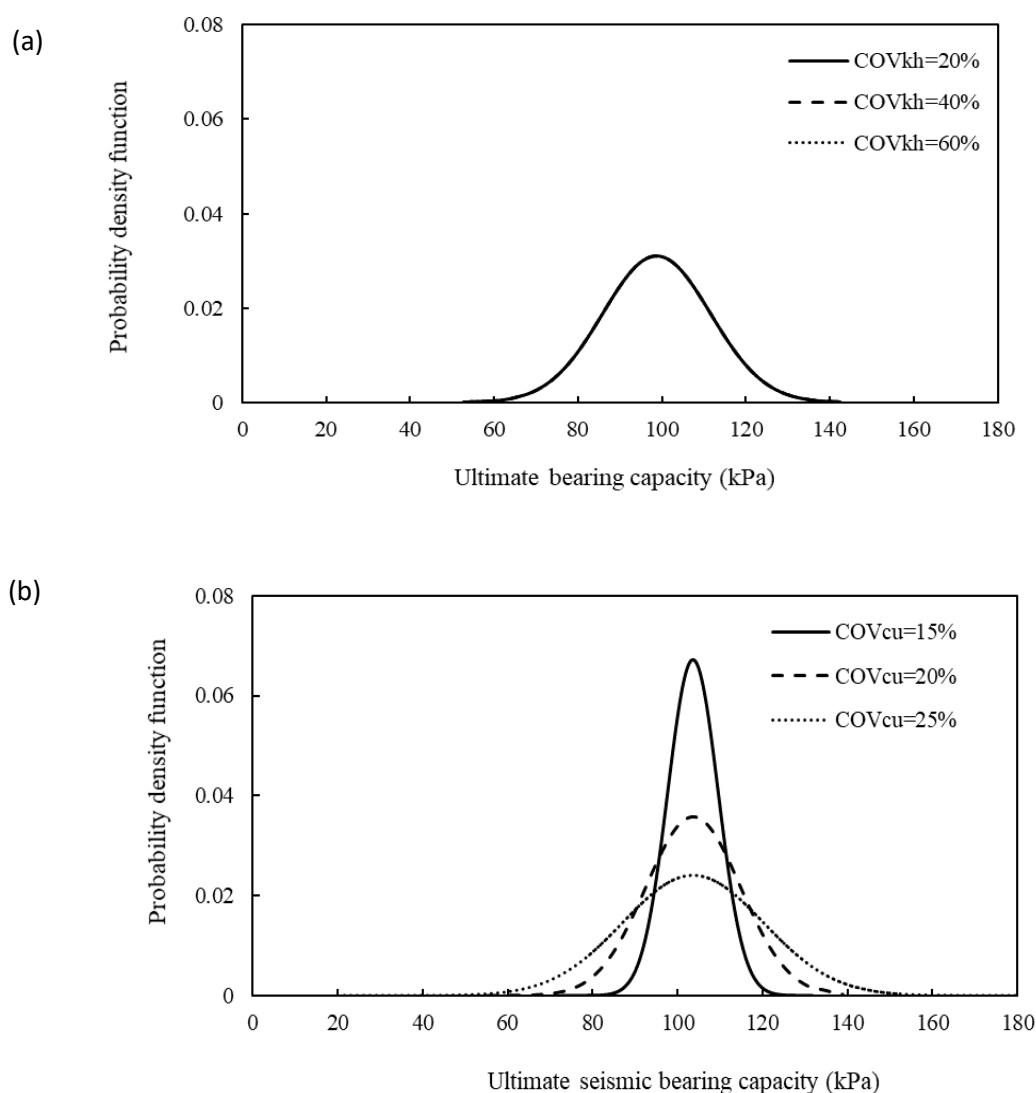


Fig. 3.10 Probability Density Function PDF of seismic bearing capacity of strip footing resting on purely cohesive soil for $\delta_h = 20m$ and $\delta_v = 2m$ for various *COVs* of: (a) seismic coefficient, (b) undrained shear strength.

3.4.3. Impact of scale of fluctuations (SOFs) on the seismic bearing capacity

Fig. 3.11 depicts the influence of variations in horizontal and vertical scale of fluctuations (SOFs) on the Probability Density Function (PDF) and failure probability of the seismic bearing capacity of a shallow strip footing on cohesive frictional soil. The results indicate that as the vertical SOF increases, the PDF becomes more dispersed. Additionally, the failure probability exhibits greater sensitivity to changes in vertical SOF compared to horizontal SOF. Similarly, in the case of the purely cohesive soil shown in Fig. 3.12, the effect of the horizontal and vertical SOF on the PDF and the failure probability of the seismic bearing capacity is

examined. Consistent with the cohesive frictional soil case, the PDF is less dispersed with increasing the horizontal SOF, and the failure probability is more responsive to changes in the vertical SOF compared to the horizontal SOF. Notably, the impact of vertical SOF on the PDF and failure probability is more pronounced than that of horizontal SOF.

Tables 3.7 and 3.8 provide insight into the influence of SOFs on the statistical moments (mean $\mu(q_u)$, standard deviation $\sigma(q_u)$ and coefficient of variation COV (q_u)) of the seismic bearing capacity. The results show slight fluctuations in the mean seismic bearing capacity, with fluctuations ranging between 0.4% and 2% for both soil types and for both horizontal and vertical SOFs. This finding aligns with the observations made by Chwala and Pula (2020) in their evaluation of the static bearing capacity of shallow foundations in a two-layered soil medium where the spatial variability in the soil strength parameters was considered only for the bottom purely cohesive layer.

Furthermore, the standard deviation of the seismic bearing capacity (σ_{q_u}) increases with increasing the horizontal or vertical SOF for both soil types. However, the coefficient of variation (COV_{q_u}) exhibits different trends, increasing for purely cohesive soil while fluctuating for cohesive frictional soil as the horizontal or vertical SOF increases.

Table 3.7. Impact of the horizontal SOF on the statistical moments of the seismic bearing capacity of a shallow strip footing for $\delta_v=6\text{m}$.

Soil type	Cohesive frictional soil			Purely cohesive soil		
δ_h (m)	μ_{q_u} (kPa)	σ_{q_u} (kPa)	COV_{q_u} (%)	μ_{q_u} (kPa)	σ_{q_u} (kPa)	COV_{q_u} (%)
20	561.14	114.61	20.43	98.15	13.55	13.81
40	560.27	124.53	22.23	97.48	13.60	13.96
60	568.76	137.88	24.24	98.30	13.81	14.05
80	568.29	131.01	23.05	98.52	13.99	14.21
100	559.05	127.71	22.85	97.73	14.50	14.85

Table 3.8. Impact of the vertical SOF on the statistical moments of the seismic bearing capacity of a shallow strip footing for $\delta_h = 60\text{m}$.

Soil type	Cohesive frictional soil			Purely cohesive soil		
δ_v (m)	μ_{q_u} (kPa)	σ_{q_u} (kPa)	COV_{q_u} (%)	μ_{q_u} (kPa)	σ_{q_u} (kPa)	COV_{q_u} (%)
2	561.14	114.61	20.43	98.15	13.55	13.81
4	573.68	141.23	24.62	98.79	15.14	15.33
6	553.93	159.89	28.86	98.78	16.08	16.29
8	563.33	151.40	26.88	99.46	16.40	16.49
10	556.56	155.99	28.03	98.39	16.52	16.80

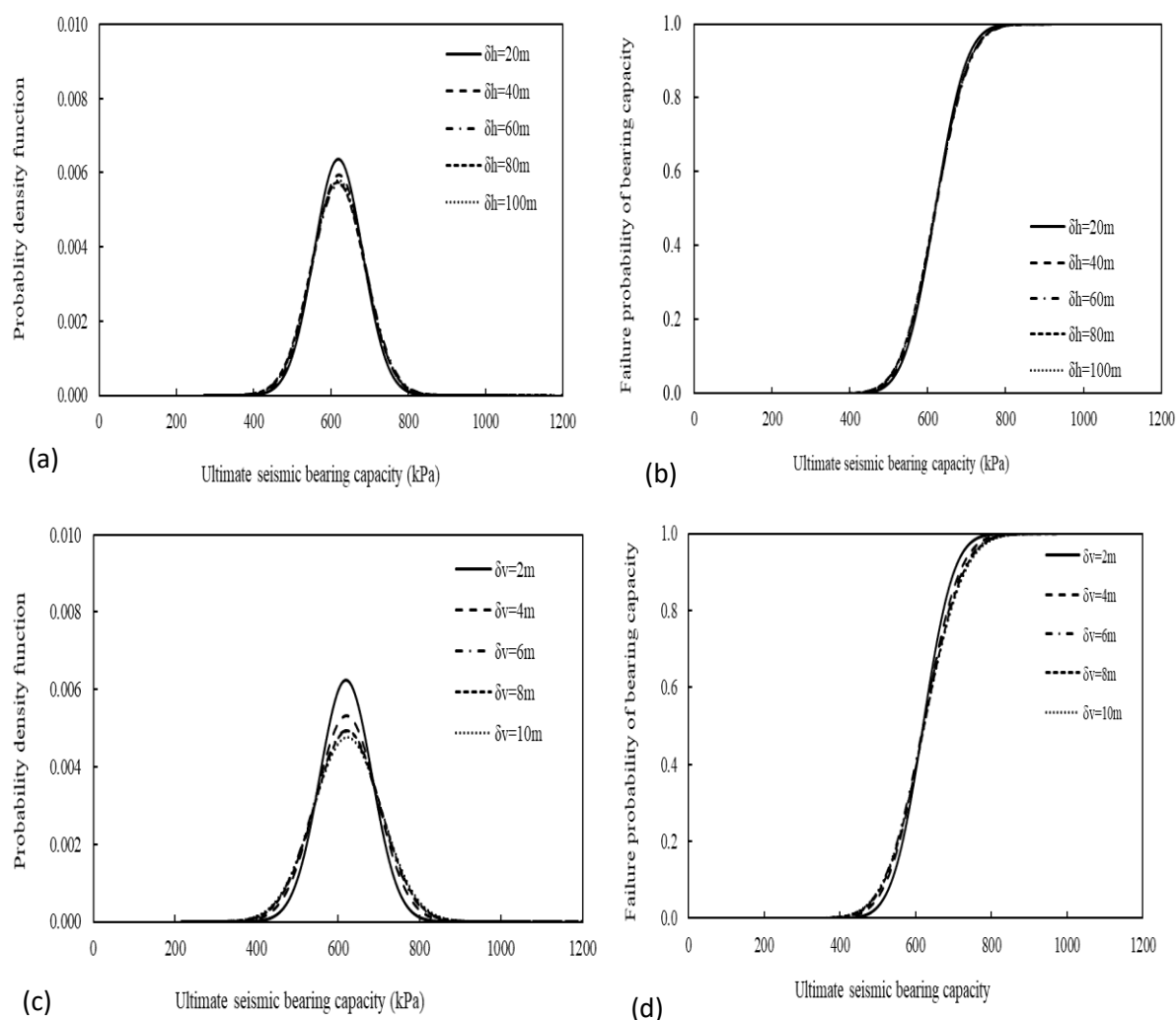


Fig. 3.11 Probability density function and failure probability of the seismic bearing capacity of a strip footing on cohesive frictional soil for various values of: (a) and (b) horizontal SOF and $\delta_v = 2\text{m}$, (c) and (d) vertical SOF and $\delta_h = 20\text{m}$.

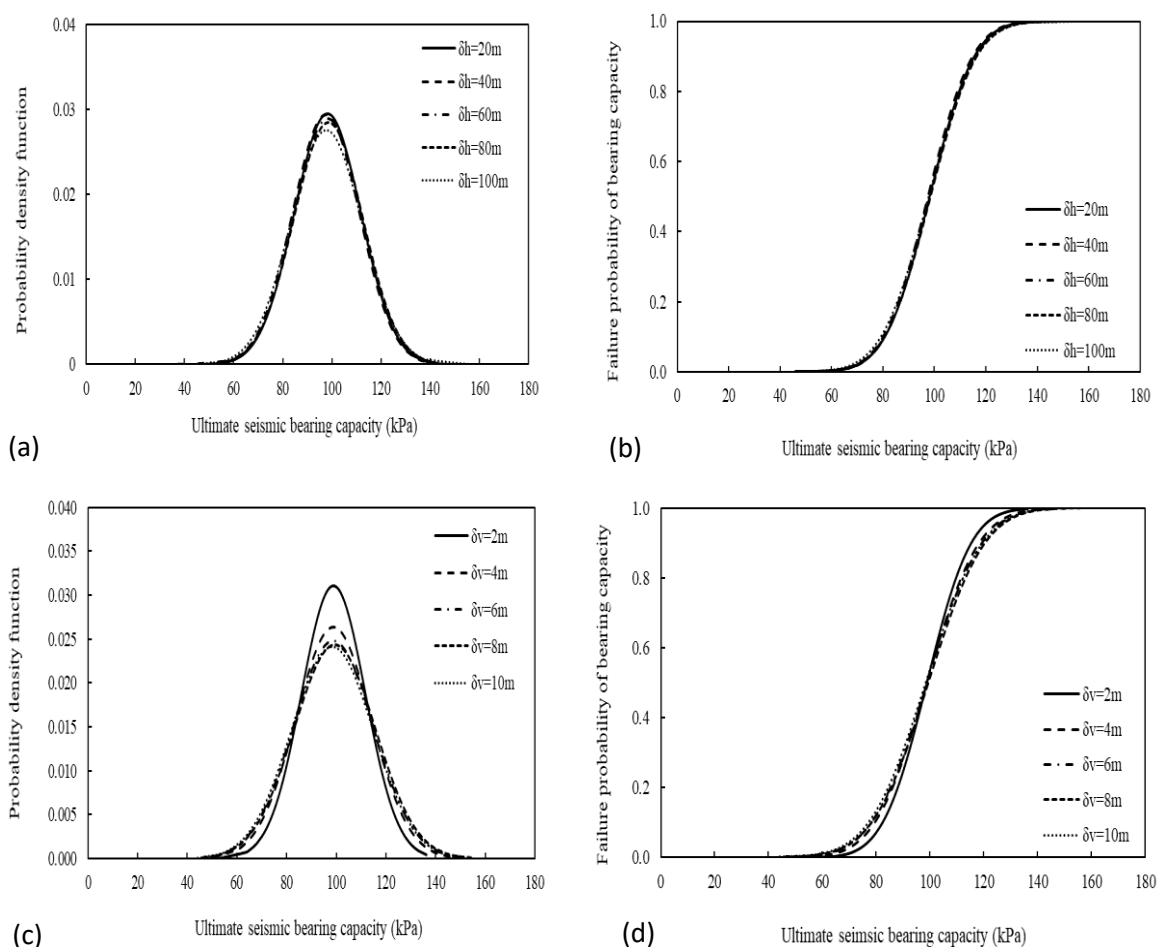


Fig. 3.12 Probability density function and failure probability of the undrained seismic bearing capacity of a strip footing on a purely cohesive soil for various values of: (a) and (b) horizontal SOF and $\delta v = 2\text{m}$, (c) and (d) vertical SOF and $\delta h = 20\text{m}$.

3.5. Conclusion

This chapter delved into the seismic bearing capacity analysis of a shallow strip footing, incorporating the variability of the shear strength properties and the seismic coefficients. The investigation was conducted in the framework of random field theory, involving reliability analysis of the seismic bearing capacity for two types of soils: purely cohesive and cohesive frictional. The Karhunen-Loève (KL) expansion method was employed to capture the randomness of the soil parameters. Results were presented in terms of statistical moments, probability density function, and failure probability of the seismic bearing capacity, accounting for the influence of the Autocorrelation Functions (ACFs), Scale of Fluctuations (SOFs) and

coefficient of variation of the random parameters. The main conclusions derived from this study include:

- The statistical moments of the bearing capacity differ only when using the SNE ACF compared to other ACF types, presenting conservative estimates for the cohesive frictional soil. However, for the purely cohesive soil, all the ACF types yield consistent results.
- The variability of the seismic bearing capacity increases with the higher coefficients of variation for the cohesion or friction angle, whereas the variability remains unaffected by increasing the coefficient of variation for the seismic coefficient.
- The mean seismic bearing capacity exhibits slight fluctuations when the horizontal SOF ranges from 20 m to 100 m and the vertical SOF ranges from 2 m to 10 m, with variations of less than 2% observed for both soil types and for both horizontal and vertical SOFs.

This study validates the reliability of the simplified formulas through comparisons with results obtained from rigorous methods, affirming their effectiveness and suitability for practical design applications.

SEISMIC BEARING CAPACITY OF
SHALLOW FOUNDATIONS IN
ANISOTROPIC NON-HOMOGENEOUS
MEDIA

4.1. Introduction

Surface waves typically arise when an earthquake originates near the Earth's surface. As their name implies, these waves travel just beneath the ground surface. While they move more slowly than S-waves, they often have larger amplitudes, making them a highly destructive type of seismic wave. The two most common types of surface waves are Rayleigh waves and Love waves.

Shallow foundations, being in direct contact with the Earth's surface, are particularly susceptible to the ground motion induced by the surface waves. The bearing capacity of these foundations, which is the ability to support vertical loads without excessive settlement or failure, becomes a critical concern in earthquake-prone regions. For this purpose, numerous studies were carried out considering the effect of these surface waves on the bearing capacity of shallow foundations (Saha and Ghosh, 2014, 2017; Pakdel et al., 2019; Izadi et al., 2022). Those studies are conducted under the assumption of a homogenous isotropic soil condition.

Another surface wave called torsional wave only propagates in non-homogeneous media (Rayleigh, 1945; Kumari and Sharma, 2014; Gupta et al., 2015; Vaishnav et al., 2017; Manna et al., 2018) did not gain any attention by researchers to take it into account through the estimation of the bearing capacity of shallow foundations.

Based on this point, the present chapter is dedicated to propose a comprehensive formula for the seismic bearing capacity of a strip footing over an anisotropic non-homogeneous soil layer covering a heterogeneous half-space taking the effects of the surface torsional wave using the pseudo-dynamic approach with the limit equilibrium method.

4.2. Torsional wave motions

To analyse the propagation of the torsional surface waves, a cylindrical coordinate system (r, θ, z), where the origin O is placed at the interface between the anisotropic non-homogeneous layer and the heterogeneous half-space, is adopted. The r -axis represents the direction of the wave propagation and the z -axis is oriented positively downward in the layered media, as depicted in Fig. 4.1. In this figure, a non-homogeneous anisotropic layer of finite thickness H is considered, where the non-homogeneity is assumed to vary exponentially with depth in the soil rigidity and mass density, along with the anisotropy in the rigidity ($N = N_0 e^{\frac{z}{\alpha}}$, $L = L_0 e^{\frac{z}{\alpha}}$,

$\rho = \rho_0 e^{\frac{z}{\alpha}}$. This layer is positioned over a heterogeneous half-space with a quadratic variation of the rigidity and the mass density ($\mu = \mu_1 \left(1 + \frac{z}{b_1}\right)$, $\rho = \rho_1 \left(1 + \frac{z}{b_1}\right)$). α and b_1 are constants having dimension equal to that of length.

Let u , v and w represent the particle displacement components along the radial (r), azimuthal (θ) and vertical (z) directions, respectively (Fig. 4.1). The torsional wave is characterized by the following displacement field (Love, 1944; Pramanik and Manna, 2022):

$$u = 0, w = 0, \quad v = v(r, z, t) \quad (4.1a)$$

The displacement component along the azimuthal direction (θ), $v(r, z, t)$, is expressed as

$$v(r, z, t) = V(z)J_1(kr)e^{i\omega t} \quad (4.1b)$$

where $V(z)$ represents the amplitude that describes how the particle displacement varies with depth. $J_1(kr)$ is the Bessel's function of the first order and first kind and k is the wave number.

For the displacement components given by Eq. (4.1a), the governing equations for the cylindrical coordinates (r, θ, z) (Kundu et al. 2014), in absence of body forces, is reduced to the following equation

$$\frac{\partial \tau_{r\theta}}{\partial r} + \frac{\partial \tau_{\theta z}}{\partial z} + \frac{2\tau_{r\theta}}{r} = \rho \frac{\partial^2 v}{\partial t^2} \quad (4.2)$$

where the stress components $\tau_{r\theta}$ and $\tau_{\theta z}$ are related to the displacement component by Eqs. (4.3a) for the non-homogeneous layer and by Eqs. (4.3b) for the heterogeneous half-space:

$$\tau_{r\theta} = N \left(\frac{\partial v}{\partial r} - \frac{v}{r} \right) \quad ; \quad \tau_{\theta z} = L \left(\frac{\partial v}{\partial z} \right) \quad (4.3a)$$

$$\tau_{r\theta} = \mu(z) \left(\frac{\partial v}{\partial r} - \frac{v}{r} \right) \quad ; \quad \tau_{\theta z} = \mu(z) \left(\frac{\partial v}{\partial z} \right) \quad (4.3b)$$

Substituting the displacement equation (Eq. (4.1b)) in the stress components (Eq. (4.3)), taking into account the variations in the rigidity and density as shown in Fig. 4.1 and setting

$$V(z) = \frac{V_1(z)}{\sqrt{L}}$$

for the layer and

$$V(z) = \frac{V_1(z)}{\sqrt{\mu}}$$

for the half-space where $V_1(z)$ is a new variable used to make the equations as unified as possible, the governing Eq. (4.2) takes the form of Eq. (4.4a) and (4.4b) for the layer and the half-space, respectively

$$\frac{d^2V_1(z)}{dz^2} + m_1^2V_1(z) = 0 \quad (4.4a)$$

$$\frac{d^2V_1(z)}{dz^2} + m_2^2V_1(z) = 0 \quad (4.4b)$$

The wave numbers in the layer and the half-space m_1 and m_2 , respectively, are given as

$$m_1 = k_T \sqrt{\left[\beta_r^{-1} \left(\frac{v_T^2}{v_s^2} - 1 \right) - \frac{1}{4} v_p^2 \right]}; \quad m_2 = k_T \sqrt{1 - \frac{v_T^2}{v_{s1}^2}}$$

in which v_T is the torsional wave velocity and v_s and v_{s1} are the shear wave velocities in the layer and the half-space, respectively ($v_s = \sqrt{\frac{N_0}{\rho_0}}$, $v_{s1} = \sqrt{\frac{\mu_1}{\rho_1}}$). The ratio N_0/L_0 is denoted as the inverse of the rigidity anisotropy of the medium along the horizontal and vertical directions, respectively ($\beta_r^{-1} = N_0/L_0$). The non-homogeneity parameter is denoted as v_p ($v_p = l/ak_T$).

The solutions of Eqs. (4.4a) and (4.4b) are the amplitudes describing the variation of the particle displacements with the depth in the layer and the half-space, respectively. They take the forms of Eqs. (4.5a) and (4.5b) for the layer and the half-space, respectively.

$$V_1(z) = A_1 \cos(m_1 z) + A_2 \sin(m_1 z) \quad (4.5a)$$

$$V_1(z) = D_1 e^{-m_2 z} \quad (4.5b)$$

Note that Eq. (4.5b) satisfies the bounded displacement condition ($V_1(z) \rightarrow 0$ as $z \rightarrow \infty$).

In Eqs. (4.5), A_i ($i = 1, 2$) and D_1 are the amplitudes of the torsional waves in the layer and the half-space, respectively.

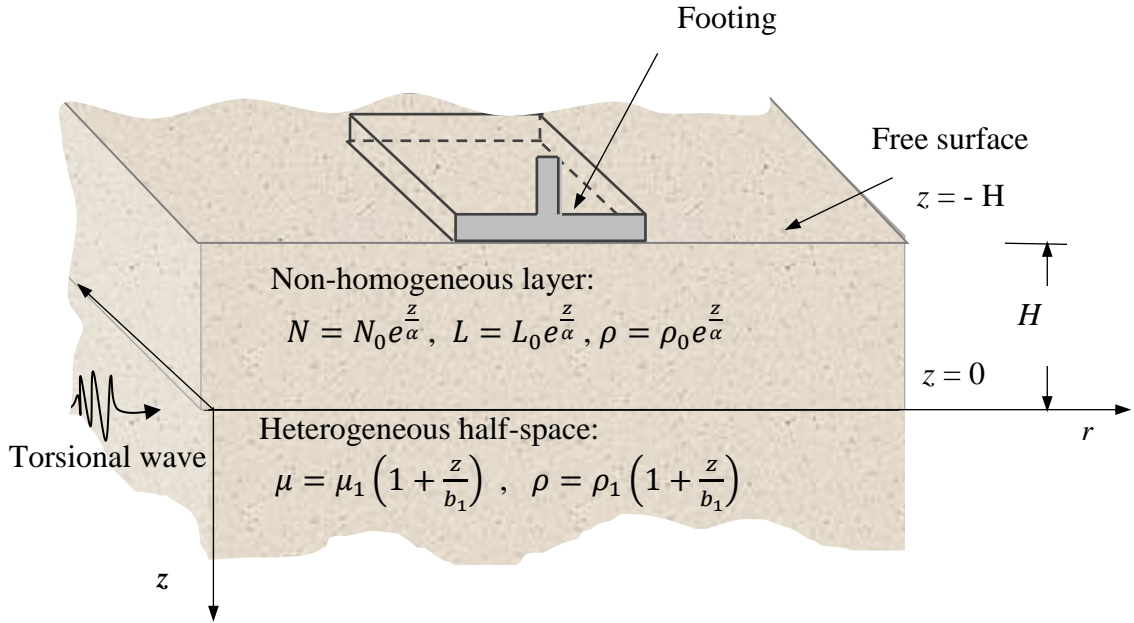


Fig. 4.1 A non-homogeneous anisotropic layer over a heterogeneous half-space.

The velocity of the torsional waves in the layer/half-space system is given from the dispersion equation obtained after eliminating the wave amplitudes (A_1 , A_2 and D_1) from the boundary conditions equations: nullity of stress at the free surface ($z = -H$), continuity of displacements and stresses at the interface layer/half-space ($z = 0$) and vanishing of the displacement in the half-space for $z \rightarrow \infty$. The dispersion equation may be written in terms of the torsional wave frequency ($K_T H$) as

$$\tan \left[K_T H \sqrt{\left\{ \beta_r^{-1} \left(\frac{v_T^2}{v_S^2} - 1 \right) - \frac{1}{4} \nu_p^2 \right\}} \right] = \frac{\mu_1}{L_0} \frac{\sqrt{\beta_r^{-1} \left(\frac{v_T^2}{v_S^2} - 1 \right) - \frac{1}{4} \nu_p^2} \left\{ \frac{1}{b_1 k} + \sqrt{\left(1 - \frac{v_T^2}{v_S^2} \frac{v_S^2}{v_{S1}^2} \right)} \right\}}{\beta_r^{-1} \left(\frac{v_T^2}{v_S^2} - 1 \right) - \frac{\mu_1}{2\alpha k L_0} \left\{ \frac{1}{b_1 k} + \sqrt{\left(1 - \frac{v_T^2}{v_S^2} \frac{v_S^2}{v_{S1}^2} \right)} \right\}} \quad (4.6a)$$

or, alternatively, in terms of the wavelength ($\lambda = 2\pi v_S/\omega$) as

$$\tan \left[2\pi \frac{H}{\lambda} \sqrt{X} \right] = \frac{\mu_1 \sqrt{\beta_r^{-1} \left(\frac{v_T^2}{v_s^2} - 1 \right) - \frac{1}{4} v_p^2} \left\{ \frac{1}{b_1 k} + \sqrt{1 - \frac{v_T^2 v_s^2}{v_s^2 v_{s1}^2}} \right\}}{\beta_r^{-1} \left(\frac{v_T^2}{v_s^2} - 1 \right) - \frac{\mu_1}{2\alpha k L_0} \left\{ \frac{1}{b_1 k} + \sqrt{1 - \frac{v_T^2 v_s^2}{v_s^2 v_{s1}^2}} \right\}} \quad (4.6b)$$

where $X = \left[\beta_r^{-1} \left(1 - \frac{v_s^2}{v_T^2} \right) - \frac{v_s^2}{v_T^2} \frac{1}{4} v_p^2 \right]$.

The torsional wave velocity can be obtained graphically or numerically as shown in Fig. 4.2 for given values of the excitation frequency, the layer thickness, the shear wave velocity, the density as well as the directional rigidities and inhomogeneity parameters in each medium (layer or half-space).

In order to obtain the torsional wave velocity, the Left-side (LS) and right-side (RS) of Eqs. (4.6) are plotted simultaneously for different values of the torsional/shear wave velocity ratio (v_T/v_s). Each intersection between the LS and RS curves corresponds to the real value of the torsional wave velocity with respect to the constraint $v_s < v_T < v_{s1}$. The first root of the dispersion equation is called the fundamental mode while the other solutions are called overtones.

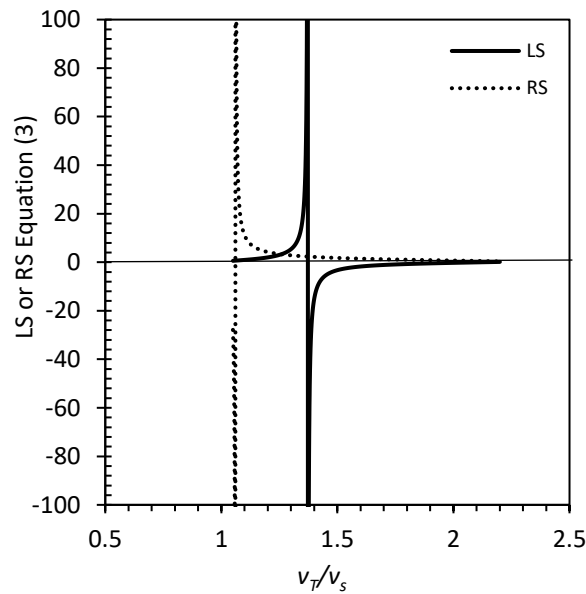


Fig. 4.2 Roots of the dispersion equation.

4.3. Anisotropy and non-homogeneity of soils

Based on the findings from previous research, it is common to apply the linear Mohr-Coulomb failure criterion to a non-homogeneous and anisotropic clay. In accordance with the study conducted by Casagrande and Carillo (1944), Fig. 4.3 displays the variation in the anisotropy of the cohesion (c). In this figure, ζ represents the angle between the maximum principal stress and the vertical direction. The cohesion of the soil, denoted as c_ζ , can be determined using the following equation

$$c_\zeta = c_h + (c_v - c_h)\cos^2\zeta \quad (4.7)$$

where the term c_v represents the vertical cohesion strength of the soil with its maximum principal stress positioned horizontally. Similarly, c_h denotes the horizontal cohesion strength of the soil where its maximum principal stress is situated vertically. Lo (1965) proved that the anisotropy coefficient, denoted as β_c ($\beta_c = c_v/c_h$), exhibits a nearly constant value, which shows the anisotropy of soil. By incorporating the anisotropy coefficient β_c into Eq. (4.7), one may obtain the following expression

$$c_\xi = c_v[\beta_c^{-1} + (1 - \beta_c^{-1})\cos^2\zeta] \quad (4.8)$$

When the inverse anisotropy coefficient β_c^{-1} equals 1.0, the soil is considered isotropic. Lo (1965) has given values of β_c^{-1} ranging from approximately 0.6 to 1.3. Additionally, Davis and Christian (1971) observed a range of β_c^{-1} values from 0.75 to about 1.56 based on extensive anisotropic strength data reported by different researchers. In the current study, the range of β_c^{-1} is set between 0.4 and 2.

The non-homogeneity of the cohesion tends to amplify as the depth z increases. Fig. 4.4 depicts the changing pattern of the cohesion non-homogeneity. It can be observed that the cohesion exhibits a linear variation with depth z . The cohesion value at a specific depth h can be determined using the following equation:

$$c_v = c_{v0} + \lambda h \quad (4.9)$$

in which, c_v represents the vertical cohesion strength when z is equal to h . Furthermore, c_{v0} denotes the vertical cohesion strength at the foundation's base ($z = 0$) and λ represents the gradient of c_v as z increases.

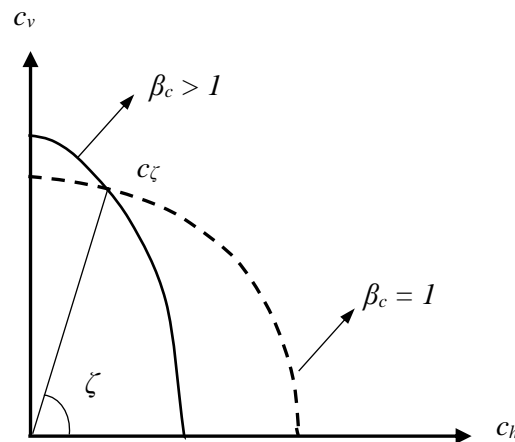


Fig. 4.3 Anisotropy of soil cohesion.

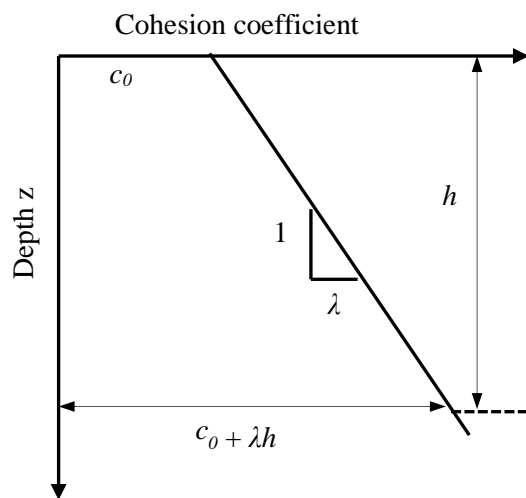


Fig. 4.4 Non-homogeneity of soil cohesion.

On the other hand, in order to take into account of the variation of the friction angle in different directions, a linear estimation in an anisotropic soil was introduced by Meyerhof (1978)

$$\varphi = \varphi_{max} - \frac{2\theta}{\pi} (\varphi_{max} - \varphi_{min}) \quad (4.10)$$

where the angle θ represents the deviation between the major principal stress and the vertical deposition direction while φ denotes the anisotropic internal friction angle. The non-homogeneity in the friction angle and anisotropy of the unit weight are not addressed in this paper due to the no availability of any data related to these aspects in the literature. On the contrary, the non-homogeneity of the unit weight is effectively incorporated in the dispersion equation of the torsional wave (Eq. 4.6) based on the assumption given in Figure 1 ($\rho = \rho_0 e^{\frac{z}{\alpha}}$). Consequently, the density value at a particular depth H can be written as

$$\rho = \rho_0 e^{\frac{H}{\alpha}} \quad (4.11)$$

By multiplying Eq. (4.11b) by the acceleration of gravity (g), the unit weight is deduced as

$$\gamma = \gamma_0 e^{\frac{k_T H}{\alpha k_T}} \quad (4.12)$$

where $K_T H$ is the torsional wave frequency and αk_T is the non-homogeneous coefficient, which can be denoted as ν_p .

4.4. Analysis method

4.4.1. Model definition and assumptions

The purpose of this subsection is to develop a model that takes into account the influence of the torsional wave propagation on the seismic bearing capacity of a shallow foundation in a non-homogeneous medium. As shown in Fig. 4.5, a shallow strip footing of width B embedded in the soil at a depth D_f from the ground surface and subject to a central vertical load (P) is considered. The environment of the footing consists in a non-homogeneous anisotropic layer of finite thickness H , of a unit weight γ and Mohr–Coulomb characteristics ($c-\phi$), resting on a heterogeneous bedrock as shown in Fig. 4.1. The layer/bedrock system extends horizontally to infinity. The Coulomb failure mechanism (Fig. 4.5) is adopted in this study due to its efficiency in the computation of the seismic bearing capacity as a viable alternative to the general shear failure mechanism as proven by Ghosh (2008), Saha and Ghosh (2017), Izadi et al. (2022), Ghosh and Debnath (2017) and Izadi et al. (2019). This failure mechanism consists of an active zone (ABC) below the footing and a passive zone (BCD) adjacent to the active zone as well as a wall interface between the two zones (BC) (Fig. 4.5).

The body forces acting on the active and passive wedges are shown in Fig. 4.6a and Fig. 4.6b, respectively, where P_A is the active thrust pushing the adjacent passive zone and P_P is the passive thrust resisting the active wedge. The interface friction angle between the active and passive wedges is denoted by δ . The inclination angles of the horizontal surface with the borders in the active and passive wedges are denoted by α and β , respectively.

In this subsection, the equivalent pseudo dynamic bearing capacity factor will be derived by the limit equilibrium method with considering the simultaneous actions of all the contributors including the soil cohesion, the loading of the footing (i.e., P) and the surcharge q , which represents the soil weight within the embedment depth. In order to account for the effects of the torsional wave propagation, the pseudo dynamic analysis will be employed.

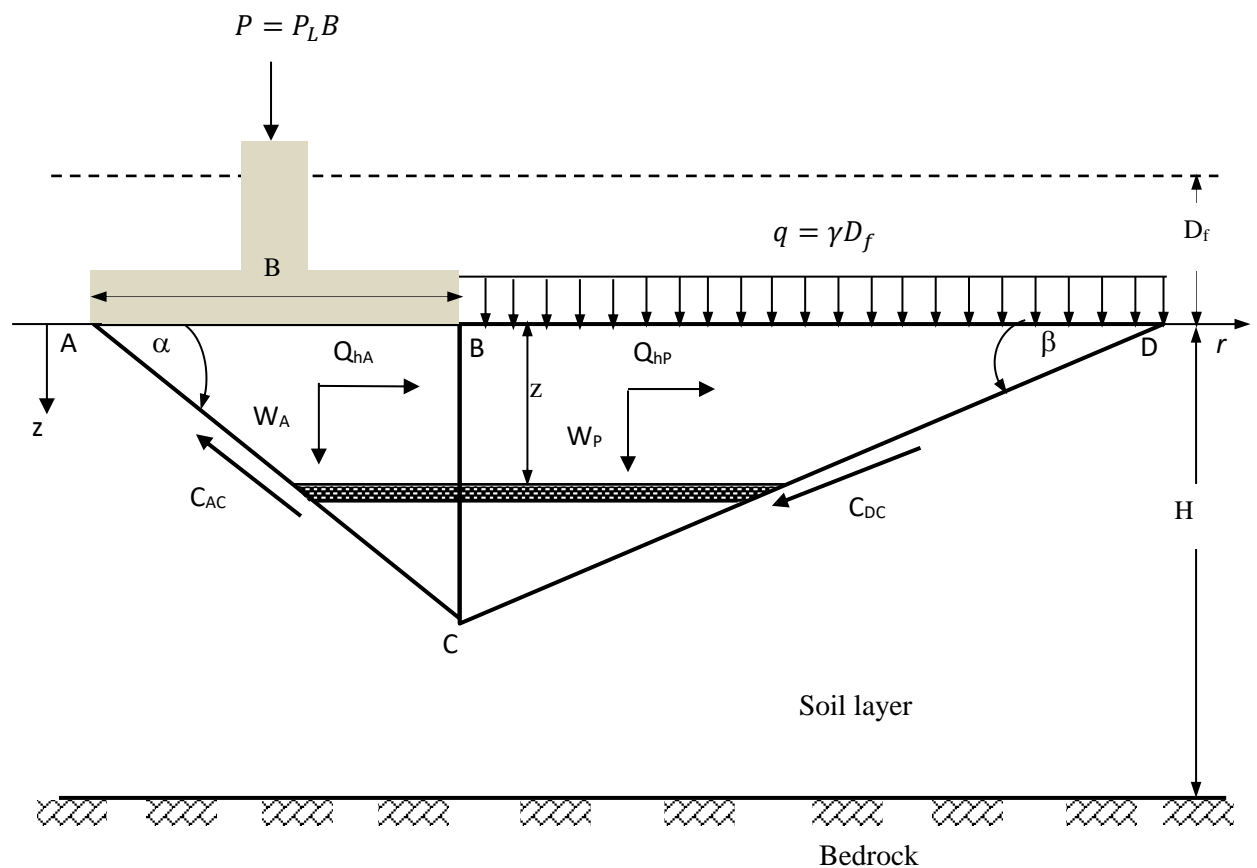


Fig. 4.5 Seismic Coulomb failure mechanism.

4.4.2. Pseudo dynamic analysis

4.4.2.1. Seismic inertia forces

The present analysis considers the torsional wave velocity v_T acting within the soil layer during the earthquake in the azimuth direction. The seismic acceleration due to the torsional wave can be found by deriving Eq. (4.1b) twice with respect to time ($a_h(r, z, t) = \frac{\partial^2 v(r, z, t)}{\partial t^2}$) and considering only the real part as well as the stress nullity condition, leading to $A_1 = A_2$ as

$$a_h(r, z, t) = \frac{\partial^2 v(r, z, t)}{\partial t^2} = -\omega^2 A_1 (\cos(m_1 z) + \sin(m_1 z)) J_1(kr) \cos(\omega t) \quad (4.14)$$

A thin element of thickness dz at a depth z from the surface top and width dr at a distance r from the wall is considered in Fig. 4.6. Its masses in the active and passive wedges are expressed by Eq. (4.15a) and (4.15b), respectively,

$$m_A(r, z) = \frac{\gamma}{g} dr dz \quad (4.15a)$$

$$m_P(r, z) = \frac{\gamma_e}{g} dr dz \quad (4.15b)$$

Where γ_e is the simultaneous action of the soil unit weight and the surcharge at the surface of the footing base, which can be expressed as

$$\gamma_e = \gamma \left(1 + \frac{2D_f}{B \tan \alpha} \right) \quad (4.16)$$

The total horizontal seismic inertia forces acting on the active and passive wedges, respectively, can be written as

$$Q_{hA}(t) = \int_0^H m_A(r, z) a_h(r, z, t) dz \quad (4.17a)$$

$$Q_{hP}(t) = \int_0^H m_P(r, z) a_h(r, z, t) dz \quad (4.17b)$$

After integration and substitution of the amplitude A_I from Eq. (4.14), the seismic inertia forces can be expressed in terms of the acceleration coefficient $k_h \left(\frac{a_h}{g} \right)$, with g is the gravity acceleration) as follow

$$Q_{hA} = \frac{\gamma k_h}{\tan \alpha} \frac{1}{K_T^2 \left[\beta_r^{-1} \left(\frac{v_T^2}{v_S^2} - 1 \right) - \frac{1}{4} v_p^2 \right]} \frac{\left\{ \left[\cos \left(K_T H \sqrt{\beta_r^{-1} \left(\frac{v_T^2}{v_S^2} - 1 \right) - \frac{1}{4} v_p^2} \right) - 1 \right] + K_T H \sqrt{\beta_r^{-1} \left(\frac{v_T^2}{v_S^2} - 1 \right) - \frac{1}{4} v_p^2} \left[\sin \left(K_T H \sqrt{\beta_r^{-1} \left(\frac{v_T^2}{v_S^2} - 1 \right) - \frac{1}{4} v_p^2} \right) + 1 \right] \right\}}{\cos \left(K_T H \sqrt{\beta_r^{-1} \left(\frac{v_T^2}{v_S^2} - 1 \right) - \frac{1}{4} v_p^2} \right) + \sin \left(K_T H \sqrt{\beta_r^{-1} \left(\frac{v_T^2}{v_S^2} - 1 \right) - \frac{1}{4} v_p^2} \right)} \quad (4.18a)$$

$$Q_{hP} = \frac{\gamma_e k_h}{\tan \beta} \frac{1}{K_T^2 \left[\beta_r^{-1} \left(\frac{v_T^2}{v_S^2} - 1 \right) - \frac{1}{4} v_p^2 \right]} \frac{\left\{ \left[\cos \left(K_T H \sqrt{\beta_r^{-1} \left(\frac{v_T^2}{v_S^2} - 1 \right) - \frac{1}{4} v_p^2} \right) - 1 \right] + K_T H \sqrt{\beta_r^{-1} \left(\frac{v_T^2}{v_S^2} - 1 \right) - \frac{1}{4} v_p^2} \left[\sin \left(K_T H \sqrt{\beta_r^{-1} \left(\frac{v_T^2}{v_S^2} - 1 \right) - \frac{1}{4} v_p^2} \right) + 1 \right] \right\}}{\cos \left(K_T H \sqrt{\beta_r^{-1} \left(\frac{v_T^2}{v_S^2} - 1 \right) - \frac{1}{4} v_p^2} \right) + \sin \left(K_T H \sqrt{\beta_r^{-1} \left(\frac{v_T^2}{v_S^2} - 1 \right) - \frac{1}{4} v_p^2} \right)} \quad (4.18b)$$

4.4.2.2. Determination of the active pressure (P_A) and passive resistance (P_P)

By applying the equilibrium of forces in the active wedge in the horizontal and vertical directions, one may get, respectively, Eq. (4.19a) and Eq. (4.19b)

$$R_A = \frac{P_A \cos \delta - Q_{hA} + C_{AC} \cos \alpha}{\sin(\alpha - \varphi)} \quad (4.19a)$$

$$P_A \sin \delta = -R_A \cos(\alpha - \varphi) + W_A - c_{AC} \sin \alpha - C_{BC} + P_L B \quad (4.19b)$$

Where W_A is the weight of the active wedge ($W_A = \frac{1}{2} \gamma B^2 \tan \alpha$). By substituting Eq. (4.19a) into Eq. (4.19b) and after some simplifications, the active force P_A is written as follow

$$P_A = \frac{Q_{hA} \cos(\alpha - \varphi)}{\cos(\alpha - \varphi - \delta)} + \frac{W_A \sin(\alpha - \varphi)}{\cos(\alpha - \varphi - \delta)} + P_L B \frac{\sin(\alpha - \varphi)}{\cos(\alpha - \varphi - \delta)} - C_{AC} \left\{ \frac{\cos \alpha \cos(\alpha - \varphi)}{\cos(\alpha - \varphi - \delta)} + \frac{\sin \alpha \sin(\alpha - \varphi)}{\cos(\alpha - \varphi - \delta)} \right\} - C_{BC} \frac{\sin(\alpha - \varphi)}{\cos(\alpha - \varphi - \delta)} \quad (4.20)$$

where

$$C_{AC} = \frac{c_v h \beta_c^{-1}}{\sin \alpha} + \frac{(1 - \beta_c^{-1}) \cos \alpha^2 c_v h}{\sin \alpha} + \frac{\lambda_c h^2 \beta_c^{-1}}{\sin \alpha} + \frac{(1 - \beta_c^{-1}) \cos \alpha^2 \lambda_c h^2}{\sin \alpha}$$

and

$$C_{BC} = c_h h + \lambda_c h^2 = c_v h \beta_c^{-1} + \lambda_c h^2$$

Similarly, applying the equilibrium of forces in the active wedge in the horizontal and vertical directions, one may obtain

$$R_P = \frac{P_P \cos \delta + Q_{HP} - C_{DC} \cos \beta}{\sin(\beta + \varphi)} \quad (4.21a)$$

$$P_P \sin \delta = R_P \cos(\beta + \varphi) - W_P - C_{DC} \sin \beta - C_{BC} \quad (4.21b)$$

Where W_P is the weight of the passive wedge ($W_P = \frac{1}{2} \gamma_e B^2 \frac{\tan \alpha^2}{\tan \beta}$). By substituting Eq. (4.21a) into Eq. (4.21b) and after some simplifications, the active force P_P is written as

$$P_P = \frac{-Q_{HP} \cos(\beta + \varphi)}{\cos(\beta + \varphi + \delta)} + \frac{W_P \sin(\beta + \varphi)}{\cos(\beta + \varphi + \delta)} + C_{DC} \left\{ \frac{\cos \beta \cos(\beta + \varphi)}{\cos(\beta + \varphi + \delta)} + \frac{\sin \beta \sin(\beta + \varphi)}{\cos(\beta + \varphi + \delta)} \right\} + C_{BC} \frac{\sin(\beta + \varphi)}{\cos(\beta + \varphi + \delta)} \quad (4.22)$$

where

$$C_{BC} = c_h h + \lambda_c h^2 = c_v h \beta_c^{-1} + \lambda_c h^2$$

and

$$C_{DC} = \frac{c_v h \beta_c^{-1}}{\sin \beta} + \frac{(1 - \beta_c^{-1}) \cos \beta^2 c_v h}{\sin \beta} + \frac{\lambda_c h^2 \beta_c^{-1}}{\sin \beta} + \frac{(1 - \beta_c^{-1}) \cos \beta^2 \lambda_c h^2}{\sin \beta}$$

4.4.2.3. Pseudo dynamic bearing capacity factor

At this stage, by equating the active pressure P_A (Eq. 4.20) and the passive resistance P_P (Eq. 4.22), the maximum load acting on the foundation (P_L) can be deduced from the following equation

$$\begin{aligned}
 P_L B \frac{\sin(\alpha-\varphi)}{\cos(\alpha-\varphi-\delta)} = & -\frac{Q_{hA} \cos(\alpha-\varphi)}{\cos(\alpha-\varphi-\delta)} - \frac{Q_{hP} \cos(\beta+\varphi)}{\cos(\beta+\varphi+\delta)} + \frac{W_P \sin(\beta+\varphi)}{\cos(\beta+\varphi+\delta)} - \frac{W_A \sin(\alpha-\varphi)}{\cos(\alpha-\varphi-\delta)} + \\
 & \left[\frac{c_v h \beta_c^{-1}}{\sin \alpha} + \frac{(1-\beta_c^{-1}) \cos \alpha^2 c_v h}{\sin \alpha} + \frac{\lambda_c h^2 \beta_c^{-1}}{\sin \alpha} + \frac{(1-\beta_c^{-1}) \cos \alpha^2 \lambda_c h^2}{\sin \alpha} \right] \left\{ \frac{\cos \alpha \cos(\alpha-\varphi)}{\cos(\alpha-\varphi-\delta)} + \right. \\
 & \left. \frac{\sin \alpha \sin(\alpha-\varphi)}{\cos(\alpha-\varphi-\delta)} \right\} + (c_v h \beta_c^{-1} + \lambda_c h^2) \left\{ \frac{\sin(\alpha-\varphi)}{\cos(\alpha-\varphi-\delta)} + \frac{\sin(\beta+\varphi)}{\cos(\beta+\varphi+\delta)} \right\} + \left[\frac{c_v h \beta_c^{-1}}{\sin \beta} + \right. \\
 & \left. \frac{(1-\beta_c^{-1}) \cos \beta^2 c_v h}{\sin \beta} + \frac{\lambda_c h^2 \beta_c^{-1}}{\sin \beta} + \frac{(1-\beta_c^{-1}) \cos \beta^2 \lambda_c h^2}{\sin \beta} \right] \left\{ \frac{\cos \beta \cos(\beta+\varphi)}{\cos(\beta+\varphi+\delta)} + \frac{\sin \beta \sin(\beta+\varphi)}{\cos(\beta+\varphi+\delta)} \right\}
 \end{aligned} \tag{4.23a}$$

as

$$\begin{aligned}
 P_L = \frac{1}{2} \gamma B \left[\frac{2}{\gamma B^2} \frac{\cos(\alpha-\varphi-\delta)}{\sin(\alpha-\varphi)} \left\{ -\frac{Q_{hA} \cos(\alpha-\varphi)}{\cos(\alpha-\varphi-\delta)} - \frac{Q_{hP} \cos(\beta+\varphi)}{\cos(\beta+\varphi+\delta)} + \frac{W_P \sin(\beta+\varphi)}{\cos(\beta+\varphi+\delta)} - \right. \right. \\
 \left. \left. \frac{W_A \sin(\alpha-\varphi)}{\cos(\alpha-\varphi-\delta)} \right\} \right] + c_v \left[\frac{h \beta_c^{-1}}{\sin \alpha} + \frac{(1-\beta_c^{-1}) \cos \alpha^2 h}{\sin \alpha} + \frac{\lambda_c h^2 \beta_c^{-1}}{c_v \sin \alpha} + \right. \\
 \left. \frac{(1-\beta_c^{-1}) \cos \alpha^2 \lambda_c h^2}{c_v \sin \alpha} \right] \frac{1}{B} \frac{\cos(\alpha-\varphi-\delta)}{\sin(\alpha-\varphi)} \left\{ \frac{\cos \alpha \cos(\alpha-\varphi)}{\cos(\alpha-\varphi-\delta)} + \frac{\sin \alpha \sin(\alpha-\varphi)}{\cos(\alpha-\varphi-\delta)} \right\} + c_v \left(h \beta_c^{-1} + \right. \\
 \left. \frac{\lambda_c h^2}{c_v} \right) \frac{1}{B} \frac{\cos(\alpha-\varphi-\delta)}{\sin(\alpha-\varphi)} \left\{ \frac{\sin(\alpha-\varphi)}{\cos(\alpha-\varphi-\delta)} + \frac{\sin(\beta+\varphi)}{\cos(\beta+\varphi+\delta)} \right\} + c_v \left[\frac{h \beta_c^{-1}}{\sin \beta} + \frac{(1-\beta_c^{-1}) \cos \beta^2 h}{\sin \beta} + \right. \\
 \left. \frac{\lambda_c h^2 \beta_c^{-1}}{c_v \sin \beta} + \frac{(1-\beta_c^{-1}) \cos \beta^2 \lambda_c h^2}{c_v \sin \beta} \right] \frac{1}{B} \frac{\cos(\alpha-\varphi-\delta)}{\sin(\alpha-\varphi)} \left\{ \frac{\cos \beta \cos(\beta+\varphi)}{\cos(\beta+\varphi+\delta)} + \frac{\sin \beta \sin(\beta+\varphi)}{\cos(\beta+\varphi+\delta)} \right\}
 \end{aligned} \tag{4.23b}$$

where the first term in the right side of Eq. (4.23b), i.e

$$\begin{aligned}
 \frac{1}{2} \gamma B \left[\frac{2}{\gamma B^2} \frac{\cos(\alpha-\varphi-\delta)}{\sin(\alpha-\varphi)} \left\{ -\frac{Q_{hA} \cos(\alpha-\varphi)}{\cos(\alpha-\varphi-\delta)} - \frac{Q_{hP} \cos(\beta+\varphi)}{\cos(\beta+\varphi+\delta)} + \frac{W_P \sin(\beta+\varphi)}{\cos(\beta+\varphi+\delta)} \right. \right. \\
 \left. \left. - \frac{W_A \sin(\alpha-\varphi)}{\cos(\alpha-\varphi-\delta)} \right\} \right]
 \end{aligned}$$

represents the contribution of the soil unit weight and surcharge (or embedment) to the bearing capacity of the shallow foundations while the remaining part of the right side of Eq. (4.23b) represents the contribution of the cohesion.

Finally, the equivalent pseudo dynamic bearing capacity factor $N_{\gamma E}$, which takes into account the effects of the torsional wave propagation in an anisotropic non-homogeneous layer over a heterogeneous half-space, is deduced from Eq. (4.13) using Eqs. (4.12) and (4.23b), in terms of the wavelength (λ) as follows

$$\begin{aligned}
 N_{\gamma E} = & \left[\frac{\tan\alpha^2 \sin(\beta+\varphi) \cos(\alpha-\varphi-\delta)}{\tan\beta \cos(\beta+\varphi+\delta) \sin(\alpha-\varphi)} \left(1 + \frac{2D_f}{B \tan\alpha} \right) - \tan\alpha \right] \exp \left(2\pi \frac{H}{\lambda} \frac{v_S}{v_T} v_p \right) - \\
 & \left[\frac{2k_h}{\tan\alpha} \frac{\tan\alpha^2}{(2\pi \frac{H}{\lambda})^2 [X]} a_{h1} \left(\frac{1}{\tan(\alpha-\varphi)} \right) \right] \exp \left(2\pi \frac{H}{\lambda} \frac{v_S}{v_T} v_p \right) - \\
 & \left[\frac{2k_h}{\tan\beta} \frac{\tan\alpha^2 \left(1 + \frac{2D_f}{B \tan\alpha} \right)}{(2\pi \frac{H}{\lambda})^2 [X]} a_{h1} \left(\frac{\cos(\beta+\varphi) \cos(\alpha-\varphi-\delta)}{\cos(\beta+\varphi+\delta) \sin(\alpha-\varphi)} \right) \right] \exp \left(2\pi \frac{H}{\lambda} \frac{v_S}{v_T} v_p \right) + \\
 & \frac{2c_v}{\gamma_0 B} \left[\frac{\tan\alpha \beta_c}{\sin\alpha} + \frac{(1-\beta_c^{-1}) \cos\alpha^2 \tan\alpha}{\sin\alpha} + v_c \frac{\tan\alpha^2 \beta_c^{-1}}{\sin\alpha} + \right. \\
 & v_c \frac{(1-\beta_c^{-1}) \cos\alpha^2 \tan\alpha^2}{\sin\alpha} \left. \right] \left\{ \frac{\cos\alpha \cos(\alpha-\varphi)}{\sin(\alpha-\varphi)} + \sin\alpha \right\} + \frac{2c_v}{\gamma_0 B} (\tan\alpha \beta_c^{-1} + v_c \tan\alpha^2) \left\{ 1 + \right. \\
 & \left. \frac{\sin(\beta+\varphi) \cos(\alpha-\varphi-\delta)}{\cos(\beta+\varphi+\delta) \sin(\alpha-\varphi)} \right\} + \frac{2c_v}{\gamma_0 B} \left[\frac{\tan\alpha \beta_c^{-1}}{\sin\beta} + \frac{(1-\beta_c^{-1}) \cos\beta^2 \tan\alpha}{\sin\beta} + v_c \frac{\tan\alpha^2 \beta_c^{-1}}{\sin\beta} + \right. \\
 & \left. v_c \frac{(1-\beta_c^{-1}) \cos\beta^2 \tan\alpha^2}{\sin\beta} \right] \left\{ \frac{\cos\beta \cos(\beta+\varphi) \cos(\alpha-\varphi-\delta)}{\cos(\beta+\varphi+\delta) \sin(\alpha-\varphi)} + \frac{\sin\beta \sin(\beta+\varphi) \cos(\alpha-\varphi-\delta)}{\cos(\beta+\varphi+\delta) \sin(\alpha-\varphi)} \right\}
 \end{aligned} \tag{4.24}$$

where

$$a_{h1} = \frac{\left\{ \left[\cos\left(2\pi \frac{H}{\lambda} \sqrt{[X]} \right) - 1 \right] + 2\pi \frac{H}{\lambda} \sqrt{[X]} \left[\sin\left(2\pi \frac{H}{\lambda} \sqrt{[X]} \right) + 1 \right] \right\}}{\cos\left(2\pi \frac{H}{\lambda} \sqrt{[X]} \right) + \sin\left(2\pi \frac{H}{\lambda} \sqrt{[X]} \right)}$$

Or, alternatively, in terms of the torsional wave frequency ($k_T H$) as

$$\begin{aligned}
 N_{\gamma E} = & \left[\frac{\tan\alpha^2 \sin(\beta+\varphi) \cos(\alpha-\varphi-\delta)}{\tan\beta \cos(\beta+\varphi+\delta) \sin(\alpha-\varphi)} \left(1 + \frac{2D_f}{B \tan\alpha} \right) - \tan\alpha \right] \exp(K_T H v_p) - \\
 & \left[\frac{2k_h}{\tan\alpha} \frac{\tan\alpha^2}{K_T H^2 \left[\beta_r \left(\frac{v_T^2}{v_S^2} - 1 \right) - \frac{1}{4\alpha^2 k^2} \right]} a_{h2} \left(\frac{1}{\tan(\alpha-\varphi)} \right) \right] \exp(K_T H v_p) - \\
 & \left[\frac{2k_h}{\tan\beta} \frac{\tan\alpha^2 \left(1 + \frac{2D_f}{B \tan\alpha} \right)}{K_T H^2 \left[\beta_r \left(\frac{v_T^2}{v_S^2} - 1 \right) - \frac{1}{4\alpha^2 k^2} \right]} a_{h2} \left(\frac{\cos(\beta+\varphi) \cos(\alpha-\varphi-\delta)}{\cos(\beta+\varphi+\delta) \sin(\alpha-\varphi)} \right) \right] \exp(K_T H v_p) + \\
 & \frac{2c_v}{\gamma_0 B} \left[\frac{\tan\alpha \beta_c^{-1}}{\sin\alpha} + \frac{(1-\beta_c^{-1}) \cos\alpha^2 \tan\alpha}{\sin\alpha} + v_c \frac{\tan\alpha^2 \beta_c^{-1}}{\sin\alpha} + \right. \\
 & v_c \frac{(1-\beta_c^{-1}) \cos\alpha^2 \tan\alpha^2}{\sin\alpha} \left. \right] \left\{ \frac{\cos\alpha \cos(\alpha-\varphi)}{\sin(\alpha-\varphi)} + \sin\alpha \right\} + \frac{2c_v}{\gamma_0 B} (\tan\alpha \beta_c^{-1} + v_c \tan\alpha^2) \left\{ 1 + \right. \\
 & \left. \frac{\sin(\beta+\varphi) \cos(\alpha-\varphi-\delta)}{\cos(\beta+\varphi+\delta) \sin(\alpha-\varphi)} \right\} + \frac{2c_v}{\gamma_0 B} \left[\frac{\tan\alpha \beta_c^{-1}}{\sin\beta} + \frac{(1-\beta_c^{-1}) \cos\beta^2 \tan\alpha}{\sin\beta} + v_c \frac{\tan\alpha^2 \beta_c^{-1}}{\sin\beta} + \right. \\
 & \left. v_c \frac{(1-\beta_c^{-1}) \cos\beta^2 \tan\alpha^2}{\sin\beta} \right] \left\{ \frac{\cos\beta \cos(\beta+\varphi) \cos(\alpha-\varphi-\delta)}{\cos(\beta+\varphi+\delta) \sin(\alpha-\varphi)} + \frac{\sin\beta \sin(\beta+\varphi) \cos(\alpha-\varphi-\delta)}{\cos(\beta+\varphi+\delta) \sin(\alpha-\varphi)} \right\}
 \end{aligned} \tag{4.25}$$

where

$$a_{h2} = \frac{\left\{ \left[\cos \left(K_T H \sqrt{\left[\beta_r^{-1} \left(\frac{v_T^2}{v_S^2} - 1 \right) - \frac{1}{4} v_p^2 \right]} \right) - 1 \right] + K_T H \sqrt{\left[\beta_r^{-1} \left(\frac{v_T^2}{v_S^2} - 1 \right) - \frac{1}{4} v_p^2 \right]} \left[\sin \left(K_T H \sqrt{\left[\beta_r^{-1} \left(\frac{v_T^2}{v_S^2} - 1 \right) - \frac{1}{4} v_p^2 \right]} \right) + 1 \right] \right\}}{\cos \left(K_T H \sqrt{\left[\beta_r^{-1} \left(\frac{v_T^2}{v_S^2} - 1 \right) - \frac{1}{4} v_p^2 \right]} \right) + \sin \left(K_T H \sqrt{\left[\beta_r^{-1} \left(\frac{v_T^2}{v_S^2} - 1 \right) - \frac{1}{4} v_p^2 \right]} \right)}$$

4.5. Conclusion

In this chapter, an equivalent seismic bearing capacity factor $N_{\gamma E}$ has been derived using the limit equilibrium method associated to the pseudo-dynamic approach considering the effect of the torsional wave. The seismic coulomb failure mechanism was used to develop a mathematical model of the seismic bearing capacity factor. The anisotropy and the non-homogeneity of the soil properties were also introduced in this mathematical model.

In the next chapter, the proposed equivalent bearing capacity factor will be validated and compared with published results, alongside a parametric study.

DETERMINISTIC AND RELIABILITY
ANALYSES OF SEISMIC BEARING
CAPACITY DUE TO TORSIONAL
WAVES

5.1. Introduction

The current chapter is considered as continuity of the previous chapter. At the first stage, an optimization of the bearing capacity factor will be done in order to find out the optimized resistance. The results of the equivalent bearing capacity factor will be validated and compared with published results. Then, a parametric study, showing the effects of various parameters governing the bearing capacity factor, will be conducted. At the second stage, a reliability analysis based on the Monte Carlo simulations will be carried out in order to investigate the influence of the soil anisotropy, soil non-homogeneity and the soil-earthquake parameter uncertainties on the equivalent seismic bearing capacity factor.

5.2. Optimization of the dynamic bearing capacity factor

In this subsection, an optimization of the equivalent dynamic bearing capacity factor $N_{\gamma E}$ with respect to the inclination angles α and β is carried out in order to find out the optimized resistance. The minimum value is taken as an optimized value. A MATLAB algorithm describing the various steps involved in the optimization of the bearing capacity factor is addressed in Fig. 5.1. The function ‘fminunc’ used in the algorithm is a part of the optimization toolbox integrated in MATLAB, which provides a set of tools for solving optimization problems. This function uses the Unconstrained Nonlinear Minimization Algorithm (UNMA), which is a gradient-based optimization method. Their advantages have made it a valuable tool for solving optimization problems in MATLAB and its ease of use, robustness, speed, flexibility and integration with MATLAB make it an excellent choice for many optimization problems.

The optimized bearing capacity factor $N_{\gamma E}$ values are listed in Table A.2 (Appendix) for the static case and in Tables A.3 to A.5 (Appendix) for the seismic case. H/λ is taken equal to 0.3 in the current study as considered for the most geotechnical structures (Ghosh, 2008; Saha and Ghosh, 2017; Saha and Ghosh, 2015). The range of variation of the parameters is practically as follows: $\varphi = 20 - 40^\circ$, $\delta = 0 - \varphi$, $k_h = 0 - 0.3$, $\frac{D_f}{B} = 0.25 - 1$, $\frac{2c_v}{\gamma_0 B} = 0 - 0.5$, $\beta_\phi = 1 - 3$, $\beta_c^{-1} = 0.4 - 2$, $v_c = 0 - 30$. The ratio of the torsional wave velocity to the shear wave velocity ($\frac{v_T}{v_S}$) is obtained graphically for the following selected parameters: $\frac{v_S^2}{v_{S1}^2} = 0.2$, $\beta_r^{-1} = 0.5 - 1$, $\frac{\mu_1}{L_0} = 1.8$ and $\frac{1}{b_1 k} = v_p = 0 - 0.5$. A parametric study will be conducted later to evaluate the impact of all these parameters.

```

// Initialize the input parameters of bearing capacity factor

$$N_{\gamma d} = f(\alpha, \beta, \varphi, \delta, \frac{v_T}{v_S}, K_T H, \frac{H}{\lambda}, k_h, \frac{D_f}{B}, \frac{2c}{\gamma B})$$

// Define the number of variables ( $\alpha$  and  $\beta$ )
m = "number of variables"
// Define the number of populations
n = "number of population"
// Define the lower and upper bounds of the variables (LB, UB)
LB = [ Lower bound of first variable, Lower bound of second variable]
UB = [Upper bound of first variable, Upper bound of second variable]
// Define the bearing capacity factor equation
fun = @(x) Nγd
// Initialize the population
for each i, where i = 1: n do
    for each j, where j = 1: m do
         $x_0(i, j) = \text{round}(LB(j) + \text{rand}() * (UB(j) - LB(j)))$ 
    end
end
// Minimization function
[x, Nγd min] = fminunc (fun, x0)
// Condition to obtain a minimum positive output
if Nγd min < 0 do
    run "file name" till condition satisfied (Nγd min > 0)
else
end
end

```

Fig. 5.1 Algorithm for optimizing the dynamic bearing capacity factor.

5.3. Validation of the model

Because of the scarcity of any solution for the dynamic bearing capacity of shallow foundations due to the effect of the torsional wave, only the static bearing capacity factors could be compared to previous findings. As shown in Fig. 5.2, the results of the current study (Table A.2 in Appendix) are compared to those of Saha and Ghosh (2017) for different values of the embedment depth ratio (D_f/B), the dimensionless cohesion ratio ($2c_v/\gamma_0 B$) and the internal

friction angle (φ). It can be noted from this Figure that the current results are in a perfect agreement with those of [Saha and Ghosh \(2017\)](#).

To assess the influence of the anisotropy and non-homogeneity of the soil, the results of the present study ([Eq. 4.23b](#)) are compared with the results of previous studies conducted under static conditions ($k_h = 0$). The comparison is presented in [Figs. 5.3 to 5.6](#).

[Fig. 5.3](#) illustrates the comparison of the unit weight bearing capacity factor, obtained from [Eq. \(4.23b\)](#) by equating c_v to zero, with the findings of [Hansen \(1970\)](#) and [Meyerhof \(1978\)](#) for the isotropic homogeneous state of the soil unit weight. The results demonstrate a remarkable similarity between the results for $\delta = \varphi/2$ and the existing results.

[Figs. 5.4 and 5.5](#) show a comparison between the present cohesive bearing capacity factor results and those obtained by [Reddy and Srinivasan \(1970\)](#), [Reddy and Rao \(1981\)](#), [Al-Shamrani and Moghal \(2005\)](#) and [Yang and Du \(2016\)](#) for an anisotropic non-homogeneous soil cohesion condition. The comparison indicates that the current bearing capacity factor values closely align with those reported by [Reddy and Srinivasan \(1970\)](#) and [Reddy and Rao \(1981\)](#). For instance, from [Fig. 5.4](#), for $\nu_c = 30$, the deviations from the [Reddy and Srinivasan \(1970\)](#) values are approximately + 5% for $\beta_c^{-1} = 0.4$, + 10% for $\beta_c^{-1} = 1.0$ and + 11% for $\beta_c^{-1} = 1.6$. Similarly, when compared to [Reddy and Rao \(1981\)](#), the differences amount to approximately - 13%, + 5%, and + 13% for $\beta_c^{-1} = 0.4, 1.0$ and 1.6 , respectively. On the other hand, from [Fig. 5.5](#), for $\beta_c^{-1} = 1.6$, the deviation from the [Reddy and Srinivasan \(1970\)](#) values are about + 7% for $\nu_c = 5$, + 11% for $\nu_c = 20$, and + 11% for $\nu_c = 30$. Similarly, when compared to [Reddy and Rao \(1981\)](#), the differences amount to approximately + 20%, + 16%, and + 13% for $\nu_c = 5, 20$, and 30 , respectively. All these deviations are reasonably expected due to disparities in the analysis methods and the utilization of different failure mechanisms.

[Fig. 5.6](#) shows the comparison of the unit weight bearing capacity factor N_γ with the findings of [Pakdel et al. \(2021\)](#) for the only anisotropic state of the soil internal friction angle. The results indicate that the current bearing capacity factor values are in a perfect agreement with those of [Pakdel et al. \(2021\)](#) due to the similarity of the used method of analysis and failure mechanism.

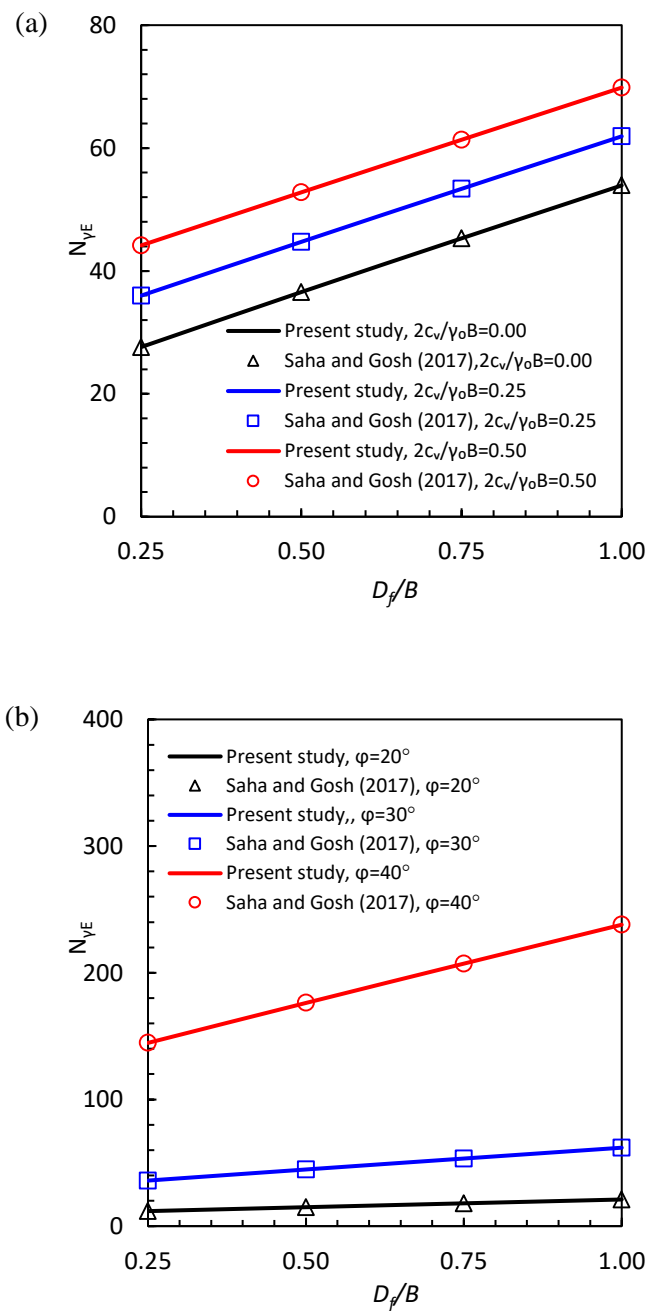


Fig. 5.2 Validation of the present static bearing capacity factor with published results: (a) $\varphi = 30^\circ$ and $\delta = \varphi/2$, (b) $\delta = \varphi/2$ and $2c_v/\gamma_0 B = 0.25$.

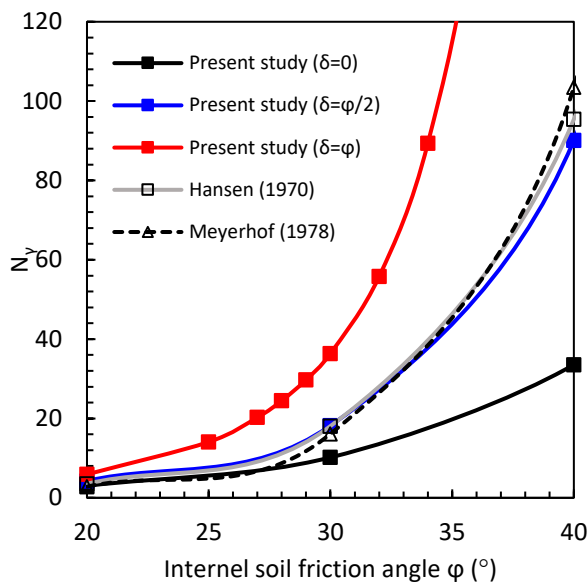
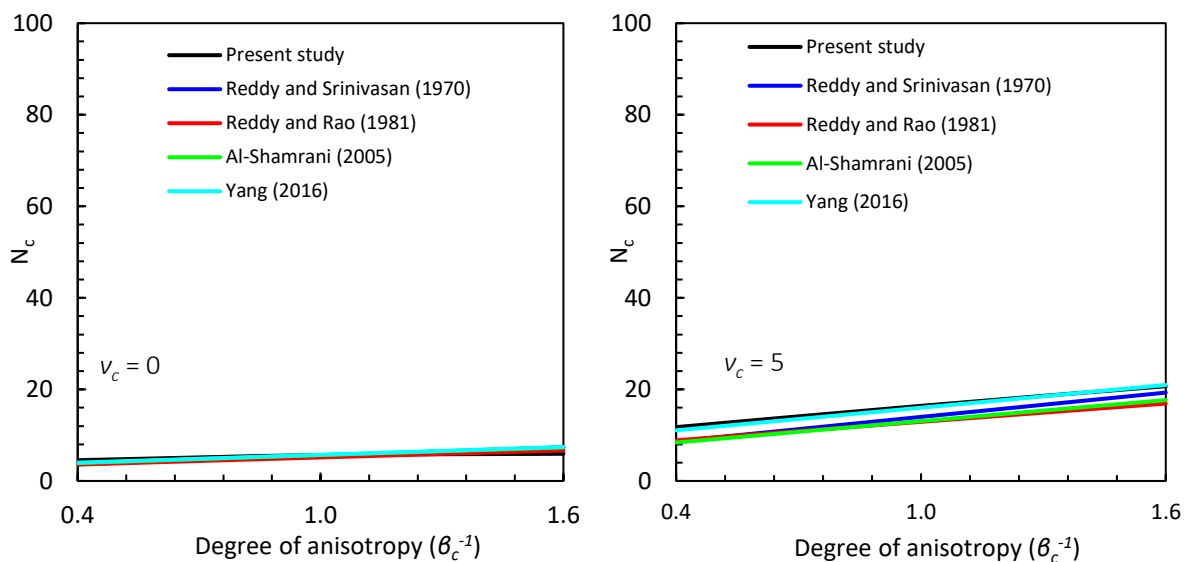


Fig. 5.3 Validation of the present N_y static bearing capacity factor with published results for isotropic homogeneous condition of soil unit weight for: $D_f/B = 0$, $\beta_r^{-1} = 1$ and $\nu_p = 0$.



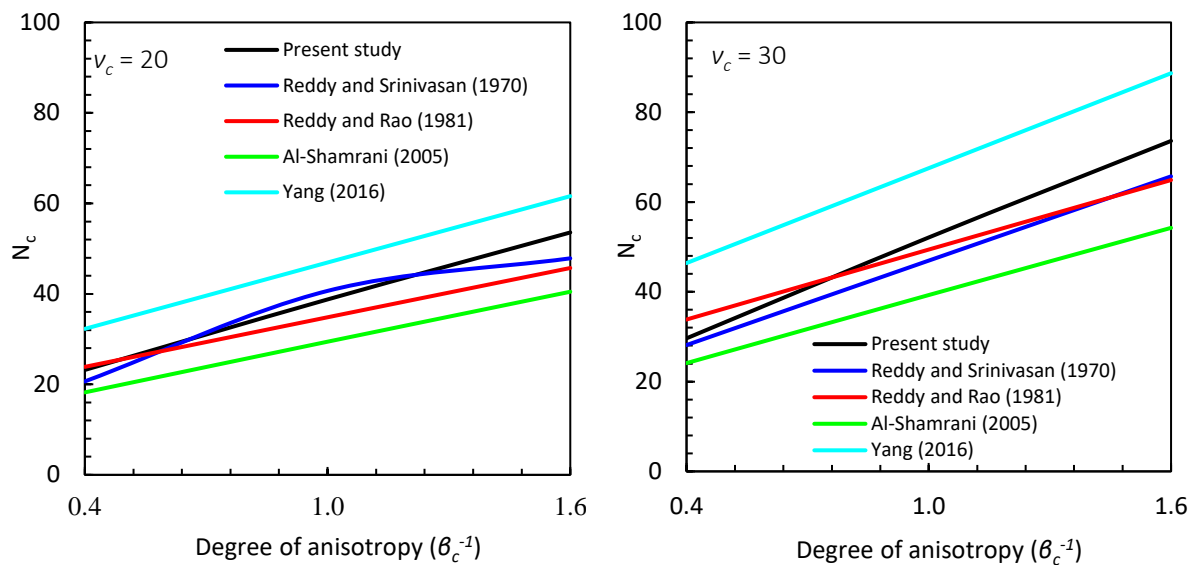
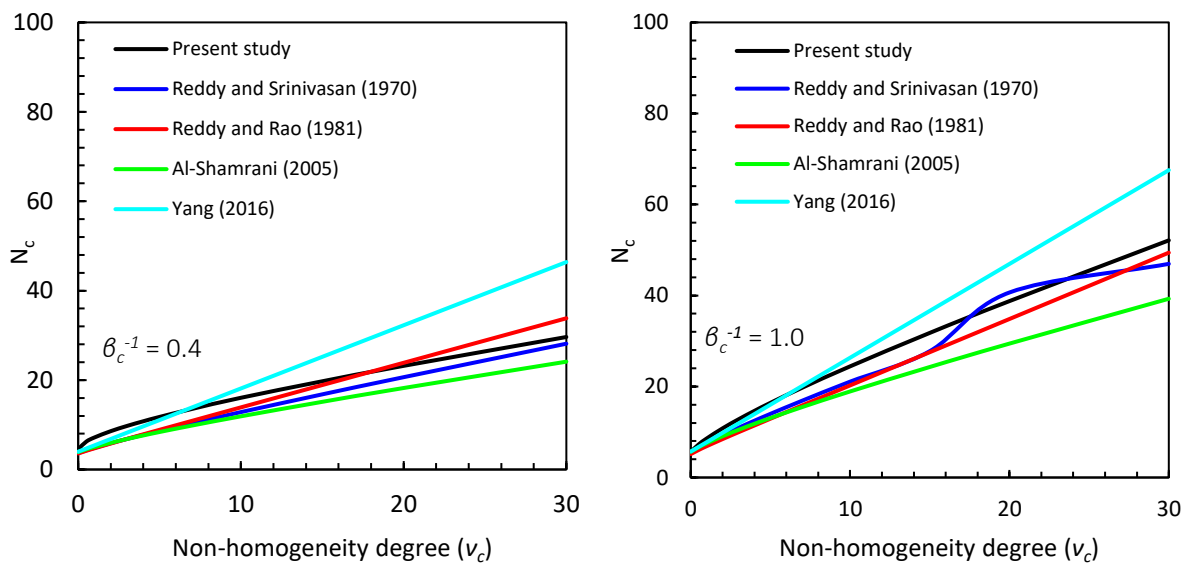


Fig. 5.4 Validation of the present N_c bearing capacity factor with published results for different anisotropic degree values of soil cohesion.



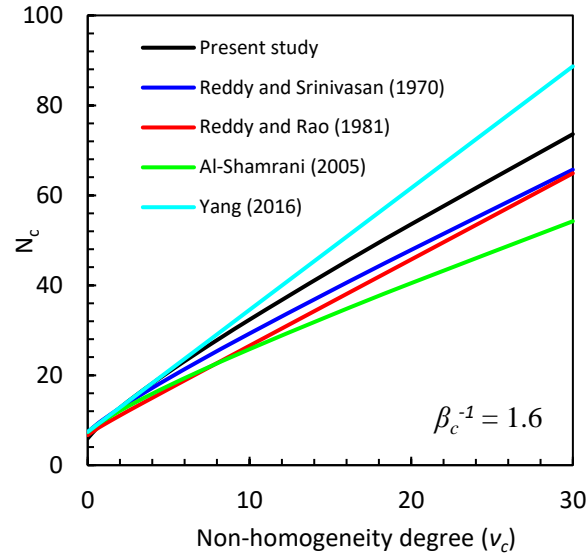


Fig. 5.5 Validation of the present N_c bearing capacity factor with published results for different non-homogeneity degree values of soil cohesion.

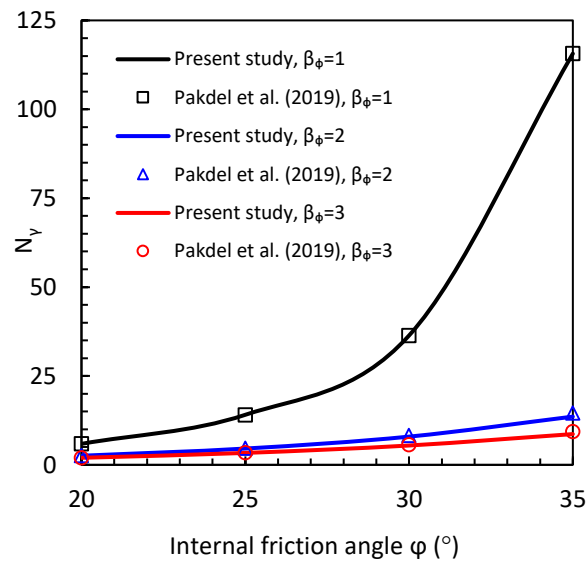


Fig. 5.6 Validation of the present N_y static bearing capacity factor with published results for different anisotropic degree values of soil friction angle for: $2c_v/\gamma_0B = 0.0$, $D_f/B = 0$, $\delta = \phi$, $\beta_r^{-1} = 1$ and $v_p = 0$.

5.4. Parametric study

The aim of this parametric study is to quantify the impact of the contributing parameters in the present seismic bearing model. In addition to the anisotropy coefficients of the cohesion and the rigidity, β_c and β_r , respectively, the anisotropy coefficient of the friction angle can also be

defined. In fact, according to Eq. (4.10) and referring to Fig. 4.6, in the active wedge, θ is assumed to be 0 , whereas in the passive wedge, θ is considered to be $\pi/2$. Pakdel et al. (2021) concluded that the active wedge exhibits the highest value of the friction angle (φ_{max}) while the passive wedge demonstrates the lowest value of the friction angle (φ_{min}) such that $\varphi_{min} = \varphi_{max} / \beta_\varphi$ with β_φ represents the anisotropic coefficient of the friction angle.

5.4.1. Impact of the internal soil friction angle φ

Fig. 5.7 shows the variation of the equivalent pseudo dynamic bearing capacity factor $N_{\gamma E}$ versus the torsional wave acceleration coefficient (k_h) when varying the soil friction angle from 20° to 40° while the other parameters are kept unchanged ($D_f/B = 0.5$, $2c_v/\gamma_0 B = 0.25$, $\delta = \phi / 2$, $\beta_r^{-1} = 0.7$, $\beta_\phi = 1.5$, $\beta_c^{-1} = 0.5$, $\nu_p = 0.1$ and $\nu_c = 15$). It can be seen from Fig. 5.7 that the bearing capacity factor increases as the soil friction angle increases. This result means that the internal resistance of the soil particles increases as the soil friction angle increases.

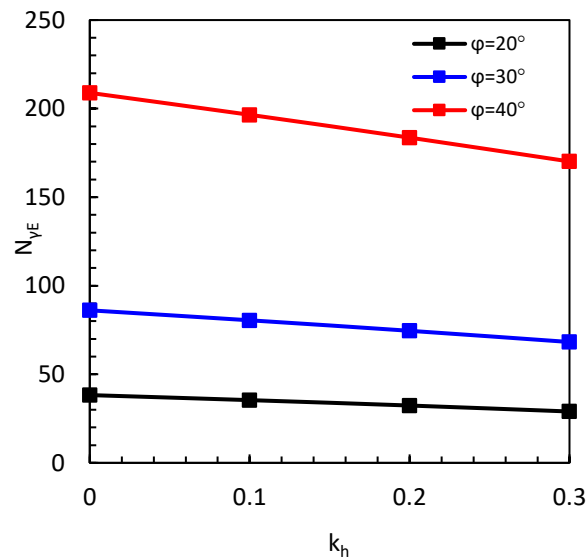


Fig. 5.7 Variation of the pseudo dynamic bearing capacity factor versus the acceleration coefficient for different values of the soil friction angle for $D_f/B = 0.5$, $2c_v/\gamma_0 B = 0.25$, $\delta = \phi / 2$, $\beta_r^{-1} = 0.7$, $\beta_\phi = 1.5$, $\beta_c^{-1} = 0.5$, $\nu_p = 0.1$ and $\nu_c = 15$.

5.4.2. Impact of the interface wall friction angle δ

Fig. 5.8 shows the variation of the equivalent pseudo dynamic bearing capacity factor $N_{\gamma E}$ versus the torsional wave acceleration coefficient (k_h) for different values of the wall friction angle ($\delta = 0$, $\delta = \varphi / 2$ and $\delta = \varphi$) while the other parameters are fixed to the values $\varphi = 30^\circ$, $D_f/B = 0.5$, $2c_v/\gamma_0 B = 0.25$, $\beta_r^{-1} = 0.7$, $\beta_\phi = 1.5$, $\beta_c^{-1} = 0.5$, $\nu_p = 0.1$ and $\nu_c = 15$. It can be seen

from this Figure that the bearing capacity factor is increasing with the increase in the wall friction angle. It is to highpoint that when δ changes from 0 to φ , the increment of variation in the pseudo dynamic bearing capacity factor is about 40%, 38%, 36% and 34% for the values of k_h equal to 0, 0.1, 0.2 and 0.3, respectively. These results may indicate that the wall friction angle increases the forces acting on the passive and active wedges in the failure mechanism, which consequently increases the soil resistance.

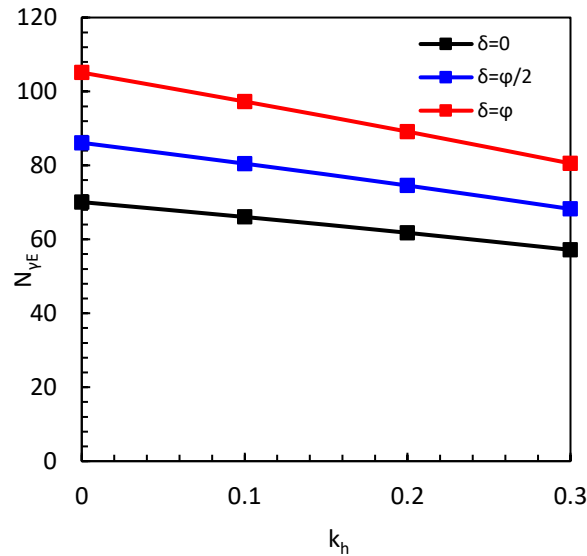


Fig. 5.8 Variation of the pseudo dynamic bearing capacity factor versus the acceleration coefficient for different values of the wall friction angle for $\varphi = 30^\circ$, $D_f/B = 0.5$, $2c_v/\gamma_0B = 0.25$, $\beta_r^{-1} = 0.7$, $\beta_\phi = 1.5$, $\beta_c^{-1} = 0.5$, $v_p = 0.1$ and $v_c = 15$.

5.4.3. Impact of the embedment depth ratio D_f/B

Fig. 5.9 shows the variation of the equivalent pseudo dynamic bearing capacity factor $N_{\gamma E}$ versus the torsional wave acceleration coefficient (k_h) for different values of the embedment depth ratio ($D_f/B = 0, 0.25, 0.5, 0.75$ and 1) when $\varphi = 30^\circ$, $2c_v/\gamma_0B = 0.25$, $\delta = \varphi/2$, $\beta_r^{-1} = 0.7$, $\beta_\phi = 1.5$, $\beta_c^{-1} = 0.5$, $v_p = 0.1$ and $v_c = 15$. It can be seen from Fig. 5.9 that the bearing capacity factor increases as the depth ratio D_f/B increases. This indicates that the footings with higher embedment depth ratio can support higher limit loads.

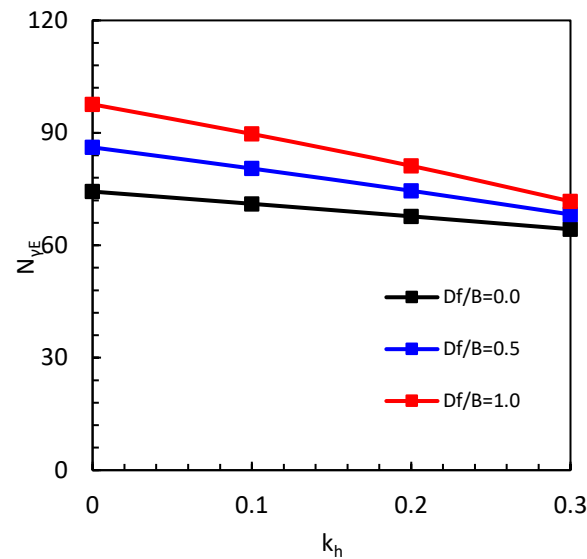


Fig. 5.9 Variation of the pseudo dynamic bearing capacity factor versus the acceleration coefficient for different values of the embedment ratio for: $\varphi = 30^\circ$, $2c_v/\gamma_0B = 0.25$, $\delta = \varphi/2$, $\beta_r^{-1} = 0.7$, $\beta_\phi = 1.5$, $\beta_c^{-1} = 0.5$, $\nu_p = 0.1$ and $\nu_c = 15$.

5.4.4. Impact of the dimensionless cohesion $2c_v/\gamma_0B$

Fig. 5.10 displays the variation of the equivalent pseudo dynamic bearing capacity factor $N_{\gamma E}$ versus the torsional wave acceleration coefficient (k_h) for different values of the dimensionless cohesion ratio ($2c_v/\gamma_0B = 0, 0.25$ and 0.5) when $\varphi = 30^\circ$, $D_f/B=0.5$, $\delta = \varphi/2$, $\beta_r^{-1} = 0.7$, $\beta_\phi = 1.5$, $\beta_c^{-1} = 0.5$, $\nu_p = 0.1$ and $\nu_c = 15$. It is clear from Fig. 5.10 that the bearing capacity factor is increasing with the increase in the dimensionless cohesion ratio.

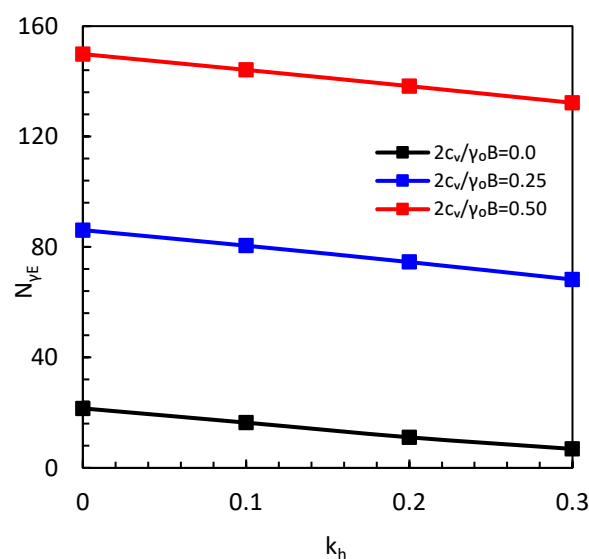


Fig. 5.10 Variation of the pseudo dynamic bearing capacity factor versus the acceleration coefficient for different dimensionless values of the cohesion ratio for: $\varphi = 30^\circ$, $D_f/B=0.5$, $\delta = \varphi/2$, $\beta_r^{-1} = 0.7$, $\beta_\phi = 1.5$, $\beta_c^{-1} = 0.5$, $\nu_p = 0.1$ and $\nu_c = 15$.

5.4.5. Impact of the wavelength and the seismic acceleration of the torsional wave

Fig. 5.11 depicts the variation of the equivalent pseudo dynamic bearing capacity factor $N_{\gamma E}$ versus the torsional wave frequency ($K_T H$) for different values of the seismic acceleration coefficient ($k_h = 0.1, 0.2$ and 0.3) when $\varphi = 30^\circ$, $D_f/B = 0.5$, $2c_v/\gamma_0 B = 0.25$, $\delta = \varphi/2$, $\beta_r^{-1} = 0.7$, $\beta_\phi = 1.5$, $\beta_c^{-1} = 0.5$, $v_p = 0.1$ and $v_c = 15$. The ratio of the torsional wave velocity to the shear wave velocity (v_T/v_s) is calculated for each torsional wave frequency value ($K_T H$) using the dispersion equation (Eq. 4.6a). Fig. 5.11 appearances that the bearing capacity factor is increasing with the increase in the torsional wave frequency. The influence of the frequency on the bearing capacity factor is significantly magnified at the maximum acceleration coefficient ($k_h = 0.3$). For example, at $k_h = 0.3$, the bearing capacity coefficient increases by 42%, 13%, 3% and 2% when $K_T H$ increases from 0.25 to 0.5, 0.5 to 0.75, 0.75 to 1 and 1 to 2, respectively. While for $k_h = 0.2$, there is an increase by about 21%, 7%, 2% and 1% for the same increase of $K_T H$, respectively. In fact, as reported by Izadi et al. (2022), the increase of the wave frequency means that the wavelength decreases and therefore a reflected effect will be noted on the bearing capacity factor. Therefore, it can be concluded that as the wavelength of the torsional wave increases, the seismic bearing capacity factor decreases. On the other hand, it can be also noted from Fig. 5.11 that the bearing capacity factor decreases as the acceleration coefficient increases.

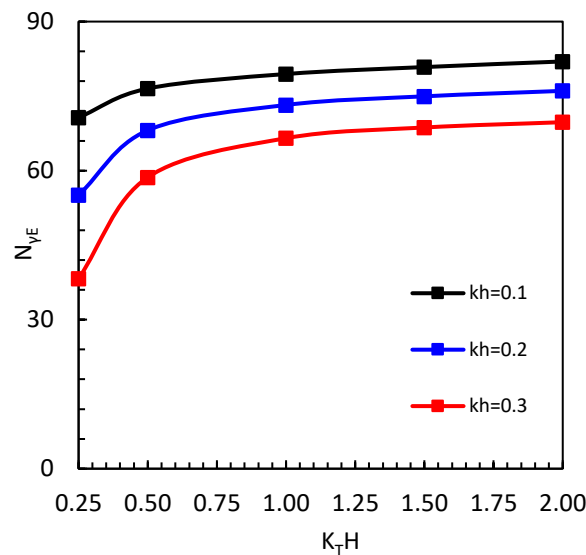


Fig. 5.11 Variation of the pseudo dynamic bearing capacity factor versus the torsional wave frequency for different values of the seismic acceleration coefficient for: $\varphi = 30^\circ$, $D_f/B = 0.5$, $2c_v/\gamma_0 B = 0.25$, $\delta = \varphi/2$, $\beta_r^{-1} = 0.7$, $\beta_\phi = 1.5$, $\beta_c^{-1} = 0.5$, $v_p = 0.1$ and $v_c = 15$.

5.4.6. Impact of soil anisotropy

Fig. 5.12 illustrates the variation of the equivalent pseudo dynamic bearing capacity factor $N_{\gamma E}$ versus the seismic acceleration coefficient for various values of the anisotropy degree of the rigidity when $\varphi = 30^\circ$, $D_f/B = 0.5$, $2c_v/\gamma_0 B = 0.25$, $\delta = \varphi/2$, $\beta_\phi = 1.5$, $\beta_c^{-1} = 0.5$, $v_\gamma = 0.1$ and $v_c = 15$. It is observed from Fig. 5.12 that as the anisotropy degree increases, there is a slight decrease in the seismic bearing capacity factor. However, this decrement remains within 5% when the anisotropy of the rigidity (β_r) increases from 1 to 2 (corresponding to a variation of β_r^{-1} from 1 to 0.5) with a specific example of $v_\gamma = 0.5$.

Fig. 5.13 illustrates the variation of the equivalent pseudo dynamic bearing capacity factor $N_{\gamma E}$ versus the seismic acceleration coefficient for various values of the anisotropy degree of the internal friction angle when $\varphi = 30^\circ$, $D_f/B = 0.5$, $2c_v/\gamma_0 B = 0.25$, $\delta = \varphi/2$, $\beta_r^{-1} = 0.7$, $\beta_c^{-1} = 0.5$, $v_p = 0.1$ and $v_c = 15$. It is noted from this figure that the seismic bearing capacity decreases as the anisotropy degree of the friction angle increases. Notably, a significant impact is evident when the anisotropy degree increases from 1 to 1.5, resulting in an estimated reduction in the bearing capacity factor of approximately 44% while from 1.5 to 2, 2 to 2.5 and 2.5 to 3 the reductions amount to approximately 18%, 10% and 6%, respectively, for $k_h = 0.3$. This observed trend can be attributed to the correlation between the anisotropy degree and the minimum internal friction angle. Increasing the anisotropy degree leads to a decrease in the minimum internal friction angle, resulting in a reduction in the shear strength within certain sub-horizontal planes.

Fig. 5.14 illustrates the variation of the equivalent pseudo dynamic bearing capacity factor $N_{\gamma E}$ versus the seismic acceleration coefficient for various values of the anisotropy degree of the cohesion when $\varphi = 30^\circ$, $D_f/B = 0.5$, $2c_v/\gamma_0 B = 0.25$, $\delta = \varphi/2$, $\beta_r^{-1} = 0.7$, $\beta_\phi = 1.5$, $v_p = 0.1$ and $v_c = 15$. It is evident from the findings that the seismic bearing capacity factor decreases as the anisotropy degree of cohesion increases. A notable impact was found when the anisotropy degree increases from 1.25 to 2.5 (corresponding to a variation of β_c^{-1} from 0.8 to 0.4) resulting in a reduction by about 43% while from 0.5 to 0.625 (corresponding to β_c^{-1} varies from 2.0 to 1.6), 0.625 to 0.83 (corresponding to a variation of β_c^{-1} from 1.6 to 1.2) and 0.83 to 1.25 (corresponding to a variation of β_c^{-1} from 1.2 to 0.8) by about 18%, 22% and 29%, respectively, for $k_h = 0.3$. Another significant finding highlights the increasing impact of the cohesion anisotropy as the seismic acceleration increases. For example, the reduction in the

bearing capacity factor when the anisotropy degree varies from 1.25 to 2.5 (corresponding to β_c^{-1} varying from 0.8 to 0.4) for $k_h = 0, 0.1, 0.2$ and 0.3 is about 33%, 35%, 38% and 43%, respectively.

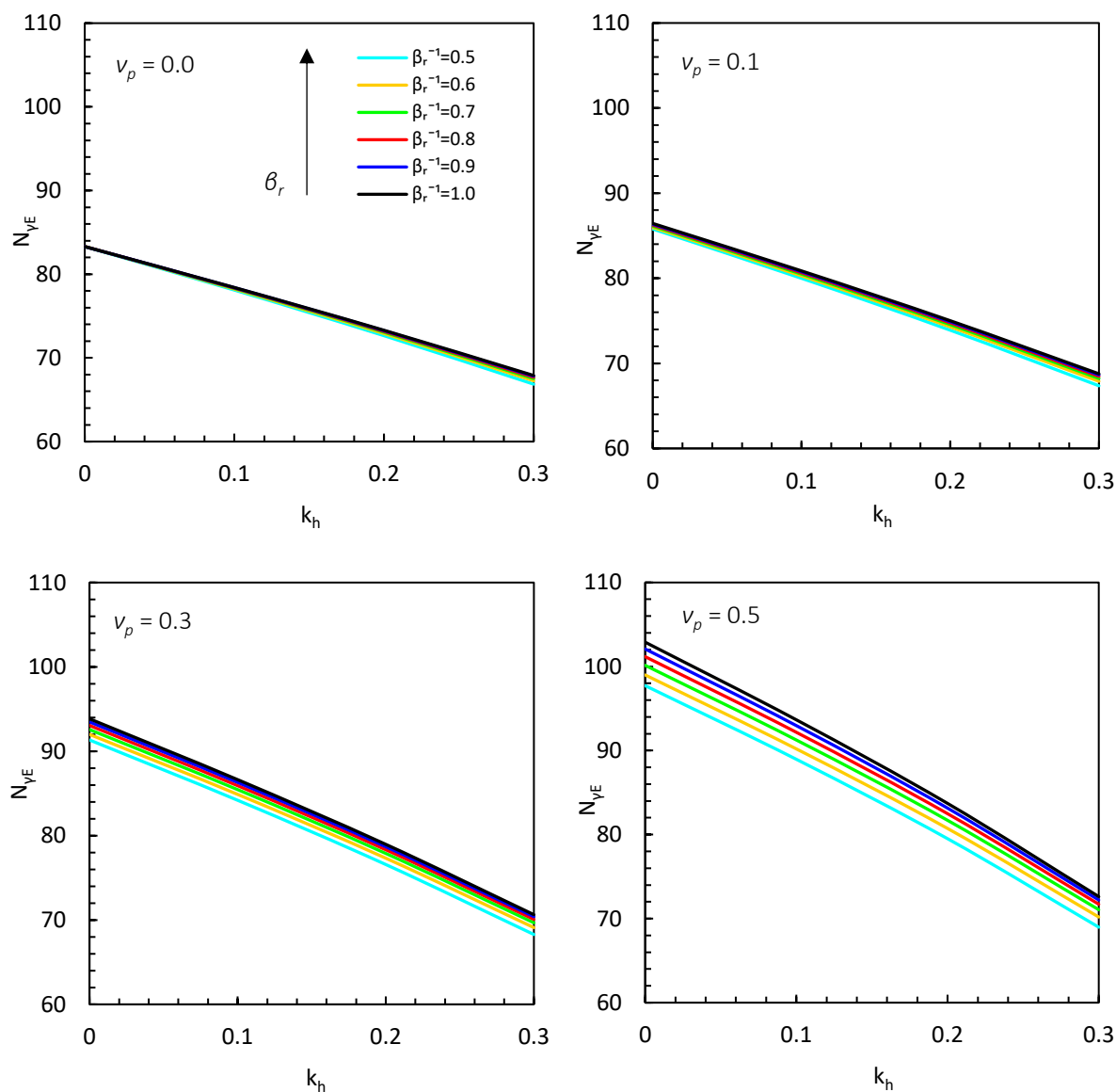


Fig. 5.12 Variation of the pseudo dynamic bearing capacity factor versus the acceleration coefficient for different values of anisotropy degree of rigidity for: $\varphi = 30^\circ$, $D_f/B = 0.5$,

$$2c_v/\gamma_0 B = 0.25, \delta = \varphi/2, \beta_\phi = 1.5, \beta_c^{-1} = 0.5, v_\gamma = 0.1 \text{ and } v_c = 15.$$

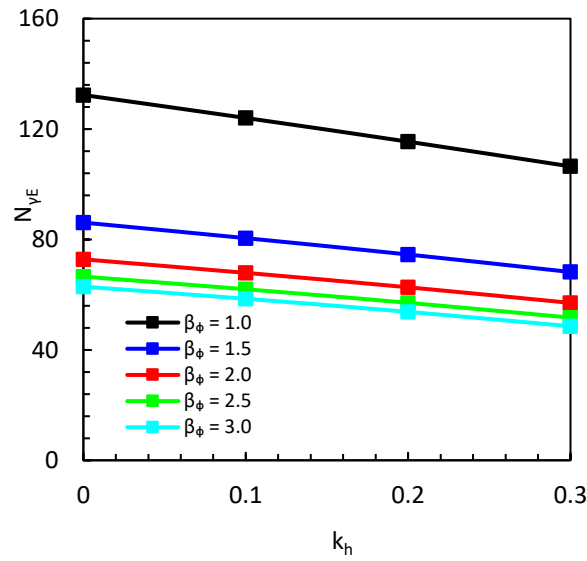


Fig. 5.13 Variation of the pseudo dynamic bearing capacity factor versus the acceleration coefficient for different values of anisotropy degree of internal friction angle for: $\varphi = 30^\circ$, $D_f/B = 0.5$, $2c_v/\gamma_0B = 0.25$, $\delta = \varphi/2$, $\beta_r^{-1} = 0.7$, $\beta_c^{-1} = 0.5$, $v_p = 0.1$ and $v_c = 15$.

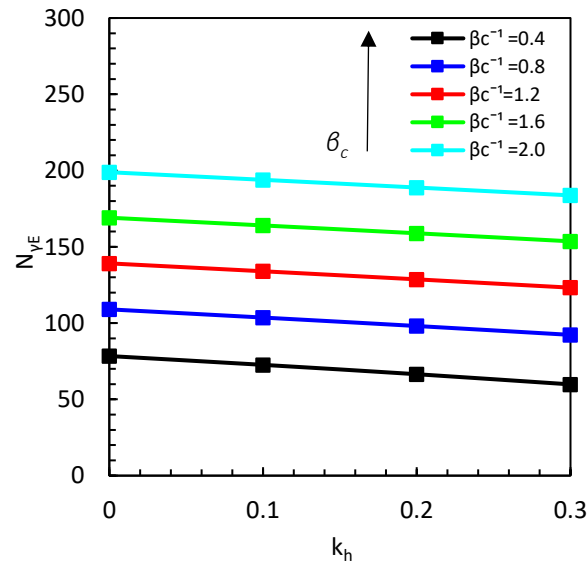


Fig. 5.14 Variation of the pseudo dynamic bearing capacity factor versus the acceleration coefficient for different values of the inverse anisotropy degree of cohesion for: $\varphi = 30^\circ$, $D_f/B = 0.5$, $2c_v/\gamma_0B = 0.25$, $\delta = \varphi/2$, $\beta_r^{-1} = 0.7$, $\beta_\phi = 1.5$, $v_p = 0.1$ and $v_c = 15$.

5.4.7. Impact of soil non-homogeneity

Fig. 5.15 shows the variation of the equivalent pseudo dynamic bearing capacity factor $N_{\gamma E}$ versus the seismic acceleration coefficient for various values of the non-homogeneity parameter coefficient when $\varphi = 30^\circ$, $D_f/B=0.5$, $2c_v/\gamma_0 B = 0.25$, $\delta = \varphi/2$, $\beta_\phi = 1.5$, $\beta_c^{-1} = 0.5$ and $\nu_c = 15$. It is noted from Fig. 5.15 that the bearing capacity factor increases as the non-homogeneity coefficient increases. This effect is particularly significant in the static cases ($k_h = 0$).

Nevertheless, when investigating the range of non-homogeneity from 0 to 0.5, the observed increase does not exceed 4%. Furthermore, it is worth noting that this increment tends to approach zero as the seismic acceleration coefficient increases.

Fig. 5.16 shows the variation of the equivalent pseudo dynamic bearing capacity factor $N_{\gamma E}$ versus the seismic acceleration coefficient for various values of the cohesion non-homogeneity coefficient when $\varphi = 30^\circ$, $D_f/B=0.5$, $2c_v/\gamma_0 B = 0.25$, $\delta = \varphi/2$, $\beta_\phi = 1.5$, $\beta_c^{-1} = 0.5$, $\beta_r^{-1} = 0.7$, $\nu_p = 0.1$. This figure reveals that the bearing capacity factor increases as the non-homogeneity coefficient increases.

Furthermore, the increment of variation in the bearing capacity factor exhibits a more significant trend when the cohesion non-homogeneity varies in the range of 0 to 15, as compared to the range of 15 to 30. As an example, when considering $k_h = 0.3$, the observed increment is approximately 160% for the non-homogeneity coefficients ranging from 0 to 15 and around 60% for coefficients ranging from 15 to 30.

Additionally, it is found that as the seismic acceleration coefficient increases, the increment of variation of the bearing capacity factor increases. For example, for the cohesion non-homogeneity ranging from 0 to 15, the maximum increment of variation is approximately 106% and 160% for $k_h = 0$ and 0.3, respectively.

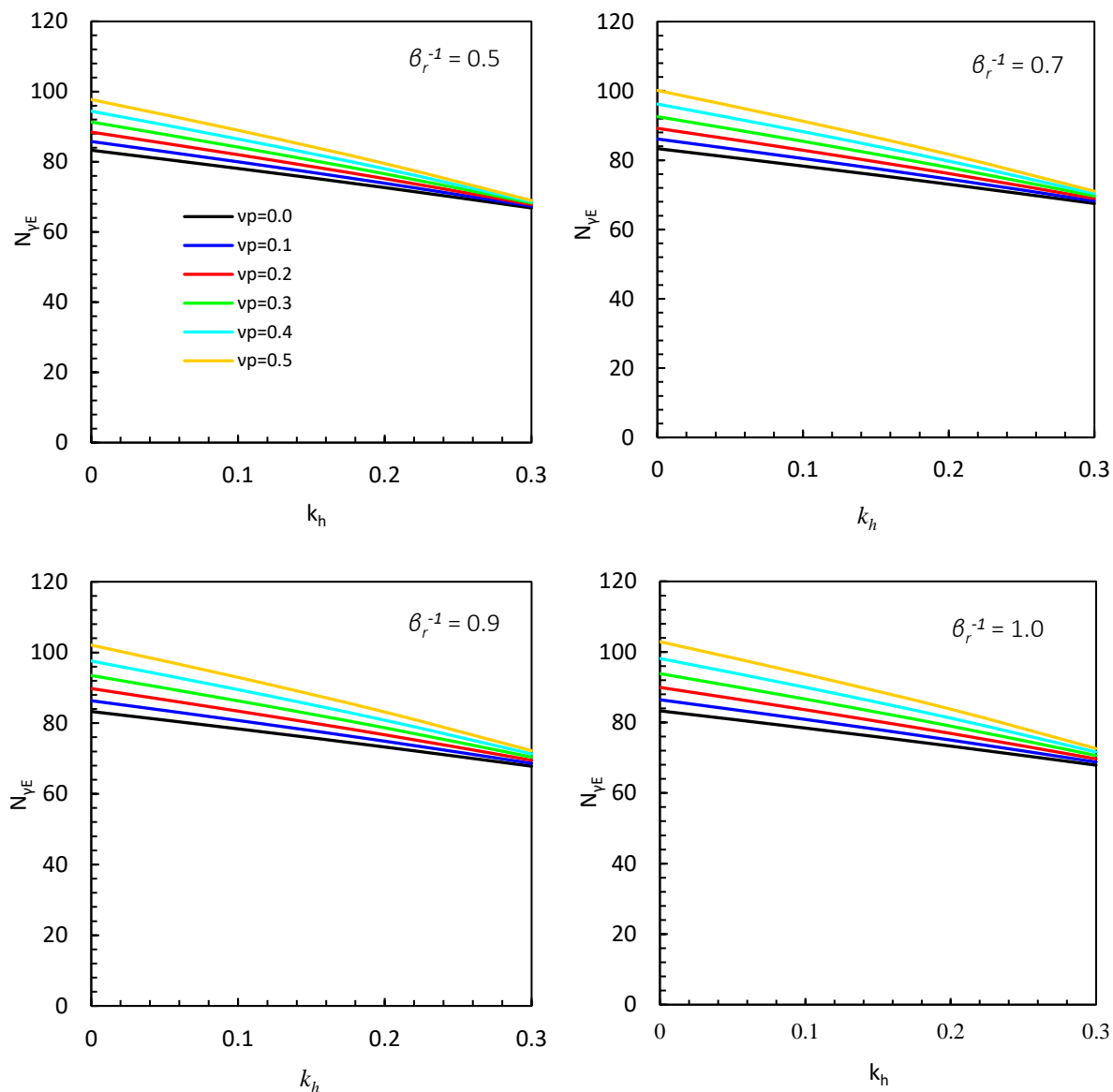


Fig. 5.15 Variation of the pseudo dynamic bearing capacity factor versus the acceleration coefficient for different values of non-homogeneity parameter for: $\varphi = 30^\circ$, $D_f/B=0.5$, $2c_v/\gamma_0B = 0.25$, $\delta = \varphi/2$, $\beta_\phi = 1.5$, $\beta_c^{-1} = 0.5$ and $v_c = 15$.

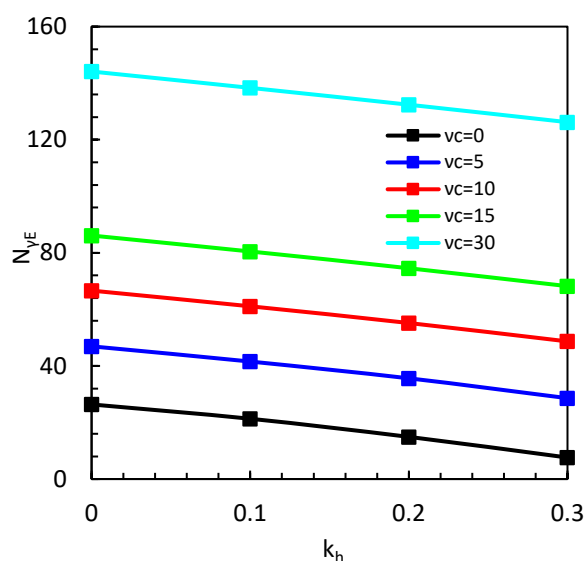


Fig. 5.16 Variation of the pseudo dynamic bearing capacity factor versus the acceleration coefficient for different values of non-homogeneity coefficient of cohesion for: $\varphi = 30^\circ$, $D_f/B=0.5$, $2c_v/\gamma_0B = 0.25$, $\delta = \varphi/2$, $\beta_\phi = 1.5$, $\beta_c^{-1} = 0.5$, $\beta_r^{-1} = 0.7$, $v_p = 0.1$.

5.5. Reliability analysis

To ensure a comprehensive and thorough investigation, this section aims to incorporate the uncertainties around the main soil and earthquake parameters that govern the seismic bearing capacity of shallow foundations (friction angle φ and seismic coefficient k_h) due to the torsional wave propagation and to study their effects on the seismic bearing capacity factor.

This study is carried out in a reliability context using the Monte Carlo simulations. The uncertainties in the above cited parameters (φ and k_h) are introduced in terms of the coefficient of variation of each parameter (COV_φ and COV_{k_h}). The concerned parameters are assumed random variables following the Log-normal distribution to avoid getting negative values of the seismic bearing capacity factor (Griffiths et al., 2002; Cherubini, 2000; Fenton and Griffiths, 2003; Babu et al., 2006). All the parameters involved in the present analysis are summarized in Table 5.1. The statistical moments such as the mean and the standard deviation of the seismic bearing capacity factor ($\mu_{N_{\gamma E}}$, $SD_{N_{\gamma E}}$) and the probability of failure (P_f) of the footing are determined for different values of the torsional wave frequency (KTH). P_f is defined as the probability that the mean bearing capacity factor value ($\mu_{N_{\gamma E}}$) is less than the deterministic value of $N_{\gamma E}$.

Table 5.1 Summary of the parameters used in the reliability analysis

Description	Parameter	Value
Friction angle	φ ($^\circ$)	30
Coefficient of variation of friction angle	COV_φ (%)	5, 10, 15
Seismic acceleration coefficient	k_h	0.2
Coefficient of variation of seismic coefficient	COV_{k_h} (%)	5, 10, 15
Torsional wave frequency	$K_T H$	0.25 - 2.0
Wall friction angle	δ ($^\circ$)	$\varphi/2$
Embedment depth	D_f/B	0.5
Dimensionless cohesion	$2c_v/\gamma_0 B$	0.25

5.5.1. Validation

The present validation is concerned with the case of the static bearing capacity factor due to the unavailability of results for the seismic case. The results of the present study are compared to those of [Massih et al. \(2008\)](#) and [Krishnan and Chakraborty \(2021\)](#) in the static case ($k_h=0$) in terms of the probability of failure ([Fig. 5.17](#)). Note that the latest authors examined the seismic bearing capacity of a strip footing resting on a (c- φ) soil using the finite element lower bound limit analysis formulation in conjunction with a modified pseudo-dynamic approach for the consideration of the seismic action. As shown in [Fig. 5.17](#), the findings of the current study align closely with those reported by [Massih et al. \(2008\)](#).

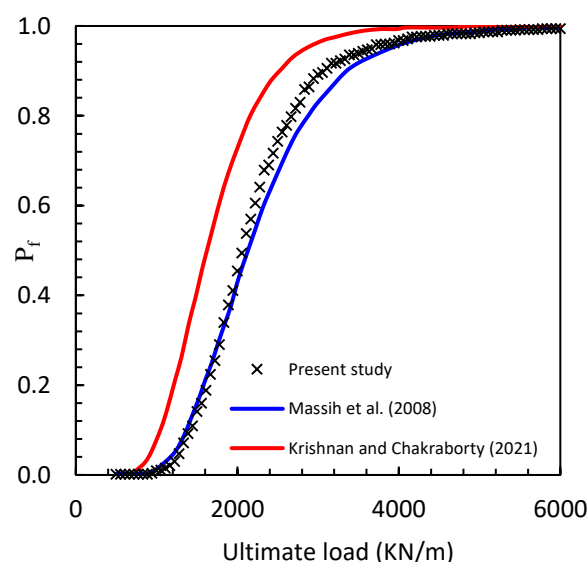


Fig. 5.17 Comparison of probability of failure with published results for $\varphi = 30^\circ$, $c = 20$ kPa, $COV_\varphi = 10\%$, $COV_c = 20\%$, and $k_h = 0$.

5.5.2. Determination of the required number of realizations

In the present seismic case, the determination of the required number of Monte Carlo simulations is based on a convergence study, as illustrated in Fig. 5.18. The figure demonstrates that the failure probability begins to converge after 500 simulations. Therefore, all the analyses in this study are conducted using 500 realizations.

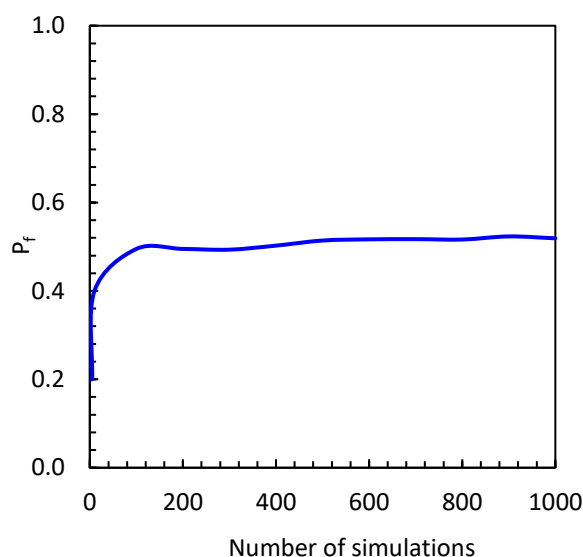


Fig. 5.18 Convergence of the failure probability with respect to the number of simulations for $\varphi=30^\circ$, $k_h = 0.2$, $COV_\varphi = 10\%$, $COV_{k_h} = 15\%$, $\beta_r^{-1} = 0.7$, $\beta_\varphi = 1.5$, $\beta_c^{-1} = 0.5$, $v_p = 0.1$ and $v_c = 15$.

5.5.3. Effects of the COV_φ and COV_{k_h} on the statistical moments of $N_{\gamma E}$ and on the failure probability

Fig. 5.19 shows the variation of the statistical moments (mean and standard deviation) of the equivalent pseudo dynamic bearing capacity factor $N_{\gamma E}$ with respect to the torsional wave frequency for different coefficients of variation of the friction angle (φ) and the seismic coefficient (k_h). It can be noted that the mean bearing capacity factor decreases as the COV_φ increases in the static case ($k_h=0$) and seismic case ($k_h=0.2$). However, the standard deviation of the bearing capacity factor increases as the COV_φ increases. A similar trend was showed by Krishnan and Chakraborty (2021) about the effect of the COV_φ on the mean bearing capacity factor in the static and seismic cases. It can also be noted that the COV_{k_h} does not exert an important impact on the mean and standard deviation of the bearing capacity factor.

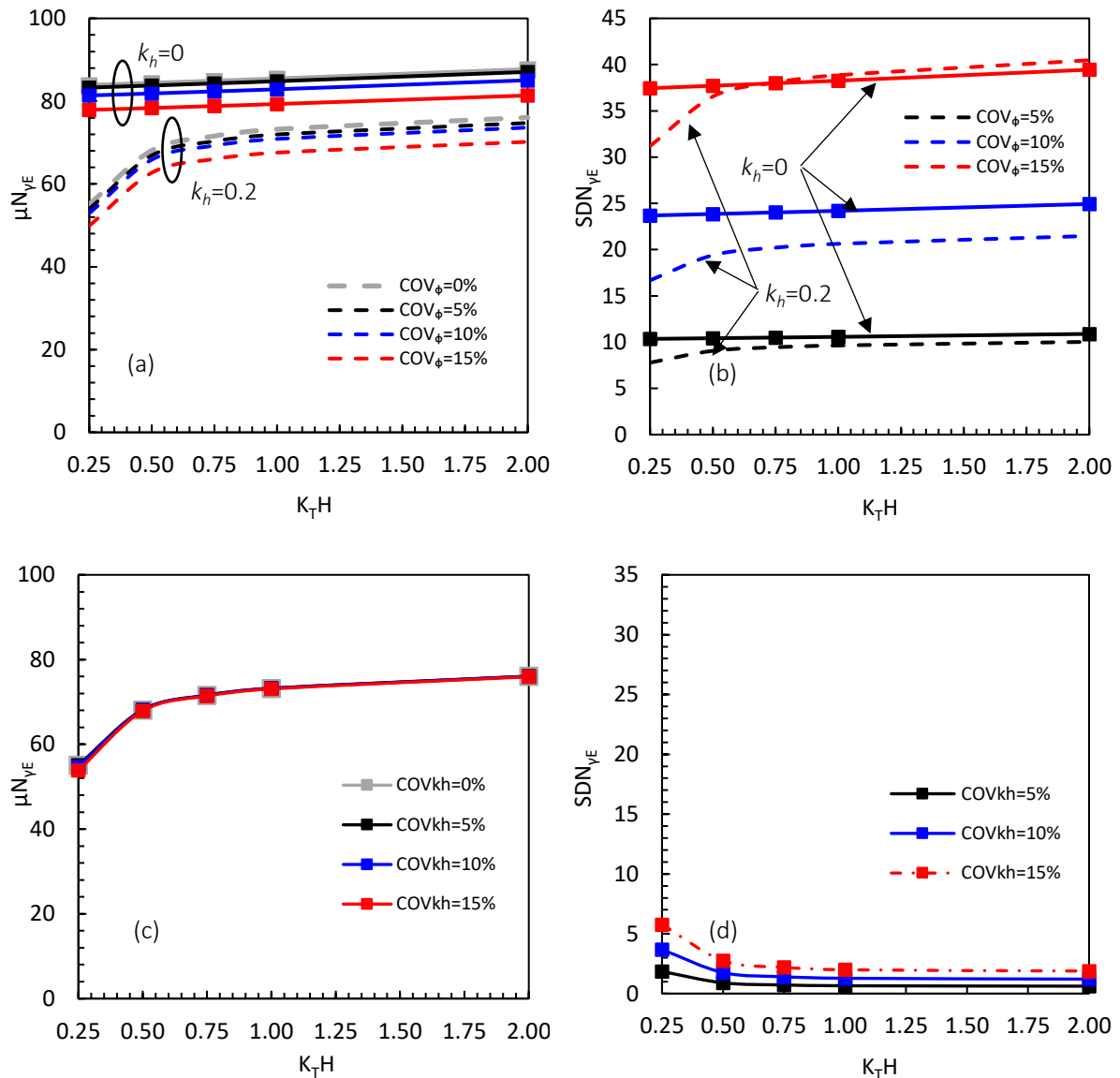


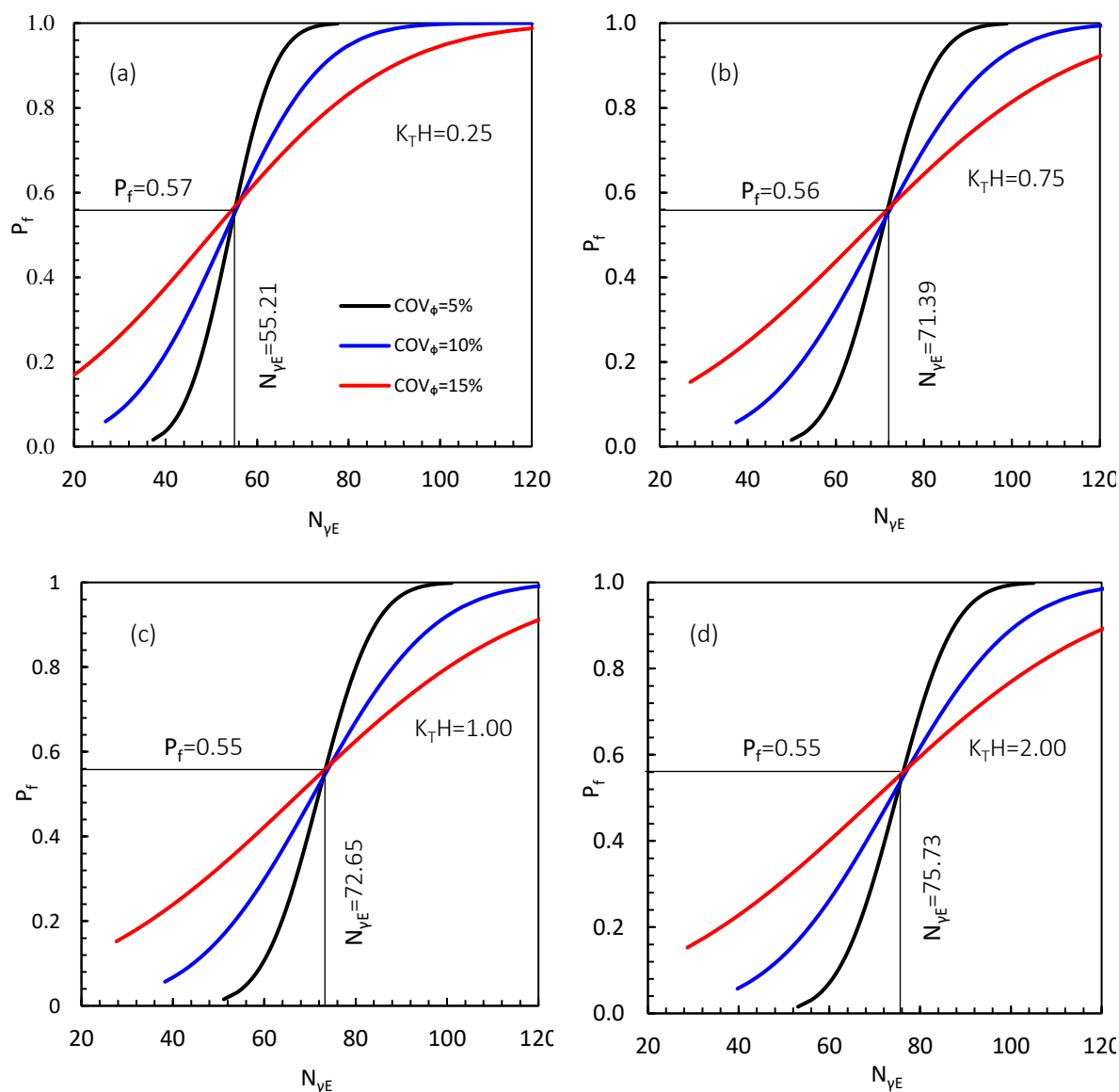
Fig. 5.19 Variation of statistical moments of pseudo dynamic bearing capacity factor versus the torsional wave frequency for different COV : (a) and (b) $\varphi = 30^\circ$, $\beta_r^{-1} = 0.7$, $\beta_\phi = 1.5$, $\beta_c^{-1} = 0.5$, $v_p = 0.1$, $v_c = 15$. (c) and (d) $\varphi = 30^\circ$, $k_h = 0.2$, $\beta_r^{-1} = 0.7$, $\beta_\phi = 1.5$, $\beta_c^{-1} = 0.5$, $v_p = 0.1$, $v_c = 15$.

Figs. 5.20a to 5.20d show the effect of the coefficient of variation of the friction angle (COV_ϕ) and Figs. 5.20e to 5.20f show the effect of the coefficient of variation of the seismic acceleration coefficient (COV_{kh}) on the probability of failure of the equivalent seismic bearing capacity factor ($N_{\gamma E}$) for different values of the torsional wave frequency ($K_T H$). The obtained failure probability was calculated as the cumulative normal distribution function of the log-

normal variables using Eq. (5.1) where a limit state function is defined as $g(\mu_{N_{\gamma E}} \leq N_{\gamma E}) = 0$ (Pula and Chwala, 2018).

$$P_f(\mu_{N_{\gamma E}} \leq N_{\gamma E}) = \Phi \left[\frac{\ln(N_{\gamma E}) - \mu_{N_{\gamma E} \ln}}{\sigma_{N_{\gamma E} \ln}} \right] \quad (5.1)$$

In Eq. (5.1), Φ denotes the cumulative normal distribution function while $\mu_{N_{\gamma E} \ln}$ and $\sigma_{N_{\gamma E} \ln}$ are the log-normally transformed mean and standard deviation of the seismic bearing capacity factor, respectively. These Figures reveal that the failure probability is more and strongly influenced by the COV_ϕ than it is by the COV_{kh} . Fig. 5.20a to 5.20d exhibit that for relatively large COV_ϕ (15%), the probability of failure is conservative (overestimated) for the smaller values of $N_{\gamma E}$ ($N_{\gamma E} \leq 76$) (Fig. 5.20d) and unconservative (underestimated) for relatively high values of $N_{\gamma E}$ ($N_{\gamma E} > 76$).



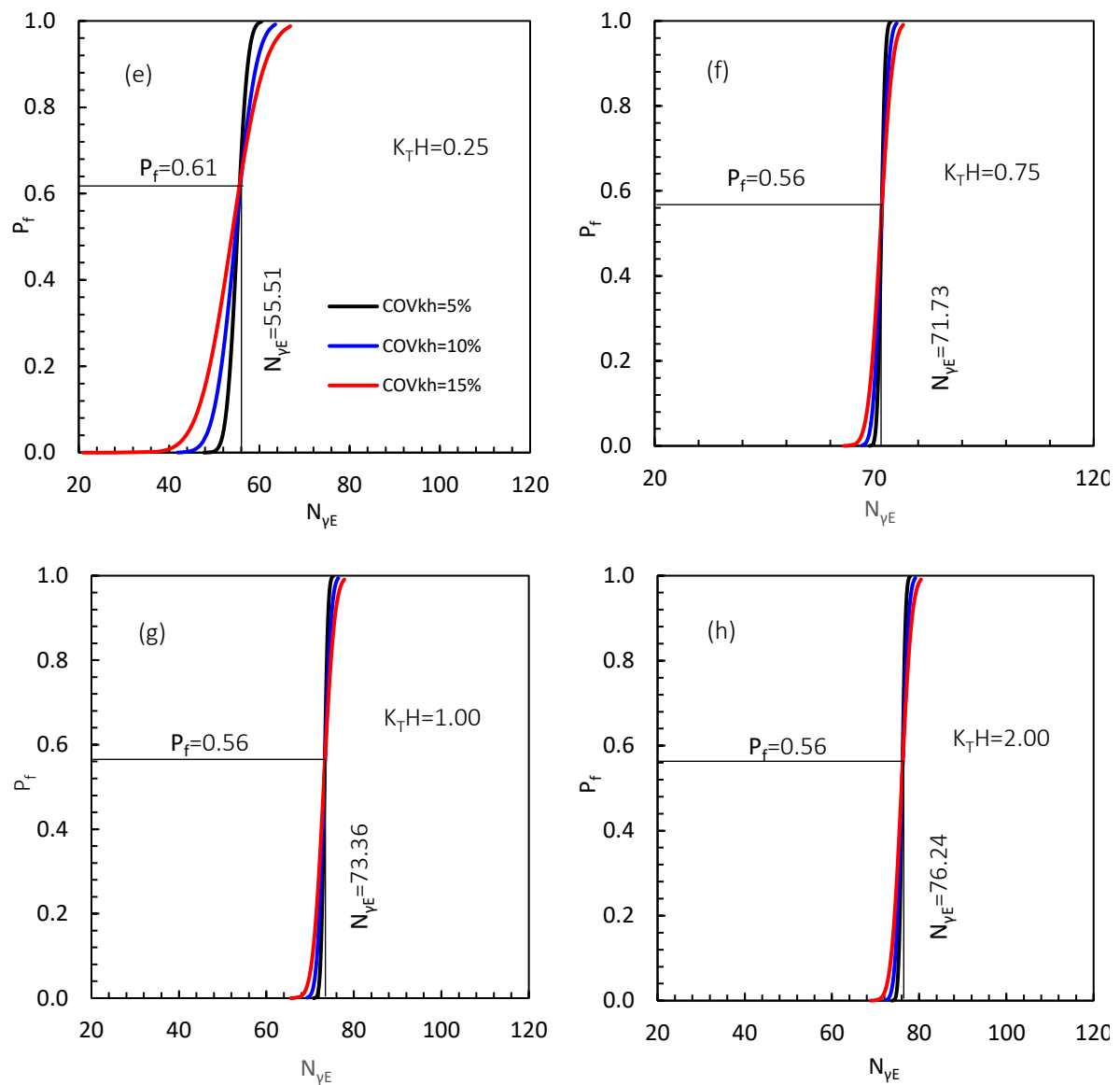


Fig. 5.20 Variation of the failure probability of $N_{\gamma E}$ factor for $\mu_{\phi} = 30^{\circ}$ and $\mu_{kh} = 0.2$ with respect to the torsional wave frequency.

5.5.4. Effects of soil anisotropy on the statistical moments of $N_{\gamma E}$ and on the failure probability

Fig. 5.21 shows the variation of the statistical moments (mean and standard deviation) of the equivalent pseudo dynamic bearing capacity factor $N_{\gamma E}$ with respect to the torsional wave frequency for different values of the rigidity anisotropy. It can be seen that the statistical moments of the seismic bearing capacity factor exhibit a decreasing trend for lower values of the wave frequency ($K_T H \leq 0.5$) as the rigidity anisotropy increases.

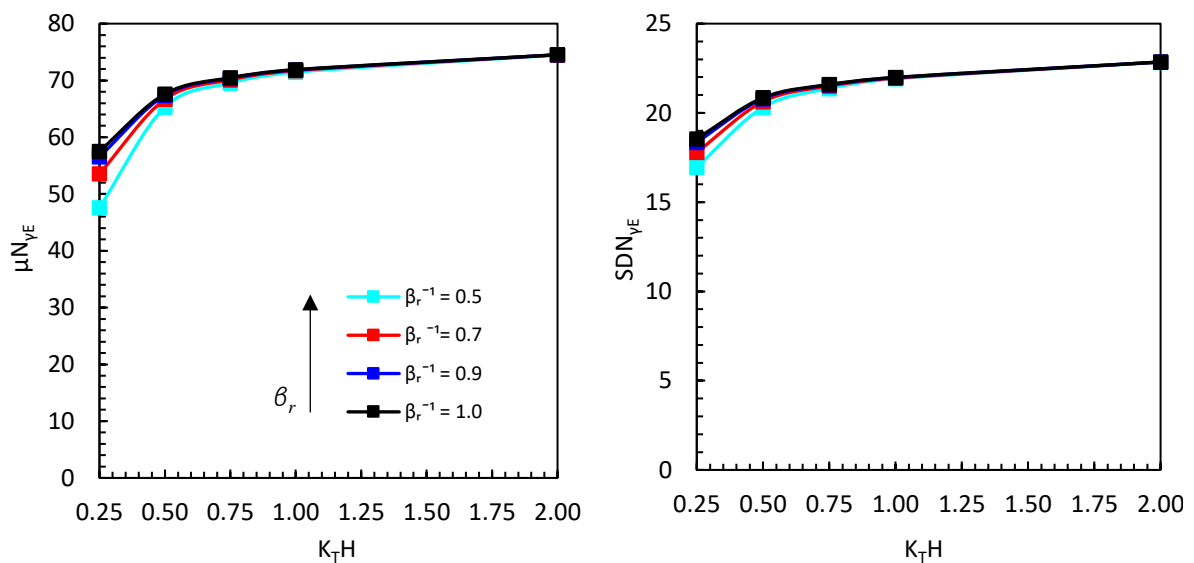


Fig. 5.21 Variation of the statistical moments of the pseudo dynamic bearing capacity factor versus the torsional wave frequency for different values of anisotropy degree of rigidity for: $\mu_\varphi = 30^\circ$, $\mu_{kh} = 0.2$, $COV_\varphi = 10\%$, $COV_{kh} = 5\%$, $\beta_\varphi = 1.5$, $\beta_c^{-1} = 0.5$, $\nu_\gamma = 0.1$ and $\nu_c = 15$.

However, for higher values of wave frequency ($K_{TH} > 0.5$), these moments tend to stabilize. Moreover, the impact of the rigidity anisotropy on the failure probability is shown in Fig. 5.22. It can be seen that the failure probability shows an increasing trend as the anisotropy increases for the lower value of the wave frequency ($K_{TH} = 0.25$). However, for higher values of the wave frequency ($K_{TH} = 0.75, 1, 2$), the failure probability tends to stabilize.

Fig. 5.23 shows the variation of the statistical moments (mean and standard deviation) of the equivalent pseudo dynamic bearing capacity factor $N_{\gamma E}$ with respect to the torsional wave frequency for different values of the internal friction angle anisotropy. It can be noted that the statistical moments decrease as the friction angle anisotropy increases. The decrease is more pronounced when the degree of anisotropy changes from 1 to 2 compared to the change from 2 to 3.

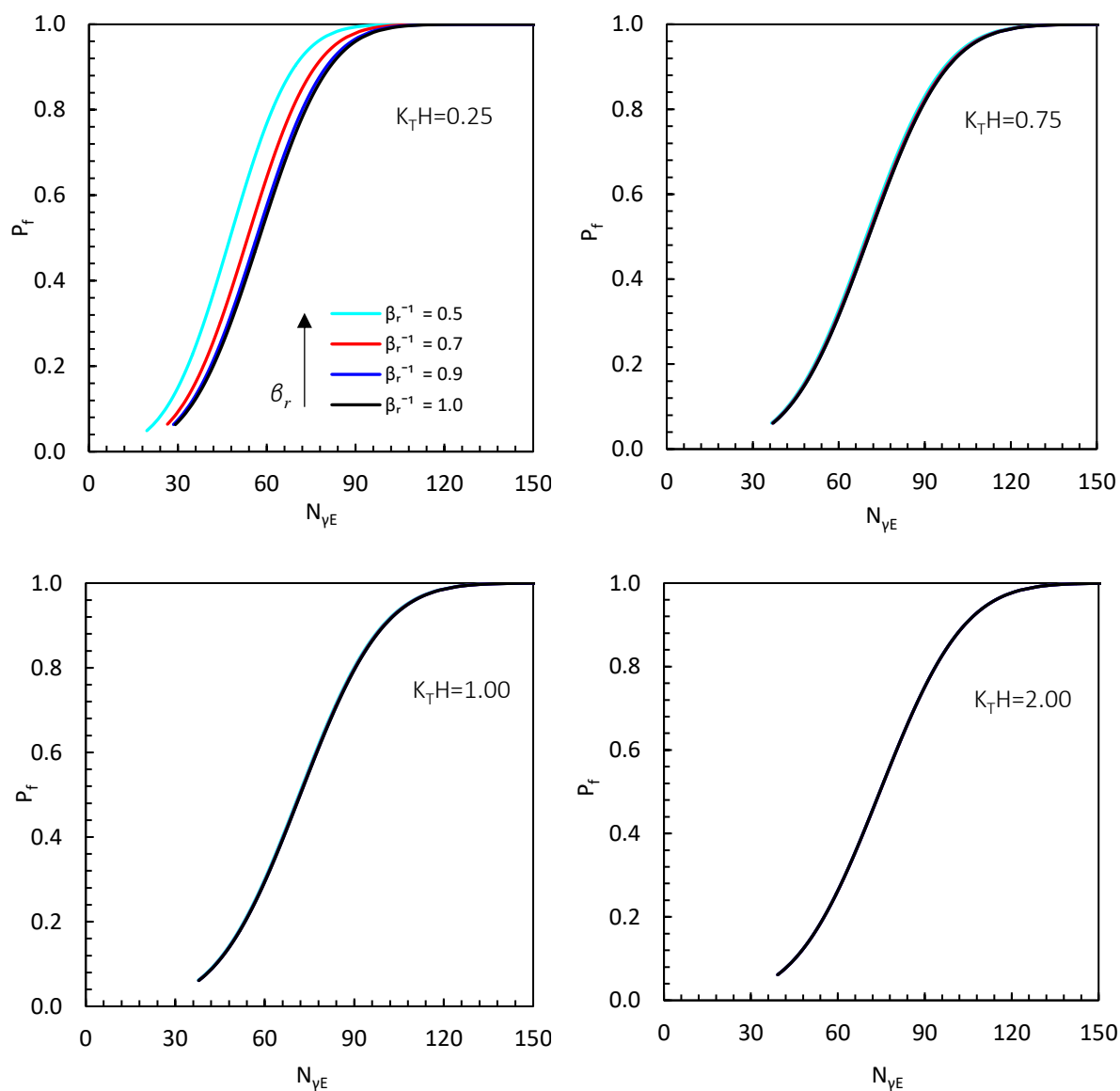


Fig. 5.22 Variation of the failure probability of the pseudo dynamic bearing capacity factor versus the torsional wave frequency for different values of non-homogeneity degree for: $\mu_\varphi = 30^\circ$, $\mu_{kh} = 0.2$, $COV_\varphi = 10\%$, $COV_{kh} = 5\%$, $\beta_\phi = 1.5$, $\beta_c^{-1} = 0.5$, $\nu_\gamma = 0.1$ and $\nu_c = 15$.

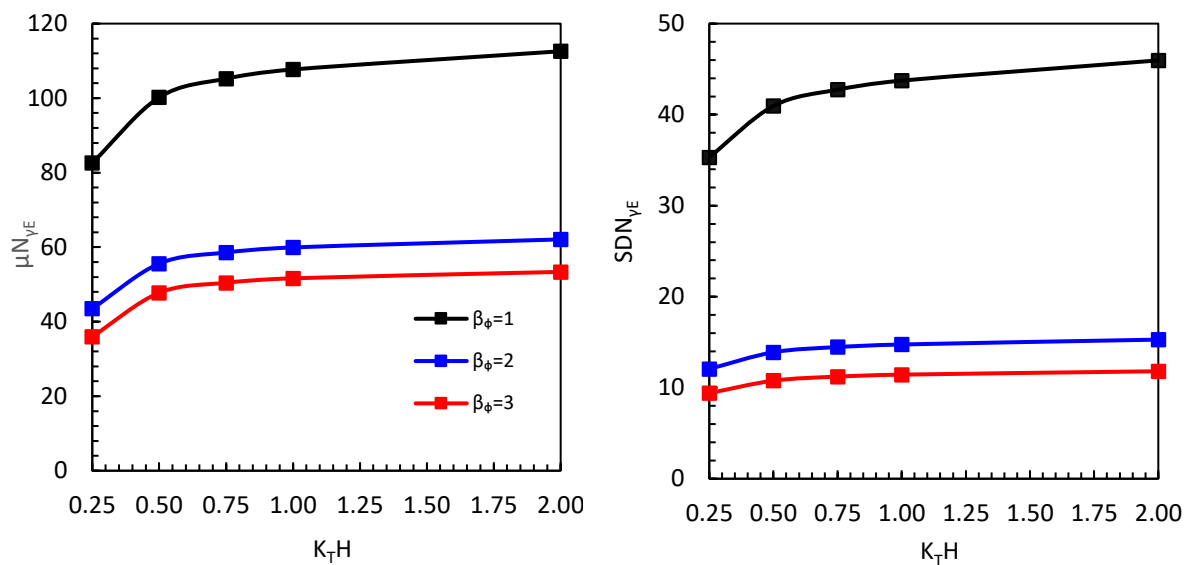


Fig. 5.23 Variation of the statistical moments of the pseudo dynamic bearing capacity factor versus the torsional wave frequency for different values of anisotropy degree of friction angle for: $\mu_\varphi = 30^\circ$, $\mu_{kh} = 0.2$, $COV_\varphi = 10\%$, $COV_{kh} = 5\%$, $\beta_r^{-1} = 0.7$, $\beta_c^{-1} = 0.5$, $\nu_p = 0.1$ and $\nu_c = 15$.

Furthermore, the impact of the internal friction angle anisotropy on the failure probability is shown in Fig. 5.24. The failure probability exhibits a significant increase as the anisotropy degree increases, with a noticeable spike when the degree of anisotropy changes from 1 to 2.

Fig. 5.25 shows the variation of the statistical moments (mean and standard deviation) of the equivalent pseudo dynamic bearing capacity factor $N_{\gamma E}$ with respect to the torsional wave frequency for different values of the anisotropy degree of cohesion. As the anisotropy degree increases, there is a noticeable decrease in the statistical moments.

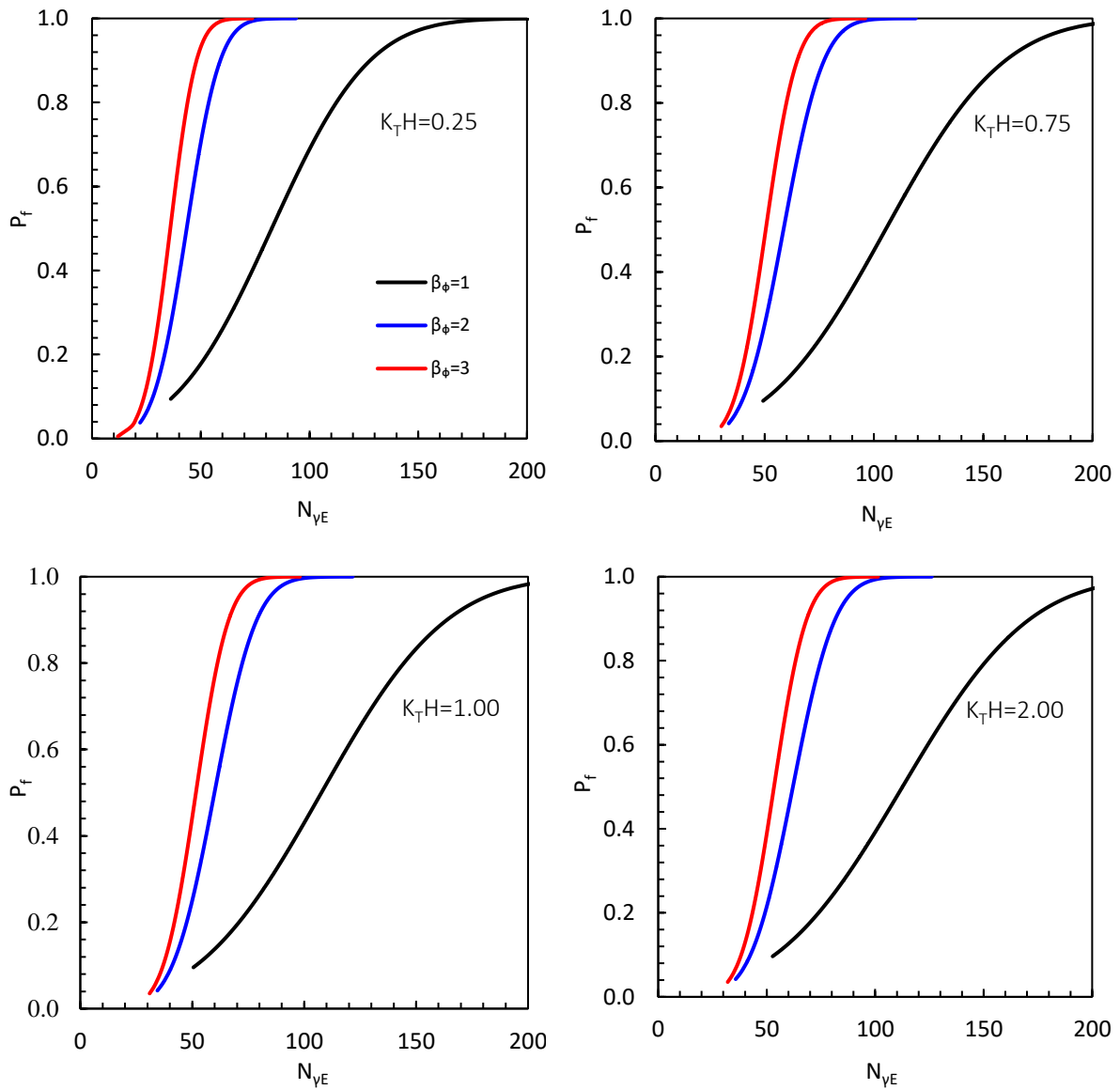


Fig. 5.24 Variation of the failure probability of the pseudo dynamic bearing capacity factor versus the torsional wave frequency for different values of anisotropy degree of friction angle for: $\mu_\phi = 30^\circ$, $\mu_{kh} = 0.2$, $COV_\phi = 10\%$, $COV_{kh} = 5\%$, $\beta_r^{-1} = 0.7$, $\beta_c^{-1} = 0.5$, $\nu_p = 0.1$ and $\nu_c =$

15.

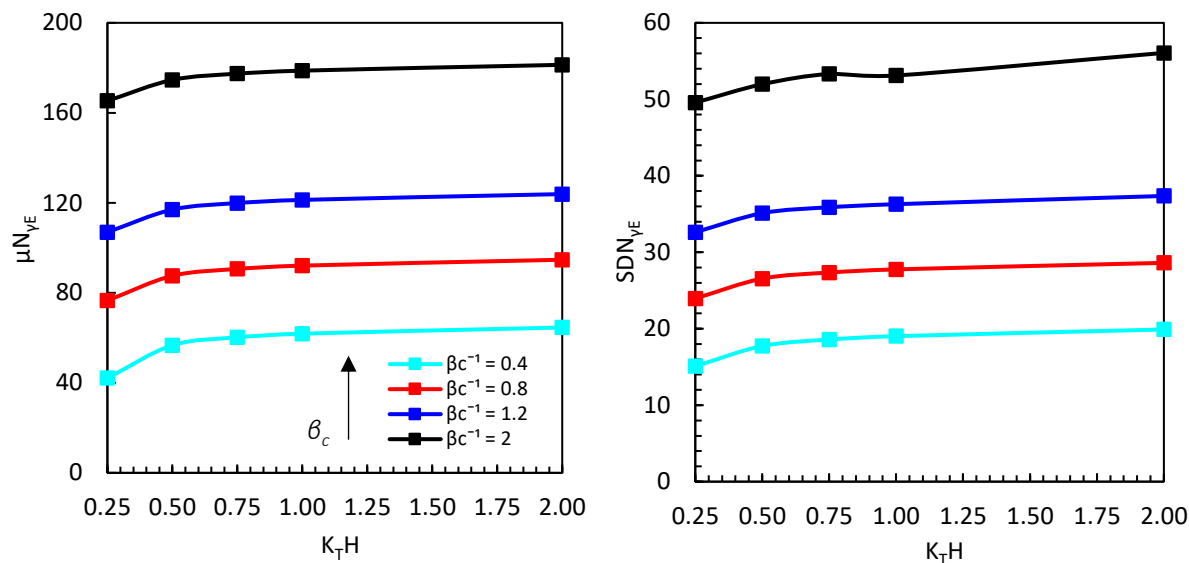


Fig. 5.25 Variation of the statistical moments of the pseudo dynamic bearing capacity factor versus the torsional wave frequency for different values of anisotropy degree of cohesion for:

$$\mu_\phi = 30^\circ, \mu_{kh} = 0.2, COV_\phi = 10\%, COV_{kh} = 5\%, \beta_r^{-1} = 0.7, \beta_\phi = 1.5, \nu_p = 0.1 \text{ and } \nu_c = 15.$$

Otherwise, the impact of the cohesion anisotropy on the failure probability is shown in Fig. 5.26. The figure clearly demonstrates that the failure probability rises with an increasing degree of anisotropy.

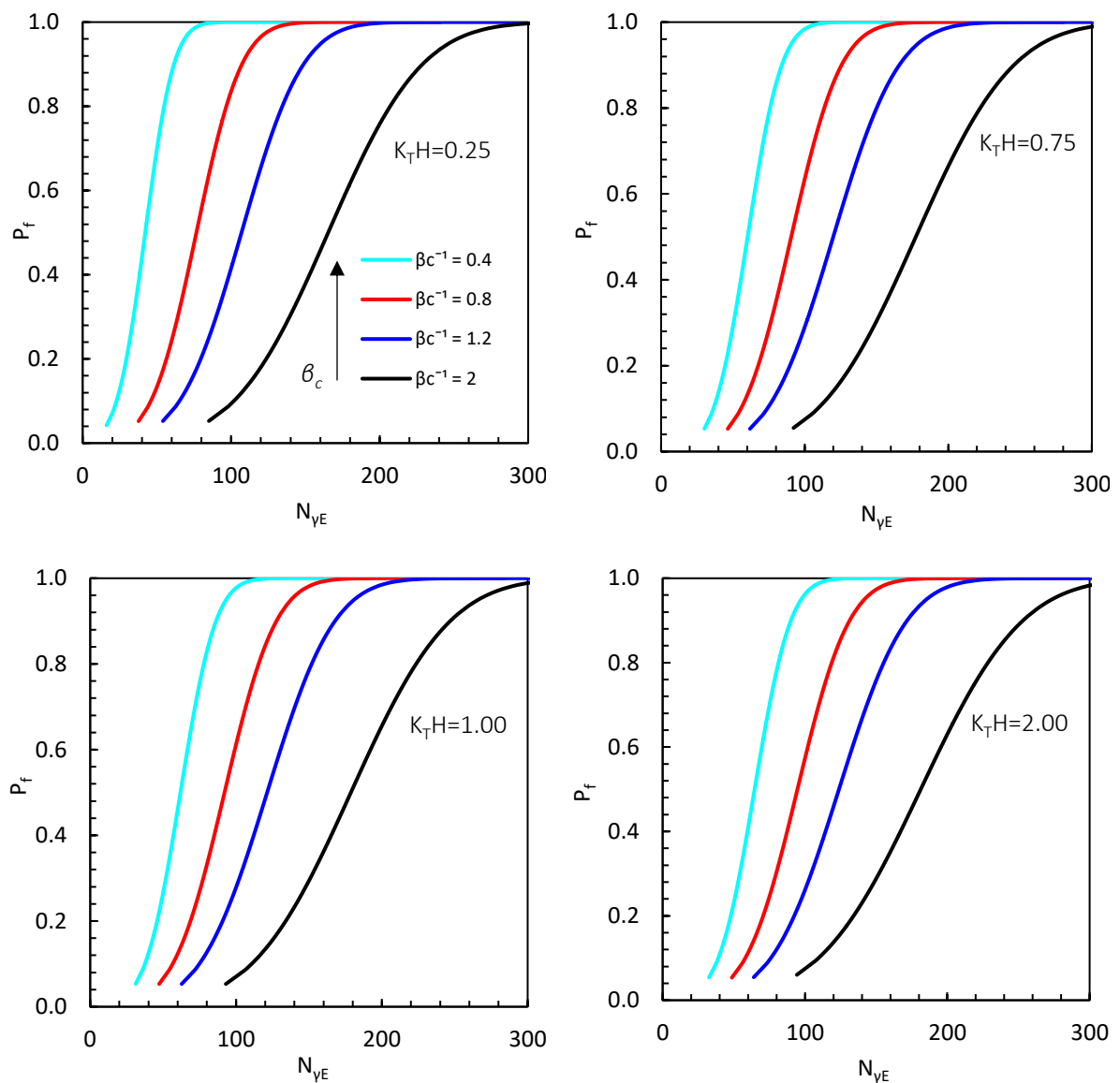


Fig. 5.26 Variation of the failure probability of the pseudo dynamic bearing capacity factor versus the torsional wave frequency for different values of anisotropy degree of cohesion for: $\mu_\phi = 30^\circ$, $\mu_{kh} = 0.2$, $COV_\phi = 10\%$, $COV_{kh} = 5\%$, $\beta_r^{-1} = 0.7$, $\beta_\phi = 1.5$, $\nu_p = 0.1$ and $\nu_c = 15$.

5.5.5. Effect of soil non-homogeneity on the statistical moments of $N_{\gamma E}$ and on the failure probability

Fig. 5.27 shows the variation of the statistical moments (mean and standard deviation) of the equivalent pseudo dynamic bearing capacity factor $N_{\gamma E}$ with respect to the torsional wave frequency for different values of non-homogeneity parameter. The findings demonstrate that the statistical moments of the seismic bearing capacity factor increases as the non-homogeneity

increases. It is evident that the impact of the non-homogeneity is more significant as the wave frequency increases.

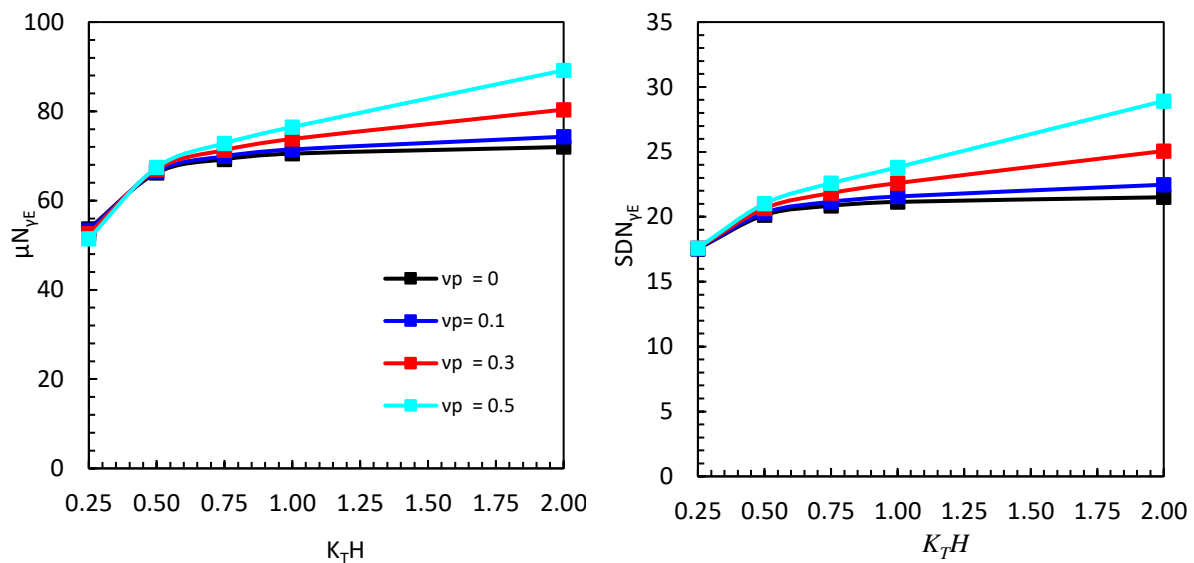


Fig. 5.27 Variation of the statistical moments of the pseudo dynamic bearing capacity factor versus the torsional wave frequency for different values of non-homogeneity parameter for: $\mu_\varphi = 30^\circ$, $\mu_{kh} = 0.2$, $COV_\varphi = 10\%$, $COV_{kh} = 5\%$, $\beta_\phi = 1.5$, $\beta_c^{-1} = 0.5$, $\beta_r^{-1} = 0.7$ and $v_c = 15$.

Besides that, the impact of the non-homogeneity parameter on the failure probability is shown in Fig. 5.28. This figure reveals that the failure probability decreases as the non-homogeneity increases.

Fig. 5.29 shows the variation of the statistical moments (mean and standard deviation) of the equivalent pseudo dynamic bearing capacity factor $N_{\gamma E}$ with respect to the torsional wave frequency for different values of the cohesion non-homogeneity. The results show that the statistical moments of the seismic bearing capacity increase as the non-homogeneity increases.

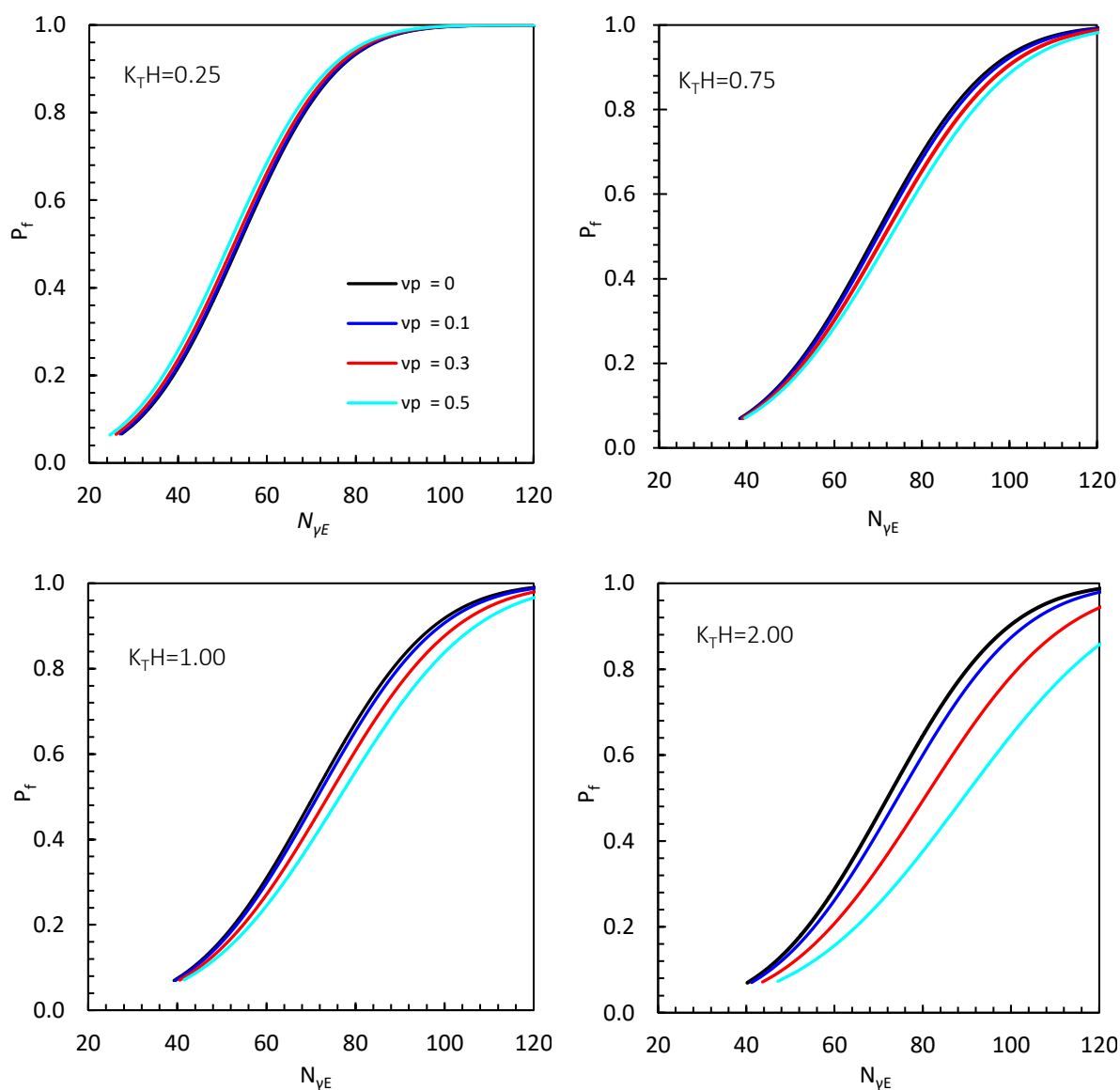


Fig. 5.28 Variation of the failure probability of the pseudo dynamic bearing capacity factor versus the torsional wave frequency for different values of non-homogeneity coefficient for: $\mu_\phi = 30^\circ$, $\mu_{kh} = 0.2$, $COV_\phi = 10\%$, $COV_{kh} = 5\%$, $\beta_\phi = 1.5$, $\beta_c^{-1} = 0.5$, $\beta_r^{-1} = 0.7$ and $v_c = 15$.

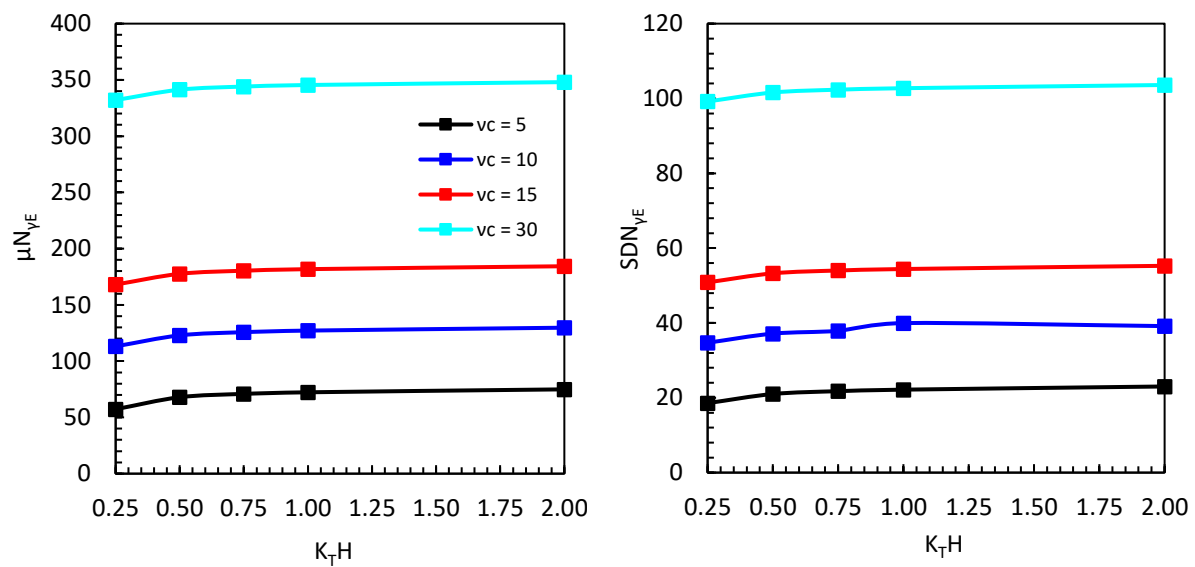


Fig. 5.29 Variation of the statistical moments of the pseudo dynamic bearing capacity factor versus the torsional wave frequency for different values of non-homogeneity coefficient of cohesion for: $\mu_\phi = 30^\circ$, $\mu_{kh} = 0.2$, $COV_\phi = 10\%$, $COV_{kh} = 5\%$, $\beta_r^{-1} = 0.7$, $\beta_\phi = 1.5$, $\beta_c^{-1} = 2$ and $\nu_p = 0.1$.

The impact of the cohesion non-homogeneity on the failure probability is also shown in Fig. 5.30, which reveals that the failure probability decreases as the non-homogeneity increases.

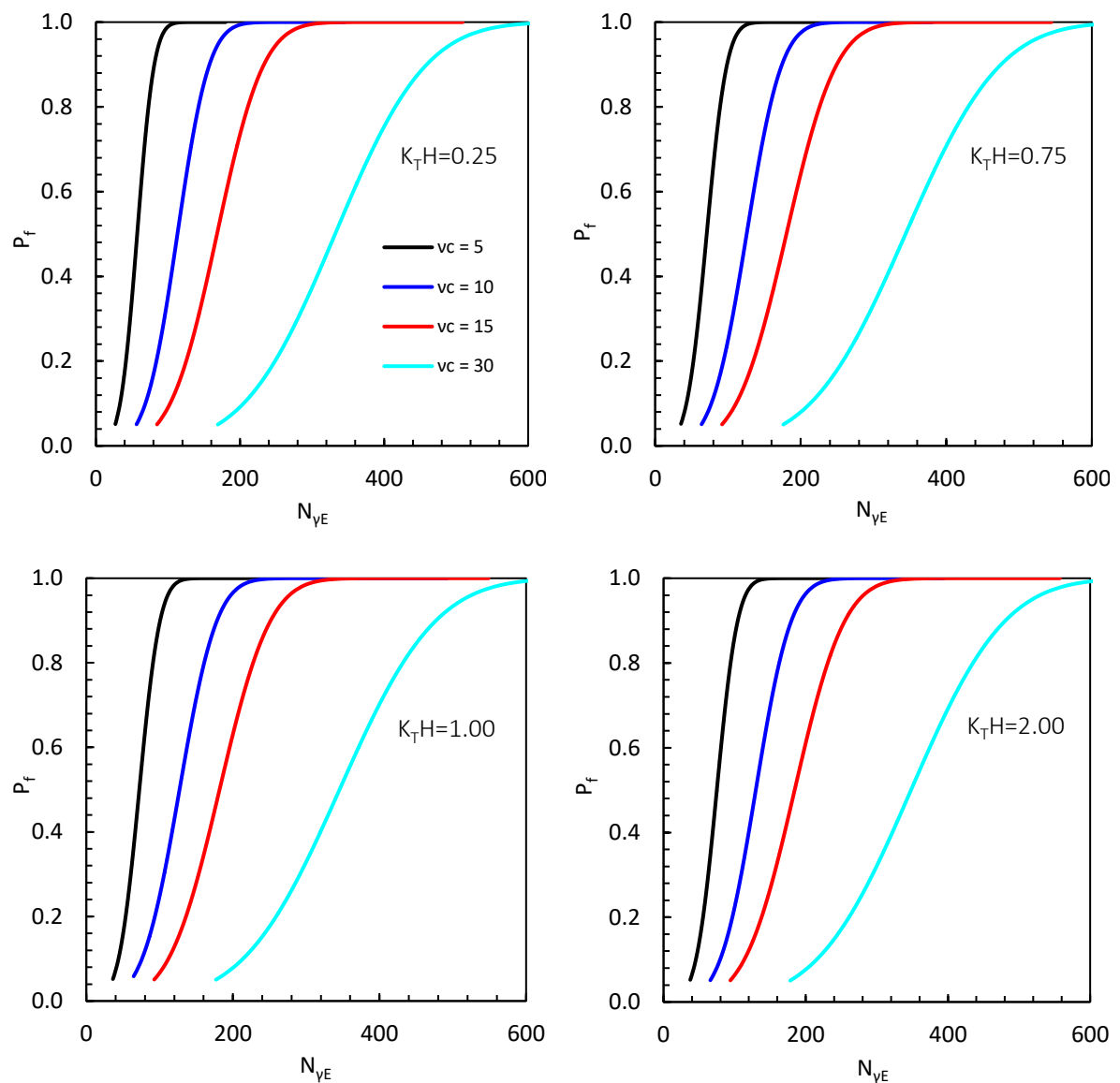


Fig. 5.30 Variation of the failure probability of the pseudo dynamic bearing capacity factor versus the torsional wave frequency for different values of non-homogeneity coefficient of cohesion for: $\mu_\phi = 30^\circ$, $\mu_{kh} = 0.2$, $COV_\phi = 10\%$, $COV_{kh} = 5\%$, $\beta_r^{-1} = 0.7$, $\beta_\phi = 1.5$, $\beta_c^{-1} = 2$ and $\nu_p = 0.1$.

5.5.6. Effect of wavelength on the failure probability

Fig. 5.31 shows the variation of the failure probability of the equivalent seismic bearing capacity factor $N_{\gamma E}$ for different torsional wave frequencies. It is observed that as the torsional wave frequency increases, the failure probability decreases. This implies that longer wavelengths of the torsional wave are associated with a higher probability of failure. It is

noteworthy that the failure probability is particularly affected by low wave frequencies ($K_{\tau H} < 0.75$), which correspond to longer wavelengths.

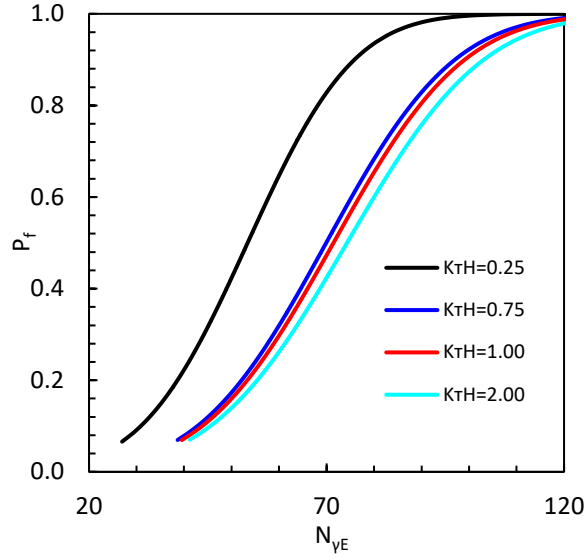


Fig. 5.31 Variation of the failure probability of $N_{\gamma E}$ factor for different torsional wave frequencies for $\mu_{\phi} = 30^{\circ}$, $\mu_{kh} = 0.2$, $COV_{\phi} = 10\%$, $COV_{kh} = 5\%$, $\beta_{\phi} = 1.5$, $\beta_c^{-1} = 0.5$, $\beta_r^{-1} = 0.7$, $\nu_p = 0.1$ and $\nu_c = 15$.

5.5.7. Effect of FOS on P_f

In order to complete the reliability analysis, the variation of the failure probability of the equivalent seismic bearing capacity factor ($N_{\gamma E}$) with respect to the factor of safety (FOS) was studied by modifying Eq. (5.2) as follows

$$P_f \left(\mu_{N_{\gamma E}} \leq N_{\gamma E} / FOS \right) = \Phi \left[\frac{\ln(N_{\gamma E} / FOS) - \mu_{N_{\gamma E}}}{\sigma_{N_{\gamma E}}} \right] \quad (5.2)$$

Generally, the factor of safety used for shallow foundations is between 3 and 4 (Griffiths et al., 2002). In the present study, the failure probability is determined for a safety factor varying from 1 to 4 with respect to different values of the COV_{ϕ} in the static and seismic case, respectively, as shown in Fig. 5.32a and Fig. 5.32b. The figures indicate that the failure probability decreases as the FOS increases. When a higher FOS is taken, the chance of the failure in the static case is reduced to 0%, 1% and 37% for $COV_{\phi} = 5\%$, 10% and 15% respectively, while in the seismic case is reduced to 0%, 6% and 49%. It is evident that for a high degree of uncertainty ($COV_{\phi} = 15\%$), a FOS greater than 4 is required in both cases.

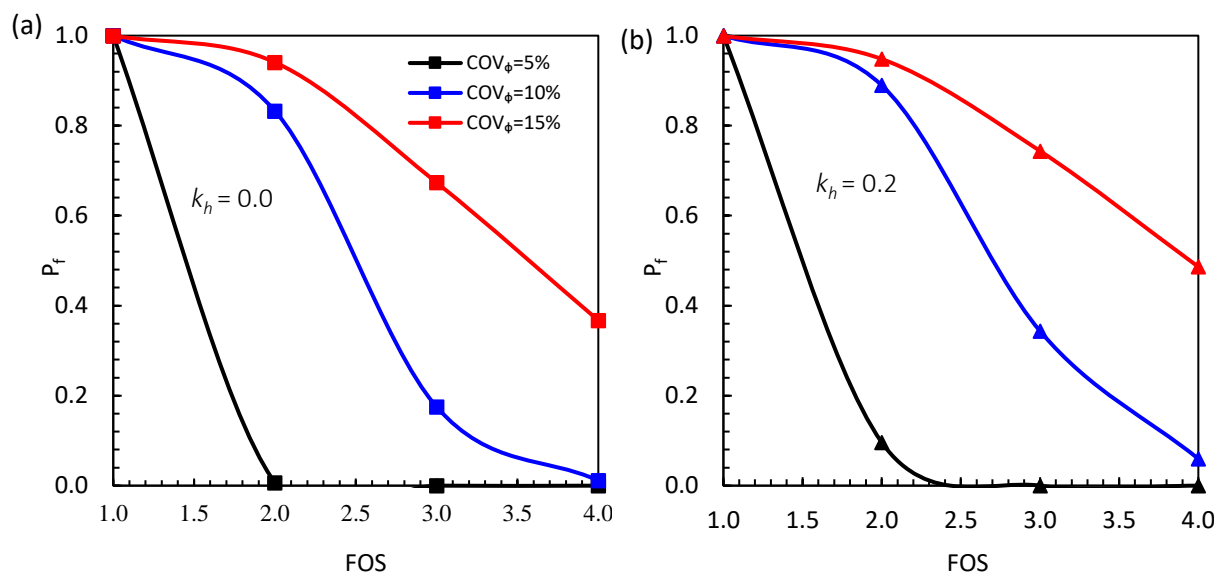


Fig. 5.32 Variation of the failure probability of $N_{\gamma E}$ factor with respect to the FOS for different values of the COV_{ϕ} for $\mu_{\phi} = 30^{\circ}$, $K_{TH} = 0.25$, $\beta_{\phi} = 3$, $\beta_c^{-1} = 0.4$, $\beta_r^{-1} = 0.5$, $v_p = 0.5$ and $v_c = 30$.

5.6. Conclusion

In this chapter, the influence of the torsional wave propagation and the soil-earthquake parameter uncertainties on the seismic bearing capacity of shallow foundations in anisotropic non-homogeneous media was investigated.

The most important conclusions that can be drawn out from the present chapter are summarized in the following points.

- 1) The increase in the soil shear strength parameters (ϕ , δ and c) as well as the depth of the footing leads to an increase in the seismic bearing capacity factor and, consequently, an increase in the ultimate seismic bearing capacity of foundations.
- 2) The anisotropy of the soil strength parameters exerts a notable effect on the seismic bearing capacity factor, which leads to a decrease in the ultimate seismic bearing capacity of foundations.
- 3) The non-homogeneity of the soil strength parameters significantly affects the seismic bearing capacity factor, leading to an increases in the ultimate seismic bearing capacity of foundations.

- 4) The seismic bearing capacity factor decreases as the acceleration coefficient of the torsional wave increases.
- 5) The seismic bearing capacity factor increases as the wave frequency increases. The increase of the wave frequency means a decrease in the wavelength and therefore a reflected effect will be noted on the bearing capacity factor. Hence, the seismic bearing capacity factor decreases as the wavelength of the torsional wave increases.
- 6) As the coefficients of variation of the soil and earthquake parameters (ϕ and k_h) increase, the mean value of the seismic bearing capacity factor decreases while the standard deviation increases.
- 7) The probability of failure of the seismic bearing capacity factor is more significantly affected by the uncertainties around the angle of internal friction than it is for the uncertainties included in the acceleration coefficient of the torsional wave.
- 8) For relatively large COV_ϕ , the probability of failure is conservative for the smaller values of $N_{\gamma E}$ ($N_{\gamma E} \leq 76$) and unconservative for relatively high values of $N_{\gamma E}$ ($N_{\gamma E} > 76$).
- 9) As the anisotropy of the soil strength parameters increases, the statistical moments of the seismic bearing capacity factor decrease accordingly. This decrease leads to an increase in the failure probability.
- 10) As the non-homogeneity of the soil strength parameters increases, the statistical moments of the seismic bearing capacity factor correspondingly increase. Consequently, this leads to a decrease in the failure probability.
- 11) The failure probability increases as the wavelength of the torsional wave increases.
- 12) Finally, the adopted safety factor (FOS) of 3 to 4 for shallow foundations may not provide sufficient guarantee for the structure's safety against failure. Therefore, it is necessary to incorporate a probabilistic analysis into the design charts to identify potential risks to structures.

GENERAL CONCLUSIONS AND
RECOMMENDATIONS FOR FUTURE
WORKS

1. General conclusions

This thesis focuses on the reliability analysis of the bearing capacity of shallow foundations under dynamic loading. It encompasses two main studies. The first one involves a numerical application that explores the impact of randomly varying soil and earthquake parameters on the seismic bearing capacity of shallow strip footing resting on: (i) a cohesive-frictional soil layer and (ii) a purely cohesive soil layer. The Karhunen-Loève (KL) expansion method within the context of random field theory was employed in that study. The second one introduces a formulation for determining the seismic bearing capacity factor of a shallow strip footing influenced by torsional surface wave propagation and resting on anisotropic heterogeneous soil. The limit equilibrium method in conjunction with the pseudo-dynamic approach were employed here. In addition to that, a reliability analysis based on the Monte Carlo simulation method was conducted in order to incorporate the soil-earthquake uncertainties and investigating their effects.

The main findings from the both studies can be outlined as follows:

- The influence of the autocorrelation function (ACF) type on the probabilistic outcomes appears to be relatively minor when contrasted with the variability in soil-earthquake parameters as represented by the coefficient of variation (COV) and the scale of fluctuation (SOF).
- The proposed seismic bearing capacity factor can be applicable in order to quantify the torsional wave propagation, the anisotropy and the non-homogeneity of the soil properties.
- The anisotropy and non-homogeneity of the soil strength parameters exerts a notable impact on the seismic bearing capacity factor.
- Torsional wavelength (or wave frequency) and the seismic acceleration significantly affect the seismic bearing capacity factor.
- The uncertainty in the soil and earthquake parameters, as indicated by the coefficient of variation, significantly impacts the statistical moment and the failure probability of the obtained seismic bearing capacity factor.
- The failure probability is influenced by the torsional wavelength, the anisotropy and the non-homogeneity.
- The necessity of the incorporation a probabilistic analysis in the seismic design of shallow foundations instead of safety factor is very important.

2. Recommendations for future works

This study presents both deterministic and probabilistic analyses of the seismic bearing capacity of shallow foundations situated on a single soil layer posed on a half-space. However, given that the Earth's surface is typically composed of non-homogeneous multiple soil layers, the assessment of the seismic bearing capacity of shallow foundations in a multi-layered soil profile would provide a more realistic insight in the geotechnical engineering field.

While the study of wave propagation in porous media has long captivated researchers' interest, the exploration of bearing capacity concerning shallow foundations on such substrates has not garnered commensurate attention. Despite the pioneering efforts of Biot, this facet remains underexplored. Consequently, delving into this area represents a promising research avenue ripe for exploration and potential breakthroughs.

In addition, Rahmani Kouadri in her thesis ([Rahmani Kouadri, 2022](#)) and [Rahmani Kouadri and co-authors \(2022\)](#) proved that the damping characteristics of the skeleton within a porous medium play a crucial role in governing wave propagation dynamics within such materials. As a result, they wield considerable influence over the bearing capacity of foundations situated within these media. Surprisingly, this aspect remains relatively unexplored by researchers, indicating a promising avenue for further investigation and potential breakthroughs in understanding and optimizing foundation performance in porous environments.

.

BIBLIOGRAPHIC
REFERENCES

Bibliographic references

Ait-Meziane Y, Souici R, Lazzali F (2018), “Relevant lessons learned from the earthquakes El Asnam, 10/10/1980 and Zemmouri, 05/21/2003 on the parasismic prevention in Algeria”, *MATEC Web of Conferences*, 149, 02040.

Alamanis N, Dakoulas P (2021), “Simulation of random fields of soil properties by the local average subdivision method and engineering applications”, *Energy Syst*, 12(4): 841-861.

Al-Bittar T, Soubra A H (2014). “Probabilistic Analysis of Strip Footings Resting on Spatially Varying Soils and Subjected to Vertical or Inclined Loads”, *Journal of Geotechnical and Geoenvironmental Engineering*, 140(4): 04013043.

Al-Bittar T, Soubra A H (2016), “Bearing capacity of spatially random rock masses obeying Hoek–Brown failure criterion”, *Georisk: Assessment and Management of Risk for Engineered Systems and Geohazards*, 11(2): 215–229.

Al-Bittar T, Soubra A H, Thajeel J (2018), “Kriging-Based Reliability Analysis of Strip Footings Resting on Spatially Varying Soils”, *Journal of Geotechnical and Geoenvironmental Engineering*, 144(10): 04018071.

Al-Shamrani M A, Moghal A A B (2012), “Upper Bound Solutions for Bearing Capacity of Footings on Anisotropic Cohesive Soils”, *GeoCongress 2012*.

Ang A H S, W H (1984), “Probability Concepts in Engineering Planning and Design: Decision, Risk and Reliability”, (2), Wiley, New York.

Asaoka A, A-Grivas D (1982), “Spatial variability of the undrained strength of clays”, *Journal of the Geotechnical Engineering Division, ASCE*, 108: 743–756.

Babu G L S, Srivastava A, Murthy D S N (2006), “Reliability analysis of the bearing capacity of a shallow foundation resting on cohesive soil”, *Canadian Geotechnical Journal*, 43(2): 217–223.

Baecher G B (1982), “Simplified geotechnical data analysis”, In: Thoft-Christensen, P. (Ed.). “Reliability Theory and Its Applications in Structural and Soil Engineering”, Reidal Publishing, Dordrecht, the Netherlands.

Baecher G B, Marr, W A, Lin, J S, Consla J (1983), “Critical Parameters for Mine Tailings Embankments”, US Bureau of Mines, Denver, CO.

- Bond A, Harris A (2008), “Decoding eurocode 7”. *Taylor and Francis*, London.
- Brahmi N, Ouahab M Y, Mabrouki A, Benmeddour D, Mellas M (2018), “Probabilistic analysis of the bearing capacity of inclined loaded strip footings near cohesive slopes”, *International Journal of Geotechnical Engineering*, 1–8.
- Britannica T Editors of Encyclopaedia (2008). “Kōbe earthquake of 1995 | Japan, Response, Casualties & Aftermath”. *Encyclopedia Britannica*. <https://www.britannica.com/event/Kobe-earthquake-of-1995>.
- Britannica T Editors of Encyclopaedia (2023), “Mexico City earthquake of 1985”. *Encyclopedia Britannica*. <https://www.britannica.com/event/Mexico-City-earthquake-of-1985>.
- Budhu M, Al-Karni A. (1993), “Seismic bearing capacity of soils”, *Géotechnique*, 43(1), 181–187.
- Carpenter L C (1980), “Computer Rendering of Fractal Curves and Surfaces”, *ACM SIGGRAPH Computer Graphics*, 14(3): 9–15.
- Casagrande A, Carillo N (1944), “Shear failure of anisotropic materials”, *Journal of Boston Society of Civil Engineers*, 31(4): 74-81.
- Cascone E, Casablanca O (2016), “Static and seismic bearing capacity of shallow strip footings”, *Soil Dynamics and Earthquake Engineering*, 84: 204–223.
- Center for Disaster Philanthropy (2022), “Earthquake in Haiti”. <https://disasterphilanthropy.org/disasters/earthquake-in-haiti/>.
- Chatzigogos C Th (2007), “Comportement sismique des fondations superficielles : Vers la prise en compte d’un critère de performance dans la conception ”. *Phd thesis*.
- Chen C, Dong W, Tang Y (2007), “Seismic ultimate bearing capacity of strip footings on slope”, *Journal of Central South University of Technology*, 14(5): 730-736.
- Cherubini C (2000), “Reliability evaluation of shallow foundation bearing capacity on c' , ϕ' soils”, *Canadian Geotechnical Journal*, 37: 264-269.
- Chiasson P, Lafleur J, Soulié M, Haw K T (1995), “Characterizing spatial variability of clay by geostatistics”, *Canadian Geotechnical Journal*, 32(1): 1–10.

Cho S E, Park H C (2010), “Effect of spatial variability of cross-correlated soil properties on bearing capacity of strip footing”, *International Journal for Numerical and Analytical Methods in Geomechanics*, 34(1): 1-26.

Choudhury D, Katdare A D (2013), “New Approach to Determine Seismic Passive Resistance on Retaining Walls Considering Seismic Waves”, *International Journal of Geomechanics*, 13(6): 852–860.

Choudhury D, Rao K S S (2002), “Seismic passive resistance in soils for negative wall friction”, *Canadian Geotechnical Journal*, 39(4): 971–981.

Choudhury D, Subba Rao K S (2005), “Seismic bearing capacity of shallow strip footings”, *Geotechnical and Geological Engineering*, 23(4): 403–418.

Chwała M, Puła W (2020), “Evaluation of shallow foundation bearing capacity in the case of a two-layered soil and spatial variability in soil strength parameters”, *PLOS ONE*, 15(4): e0231992.

Constantine P (2022), “Random field simulation”. Retrieved in December 21, 2021, from <https://www.mathworks.com/matlabcentral/fileexchange/27613-random-field-simulation>

Conti R (2018), “Simplified formulas for the seismic bearing capacity of shallow strip foundations”, *Soil Dynamics and Earthquake Engineering*, 104: 64-74.

Costet J, Sanglerat G (1983), “Cours pratique de mécanique des sols“. Tomes 1 et 2. 3ème édition, Dunod, Paris.

Davis E H, Christian J T (1971), “Bearing capacity of anisotropic cohesive soil”, *Journal of the Soil Mechanics and Foundations Division*, 97(5): 753-769.

De Jong D J G (1957), “Graphical method for the determination of slip-line fields in soil mechanics”. *Ingenieur*, 69(29): 61-65 (in Dutch).

Debnath L, Ghosh S (2018), “Pseudostatic Analysis of Shallow Strip Footing Resting on Two-Layered Soil”, *International Journal of Geomechanics*, 18(3): 04017161.

DeGroot D J, Baecher G B (1993), “Estimating autocovariance of in-situ soil properties”, *Journal of Geotechnical Engineering, ASCE*, 119(GT1): 147–166.

Dembicki E, Dravtchenko J, Sibille E (1964), “Sur les solutions analytiques approchées des problèmes d'équilibre limite plan pour milieux cohérents et pesants”, *Mec*, 3 : 277-312.

Der Kiureghian A, Ditlevsen O (2009). “Aleatory or epistemic? Does it matter?” *Structural Safety*, 31(2): 105-112.

Deutsch C V, Journel A G (1997), “GSLIB: Geostatistical Software Library and User’s Guide (Applied Geostatistics)”. Oxford University Press, Oxford, 384.

Dobrzański J, Kawa M (2021), “Bearing capacity of eccentrically loaded strip footing on spatially variable cohesive soil”, *Studia Geotechnica et Mechanica*, 43(4): 425-437.

Drucker D C, Prager W (1952), “Soil mechanics and plastic analysis or limit design”, *Q. Appl Math*, 10: 157-165.

Elkateb T, Chalaturnyk R, Robertson PK (2002), “An overview of soil heterogeneity: quantification and implications on geotechnical field problems”, *Canadian Geotechnical Journal*, 40:1–15.

Fenton G A, Griffiths DV (2003), “Bearing-capacity prediction of spatially random $c - \phi$ soils”, *Canadian Geotechnical Journal*, 40(1): 54–65.

Fenton G A, Vanmarcke E H (1990), “Simulation of random fields via local average subdivision”, *Journal of Engineering Mechanics*, 116(8): 1733–1949.

Fournier A, Fussell D, Carpenter L (1982), “Computer rendering of stochastic models”, *Communications of the ACM*, 25(6): 371–384.

Ghanem R G, Spanos P D (1991), “Stochastic Finite Element—A Spectral Approach”. Springer, New York.

Ghosh P (2008), “Upper bound solutions of bearing capacity of strip footing by pseudo-dynamic approach”, *Acta Geotechnica*;3(2): 115-123.

Ghosh S, Debnath L (2017), “Seismic Bearing Capacity of Shallow Strip Footing with Coulomb Failure Mechanism using Limit Equilibrium Method”, *Geotechnical and Geological Engineering*, 35(6): 2647–2661.

Griffiths D V, Fenton G A, Manoharan N (2002), “Bearing Capacity of Rough Rigid Strip Footing on Cohesive Soil: Probabilistic Study”, *Journal of Geotechnical and Geoenvironmental Engineering*, 128(9): 743–755.

Gupta S, Kundu S, Vishwakarma SK (2015), “Propagation of torsional surface waves in an inhomogeneous layer over an initially stressed inhomogeneous half-space”, *Journal of Vibration and Control*, 21(7):1286-1298.

Hamrouni A, Sbartai B, Dias D (2021), “Ultimate dynamic bearing capacity of shallow strip foundations - Reliability analysis using the response surface methodology”, *Soil Dynamics and Earthquake Engineering*, 144: 106690.

Hansen J B (1970), “A Revised and Extended Formula for Bearing Capacity”, Bulletin No. 28, Danish Geotechnical Institute, Copenhagen.

Izadi A, Chenari RJ, Javankhshdel S, Masouleh FH (2022), “Effect of love wave propagation on the equivalent seismic bearing capacity of shallow foundations using 3d coulomb failure mechanism”, *Geotechnical and Geological Engineering*, 40(5): 2781–2797.

Izadi A, Nazemi Sabet Soumehsaraei M, Jamshidi Chenari R, Ghorbani A (2019), “Pseudo-static bearing capacity of shallow foundations on heterogeneous marine deposits using limit equilibrium method”, *Marine Georesources & Geotechnology*, 1–12.

Jha S K (2016), “Reliability-Based Analysis of Bearing Capacity of Strip Footings Considering Anisotropic Correlation of Spatially Varying Undrained Shear Strength”, *International Journal of Geomechanics*, 16(5): 06016003.

Johari A, Hosseini S M, Keshavarz A (2017), “Reliability analysis of seismic bearing capacity of strip footing by stochastic slip lines method”, *Computers and Geotechnics*, 91: 203–217.

Katdare A, Choudhury D (2012), “Effect of Rayleigh wave on seismic active earth pressure behind retaining wall”, *Disaster Advances*, 5(4):1154–1159.

Keaveny J M, Nadim F, Lacasse S (1989), “Autocorrelation functions for offshore geotechnical data”, Proceedings of the Fifth International Conference on Structural Safety and Reliability, Vol. 1. Vancouver, BC, 263–270.

Kouadri R R, Harichane Z, Bouaricha L (2022), “Amplification of seismic wave motions in partially fluid-filled poroviscoelastic media”, *Soil Dynamics and Earthquake Engineering*, 160: 107382.

Kouadri R R, Harichane Z (2022), “Etude de la propagation des ondes sismiques dans les milieux poreux : Applications Pratiques”, *Phd thesis*.

Kötter F, (1903), “Die Bestimmung des Druckes an gekrümmten Gleitflächen”, eine Aufgabe aus der Lehre vom Erddruck. Monatsber, Akad, Wiss, Berlin, 229-233.

Kotzias P C, Stamatopoulos A C, Kountouris P J (1993), “Field quality control on earth-dam: Statistical graphics for gauging”, *Journal Geotechnical Engineering, ASCE*, 119(5): 957–964.

Krishnan K, Chakraborty D (2021), “Seismic bearing capacity of strip footing over spatially random soil using modified pseudo-dynamic approach”, *Computers and Geotechnics*, 136: 508–519.

Kulatilake P H S W, Ghosh A (1988), “An investigation into accuracy of spatial variation estimation using static cone penetrometer data”, *Proceedings of the First International Conference on Penetration Testing*, Orlando, FL, 815–821.

Kumar J, Mohan Rao V B K (2002), “Seismic bearing capacity factors for spread foundations”, *Geotechnique*, 52(2): 79–88.

Kumari P, Sharma VK (2014), “Propagation of torsional waves in a viscoelastic layer over an inhomogeneous half space”, *Acta Mechanica*, 225: 1673–1684.

Kundu S, Gupta S, Saha A, Manna S (2014), “Propagation of a torsional surface wave in a non-homogeneous anisotropic layer over a heterogeneous half-space”, *Journal of Vibration and Control*, 1-12.

Lacasse S, de Lamballerie J Y N (1995), “Statistical treatment of CPT data”. *Proceedings of International Symposium on Cone Penetration Testing*, Linköping, Sweden, 369–380.

Lacasse S, Nadim F (1996), “Uncertainties in characterizing soil properties”, In: Shackelford, C.

Lo K Y (1965), “Stability of slopes in anisotropic soils”, *Journal of the Soil Mechanics and Foundations Division ASCE*, 91(4): 85-106.

Love A E H (1944), “Mathematical Theory of Elasticity”, Dover Publications, 4th Edition.

Lumb P (1970), “Safety factors and the probability distribution of soil strength”, *Canadian Geotechnical Journal*, 7: 225-242.

Lumb P (1972), “Precision and accuracy of soil tests.” In *Statistics and Probability in Civil Engineering*, Hong Kong University Press.

Lumb P (1974), “Application of statistics in soil mechanics”. In: Lee, I. K. (Ed.). *Soil Mechanics: New Horizons*. Butterworth and Company Publishers Limited, London, 44–111.

Luo N, Bathurst R J (2017), “Reliability bearing capacity analysis of footings on cohesive soil slopes using RFEM”, *Computers and Geotechnics*, 89: 203-212.

Manna S, Kundu S, Misra JC (2018), “Theoretical analysis of torsional wave propagation in a heterogeneous aeolotropic stratum over a voigt-type viscoelastic half-space”, *International Journal of Geomechanics*, 18(6): 04018050.

Martin C M (2005), “Exact bearing capacity calculations using the method of characteristics”, *Turin* 4, 441–450.

Meyerhof G G (1963), “Some Recent Research on the Bearing Capacity of Foundations”, *Canadian Geotechnical Journal*, 1(1): 16–26.

Meyerhof G G (1978), “Bearing capacity of anisotropic cohesionless soils”, *Canadian Geotechnical Journal*, 15(4):592–595.

Nadgouda K, Choudhury D (2019), “Seismic bearing capacity factor $N_{\gamma e}$ for dry sand beneath strip footing using modified pseudo-dynamic method with composite failure surface”, *International Journal of Geotechnical Engineering*, 1–10.

Novotortsev V I (1938), “Application of the theory of plasticity to problems of determining the bearing capacity of building foundations”, *Izv., VNIG* 22.

Pakdel P, Jamshidi Chenari R, Veiskarami M (2021), “Seismic bearing capacity of shallow foundations rested on anisotropic deposits”, *International Journal of Geotechnical Engineering*, 15(2): 181-192.

Pane V, Vecchiotti A, Cecconi M (2016), “A numerical study on the seismic bearing capacity of shallow foundations”, *Bulletin of Earthquake Engineering*, 14(11): 2931–2958.

Paolucci R, Pecker A (1997), “Seismic Bearing Capacity of Shallow Strip Foundations on Dry Soils”, *Soils and Foundations*, 37(3): 95–105.

Phoon K K, Kulhawy F H (1996), “On quantifying inherent soil variability”. *Uncertainty in the Geologic Environment, from Theory to Practice*, Proceedings of Uncertainty 96, Madison, WI. Geotechnical Special Publication (GSP) 58, ASCE, Reston, VA, 326–340.

Phoon K K, Kulhawy F H (1999), “Characterization of geotechnical variability”, *Canadian Geotechnical Journal*, 36(4): 612–624.

Popescu R, Prevost J H, Vanmarcke E H (1995), “Numerical simulations of soil liquefaction using stochastic input parameters”, Proceedings of the 3rd International Conference on Recent Advances in Geotechnical Earthquake Engineering and Soil Dynamics, St. Louis, MO, 275–280.

Pramanik D, Manna S (2023), “Love-like wave dispersion in a highly non-homogeneous viscoelastic orthotropic layer under the effect of non-local elasticity”, *Mathematical Methods in the Applied Sciences*, 46 (14): 15048-15072

Prandtl L (1920), Über die Härte plastischer Körper. Nachr. K. Ges. Wiss. Gott., Math.-Phys. Kl, 1920: 74-85.

Puła W, Chwała M (2015), “On spatial averaging along random slip lines in the reliability computations of shallow strip foundations”, *Computers and Geotechnics*, 68: 128–136.

Puła W, Chwała M (2015), “On spatial averaging along random slip lines in the reliability computations of shallow strip foundations”, *Computers and Geotechnics*, 68: 128–136.

Puła W, Chwała M (2018), “Random bearing capacity evaluation of shallow foundations for asymmetrical failure mechanisms with spatial averaging and inclusion of soil self-weight”, *Computers and Geotechnics*, 101: 176–195.

Puła W, Chwała M (2018), “Random bearing capacity evaluation of shallow foundations for asymmetrical failure mechanisms with spatial averaging and inclusion of soil self-weight”, *Computers and Geotechnics*, 101: 176–195.

Rayleigh L (1945), “Theory of sound. Dover”, New York.

Reddy A S, Rao KV (1981), “Bearing capacity of strip footing on anisotropic and nonhomogeneous clays”, *Soils and Foundations*, 21(1):1–6.

Reddy AS, Srinivasan R (1970), “Bearing capacity of footings on anisotropic soils”, *Journal of the Soil Mechanics and Foundations Division*, 96(6):1967–1986.

Reissner H (1924), Zum Erddruckproblem. In: C.B. Biezend and J.M. Burgers (Editors), Proc. 1st Int. Congr. Appl. Mech., Delft, 295-311.

Sturzenegger S (2015). “Loma Prieta Earthquake, 1989 Historical Essay”. FoundSF. https://www.foundsf.org/index.php?title=Loma_Prieta_Earthquake,_1989.

Tang W H (1979), “Probabilistic evaluation of penetration resistances”, *Journal of the Geotechnical Engineering Division, ASCE*, 105(GT10): 1173–1191.

Taylor A. (2016), Nepal’s earthquakes: One year later. The Atlantic. <https://www.theatlantic.com/photo/2016/04/nepals-earthquakes-one-year-later/479772/>.

Taylor D W (1948), “Fundamentals of Soil Mechanics”, Wiley, New York.

Terzaghi K (1943), “Theoretical Soil Mechanics”, Wiley, New York.

Vaishnav PK, Kundu S, Abo-Dahab SM, Saha A (2017), “Torsional surface wave propagation in anisotropic layer sandwiched between heterogeneous half-space”, *Journal of Solid Mechanics*, 9(1): 213-224.

Vanmarcke E H (1977), “Probabilistic modeling of soil profiles.” *Journal of the Geotechnical Engineering Division, ASCE*, 103(11): 1227-1246.

Vanmarcke E H (1983), “Random fields: Analysis and synthesis” M.I.T, Press, Cambridge, Mass, 382.

Vesic A S (1973), “Analysis of ultimate loads of shallow foundations”, *J. Soil Mech. Found. Eng. Div.*, 99(1): 45.

Vrouwenvelder T, Calle E (2003), “Measuring spatial correlation of soil properties”, *Heron*, 48(4): 297–311.

Wikipedia (2024), “Christchurch earthquake 2011”. Wikipedia. https://en.wikipedia.org/wiki/2011_Christchurch_earthquake.

Wolff T F (1996), “Probabilistic slope stability in theory and practice”, *Uncertainty in the Geologic Environment, from Theory to Practice, Proceedings of Uncertainty 96*, Madison, WI. Geotechnical Special Publication (GSP) 58, ASCE, Reston, VA, 419–433.

Wolff T H (1985), “Analysis and design of embankment dam slopes: A probabilistic approach.” Ph.D thesis, Purdue Univ., Lafayette, Ind.

Wu T H (1974), “Uncertainty, safety, and decision in soil engineering”, *Journal of Geotechnical Engineering*, 100(3), 329–348.

- Richards R, Elms D G, Budhu M (1993), “Seismic Bearing Capacity and Settlements of Foundations”, *Journal of Geotechnical Engineering*, 119(4): 662–674.
- Saha A, Ghosh S (2013), “Pseudo-dynamic passive resistance of battered-faced retaining wall supporting c - Φ backfill considering Rayleigh wave”, *International Journal of Geotechnical Engineering*, 8(4): 396–405.
- Saha A, Ghosh S (2014), “Pseudo-dynamic analysis for bearing capacity of foundation resting on c - Φ soil”, *International Journal of Geotechnical Engineering*, 9(4): 379-387.
- Saha A, Ghosh S (2017), “Modified pseudo-dynamic bearing capacity analysis of shallow strip footing considering total seismic wave”, *International Journal of Geotechnical Engineering*.
- Saha A, Nama S, Ghosh S (2019), “Application of HSOS algorithm on pseudo-dynamic bearing capacity of shallow strip footing along with numerical analysis”, *International Journal of Geotechnical Engineering*, 1–14.
- Sarma S K, Iossifelis I S (1990), “Seismic bearing capacity factors of shallow strip footings”, *Géotechnique*, 40(2): 265–273.
- Simões J T, Neves L C, Antão A N, Guerra N M C (2020), “Reliability assessment of shallow foundations on undrained soils considering soil spatial variability”, *Computers and Geotechnics*, 119: 103369.
- Simões J T, Neves L C, Antão A N, Guerra, N M C (2020), “Reliability assessment of shallow foundations on undrained soils considering soil spatial variability”, *Computers and Geotechnics*, 119: 103369.
- Smith C C (2005), “Complete limiting stress solutions for the bearing capacity of strip footings on a Mohr–Coulomb soil”, *Geotechnique*, 55: 607–612.
- Sokolovskii VV (1965), “Statics of Granular Media”, Pergamon Press, New York.
- Soubra A H (1999), “Upper-Bound Solutions for Bearing Capacity of Foundations”, *Journal of Geotechnical and Geoenvironmental Engineering*, 125(1): 59–68.
- Spencer A J M (1962), “Perturbation methods in plasticity”. III, Plane strain of ideal soils and plastic solids with body forces./ *Mech. Phys. Solids*, 10: 165-177.
- Steedman R S, Zeng X (1990), “The influence of phase on the calculation of pseudo-static earth pressure on a retaining wall”, *Géotechnique*, 40(1): 103–112.

Wu Y, Zhou X, Gao Y, Zhang L, Yang J (2019), “Effect of soil variability on bearing capacity accounting for non-stationary characteristics of undrained shear strength”, *Computers and Geotechnics*, 110: 199–210.

Yamamoto K (2010), “Seismic bearing capacity of shallow foundations near slopes using the upper-bound method”, *International Journal of Geotechnical Engineering*, 4(2): 255–267.

Yang X-L, Du D-C (2016), “Upper bound analysis for bearing capacity of nonhomogeneous and anisotropic clay foundation”, *KSCE Journal of Civil Engineering*, 20(7): 2702–2710.

Youssef Abdel Massih D S, Soubra A H, Low B K (2008), “Reliability-Based Analysis and Design of Strip Footings against Bearing Capacity Failure”, *Journal of Geotechnical and Geoenvironmental Engineering*, 134(7): 917–928.

Yucemen M S, Tang W H, Ang A H S (1973), “A probabilistic study of safety and design of earth slopes.” *Civil Engineering Studies, Structural Research Series 402*, University of Illinois, Urbana.

Zhou X-P, Gu X-B, Yu M-H, Qian Q-H (2015), “Seismic bearing capacity of shallow foundations resting on rock masses subjected to seismic loads”, *KSCE Journal of Civil Engineering*, 20(1): 216–228.

APPENDIX

$$A = \sin(\varphi - \alpha_i - i) \sec i \cos \varphi \times \exp(-\psi \tan \varphi) / \sin(2\varphi - \alpha_1 - \alpha_4) \quad (\text{A.1})$$

$$M = \sin(\varphi + \alpha_2 + \alpha_3) \sec i \times \cos \varphi / \sin(2\varphi - \alpha_2 - \alpha_3) \quad (\text{A.2})$$

$$D = \{L_1 \cos \varphi - r_1 \cos(\varphi + \alpha_2 + \alpha_3)\} \times \frac{\cos \varphi}{\sin(2\varphi + \alpha_2 + \alpha_3)} \\ - \{L_0 \cos \varphi - r_0 \cos(\varphi - \alpha_1 - \alpha_4)\} \times \frac{\cos \varphi \exp(-\psi \tan \varphi)}{\sin(2\varphi - \alpha_1 - \alpha_4)} \\ + r_1 \{1 - \exp(-2\psi \tan \varphi)\} / \tan \varphi \quad (\text{A.3})$$

$$R = \delta r_1^2 \sec i \cos \mu \{ \exp(-b \tan \mu) \times \sin(\alpha_3 + \psi + i - \mu) - \sin(\alpha_3 + i - \mu) \} \\ + r_1 L M \sin \alpha_3 - A L_0 \sin \alpha_1 \quad (\text{A.4})$$

$$\mu = \tan^{-1}(3 \tan \varphi) \quad (\text{A.5})$$

$$i = \tan^{-1}(k_c) \quad (\text{A.6})$$

$$\psi = \pi - \alpha_3 - \alpha_4 \quad (\text{A.7})$$

$$r_0 = \sin(\alpha_1) / \sin(\alpha_1 + \alpha_4) \quad (\text{A.8})$$

$$r_1 = r_0 e^{\psi \tan \varphi} \quad (\text{A.9})$$

$$L_0 = \sin(\alpha_4) / \sin(\alpha_1 + \alpha_4) \quad (\text{A.10})$$

$$L_1 = r_1 \sin(\alpha_3) / \sin(\alpha_2) \quad (\text{A.11})$$

$$L = r_1 \sin(\alpha_2 + \alpha_3) / \sin(\alpha_2) \quad (\text{A.12})$$

The dimensions r_0 , r_1 , L_0 , L_1 and L can be obtained as fraction of foundation width B as defined in the Fig. 1.14. The angles α_1 , α_2 , α_3 and α_4 are shown also in the same figure.

$$\alpha_i = w_i \sin(\varphi - \beta_i) + R_i \cos\varphi + S_{i+1} \sin(\varphi - \beta_i - \delta_{i+1}) - S_i \sin(\varphi - \beta_i - \delta_i) \quad (\text{A.13})$$

$$p_i = w_i \cos(\varphi - \beta_i) \quad (\text{A.14})$$

$$R_i = cb_i \sec(\beta_i) \quad (\text{A.15})$$

$$S_i = cd_i \quad (\text{A.16})$$

Table A.1. Seismic bearing capacity formulas for cohesive-frictional and purely cohesive soils (Conti 2018).

	Cohesive-frictional soil	Purely cohesive soil
Ultimate seismic bearing capacity	$q_{uE} = \frac{1}{2} \gamma B N_{\gamma E} + c N_{cE} + q N_{qE}$	
Seismic bearing capacity factors	$N_{qE} = e_q^k N_{qS}$ $N_{cE} = e_c^k N_{cS}$ $N_{\gamma E} = e_\gamma^k N_{\gamma S}$	$N_{qE} = e_q^k N_{qS}$ $N_{cE} = e_c^k N_{cS}$ $N_{\gamma E} = e_\gamma^k$
Static bearing capacity factors	$N_{qS} = \left(\frac{1 + \sin\varphi}{1 - \sin\varphi} \right) e^{\pi \tan\varphi}$ $N_{cS} = (N_{qS} - 1) \cot\varphi$ $N_{\gamma S} = 1.5(N_{qS} - 1) \tan\varphi$	$N_{qS} = 1$ $N_{cS} = 2 + \pi$ $N_{\gamma S} = 0$
Soil inertia	$e_q^k = \left(1 - \frac{k_h}{\tan\varphi} \right)^{(0.37 \tan\varphi)^{0.5}}$ $e_c^k = 1$ $e_\gamma^k = \left(1 - \frac{k_h}{\tan\varphi} \right)^{0.47}$	$e_q^k = 1 - a_q \left(\frac{k_h}{k_{h,lim}} \right) - b_q \left(\frac{k_h}{k_{h,lim}} \right)^2$ $e_c^k = 1$ $e_\gamma^k = -a_\gamma \left(\frac{k_h}{k_{h,lim}} \right) - b_\gamma \left(\frac{k_h}{k_{h,lim}} \right)^2$
		<p>Where:</p> $a_q = 0.75 k_{h,lim} \quad b_q = 1.4 k_{h,lim}$ $a_\gamma = 1.75 k_{h,lim} \quad b_\gamma = 1.4 k_{h,lim}$ $k_{h,lim} = \frac{c_u}{\gamma(D + \frac{B}{2})}$

Table A.2. Static bearing capacity factor $N_{\gamma s}$.

δ	$2c_v/\gamma_0 B$	D_f/B											
		$\varphi = 20^\circ$				$\varphi = 30^\circ$				$\varphi = 40^\circ$			
		0.25	0.5	0.75	1	0.25	0.5	0.75	1	0.25	0.5	0.75	1
0	0	5.45	7.72	9.93	12.10	15.38	20.32	25.13	29.87	45.65	57.26	68.60	79.78
	0.25	8.84	11.04	13.22	15.37	20.90	25.72	30.46	35.16	55.34	66.74	77.96	89.06
	0.5	12.11	14.28	16.44	18.59	26.25	31.01	35.71	40.38	64.79	76.07	87.20	98.24
$\varphi/2$	0	7.66	10.86	13.97	17.03	27.61	36.56	45.30	53.92	123.33	155.31	186.64	217.56
	0.25	11.85	14.95	18.00	21.03	35.98	44.73	53.36	61.90	144.65	176.17	207.21	237.94
	0.5	15.91	18.96	21.99	25.00	44.15	52.79	61.34	69.84	165.62	196.81	227.64	258.21
φ	0	10.61	15.05	19.38	23.65	55.45	73.69	91.53	109.15	-	-	-	-
	0.25	15.99	20.29	24.55	28.78	70.84	88.72	106.37	123.86	-	-	-	-
	0.5	21.20	25.44	29.66	33.87	85.91	103.58	121.09	138.49	-	-	-	-

Appendix

Table A.3. Equivalent pseudo dynamic bearing capacity factor $N_{\gamma E}$ for different anisotropy degree of rigidity and non-homogeneity parameter when $k_h=0.2$

$D_f/B = 0.5, \beta_\phi = 1.5, \beta_c^{-1} = 0.5, \text{ and } \nu_c = 15$														
φ	δ	$2c_v/\gamma_0 B$	$\beta_r^{-1} = 0.5$				$\beta_r^{-1} = 0.7$				$\beta_r^{-1} = 1.0$			
			ν_p											
			0.0	0.1	0.3	0.5	0.0	0.1	0.3	0.5	0.0	0.1	0.3	0.5
20°	0	0	-	-	-	-	-	-	-	-	-	-	-	-
		0.25	28.70	28.99	29.60	30.21	28.88	29.25	30.05	30.12	28.98	29.41	30.38	31.51
		0.5	55.41	55.72	56.38	57.06	55.58	55.97	56.82	56.88	55.68	56.13	57.16	58.36
	$\varphi/2$	0	-	-	-	-	-	-	-	-	-	-	-	-
		0.25	31.71	32.06	32.75	33.45	31.93	32.36	33.29	33.38	32.05	32.55	33.69	34.99
		0.5	61.11	61.48	62.24	63.04	61.31	61.77	62.77	62.84	61.43	61.96	63.17	64.59
	φ	0	-	-	-	-	-	-	-	-	-	-	-	-
		0.25	34.74	35.12	35.88	36.63	34.99	35.47	36.51	36.62	35.14	35.71	36.97	38.40
		0.5	66.93	67.38	68.19	69.07	67.17	67.68	68.81	68.90	67.31	67.91	69.27	70.86
30°	0	0	-	-	-	-	-	-	-	-	-	-	-	
		0.25	60.32	61.29	63.37	65.66	60.62	61.77	64.35	64.39	60.79	62.11	65.16	68.83
		0.5	113.70	114.68	116.79	119.13	113.99	115.16	117.77	117.80	114.16	115.49	118.58	122.31
	$\varphi/2$	0	-	-	-	-	-	-	-	-	-	-	-	-
		0.25	72.65	73.89	76.57	79.51	73.06	74.55	77.89	77.95	73.29	75.00	78.96	83.70
		0.5	136.37	137.63	140.37	143.38	136.77	138.28	141.67	141.73	137.00	138.73	142.75	147.58
	φ	0	-	-	-	-	-	-	-	-	-	-	-	-
		0.25	86.74	88.26	91.51	95.04	87.30	89.13	93.21	93.34	87.62	89.73	94.59	100.39
		0.5	162.68	164.23	167.57	171.22	163.23	165.09	169.26	169.37	163.54	165.68	170.64	176.58
40°	0	0	19.71	22.41	28.30	34.91	20.32	23.48	30.63	30.55	20.66	24.24	32.62	42.78
		0.25	131.93	134.68	140.70	147.47	132.48	135.70	142.98	142.87	132.79	136.44	144.96	155.30
		0.5	243.52	246.28	252.33	259.13	244.07	247.30	254.61	254.50	244.38	248.04	256.60	266.99
	$\varphi/2$	0	28.30	32.22	40.76	50.28	29.37	34.00	44.45	44.47	29.96	35.24	47.54	62.43
		0.25	178.00	182.01	190.77	200.58	178.89	183.61	194.25	194.17	179.40	184.75	197.25	212.39
		0.5	326.51	330.54	339.35	349.23	327.39	332.13	342.83	342.73	327.89	333.27	345.83	361.05
	φ	0	39.14	44.66	56.61	69.83	40.94	47.52	62.30	62.52	41.95	49.47	66.95	88.07
		0.25	245.40	251.08	263.44	277.19	246.89	253.61	268.76	268.79	247.74	255.40	273.26	294.81
		0.5	449.47	455.19	467.65	481.52	450.94	457.71	472.95	472.97	451.78	459.49	477.45	499.16

Appendix

Table A.4. Equivalent pseudo dynamic bearing capacity factor $N_{\gamma E}$ for different anisotropy degree of internal friction angle for $k_h=0.2$.

$\beta_r^{-1} = 0.7, \beta_c^{-1} = 0.5, v_p = 0.1$ and $v_c = 15$														
φ	δ	$2c_v/\gamma_0 B$	$\beta_\phi = 1.0$				$\beta_\phi = 2.0$				$\beta_\phi = 3.0$			
			D_f/B											
			0.25	0.50	0.75	1.00	0.25	0.50	0.75	1.00	0.25	0.50	0.75	1.00
20°	0	0	-	-	-	-	-	-	-	-	-	-	-	-
		0.25	31.91	33.83	35.72	37.57	26.23	27.25	28.21	29.13	24.64	25.41	26.10	26.71
		0.5	61.03	62.98	64.91	66.82	51.82	52.90	53.95	54.98	49.21	50.17	50.88	51.66
	$\varphi/2$	0	-	-	-	-	-	-	-	-	-	-	-	-
		0.25	38.15	40.50	42.80	45.06	28.23	29.31	30.33	31.28	25.94	26.73	27.43	28.04
		0.5	72.52	74.91	77.28	79.62	55.66	56.82	57.94	59.04	51.73	52.62	53.47	54.29
	φ	0	-	-	-	-	-	-	-	-	-	-	-	-
		0.25	46.84	49.72	52.54	55.30	29.89	31.00	32.03	32.99	26.74	27.53	28.23	28.81
		0.5	88.69	91.63	94.54	97.41	58.91	60.12	61.28	62.42	53.36	54.26	55.12	55.94
30°	0	0	11.31	15.55	19.66	23.70	-	-	-	-	-	-	-	-
		0.25	73.67	78.30	82.85	87.35	53.28	55.33	57.35	59.33	48.26	49.72	51.13	52.48
		0.5	135.88	140.54	145.17	149.76	102.97	105.07	107.16	109.22	94.68	96.22	97.73	99.22
	$\varphi/2$	0	18.91	25.70	32.32	38.84	-	-	-	-	-	-	-	-
		0.25	108.18	115.43	122.60	129.69	60.34	62.69	64.98	67.22	52.21	53.78	55.29	56.73
		0.5	197.22	204.53	211.79	219.00	116.33	118.74	121.12	123.48	102.31	103.98	105.61	107.22
	φ	0	34.72	46.86	58.73	70.43	-	-	-	-	-	-	-	-
		0.25	186.94	199.80	212.51	225.10	65.93	68.44	70.88	73.27	53.80	55.37	56.86	58.28
		0.5	338.50	351.48	364.36	377.16	127.11	129.71	132.27	134.80	105.55	107.23	108.88	110.49
40°	0	0	39.66	50.45	60.98	71.33	-	-	-	-	-	-	-	-
		0.25	181.97	193.49	204.87	216.13	112.05	116.17	120.24	124.28	97.51	100.28	103.00	105.68
		0.5	323.68	335.32	346.87	358.34	212.43	216.59	220.73	224.84	188.38	191.23	194.05	196.85
	$\varphi/2$	0	98.56	124.90	150.68	176.10	-	-	-	-	-	-	-	-
		0.25	386.84	414.23	441.33	468.18	134.33	139.37	144.35	149.28	107.87	110.93	113.94	116.88
		0.5	674.79	702.37	729.76	756.98	253.87	258.97	264.05	269.09	208.19	211.36	214.49	217.60
	φ	0	623.87	790.64	954.35	1116.20	-	-	-	-	-	-	-	-
		0.25	-	-	-	-	-	-	-	-	-	-	-	-
		0.5	-	-	-	-	-	-	-	-	-	-	-	-

Appendix

Table A.5. Equivalent pseudo dynamic bearing capacity factor $N_{\gamma E}$ for different anisotropy degree and non-homogeneity coefficient of cohesion for $k_h = 0.2$.

$D/B = 0.5$, $\beta_r^{-1} = 0.7$, $\beta_\phi = 1.5$ and $v_p = 0.1$

φ	δ	$2c_v/\gamma_0 B$	$\beta_c^{-1} = 0.4$				$\beta_c^{-1} = 1.2$				$\beta_c^{-1} = 2.0$			
			v_c											
			0	5	15	30	0	5	15	30	0	5	15	30
20°	0	0	-	-	-	-	-	-	-	-	-	-	-	-
		0.25	-	12.25	25.97	46.03	-	21.23	51.01	95.35	-	29.69	75.13	142.99
		0.5	-	22.48	49.58	89.56	8.21	39.73	99.02	187.60	9.14	56.42	147.06	282.71
	$\varphi/2$	0	-	-	-	-	-	-	-	-	-	-	-	-
		0.25	-	13.71	28.68	50.56	-	23.79	56.80	105.89	-	33.27	83.87	159.39
		0.5	-	25.09	54.61	98.21	9.49	44.38	110.03	208.08	10.27	63.04	163.90	314.84
	φ	0	-	-	-	-	-	-	-	-	-	-	-	-
		0.25	-	15.12	31.37	55.10	-	26.38	62.82	116.98	-	36.96	93.13	176.93
		0.5	-	27.71	59.70	106.97	10.71	49.21	121.62	229.76	11.32	69.98	181.90	349.36
30°	0	0	-	-	-	-	-	-	-	-	-	-	-	-
		0.25	11.36	26.69	55.29	97.70	12.65	44.39	105.20	196.07	13.80	61.44	153.47	291.19
		0.5	14.96	45.40	102.33	187.02	17.71	80.17	201.50	383.12	20.12	113.97	297.77	573.13
	$\varphi/2$	0	-	-	-	-	-	-	-	-	-	-	-	-
		0.25	14.74	32.75	66.49	116.52	16.08	54.82	128.67	238.96	17.27	76.00	188.88	357.71
		0.5	19.66	55.26	122.38	222.27	22.56	98.41	245.67	466.08	25.07	140.33	365.65	703.18
	φ	0	-	-	-	-	-	-	-	-	-	-	-	-
		0.25	18.25	39.43	79.10	137.90	19.62	66.90	156.75	290.86	20.80	93.28	232.20	439.92
		0.5	24.81	66.49	145.34	262.72	27.84	120.10	299.15	567.12	30.39	172.25	449.46	864.70
40°	0	0	23.48	23.48	23.48	23.48	23.49	23.48	23.48	23.50	23.48	23.48	23.48	23.48
		0.25	28.95	60.67	122.27	214.10	31.64	97.29	226.14	419.00	34.30	132.92	326.89	617.46
		0.5	34.09	97.64	220.52	403.98	39.64	170.34	427.70	813.29	45.04	241.25	628.87	1209.90
	$\varphi/2$	0	34.00	34.00	34.00	34.00	34.00	34.00	34.00	34.00	34.00	34.00	34.00	34.00
		0.25	42.46	83.78	164.45	284.80	45.80	136.21	313.18	577.93	49.09	187.18	457.96	863.42
		0.5	50.33	133.08	294.06	534.54	57.25	236.76	590.06	1119.30	63.94	338.00	878.90	1689.60
	φ	0	47.52	47.52	47.52	47.52	47.52	47.52	47.52	47.52	47.52	47.52	47.52	47.52
		0.25	60.85	116.49	225.19	387.34	65.06	194.47	447.42	825.77	69.16	270.52	665.26	1256.30
		0.5	73.22	184.47	401.31	725.28	81.98	338.49	843.35	1599.7	90.35	489.54	1278.00	2459.70